“ FROM AMPHIPHILIC BLOCK COPOLYMERS TO FERROCENYL-FUNCTIONALIZED POLYMERS FOR BIOSENSORIC APPLICATIONS ”

Dissertation
zur
Erlangung des Grades

„ Doktor der Naturwissenschaften ”

am Fachbereich Chemie, Pharmazie und Geowissenschaften
der Johannes Gutenberg – Universität in Mainz

Francisco Javier López Villanueva

geboren in Rüsselsheim (Deutschland)

Mainz 2007

Ein guter Ingenieur ist immer
ein bisschen konservativ …
zumindest auf dem Papier.

Scotty (in StarTrek – TNG)

The present thesis can be divided in three main parts. In all parts new polymer architectures were synthesized and characterized concerning their special features.
The first part will emphasize the advantage of a polystyrene-*block*-(hyperbranched polyglycerol) copolymer in comparison to an analogue polystyrene-*block*-(linear polyglycerol) copolymer. Therefore a synthethic route to prepare linear block copolymers has been developed. Two strategies were examined. One strategy was based on the classic, sequential anionic polymerization; the second strategy was based on a "Click-Chemistry" coupling reaction. In a following step glycidol was hypergrafted from these block copolymers by applying a hypergrafting reaction with glycidol. The behavior of the amphiphilic block copolymers synthesized was studied in different solvents. Furthermore the polarity of the solvent was changed to form the corresponding inverse micelles. DLS, SLS, SEC-MALLS-VISCO, AFM and Cyro TEM measurements were performed to obtain a visual image from the appearance of the aggregates. It was found that a linear-hyperbranched architecture is necessary, if well defined, monodisperse aggregates are required, e.g. for the preparation of ordered nanoarrays. Linear-linear block copolymers formed only polydisperse aggregates. Additionally it was found that size distribution could be improved dramatically by passing the aggregates through a SEC column with large pores. The SEC columns acted like a template in which the aggregates adopt a more stable conformation.
In the second part anionic polymerization was employed to synthesize silane-endfunctionalized macromonomers with different molecular weights based on polybutadiene and polyisoprene. These were polymerized by a hydrosilylation reaction in bulk to obtain branched polymers, using Karstedt's catalyst. Surprisingly the addition of monofunctional silanes during the polymerization had only a minimal effect concerning the degree of polymerization. It was possible to introduce silanes without increasing the overall number of reaction steps by a very convenient "pseudo-copolymerization" method. All branched polymers were analyzed by SEC, SEC-MALLS, SEC-viscometry, ^{1}H-NMR-spectroscopy and DSC concerning their branching ratio. The branching parameters for the branched polymers exhibited similar characteristics as hyperbranched polymers based on AB_2 monomers. Detailed kinetic study showed that the polymerization occurred very rapidly in comparison to the hydrosilylation polymerization of classical AB_2 type carbosilanes monomers.
The last part will deal with ferrocenyl-functionalized polymers. On the one hand, ferrocenyl-functionalized polyglycerols (PG) were studied. Esterification of PGs with different molecular weight using ferrocenemonocarboxylic acid gave the ferrocenyl funtionalized polymers in high yields. On the other hand three different block copolymers were prepared with different ratios of styrene to butadiene units (10:1, 4:1, 2:1). The double bonds of the 1,2-PB block were hydrosilylated using silanes bearing one ($HSiMe_2Fc$) or two ($HSiMeFc_2$) ferrocene units. High degrees of functionalization were obtained (up to 83 %). In this manner, six different ferrocenyl-rich block copolymers with different fractions of ferrocene were prepared and analyzed, employing NMR-spectroscopy, SEC, SEC/MALLS/viscometry, DLS and cyclic voltammetry. The redox properties of the studied polymers varied primarily with the nature of the silane unit attached. Additionally, the redox properties in solution of the studied polymers were influenced by the block length ratio of the block copolymers. Unexpectedly, with increasing block length of the ferrocenyl block the fraction of active ferrocenes decreased. Nevertheless, in case of thin monolayer films this behaviour was not observed. All polymers (PG and PS-*b*-PB based) exhibited good electrochemical properties in a wide range of solvents, which rendered them very interesting for biosensoric applications.

ADH	alcohol dehydrogenase
AFM	atomic force microscopy
CV	cyclic voltammetry
DB	degree of branching
DBU	1,8-diazabicyclo[5.4.0]undec-7-ene
DIC	Diisopropylcarbodiimide
DLS	dynamic light scattering
DMF	dimethylformamide
DNA	deoxyribonucleic acid
DPTS	4-(Dimethylamino)pyridinium 4-toluenesulfonate
DSC	differential scanning calometry
EDC	endocrine-disrupting compound
EDTA	ethylenediaminetetraacetic acid
EEGE	ethoxy ethyl glycidyl ether
ESI-MS	electron spray ionization mass spectrometry
Fc	ferrocene
$[\eta]$	intrinsic viscosity
h	hour
HOPG	highly-ordered pyrolytic graphite
HPLC	high-performance liquid chromatography
$HSiMe_2Fc$	ferrocenyldimethylsilane
$HSiMeFc_2$	diferrocenylmethylsilane
hypPG	hyperbranched polyglicidol
hypPG-PS-hypPG	hypPG-*block*-polystyrene-*block*-hypPG copolymer
linPG	linear polyglycerol
linPG-PS-linPG	linPG-*block*-polystyrene-*block*-linPG copolymer
LS	light scattering
MALLS	multi angle laser light scattering
MALDI-ToF	Matrix Assisted Laser Desorption/Ionization Time-of-Flight
Me	methyl
min	minute
M_n	number average of the molecular weight
MS	mass spectrometry
N_3-PS-N_3	α,ω functional polystyrene with azide endgroups

NADH	dihydronicotinamide adenine dinucleotide
NMR	nuclear magnetic resonance
PB	polybutadiene
PDI	polydispersity index
PEEGE	poly(ethoxy ethyl glycidyl ether)
PEEGE-PS-PEEGE	PEEGE-*block*-polystyrene-*block*-PEEGE copolymer
PG	polyglycerol
PI	polyisoprene
P_n	number average of the degree of polymerization
PS	polystyrene
PS-N_3	polystyrene with azide endgroup
PS-linPG	polystyrene-*block*-linear PG copolymer
PS-hypPG	polystyrene-*block*-hyperbranched PG copolymer
PS-PEEGE	polystyrene-*block*-PEEGE copolymer
PS-OH	polystyrene with hydroxyl endgroup
PS-Tos	polystyrene with tosylate endgroup
R_g	radius of gyration
R_h	hydrodynamic radius
RI	refractive index
ROMBP	ring opening multibranching polymerization
s	second
SCVP	self-condensing vinyl polymerization
SEC	size exclusion chromatography
SLS	static light scattering
TBAH	tetra-n-butylammonium hexafluorophosphate
TEM	transmission electron microscopy
T_g	glass transition temperature
THF	tetrahydrofuran
TCF	time correlation function
TEM	transmission electron microscopy
TGA	thermo gravimetric analysis
TMP	1,1,1-tris(hydroxymethyl)propane
TNG	the next generation
Tos-PS-Tos	α,ω functional polystyrene with tosylate endgroups

UV-vis	ultraviolet-visible
wt.-%	weight percent

1. Introduction

1.1. Hyperbranched Polymers

1.1.1. Natural Origins

Roughly spoken, a linear polymer can be defined as long chain with two ends. A branched polymer possesses branching units in addition to the “normal” chain segments. From these units new linear chains are grown. Depending on the amount of these branching units, a branched polymer is characterized by multiple chain ends (termini). Of course, branched or “hyperbranched” polymers have not been invented by mankind. In fact, Nature is the true outrider concerning the development of randomly cascade-branched structures.[1-4] The most famous examples are glycogen, amylopectin and dextran, which are produced on a 10^9 ton/year scale (Figure 1).

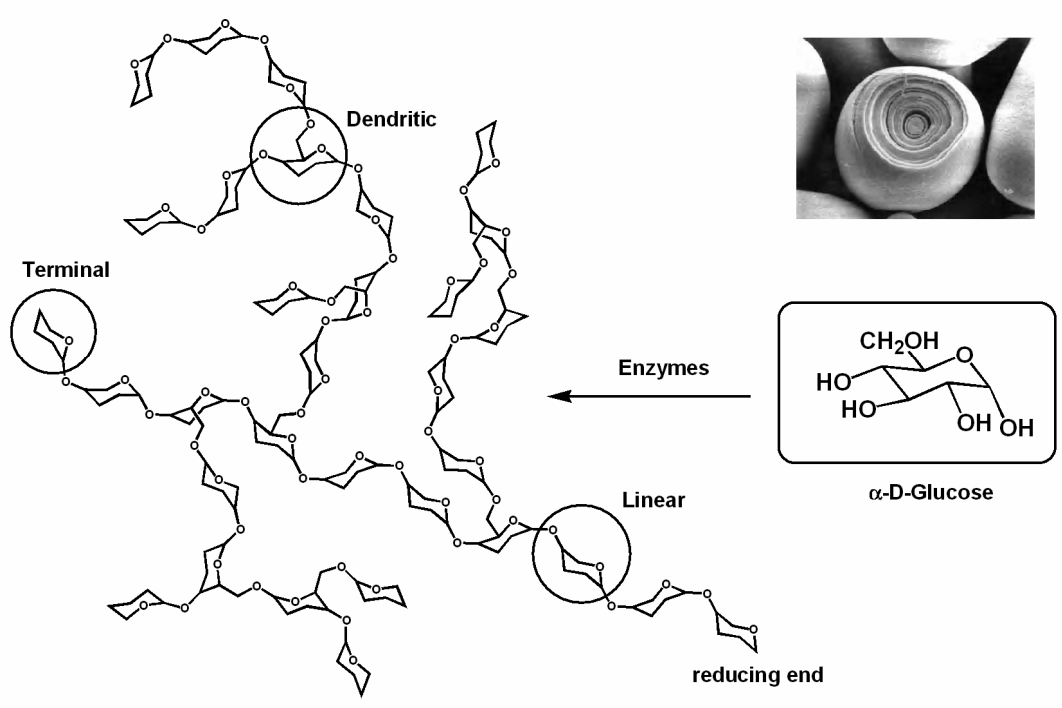

Figure 1 Enzymatic polymerization of α-D-glucopyranose leading to hyperbranched glycogen (idealized structure). The inset shows a SEM image of a starch grain with layer structure.[5]

The branched structure of these natural products was first identified by Staudinger (1930)[6] and closer examined later on by Meyer and Bernfeld (1940).[7] Nature takes

advantage of the fact that multibranching results in a structure with numerous reduceable endgroups, allowing therefore the easy and fast release of energy via the cleavage of glucose.

The enzyme-controlled synthesis of these polysaccharides yields very precisely defined macromolecules regarding the branching sites. The three polymers differ from each other only by the linkage and the amount of branching sites. Linear units are $\alpha(1\rightarrow6)$ or $\alpha(1\rightarrow4)$ and branching units are $\alpha(1\rightarrow3)$ or $\alpha(1\rightarrow6)$. Nature is able to synthesize macromolecules with hundreds of millions gram per mol, which is generally beyond the molar masses from synthetic approaches (Table 1). The degrees of branching (DB) of natural glycopolymers is in generally low, ranging between 16 and 60 %.

Table 1 Structural and molar data of branched polysaccharides.[8]

	M_w / gmol^{-1}	linkage		DB / %
		linear	branching	
dextran	2 x 10^6	$\alpha(1\rightarrow6)$	$\alpha(1\rightarrow3)$	< 60
glycogen	2 – 300 x 10^6	$\alpha(1\rightarrow4)$	$\alpha(1\rightarrow6)$	< 16
amylopectin	70 – 120 x 10^6	$\alpha(1\rightarrow4)$	$\alpha(1\rightarrow6)$	< 10

1.1.2. Mankind's Answer

The interest of researchers in branched structures was focused on dendrimers since the mid-1980ies.[9-11] The perfect branch-on-branch structures of dendrimers are synthesized by multi-step protocols, including alternating build-up reactions of the shell and purification steps. These synthetic approaches permit access to symmetric and monodisperse polymers of unprecedented structural precision. Due to their perfectly branched structure, dendrimers were believed to be very promising candidates for a wide range of applications in materials science.[12-14] Use in coatings, as viscosity mediators, and to prevent gas hydrate–ice crystal formation in oil pipelines has been investigated.[15] Encouraged by the rapid advances regarding the scale-up synthesis of dendrimers, a large number of materials scientists have focused their research on functional dendrimers.[14,16,17] Nevertheless, because of the unavoidable multistep

synthesis, dendrimers are very expensive materials, especially when going to higher generations.

To solve this “scale-up” and also economic problems, scientists went back to the first approaches of branched or hyperbranched polymers, which were based on Flory’s seminal work.[18] This basic concept of a polycondensation using AB_2-monomers with complementary A and B functionalities (e.g., hydroxyl and carboxyl groups) leading to branched or “hyperbranched” polymers is today one of the mainly employed methods, with more than 150 examples for suitable monomers published since 1990. Some of these examples are presented in Figure 2.

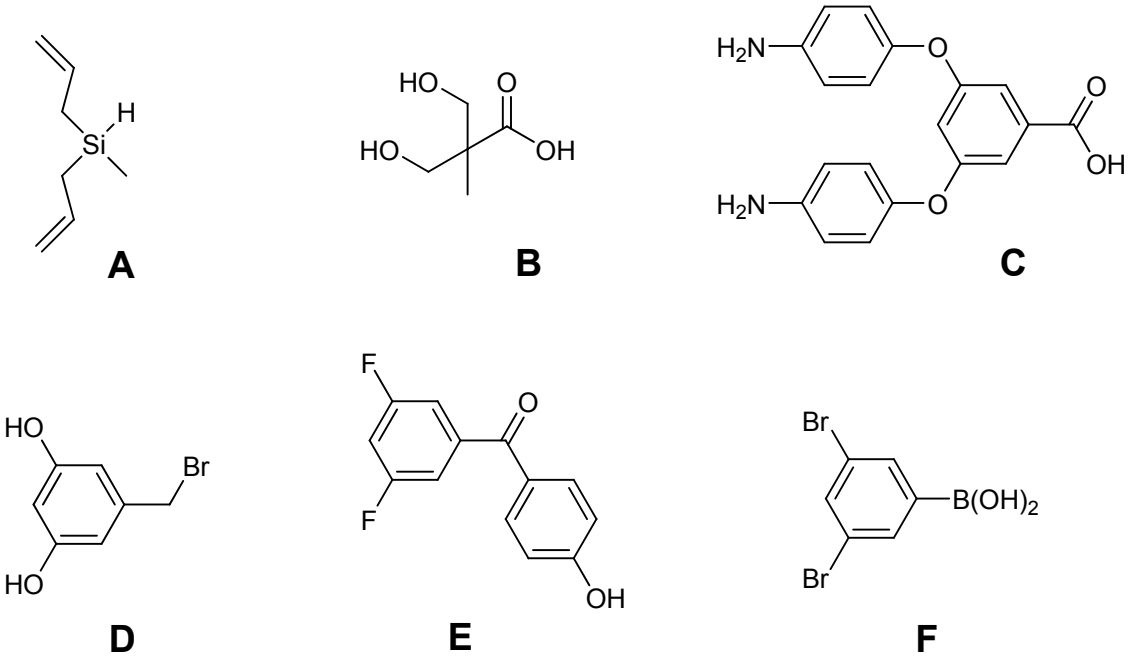

Figure 2 Examples of AB_2-monomers leading to hyperbranched (A) polycarbosilanes,[19,20] (B) polyesters,[21] (C) polyamides,[22] (D) polyethers,[23] (E) poly(ether ketones),[24] and (F) polyphenylenes.[25]

The last example (F) was published by Kim and Webster, who introduced with this polymer also the terms “hyperbranching” and “hyperbranched”.[25] It was one of the first approaches toward synthetically constructed branched macromolecules since the works of Flory and could be understood as the birthday of hyperbranched polymers. Since (hyper-)branched polymers exhibit similar properties to dendrimers by straightforward and more economical syntheses, their influence has significantly increased in recent years.[26]

The following characteristics were of particular interest to materials scientists:[27,28]

i a globular relatively compact structure
ii a high number of surface functionalities
iii absence of entanglements, in contrast to linear polymer chains

These structural peculiarities usually result in amorphous materials, since branching prevents crystallization and leads to low viscosity in bulk and solution.[29,30] Hyperbranched polymers are usually not very tough materials due to the lack of chain entanglement and the high concentration of endgroups. Thus their physical properties depend strongly on the glass transition temperature (T_g), e.g. high T_g results in brittle materials and low T_g in oils.

From a topological point of view, hyperbranched polymers are characterized by the absence of a connecting line between any two endgroups that passes all branching points. This definition translates to a structure that contains at maximum one closed cycle per macromolecule, i.e., no gelation can occur.[31]

Numerous possible applications have been proposed for these materials: the low viscosity in combination with high functionality is useful for functional crosslinkers, additives, rheology modifiers for components in adhesives, advanced coatings, structured hydrogels and dental composites. Furthermore, examples in the fields of biomedicine and biochemistry as carriers for the controlled release of drugs are under investigation.[8,26,27,32,33]

1.1.3. Degree of Branching

The degree of branching (DB) is a crucial parameter for polymer chemists working in the field of tree-like branched macromolecules. Dendrimers do not posses linear units and therefore only contain dendritic and terminal units. Thus the DB for them is defined to be unity (Figure 3).

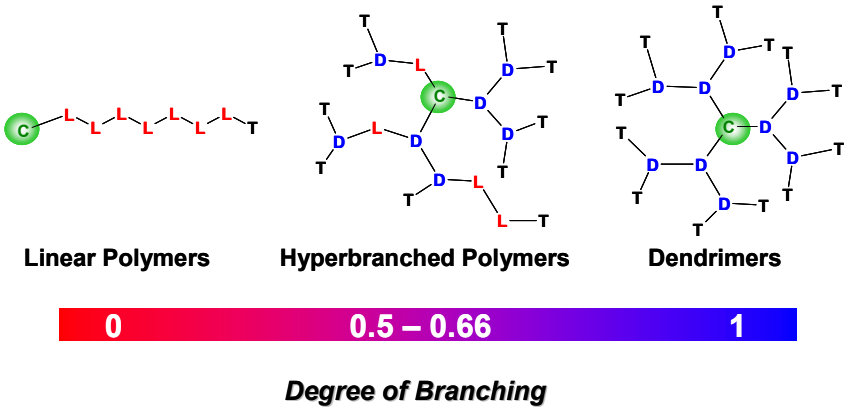

Figure 3 Comparison of polymeric architectures as a function of the degree of branching DB (D, L, T: dendritic, linear and terminal units, respectively).

In contrast, a linear polymer contains only linear segments leading to a DB of zero. Consequently (hyper)branched polymers are situated in the region between zero and one.

A first definition of the DB for AB_2 based monomers was introduced by Fréchet et al. in 1991:[34]

$$DB_{Fréchet} = \frac{D+T}{D+T+L} \tag{1.1}$$

D, L, T represent the relative abundances (%) of the dendritic, linear and terminal units respectively. In equation (1.1) the linear direction is also counted as a branching point, which leads in case of low molecular weight polymers to an overestimation of the DB.

Based on theoretical studies performed by Frey et al. a new expression valid for AB_n ($n \geq 2$) monomers was defined that could estimate the DB more accurate in the low molecular weight regime.[35,36]

$$DB_{Frey} = \frac{2D}{2D+L} \tag{1.2}$$

In equation (1.2) the formation of cycles during the polymerization is neglected. To calculate the DB it is necessary to know the relative abundances. Generally this is achieved by NMR spectroscopy.

1.1.4. Contraction Factors

Equations (1.1) and (1.2) are only suitable, if it is possible to distinguish the dendritic, linear and terminal units. Unfortunately, this is not possible for all hyperbranched polymers. Often the characteristical responses, e.g. in NMR experiments, are very similar, making it impossible to obtain relative abundances as in the case of highly branched poly(ethylene)s synthesized by Ziegler-Natta-type catalysts.[37-40]

In this case the determination of the contraction factors becomes more useful. It is possible to treat the decrease of R_{gb} (radius of gyration of a branched polymer) and $[\eta]_b$ (intrinsic viscosity of a branched polymer) quantitatively as a result of branching. This was done for the first time by Zimm and Stockmayer for the radius of gyration (g-parameter), and somewhat later by Stockmayer and Fixman for the intrinsic viscosity (g'-parameter).[41,42] They introduced the following shrinking or contraction factors: the radii of gyration for a Gaussian segment distribution can in principle be calculated analytically without introducing any physical approximations. For the intrinsic viscosity this is not the case since hydrodynamic interactions among the segments have to be taken into account. So far these can be calculated only under certain approximations whose physical relevance remains not fully understood.[43-45]

$$g = \left.\frac{\left(R_g^2\right)_{br}}{\left(R_g^2\right)_{lin}}\right|_M \tag{1.3}$$

$$g' = \left.\frac{[\eta]_{br}}{[\eta]_{lin}}\right|_M \tag{1.4}$$

Nevertheless the g and g' (also termed as branching ratio's) are very useful parameters to estimate the compactness of branched macromolecules in comparison to the linear analogues. Roughly speaking, the contraction factors are a volume fraction, giving an estimate about how much "smaller" a branched polymer is in contrast to a linear coil analogue.

1.2. Synthetic Concepts

1.2.1. Inimer Concept

Besides the long-known condensation of AB_n monomers (*vide supra*), numerous materials scientists worked on alternative concepts to increase the size of the polymers and to decrease the polydispersity in the 1990ies.

The Williamson etherification, as an example for step-growth, of a benzylic bromide group with one of the phenolic groups of another monomer unit yields a dimer (Figure 4 A). The overall growth process involves two monomers containing a total of six potential reactive centers (2A + 4B) and gives rise to a dimer with only four reactive centers remaining (1A + 3B). Therefore, bond formation consumes two reactive centers (one A and one B), whereas the newly formed ether bond is incapable of participation in any further growth process. Hyperbranched polymers formed by this kind of step-growth synthesis have a very broad PDI (≈ 5).

In 1995 Fréchet et al. introduced for the first time the "inimer" concept.[46] This concept, also termed self-condensing vinyl polymerization (SCVP), has the advantage of producing and not consuming reactive sites during polymerization.

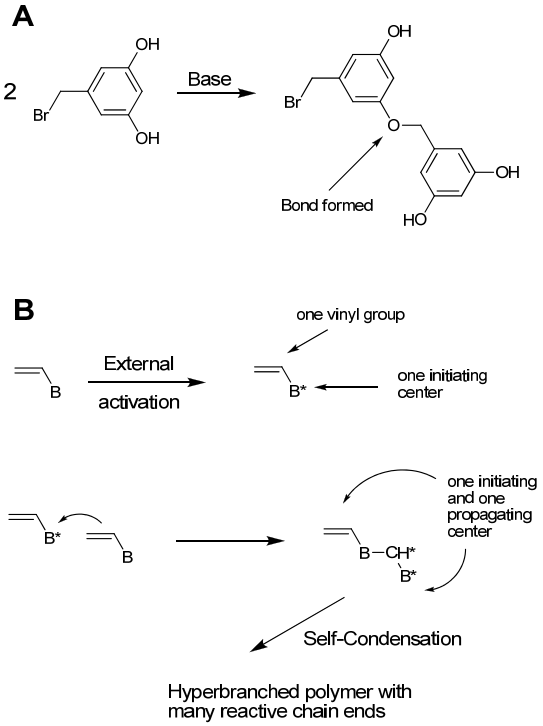

Figure 4 Step-growth polycondensation vs. SCVP.[46]

In the case of the AB vinyl monomer (Figure 4, B), in which A is a vinyl group and B is a pendant group (for example, the aromatic ring of styrene), the polymerization is started by an activated initiating moiety, I*. Depending on the type of polymerization, I* could be a "living" free radical, an electrophilic cationic moiety, or a carbanion. In addition, reaction of I* with one carbon atom of the double bond results in the consumption of two reactive centers with concurrent formation of a bond that is usually incapable of further reaction. However, the process also creates a new active site on the second carbon atom of the double bond that is capable of reacting with yet another double bond in the process of propagation. Because the double bond behaves as an effective difunctional moiety, the foundation may be laid for growth of highly branched structures through appropriate manipulations of the pendant group B. Especially *p*-(1-chloroethyl)-styrene could be employed very successfully under radical conditions.[46] Today many examples for the SCVP were developed including acrylate monomers and/or ionic reaction conditions.[47-49]

1.2.2. Slow Monomer Addition

The step-growth polycondensation as well as the SCVP still possess one major disadvantage. If the polymerization is performed under bulk conditions, the obtained PDIs are rather high. The main parameters influencing the PDI, the degree of polymerization and the DB of hyperbranched polymers were discussed in a computer simulation study.[50] It was found that the slow monomer addition of suitable AB_n monomers would allow a control of the molecular weight via the monomer/core ratio. Additionally, it was concluded that the polydispersity would behave reciprocal to the number of functional groups in the core (PDI≈1+1/f with f = core functionality), which is also illustrated in Figure 5.

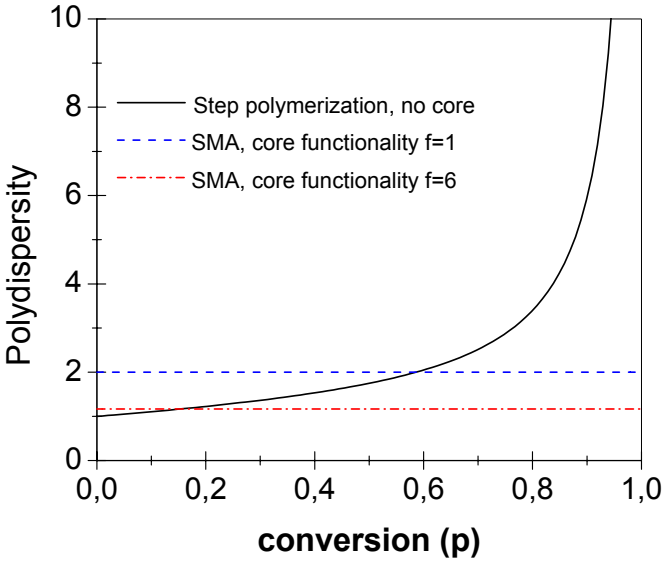

Figure 5 Polydispersity vs. conversion for an AB_2 monomer in the case of step-growth reaction and slow monomer addition with arbitrary core functionality values (f=1 and 6).

A parallel theoretical work from Müller et al. confirmed the conclusions for the analogous SCVP using core forming molecules.[51] The first example of the slow monomer addition was reported by Moore et al. for the synthesis of hyperbranched polyphenylacetylenes.[52,53] The efficiency of the slow monomer addition technique can be directly related to the reactivity of the added monomer. Highly reactive monomers that are added instantaneously to the core have a lower tendency for the formation of unwanted homopolymers (e.g. monomer itself does not act as initiator).

A very interesting “candidate” in this context is the glycidol (oxiran-2-yl-methanol) monomer. Concerning a ring opening polymerization this monomer increases the number of active sides after each addition step by one.

Therefore it is also termed a “latent AB_2 monomer”. Penczek and Dworak presented in 1994 and 1995 the cationic ring-opening polymerization of glycidol leading to hyperbranched polyether polyols.[54,55] In 1999 was the anionic ring-opening multibranching polymerization of glycidol was developed.[56,57]

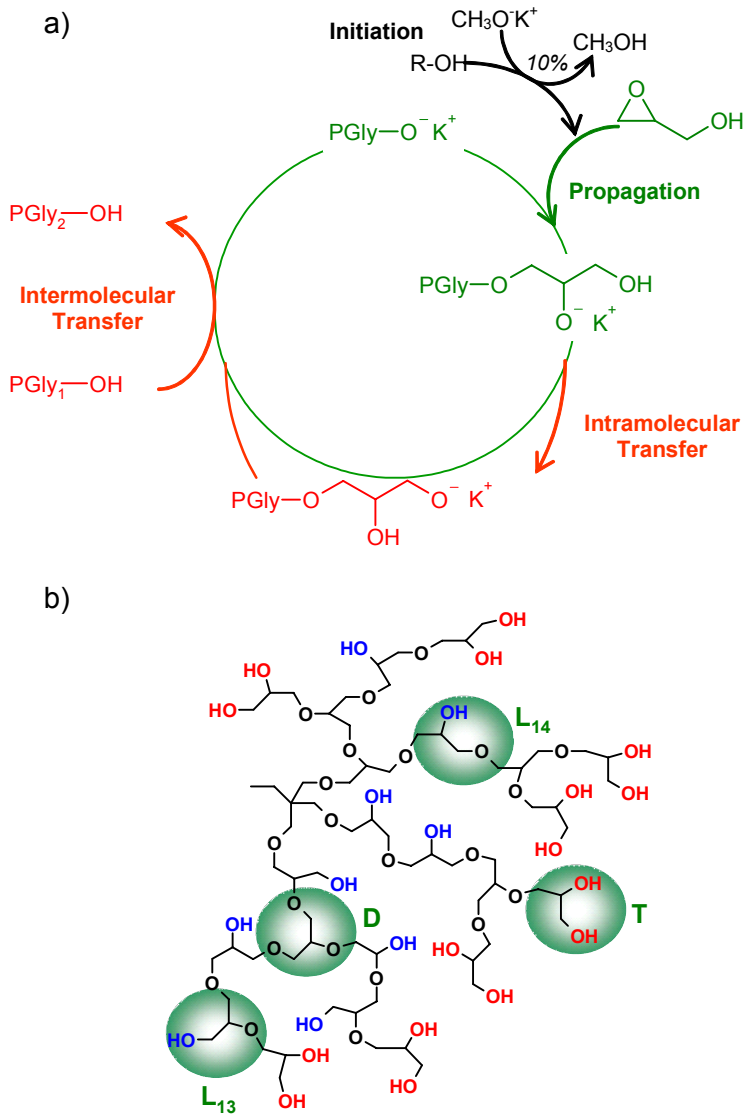

Figure 6 a) Mechanistic pathway of the base-catalyzed ring-opening multibranching polymerization of glycidol. b) Structure of the resulting hyperbranched polyglycerol, which represents only a small idealized fragment of the large polymer.

The latent AB_2 monomer is slowly added to partially deprotonated 1,1,1-tris(hydroxymethyl)propane (TMP), representing a trifunctional core-initiator for the polymerization. Due to the fast proton exchange during the polymerization the different chain ends (secondary and primary alcohols) are able to grow simultaneously into a branched structure as shown in Figure 6. The materials reported were transparent and viscous liquids. The polymers studied exhibited a DB between 0.53 and 0.59 for molar masses between 2 000 and 20 000 g mol^{-1}. It was shown that with increasing molecular weights the polydispersity broadens and a second distribution at low molar masses appears which is ascribed to impeded diffusion of the glycidol monomer with increasing viscosity of the system. Also small amounts of cyclic products were found. An optimized polymerization procedure based on an improved reac-

tion setup and with diglyme as emulsifying agent reduced some of these problems.[58] Recently Brooks et al. reported a procedure for the synthesis of high molecular weight polyglycerols (PGs) with dioxane as emulsifying agent.[59] Very high molecular weight hyperbranched PGs with narrow polydispersity were obtained (M_n up to 700 000, PDI = 1.1-1.4). However, no clear explanation for the formation of high molecular weights was given in this paper. The polyglycerols formed are currently tested in blood-extender formulations and blood substitute mixtures and have also been patented for this purpose.

1.3. Block Copolymers

1.3.1. Structural Considerations

Block copolymers are a fascinating class of polymeric materials belonging to a large family known as "soft materials." This class of polymers is made by the covalent bonding of two or more polymeric chains which are thermodynamically incompatible giving rise to a rich variety of microstructures in bulk and in solution. The length scale of these microstructures is comparable to the size of the block copolymer molecules (typically 5-50 μm); therefore the microstructures are highly coupled to the physical and chemical characteristics of the molecules. The variety of microstructures gives rise to materials with applications ranging from thermoplastic elastomers and high-impact plastics to pressure-sensitive adhesives, additives, foams, etc. In addition, block copolymers are very good candidates for potential applications in advanced technologies such as information storage, drug delivery and photonic crystals.[60]

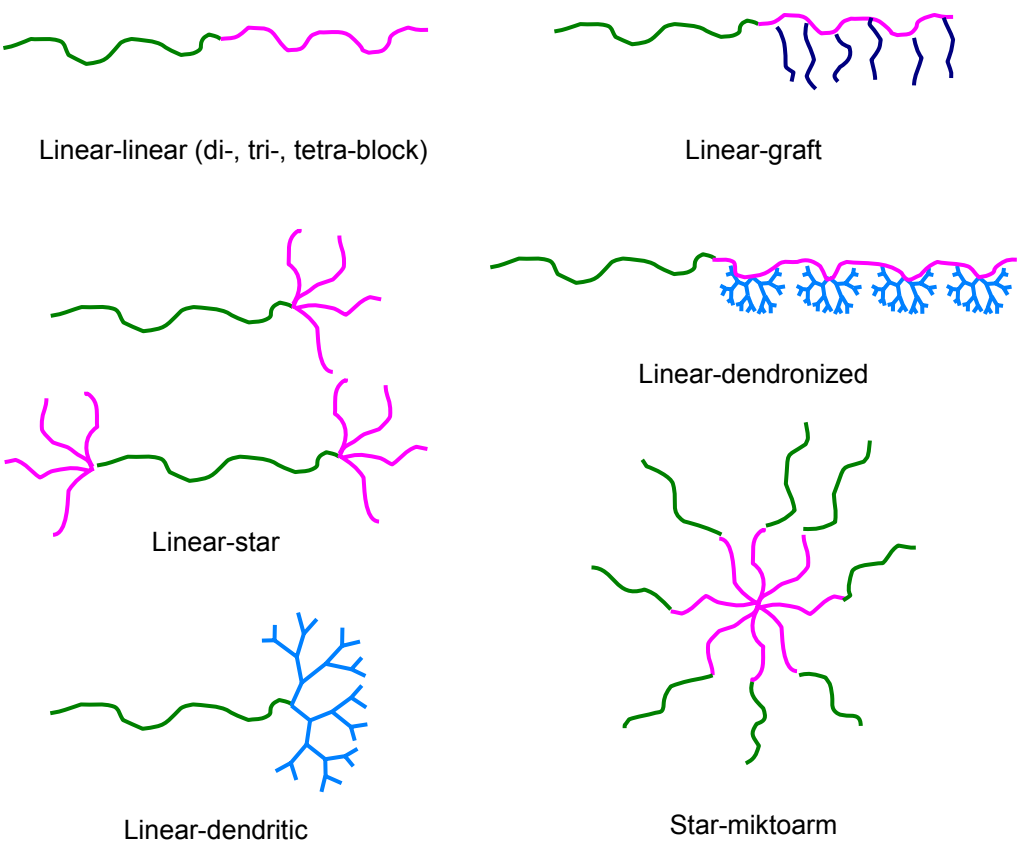

Figure 7 Schematic images of different block copolymer architectures.

Figure 7 shows some examples of the possible structures of block copolymers. Linear AB diblock copolymers are nowadays very common and in some cases also commercially available. Commercial examples are the polystyrene-polybutadiene elastomers from BASF (Styrolux® and Styroflex®).[61] The coupling of telechelic polymers with AB_n-structure, in which preformed polymer segments react with each other represents an approach that has been applied extensively to the synthesis of well-defined structures such as stars,[62,63] dendritic stars,[64] macromolecular "dumbbells",[65] dendrigrafts,[66] H-shaped[67] as well as arborescent polymers.[68] This has led to a better understanding of the respective structure-property relationships.[69,70] Recently also triblock copolymers have attracted the interest of many materials scientists as these materials are capable of forming a much richer diversity due to phase separation in bulk and suprastructure formation in solution.[71-73]

1.3.2. Linear-Dendritic Block Copolymers

The rapid development of dendrimers and hyperbranched polymers - cascade-branched structures that are often summarized as “dendritic polymers” - has greatly enhanced the spectrum of potential building blocks for segmented macromolecular architectures. Dendritic structures lead to a compact, globular shape of the macromolecules due to spatial restrictions of the branched topology. In addition, dendritic blocks are unlikely to form entanglements (*vide supra*).

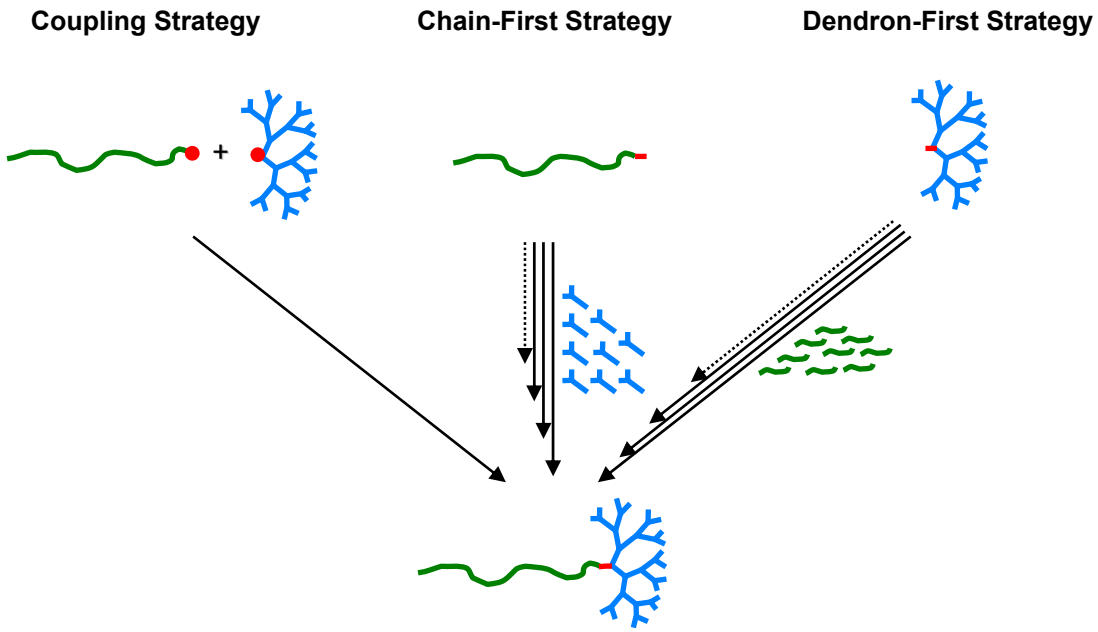

Figure 8 Schematic illustration of the different fundamental strategies for the synthesis of linear-dendritic block copolymers.

The three main approaches to linear-dendritic block copolymers are summarized in Figure 8. First examples for linear-dendritic block copolymers date back to the mid 1990ies. Especially Fréchet and Meijer focused their attention early on this field of science and developed linear-dendritic block copolymers based on their experience with dendrimers. Fréchet et al. developed a convergent route, by which a polyethylene glycol was coupled with a poly benzyl ether dendron via the well-known Williamson etherification.[74] Slightly later Meijer et al. described linear-dendritic polymers based on a functional polystyrene with a divergently formed poly(propylene imine) dendron by consecutive Michael additions of acrylonitrile.[75,76]

Another very interesting class of dendritic polymers are the “dendronized polymers”. In this case the dendritic wedges are aligned on the polymer chain. Because of the generally increasing demand of space for the dendritic wedges, these polymers as-

sume a more stretched conformation with increasing dendrimer generation (Figure 9).[77,78]

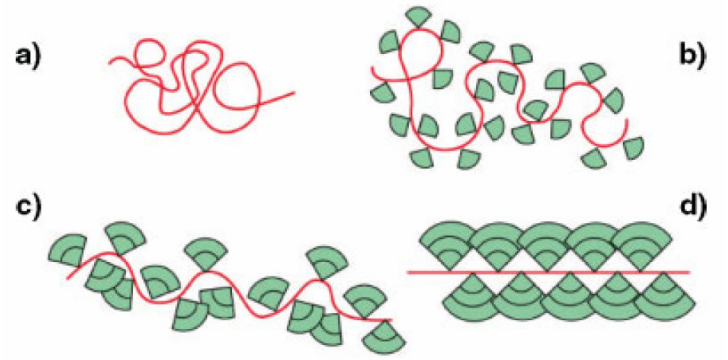

Figure 9 Cartoon representation of a coiled polymer backbone stretching via the attachment of increasingly sterically demanding dendrons. Polymer backbone with a) no dendrons; b) dendrons of the first generation; c) second generation; d) third generation.[77]

1.3.3. Linear-Hyperbranched Block Copolymers

Linear-dendritic block copolymers suffer from the same disadvantages as dendrimers. The synthesis generally requires tedious multiple steps synthesis and the final product is often available only in small quantities. A possible solution could be the exchange of the dendritic block by a synthetic more easily accessible hyperbranched block. The fundamental strategies for the block copolymer formation are still the same (Figure 8) and the physical properties of the hyperbranched block should not differ too much from a dendritic block (*vide supra*).

In this context the "hypergrafting" concept has shown to be a very suitable strategy. To generate a linear-hyperbranched block copolymer a long linear block is combined with a short polyfunctional B_f-type structure that is used as an initiator-core for the ensuing hypergrafting procedure. Thus hypergrafting means the "pseudo-living" addition of suitably reactive AB_2 monomers onto the B_f-block. This synthetic approach was first established for the preparation of polystyrene-*block*-(1,2-polybutadiene-*hypergrafted*-polycarbosilane) using alkenyl silane monomers.[79] Unfortunately the grafting efficiency was very low (30-60 %) because the carbosilane monomers employed were not very reactive and showed intramolecular cyclization. Nevertheless the very narrow dispersed block copolymers (PDI = 1.02-1.07) showed a high diversity in their morphology. The morphology was strongly influenced by the size of the branched block.

To increase the hypergrafting efficiency, recently another approach based on the more reactive glycidol monomers was studied (Figure 10).[80]

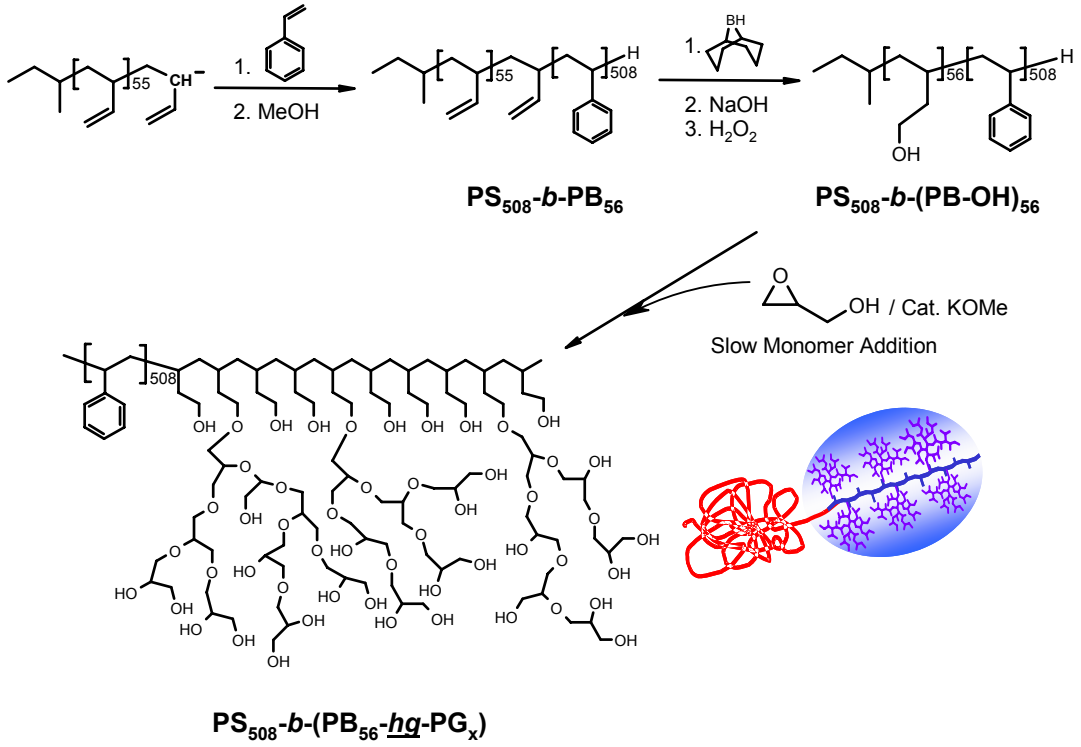

Figure 10 Synthetic strategy for the preparation of PS_{508}-*b*-(PB_{56}-*hg*-PG_x).

A convenient three-step strategy was developed for the preparation of well-defined amphiphilic, linear-hyperbranched block copolymers via hypergrafting. The procedure was a combination of the carbanionic polymerization with the alkoxide-based, controlled ring-opening multibranching polymerization of glycidol. The materials consisting of a linear polystyrene block and a hyperbranched polyglycerol block exhibited narrow polydispersity (1.01-1.02 for 5.4% to 27% wt. PG and 1.74 for 52% wt. PG) combined with a high grafting efficiency (60-76 %).

Detailed investigation of the solution properties of the block copolymers with linear polystyrene blocks showed that the block copolymer micelles were stabilized by the highly branched block. Spin-coated on graphite these aggregates showed interesting features, with respect to the presence of a very dense, functional and stable hyperbranched block (Figure 11). This could give rise to promising potential applications, e.g. nanopatterning of surfaces.

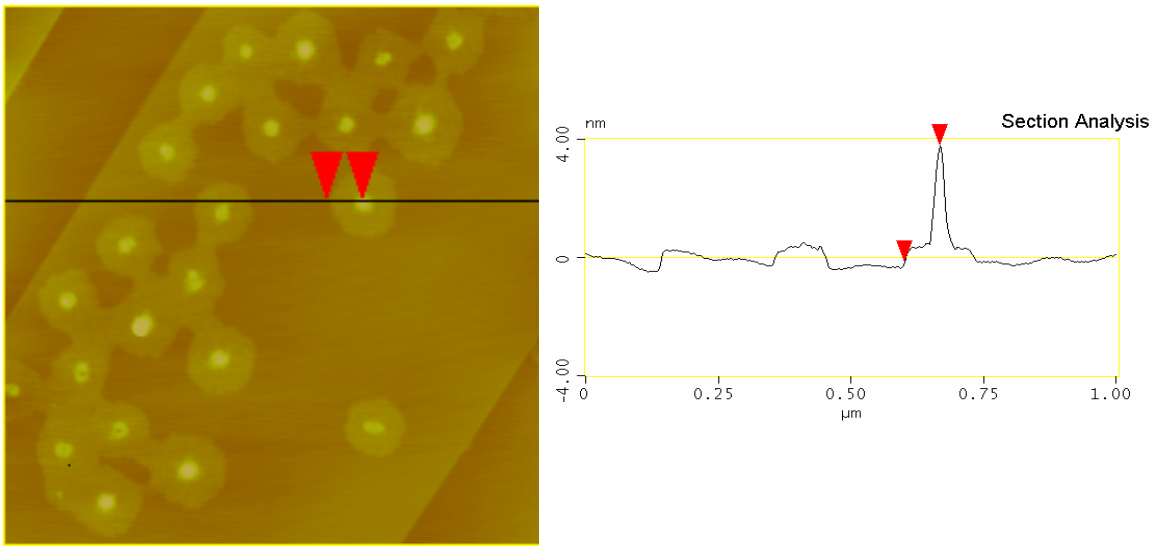

Figure 11 AFM-micrographs from a toluene solution (0.5 g/L) on a graphite substrate in tapping mode (radius ≈ 67 nm).

Nevertheless, based on this context it was not possible to discuss the very important question if the hyperbranched structure was really necessary for the formation of the well defined structures or if only linear block copolymers would yield the same results. The answer to this question will be the subject of the following work.

2. Objectives

2.1. Introduction

Polymers were and are very important for the life of mankind. Polysaccharides as well as the DNA are examples how nature uses specifically designed polymers with special functions to enable life on this planet. Very complex and diverse structures are constructed by Nature from a reduced choice of building units (amino acids, lipids, etc.). Proteins, for instance, are formed from a few amino acids and exhibit different secondary conformations, e. g. α-helix, β-sheet, or coiled. Proteins with well-defined tertiary and quaternary structures are constituted of folded peptide segments. Even higher in complexity, cells are produced in large variety by Nature to address specific functions in the organism. Cell functions are fulfilled through the concerted action of few perfectly defined proteins, i.e. not every cell possesses the same proteins and only the appropriate ones can perform a determined function (Figure 12).

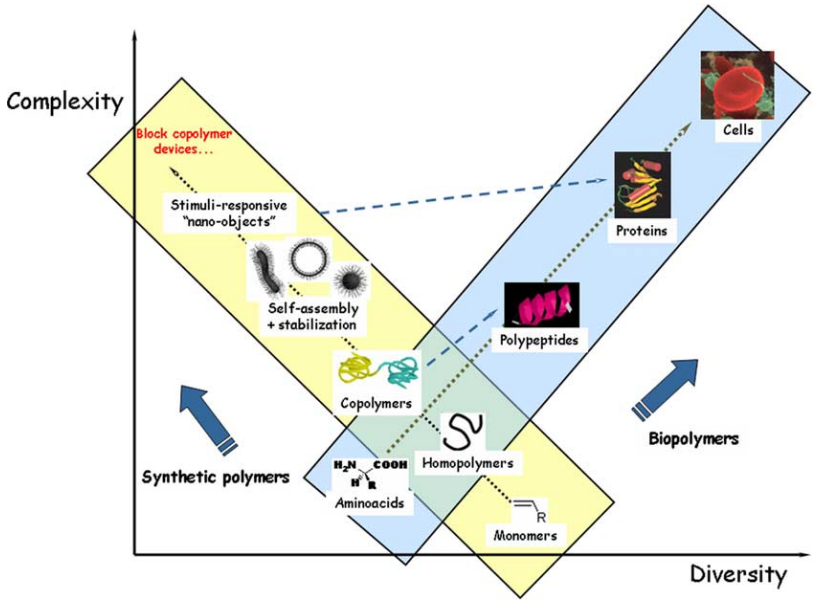

Figure 12 Schematic representation of diversity vs. complexity in natural and synthetic polymers.[81]

In contrast to natural macromolecules, synthetic polymers can be obtained from a very large variety of monomers. Polymerization of these monomers affords different kinds of more or less complex homopolymers and copolymers; and macromolecular engineering of these gives access to unusual architectures and shapes. However, none of these structures exhibits the sophistication and complexity attained by those

derived from the combination of a mere 20 amino acids (natural monomers) used by nature.[81]

Thus, polymer scientists have learned that it is crucial to build more complex structures to compete with diversity and functionality in Nature. Therefore they have focused their scope on the development of polymer structures with special functions or functionalities that can be used in special applications or that have similar self-organizing capabilities as the polymers from Nature.[11,82,83] Block copolymers are a specific class of polymers that were believed to fulfill these requirements, as their ability to form supramolecular structures or to phase separate rendered them highly interesting.[84-86] Especially the demand for structures with a size below 100 nm in the field of microtechnology was a strong driving force to examine the potential of block copolymers.[87] Especially amphiphilic block copolymers offer promising potential with respect to the formation of supramolecular structures in solution[88-91] that may serve, e.g., as nanoreactors or templates for nanometer-sized objects.[92] Also their interfacial properties can be exploited, e.g., for the preparation of organic/inorganic hybrid structures, in biomineralization as well as for materials with novel optic, magnetic and catalytic properties. Excellent reviews describe the enormous potential in this field.[84,93]

On the other hand functional polymers attract also increased attention. In the beginning polymers were classified more as structural polymers, e.g. in plastic tools. Today the demand for polymers with special functionality to solve a specific problem and which are only used as an additive has become very important. Indeed many applications devoted to an increase of the quality of life are solved by industrial companies on the base of functional polymers. Applications like laundry-detergents, paper and textile manufacturing, pharmaceutical formulations, food processing and cosmetics, functional polymers have become very important key factors.[94,95] The synthetic modification or functionalization of polymers by introducing different functional groups is an efficient strategy to obtain new materials with enhanced or specific physical and chemical properties.[96] In this context dendrimers and also the more easily accessible hyperbranched polymers became very interesting because of the high density of functional groups on the surface of a globular polymer.

2.2. Particular Objectives

2.2.1. Amphiphilic Block Copolymers – Synthesis

The field of amphiphilic block copolymers has been extensively studied, since these materials exhibit promising properties for future nanotechnology and interface modification (*vide supra*). Numerous linear amphiphilic AB-diblock copolymer architectures have been reported, but only limited efforts have been described that aim at linear-dendritic architectures with amphiphilic structure.[97] Based on a publication by Frey et al. (chapter 1.3.3.) it was the objective to compare the structural influence for block copolymers based on polystyrene and hyperbranched polyglycerol. In this context the advantage of a hyperbranched polyglycerol block should be studied in comparison to a fully linear analogue polystyrene-*block*-polyglycerol copolymer. Therefore a synthethic route to synthesize analogous linear block copolymers had to be developed. The synthesis of block copolymers based on two different strategies is shown in chapter 3. One strategy was based on the classic sequential anionic polymerization, with polystyrene as a first block and polyglycerol as a second. This technique is already very well known for block copolymers based on polyethylenglycol as hydrophilic block.[98] The second strategy was based on a “Click-Chemistry” coupling reaction.[99] Thus, were suitably preformed azide- and alkyne-functionalized homopolymers coupled to form of a triazole linking unit. In a following step glycidol was hypergrafted on this block copolymer by applying the hypergrafting reaction. Thus the hydroxyl groups of the linear block acted as a B_f core. Different sized polymers were synthesized with pure linear and linear-hyperbranched structure.

2.2.2. Amphiphilic Block Copolymers – Aggregation

The advantage of amphiphilic block copolymers is based on the ability to self organization in selective solvents and to form under special conditions very interesting supramolecular structures (*vide supra*). The behavior of the amphiphilic block copolymers synthesized in chapter 3 were studied in different solvents. Also the polarity of the solvent was changed to form the corresponding inverse micelles. Light scattering was employed to study the supramolecular structures in solution because it is the

most versatile method to gain direct information concerning size and polydispersity.[100-102] Additionally AFM and Cryo TEM measurements were performed to obtain a visual image from the appearance of the particles. Chapter 4 emphasizes the structural difference between a pure linear-linear and a linear-hyperbranched block copolymer.

2.2.3. Branched Polydienes

Despite the numerous strategies developed for the preparation of branched polymers in recent years (*vide supra*), there are still a limited number of simple synthetic strategies based on common vinyl monomers. Interesting work in this area has been performed by Baskaran[103] and Yan et al.[48] An innovative macromonomer route for branched polymer structures has been presented in a recent work by Hutchings et al.[104,105] who exploited endcapping of an α-functional, anionically prepared polystyrene with suitable difunctional 1,1-diphenyl(ethylene) units. In this manner, α,ω-functional AB_2-type macromonomers were obtained that were converted to branched polystyrene by subsequent poly(benzyl ether) formation.
In analogy to this work, yet simplifying the general approach further, a facile two-step synthesis for branched poly(diene)s by polycondensation of AB_n type macromonomers is described in Chapter 5. The synthesis of the macromonomers was conducted in one step by conventional anionic polymerization of the dienes, leading to well-defined polymers with respect to molecular weight and polydispersity. Quantitative end-capping of the polymers was achieved with chlorodimethylsilane. In the resulting AB_n-macromonomers the silane Si-H end-group represents the single A-functionality, while the alkenyl groups of the polydiene chain represent the B-groups for the ensuing hydrosilylation-based polyaddition that leads to branched polymers.

Today functional polymers are one of the fastest growing fields in materials science. The synthesis of macromolecules with special properties that may be tuned by changing their functionality is of great interest not only for academic science. In applications like laundry-detergents, paper and textile manufacturing, pharmaceutical formulations, food processing and cosmetics, functional polymers became important key factors.[94,95] The synthetic modification or functionalization of polymers by intro-

ducing different functional groups is an efficient strategy to obtain new materials with enhanced or specific physical and chemical properties.[96]
In addition to the innovative method above a “pseudo-copolymerization” technique to obtain functionalized and branched polydienes without increasing the number of steps is additionally presented in chapter 5.

2.2.4. Ferrocenyl Functionalized Polyglycerols

Currently ferrocenyl containing compounds are receiving increased attention. Especially the high chemical and thermal stability in combination with the electrochemical properties of the ferrocene group are very attractive.[106] The range of possible applications today reaches areas from the military hardware development to the peaceful development of anticancer drugs.[107] Encouraged by the rapid advances in this field of chemistry, a large number of material scientists have focused their research on functional dendrimers, with some of them involving interactions with biological molecules.[11,14,16,17,108] Therefore the development of ferrocenyl functionalized dendrimers was soon investigated and numerous examples are already known in literature.[109-115] A major drawback of this concept relies in the fact that structurally perfect dendrimers are usually available in small quantities only, due to the unavoidable multistep synthesis (*vide supra*).
In Chapter 6 the facile two step synthesis of ferrocenyl functionalized polyglycerols is described. Additional electrochemical properties were investigated by the use of cyclic voltammetry (CV) experiments in different solvents.

2.2.5. Ferrocenyl Functionalized PS-*block*-PB Copolymers

During the last decade a large number of research groups have investigated different polymeric systems with ferrocenyl containing structures. Thus macromolecules were developed containing the ferrocene as part of the backbone or as side group of a linear chain.[116-122]

The advantages of block copolymers concerning their abilities to form supramolecular structures and to establish micropatterned surfaces made them also very interesting for this field of science (*vide supra*). Therefore the development of ferrocenyl-containing block copolymers has been an important challenge. The methods developed by Nuyken et al. and Frey et al. are based on controlled anionic or radical polymerization and were successfully applied for the copolymerization of vinylferrocene with styrene or other olefinic monomers.[123,124] Balsara et al. have shown that a polyvinylferrocene-*b*-polyisoprene copolymer could be successfully applied as heterogeneous catalyst for Michael additions.[125] Especially, the research performed by Manners et al. has led to a wide range of examples concerning block copolymers with well-defined ferrocene containing blocks.

Chapter 7 presents a comparison of the electrochemical properties of diblock copolymers consisting of a 1,2-polybutadiene block (PB) with ferrocenyl side groups as electroactive part and a polystyrene (PS) block that imparts additional polymer properties and may be considered as insulator. The ferrocenyl side groups are based on mono- and diferrocenylsilanes and were especially developed for this purpose. The block length ratio and the structure of the ferrocenyl side groups were varied, leading to polymers with variable ferrocene content and electrochemical properties.

3. Amphiphilic Block Copolymers – Synthesis

3.1. Introduction

3.1.1. "Click-Chemistry"

The advantages of amphiphilic block copolymers have already been described in the chapters 1 and 2. Therefore, this brief introduction will summarize the recent advances of a method that has become very popular, the so called "Click-Chemistry".[126] The term "Click-Chemistry" was introduced in 2001 by Sharpless et al. The objective was to develop an expanding set of powerful, selective, and modular "blocks" that worked reliably in both small- and large-scale applications. They termed the foundation of this approach "Click-Chemistry", and have defined a set of stringent criteria that a process must meet to be useful in this context. Suitable reactions have to:

i be modular, wide in scope and give very high (ideally quantitative) yields
ii generate only inoffensive byproducts
iii be purified by nonchromatographic methods
iv be stereospecific (but not necessarily enantioselective)
v be performed under simple reaction environments (air, water, etc.)

These very strong criteria were nevertheless fulfilled by a few types of reactions. The following reactions were then chosen to be useful candidates:

- cycloadditions of unsaturated species, especially 1,3-dipolar cycloaddition reactions, but also the Diels–Alder family of transformations
- nucleophilic substitution chemistry, particularly ring-opening reactions of strained heterocyclic electrophiles such as epoxides, aziridines, aziridiniumions and episulfoniumions
- carbonyl chemistry of the "non-aldol" type, such as formation of ureas, thioureas, aromatic heterocycles, oxime ethers, hydrazones, and amides
- additions to carbon–carbon multiple bonds, especially oxidative cases such as epoxidation, dihydroxylation, aziridination, and sulfenyl halide addition, but also Michael additions of Nu-H reactants

Especially the 1,3 dipolar cycloaddition of alkynes and triazoles became very famous in this context and was especially emphasized one year later in follow-up work by Sharpless et al.[127]

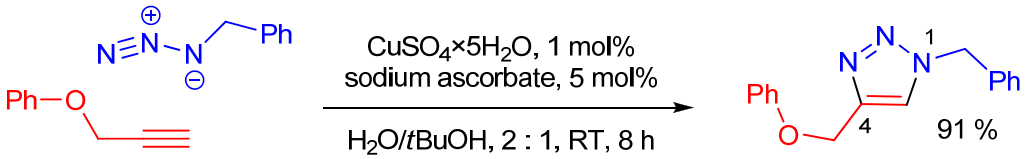

Figure 13 General scheme for click reactions based on the Huisgen-type 1,3-dipolar cycloaddition

This reaction in fact was not new. These reactions are very well known since the late 60ies as Huisgen-type cycloadditions.[128] Nevertheless the reaction pathway under thermal conditions was not stereospecific and gave always a 1 : 1 mixture of the 1,4 and 1,5 product. The innovation achieved by Sharpless lies in the copper catalyst used. The reaction can be performed very fast under mild conditions, with excellent yields and without interference of most functional groups (Figure 13). Additionally 1,2,3-triazoles are among the most stable nitrogen heterocycles: they are resistant to severe hydrolytic, reductive, and oxidative conditions.

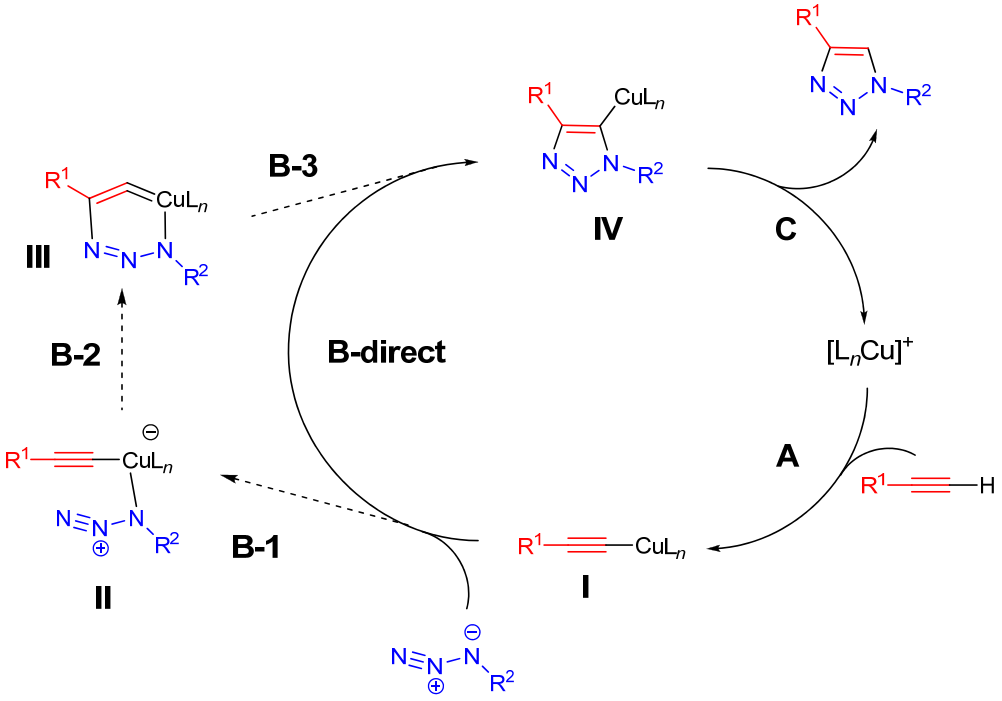

Figure 14 Proposed catalytic cycle for the Cu^{I}-catalyzed ligation.

Figure 14 shows the proposed catalytic cycle for the copper(I)-catalyzed ligation. In a first step copper(I) acetylide **I** is formed. No reaction was observed with internal al-

kynes. The next step was very intensely analyzed by density functional theory calculations. Surprisingly the calculation disfavored the concerted mechanism. The stepwise formation of the six membered ring **III** turned out to be more favored by about 12 - 15 kcal.

The obvious advantages of chemical reactions without interference of other functional groups have inspired many chemists in various areas. Also polymer scientists became fast attracted by the Click-Chemistry. Thus Click-Chemistry has been used to synthesize endfunctionalized polymers,[129] dendronized polymers,[130] functionalized carbon nanotubes,[131] hydrogels[132] and also block copolymers.[99]

3.2. Synthesis of Linear Block Copolymers

3.2.1. By Sequential Anionic Polymerization

In the context of this work, click-chemistry was considered to be an attractive method for the preparation of linear-hyperbranched block copolymers. To obtain linear-hyperbranched block copolymers, in the first step linear block copolymers with a functional block had to be created. The pathway for this reaction is shown in Figure 15. Polystyrene was prepared by classical anionic polymerization.[133-135] Anionic polymerization represents a powerful method for the controlled manipulation of macromolecular architecture and is crucial for the synthesis of a wide variety of materials with a high degree of molecular and compositional homogeneity.[70,136,137] This advantage makes living anionic polymerization very attractive for the synthesis of the model polymers that are required for establishing relationships between structure and physical properties. However, the high reactivity of anionic centers towards atmospheric (moisture, oxygen, carbon dioxide) and other contaminants dictates specially designed apparatuses and appropriate techniques in order to avoid premature living chain termination. Both inert atmosphere and high vacuum techniques are established for anionic living polymerization.

Nevertheless, the disadvantage of the strict, inert conditions because of the highly reactive living species possesses one very significant advantage. At present, anionic

polymerization has become a key technique for the synthesis of end-functional polymers. Indeed, in addition to predictable molecular weights and narrow molecular weight distribution, well-defined end groups can be quasi-quantitatively attached to the chains by the appropriate choice of either initiator or terminating agent or both of them.[138-140]

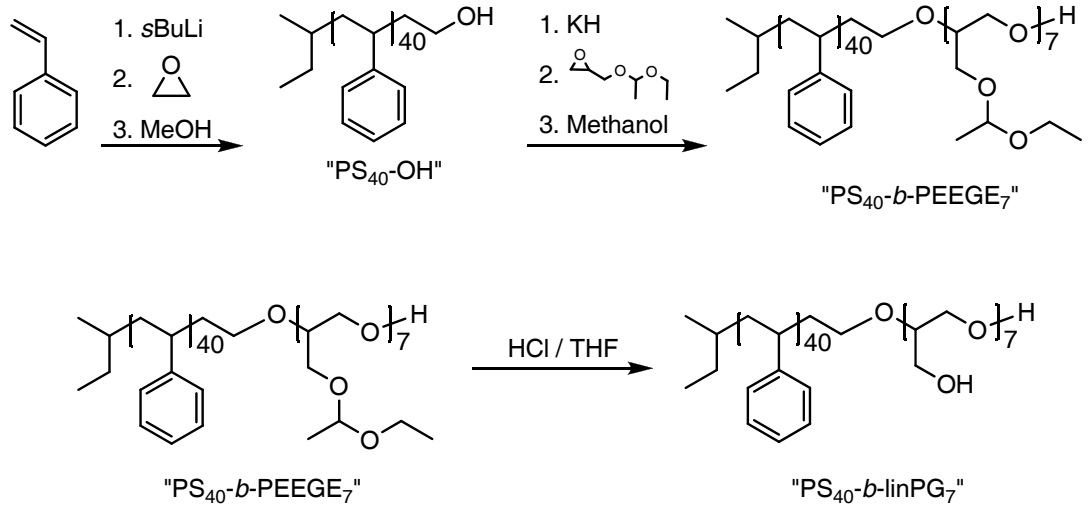

Figure 15 Synthesis of **PS_{40}-*b*-$linPG_7$** via sequential anionic polymerization

Concerning literature the addition of a carbanion to the cyclic ethylene oxide can be also viewed as a “click-reaction” because of the high addition speed and the lack of side reactions (except for the inert conditions). The reaction can be very easily monitored by the disappearance of the characteristic color of the living polystyrene carbanions. After functionalization the polymer was worked up by precipitation into methanol and dried in vacuum.

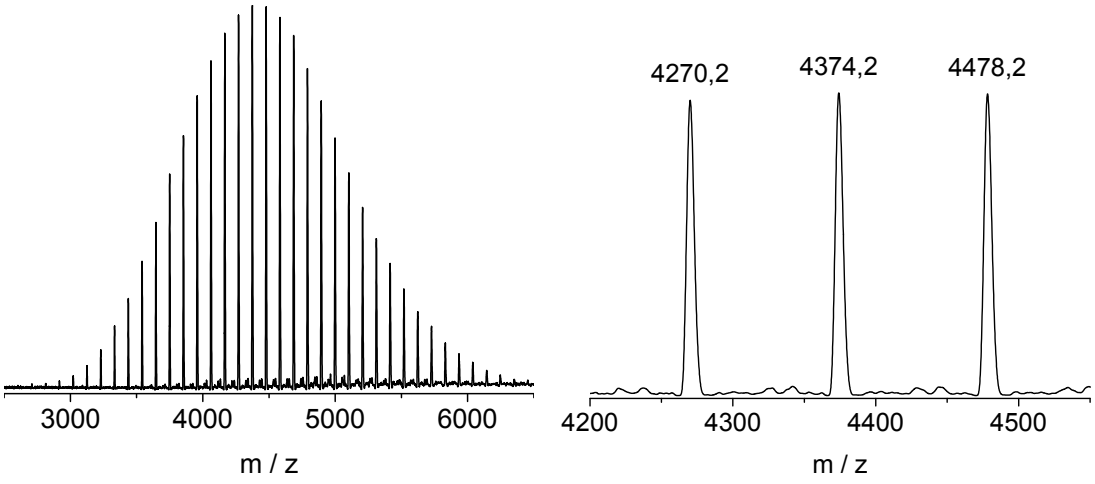

Figure 16 MALDI-ToF spectra of **PS_{40}-OH** using dithranol as a matrix and silver trifluoroacetate as cationizing agent.

A very useful technique to obtain information concerning the end groups of a polymer and its degree of terminal functionalization is MALDI-ToF.[141] MALDI makes use of short pulses of laser light to induce the formation of intact gaseous ions of a polymer dissolved in low concentration in a UV-absorbing, low molecular weight matrix. Therefore MALDI-ToF is well known to be a very mild ionization technique as most molecules are ionized without disintegration. A schematic representation of a MALDI-ToF mass spectrometer can be found in the appendix (Figure 139, page 183).

Figure 16 shows the MALDI-ToF spectrum of **PS_{40}-OH** using dithranol as a matrix and silver trifluoroacetate as cationizing agent. Clearly only one distribution is visible with peak separations identical to the styrene monomer mass. The enlarged region of the maximum shows the three peaks belonging to **PS_{39}-OH**·Ag^+, **PS_{40}-OH**·Ag^+ and **PS_{41}-OH**·Ag^+. The appearance of only one distribution strongly supports the quantitative endcapping reaction.

Linear polyglycerols can be conveniently synthesized via ring-opening polymerization of the acetal-protected glycidol (ethoxy ethyl glycidyl ether, EEGE) monomer followed by cleavage of the acetal protecting groups under acidic conditions.[142,143] Unfortunately, the controlled synthesis of linear polyglycerols for high molecular weight polymers is not trivial. Side reactions similar to the self-initiation of the propylene oxide from acidic protons become more probable with increasing conversion.[144,145]

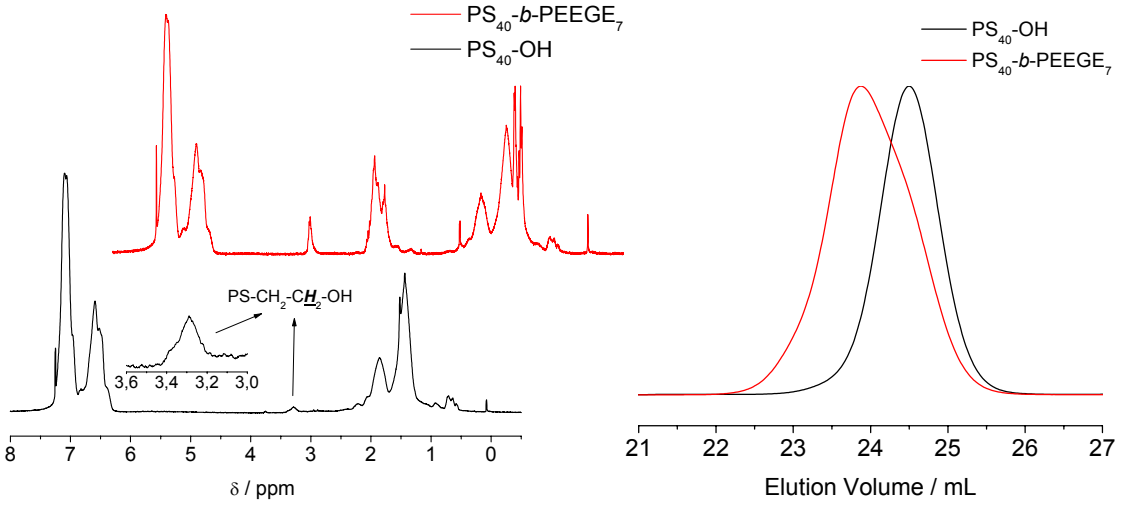

Figure 17 ^{1}H-NMR in $CDCl_3$ (left) and SEC elugram in THF (right): **PS_{40}-OH** vs. **PS_{40}-*b*-PEEGE$_7$**.

These side reactions are more pronounced with potassium as counter ion than with heavier alkali metals.[146] Nevertheless, if a polymer is used as a macroinitiator, the

most convenient method to obtain the corresponding alkoxide as initiator is by the use of potassium hydride.[147] If the degrees of polymerization are kept low, very well-defined block copolymers containing a linear polyglycerol segment can be obtained.
Informations concerning molecular weight and polydispersity were collected by size exclusion chromatography (SEC). SEC is a special application of the high performance liquid lhromatography (HPLC), but in the ideal case without interaction due to absorption or partition. Particles are therefore separated only diffusion-controlled by their size (i.e., hydrodynamic volume), whereas smaller particles remain longer in the columns than larger ones.[148]
Figure 17 (right) shows the SEC elugram of the **PS_{40}-OH** macroinitiator and the corresponding block copolymer. The number average molecular weight (M_n) of the macroinitiator was determined to be 4 200 with a very narrow polydispersity (PDI = 1.05). Obviously, the block copolymer becomes not only larger (peak shifted to lower elution volumes) its distribution is also slightly broader. The block copolymer possesses an M_n of 5 600 g/mol and a polydispersity of 1.13 (vs. polystyrene standards). Nevertheless, the block copolymer is still very narrowly distributed. ^{1}H-NMR spectra recorded in $CDCl_3$ before and after the formation of the block copolymer also confirm the successful synthesis (Figure 17, left).

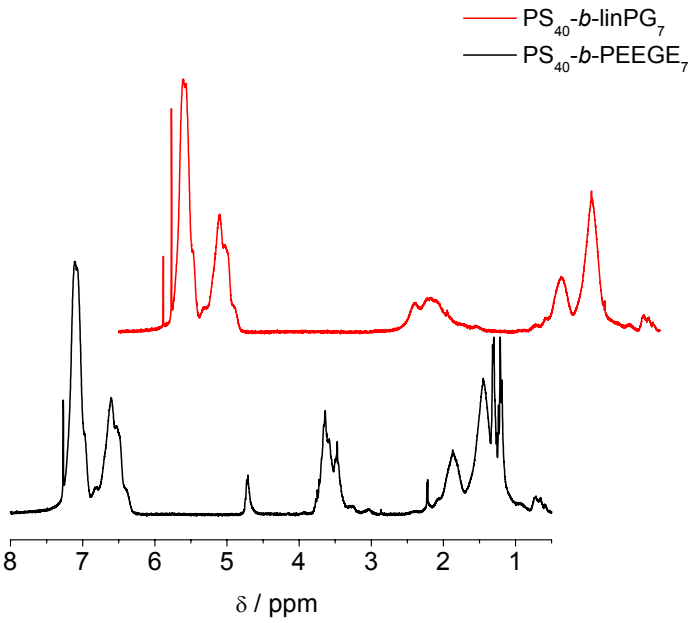

Figure 18 ^{1}H-NMR spectra ($CDCl_3$) for **PS_{40}-*b*-$PEEGE_7$** and **PS_{40}-*b*-$linPG_7$**.

The macroinitiator shows the typical polystyrene signals and also the signal for the characteristic methylene unit next to the hydroxyl group (at 3.3 ppm). By integration of this signal the M_n of the macroinitiator has also been proven. The block copolymer

has signals that are characteristic for both blocks. In addition to the polystyrene signals at 1.2 and 1.3 ppm the methyl signals of the PEEGE block are visible. At 3.5 ppm all methylene signals resonate and at 4.7 ppm the signals for the acetal group are observed. Comparison of the acetal signal to the aromatic signals from the polystyrene yields directly the composition, i.e., **PS_{40}-*b*-$PEEGE_7$**.

Cleavage of the acetal groups was performed under acidic conditions, yielding the targeted **PS_{40}-*b*-linPG$_7$** copolymer. Figure 18 shows the ^{1}H-NMR spectra recorded in $CDCl_3$ before and after cleavage of the acetal groups. The signals for the acetal group or the methyl protons have vanished. The signals for the methylene groups of the linear polyglycerol are still clearly visible at 3.6 ppm.

3.2.2. "Click"-Coupling to AB-type Copolymers

The synthetic pathway described in chapter 3.2.1. had the disadvantage of yielding only linear polyglycerol segments with low degrees of polymerization. As the reaction for the polymerization of the acetal-protected glycidol monomer proceeds more controlled when using cesium as a counterion, a new strategy was developed.[149]

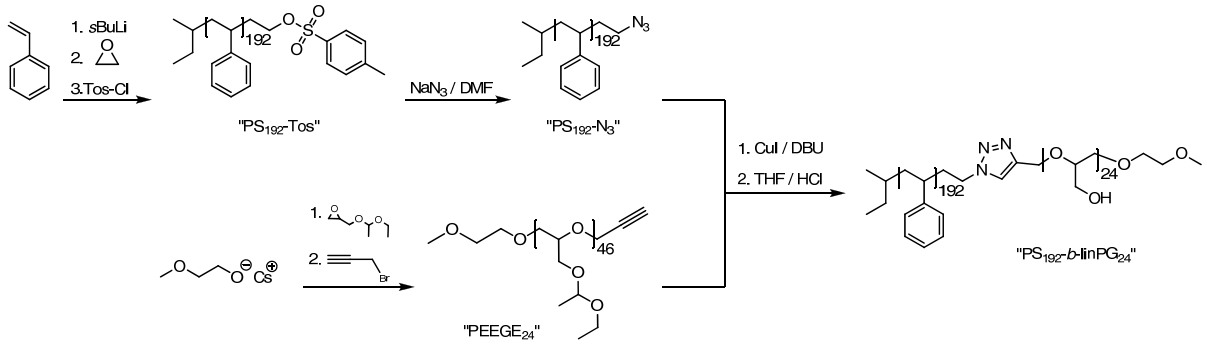

Figure 19 Synthesis of **PS_{192}-*b*-linPG$_{24}$** by "Click"-coupling.

Since reactions based on cesium or cesium hydrides require very inert conditions, which were not achieved in the timescale of this work, an alternative route to the macroinitiator pathway had to be developed. Recently it was reported that "Click-Chemistry" could also be very successfully employed to synthesize block copolymers from suitable alkyne- and azide-functionalized polymers.[99] Figure 19 shows the respective synthetic pathway to obtain a block copolymer by click-coupling of an azide-functionalized polystyrene and an alkyne-functionalized PEEGE.

The PEEGE synthesis was initiated by the 2-methoxyethanol alkoxide, which was formed in situ from $CsOH \cdot H_2O$ prior to the reaction. End group functionalization was performed by a Williamson synthesis with propargyl bromide, which was added in a ten fold excess and thus yielded the alkyne-functionalized PEEGE.

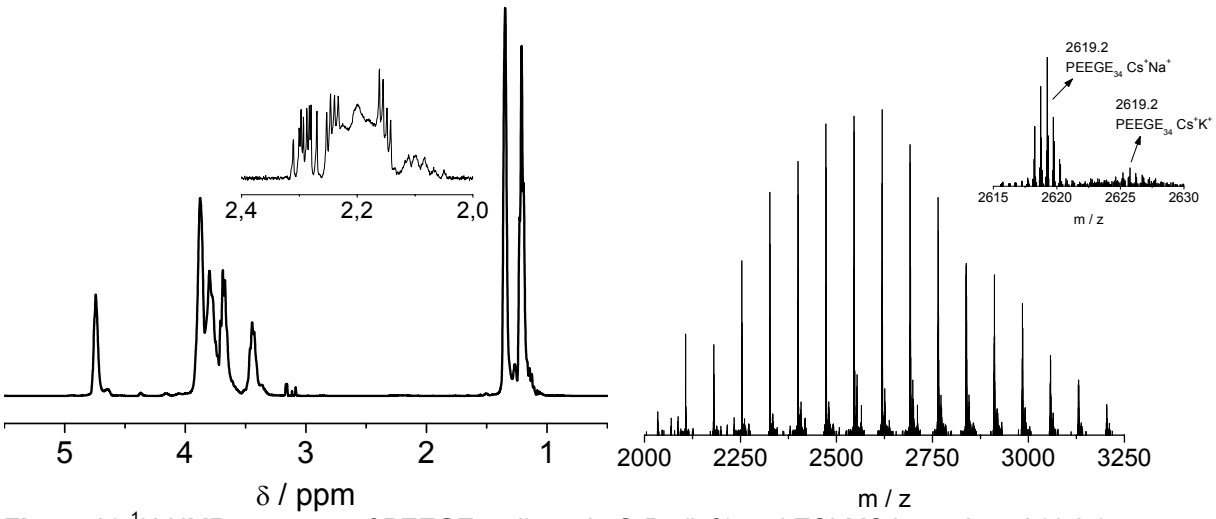

Figure 20 ^{1}H-NMR spectrum of **$PEEGE_{34}$**-alkyne in C_6D_6 (left) and ESI-MS in methanol (right).

Figure 20 (left) shows the ^{1}H-NMR spectrum in C_6D_6 of a **$PEEGE_{34}$** with alkyne end group. Employing SEC with polystyrene standard calibration, a narrowly distributed polymer was obtained (M_n = 5 900 g/mol, PDI = 1.12). The PEEGE signals were identical with the directly synthesized block copolymer in chapter 3.2.1. The single signal of the alkyne proton (2.2 ppm) was very weak, and according to its integral intensity it would yield a PEEGE polymer with an M_n of 11 000 g/mol. In this place it should be pointed out that detection of the end groups by NMR techniques is quite difficult, particularly in this case, when the characteristic signal is caused by a single proton from a large polymer structure.

To ensure the formation of the alkyne endfunctionalized PEEGE, ESI mass spectrometry was performed. ESI-MS is similar to the MALDI-ToF technique with respect to the mild treatment of the analyte. In contrast to MALDI-ToF, however, also multiple charged ions can occur.[150] Figure 20 (right) shows the corresponding ESI spectrum for **$PEEGE_{34}$** with alkyne end group. Obviously, only one single distribution can be observed. A smaller second distribution belongs to another cationizing ion pair. Because of the double-charged macromolecules, the distance between two peaks is only half of the monomer size. The peak maximum was found at 5200 g/mol which coincides with the molar mass obtained by SEC. A MALDI-ToF experiment gave an

analogous result (see appendix Figure 140, page 183), supporting the successful synthesis.

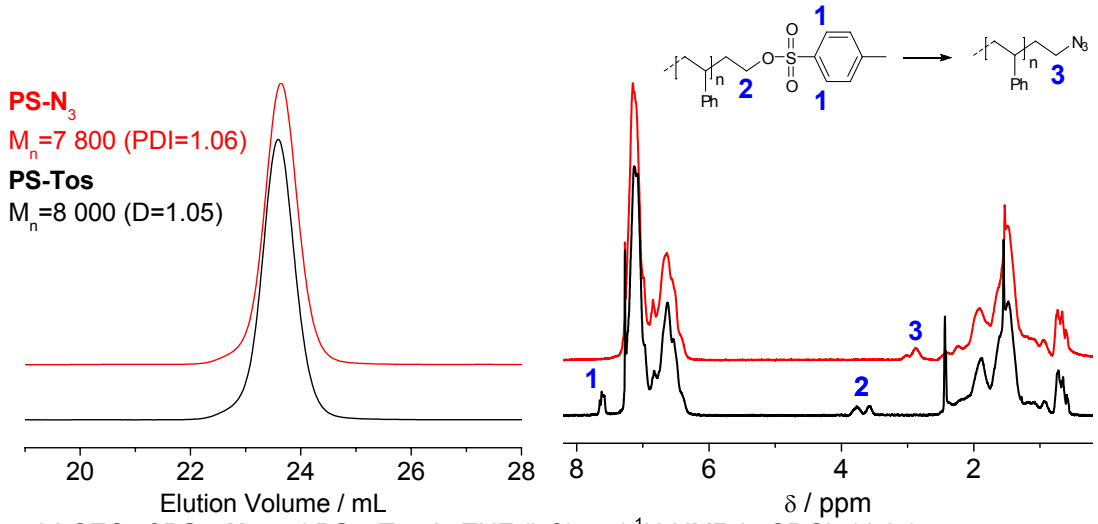

Figure 21 SEC of **PS_{75}-N_3** and **PS_{75}-Tos** in THF (left) and ^{1}H-NMR in $CDCl_3$ (right).

The azide-functionalized polystyrene was prepared by an anionic polymerization route. The synthesis was analogous to the synthesis of **PS_{40}-OH** from chapter 3.2.1. except that the lithium alkoxides were quenched directly with tosyl chloride instead of methanol. This end group could be very easily substituted nucleophilically by sodium azide. Figure 21 (left) shows the SEC traces of the samples **PS_{75}-Tos** and **PS_{75}-N_3**. Both polymers are very well-defined (PDI ≤ 1.06) and, as expected, the azide functionalized polymer was of slightly lower molecular weight, because of the smaller end group (peak for the PS-N_3 shifted to higher elution volumes). The ^{1}H-NMR spectrum also shows that the end groups were fully exchanged (Figure 21, right). **PS_{75}-Tos** shows the characteristic signals of the tosylate group at 7.6 ppm and 3.7 ppm. In case of the **PS_{75}-N_3**, these signals vanished or shifted to higher field (2.8 ppm).

To obtain a more significant difference concerning the block length in comparison to the block copolymer described in chapter 3.2.1., a higher molecular weight polystyrene with azide functionality and a larger PEEGE block with alkyne functionality were synthesized. Of course, with increasing length of the homopolymer also the difficulty concerning end group analysis increases. For the block copolymer synthesis a **PS_{192}-N_3** and a **$PEEGE_{46}$** were chosen. Both polymers were synthesized according to the procedure mentioned above and were very well-defined. The **PS_{192}-N_3** had a M_n of 20 700 (PDI = 1.06) and the **$PEEGE_{46}$** had a M_n of 6 700 (PDI = 1.20).

The coupling reaction of the blocks is based on a procedure described by van Hest et al.[99] The catalyst was a mixture of copper(I) iodide and DBU. DBU is a necessary ligand to dissolve the copper ions and also to increase their reactivity in THF. The reaction was stirred overnight at 50 °C with **PEEGE$_{46}$** in threefold excess.

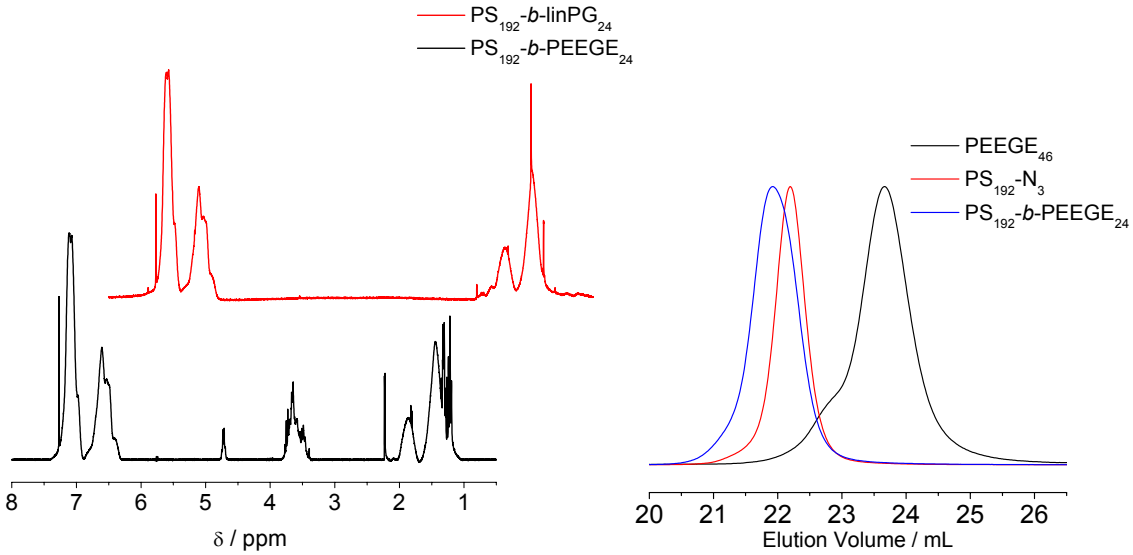

Figure 22 ^{1}H-NMR spectra in $CDCl_3$ for the block copolymers of **PS$_{192}$-*b*-PEEGE$_{24}$** and **PS$_{192}$-*b*-linPG$_{24}$** (left). SEC chromatogram of **PEEGE$_{46}$**, **PS$_{192}$-N$_3$** and **PS$_{192}$-*b*-PEEGE$_{24}$** in THF (right).

Figure 22 (right) shows the SEC chromatograms of the two samples **PEEGE$_{46}$** and **PS$_{192}$-N$_3$** homopolymers and the resulting block copolymer after the “Click”-coupling. After purification by repetitive precipitation from THF in methanol the block copolymer does not contain any traces of homopolymer. M_n was found to be 25 300 g/mol (PDI = 1.09). This value is slightly lower than the sum of both homopolymers. Nevertheless this result was confirmed by ^{1}H-NMR spectroscopy, and the composition was determined to be **PS$_{192}$-*b*-PEEGE$_{24}$**. This result was somehow surprising, because SEC gave no signal for remaining homopolymer (narrow PDI and no shoulder), but the expected length for the **PEEGE** block should have been twice larger. Possibly smaller endfunctionalized polymers may react faster than a larger polymer, because the mobility of the end group is related to diffusion. Unfortunately the molecular weight of the polymer was too large to perform detailed characterization via MALDI-ToF spectrometry.

Subsequently, the acetal protecting groups were removed analogous to the block copolymer in chapter 3.2.1. In case of the resulting block copolymer **PS$_{192}$-*b*-linPG$_{24}$** the methylene groups of the linear PG segment are not visible in the ^{1}H-NMR spectra recorded in $CDCl_3$. This is a clear indication for aggregation with the polar linear PG

segment in the core. Since the micellar core is in a solid like state, the relaxation time of the protons are very slow, resulting in very broad signals.[151]

3.2.3. "Click"-Coupling to ABA-type Copolymers

The synthetic pathway developed in chapter 3.2.2. was slightly modified to obtain linear ABA-type block copolymers with linear PG as the A blocks (Figure 23).

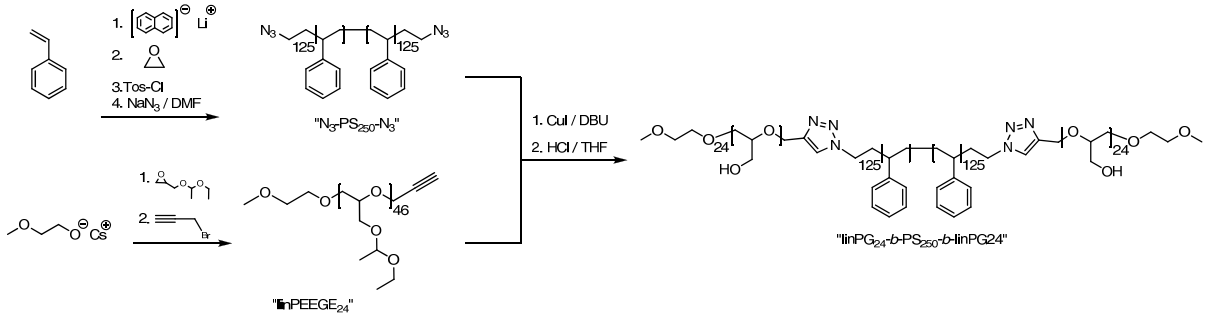

Figure 23 Synthesis of **linPG-*b*-PS-*b*-linPG** via Click coupling

In order to obtain a polystyrene with two azide-functionalized end groups another initiator had to be chosen. A very convenient difunctional initiator is the naphthyl/Li initiator system.[152,153] The naphthyl anion transfers an electron to a styrene monomer, which is transformed to a radical anion that is stabilized by coupling with a second radical anion, resulting in the formation of a dianion. Thus, in this case propagation proceeds from both ends of the polymer.

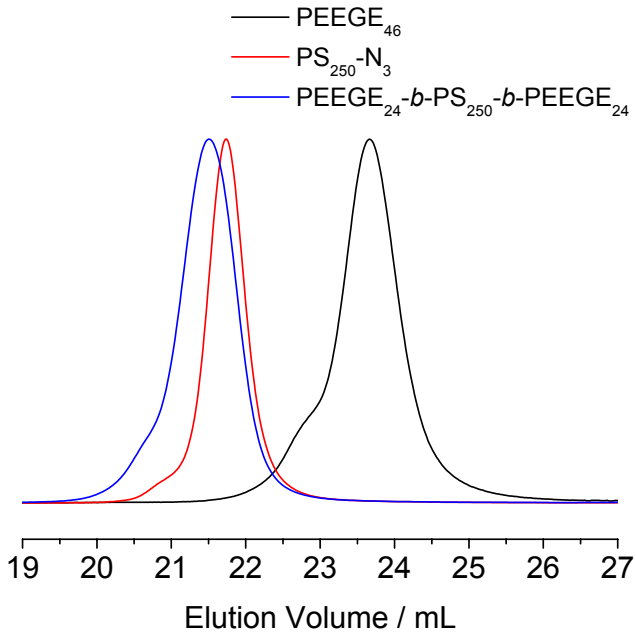

Figure 24 SEC chromatogram of **$PEEGE_{46}$**, **N_3-PS_{192}-N_3** and **$PEEGE_{24}$-*b*-PS_{192}-*b*-$PEEGE_{24}$** in THF.

End-functionalization was again performed with ethylene oxide. Surprisingly, the solution was instantly transformed into a gel. This is tentatively explained by the fact that chains with alkoxides at both ends may tend to interact physically, resulting in a gel. Nevertheless, the endcapping reaction was achieved over night (red color disappeared) and after the addition of the tosyl chloride the gel dissolved. In SEC characterization (Figure 24) the obtained **Tos-PS$_{250}$-Tos** polymer exhibited a very narrow distribution (M_n of 25 300 g/mol, PDI = 1.04). After treatment with sodium azide the polymer was converted into the corresponding **N$_3$-PS$_{250}$-N$_3$**.The SEC characteristics did not change significantly (M_n = 25 700 g/mol, PDI = 1.04). The "Click"-coupling reaction was performed in full analogy to the block copolymer formation in chapter 3.2.2. The results from SEC for **PEEGE$_{24}$-*b*-PS$_{192}$-*b*-PEEGE$_{24}$** also showed in analogous manner a narrowly distributed triblock copolymer (M_n = 35 700 g/mol, PDI = 1.13).

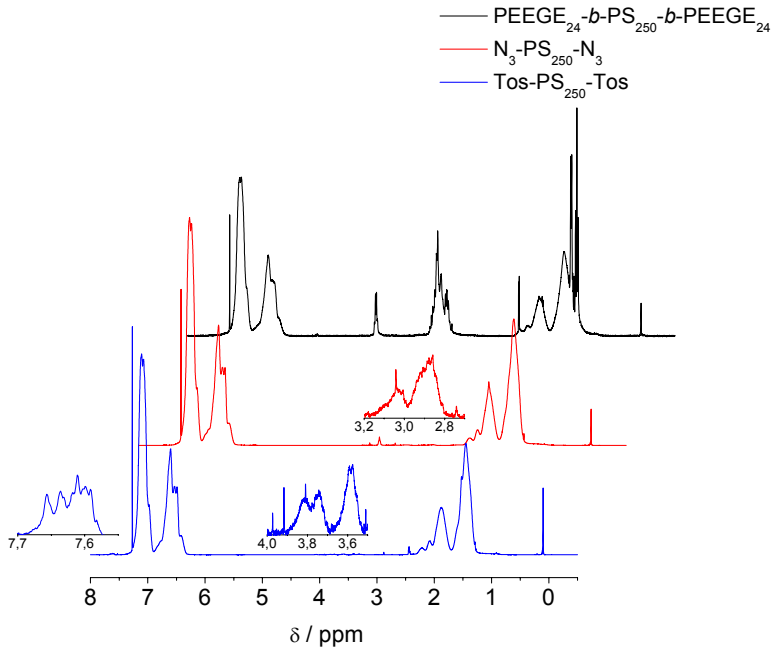

Figure 25 ^{1}H-NMR spectra of **Tos-PS$_{192}$-Tos**, **N$_3$-PS$_{192}$-N$_3$** and **PEEGE$_{24}$-*b*-PS$_{192}$-*b*-PEEGE$_{24}$** in $CDCl_3$.

^{1}H-NMR supports the conclusions from SEC (Figure 25). The characteristic tosylate signals disappeared or shifted to higher field after nucleophilic substitution by the azide. The final triblock copolymer exhibited the same signals as the block copolymers described in chapter 3.2.1. and 3.2.2. Again, it should be pointed out that the addition of a **PEEGE$_{46}$** alkyne-functionalized polymer yielded only **PEEGE$_{24}$** segments in the block copolymer. The protecting acetal group was also cleaved under acidic conditions to obtain finally the **linPG$_{24}$-*b*-PS$_{192}$-*b*-linPG$_{24}$**.

3.3. Hypergrafting of the linear block copolymers

The “hypergrafting” concept was already introduced in chapter 1.3.3. The basic principle is to take use of a multifunctional core and to add a latent AB_2 monomer to obtain a well-defined hyperbranched polymer (*vide supra*).

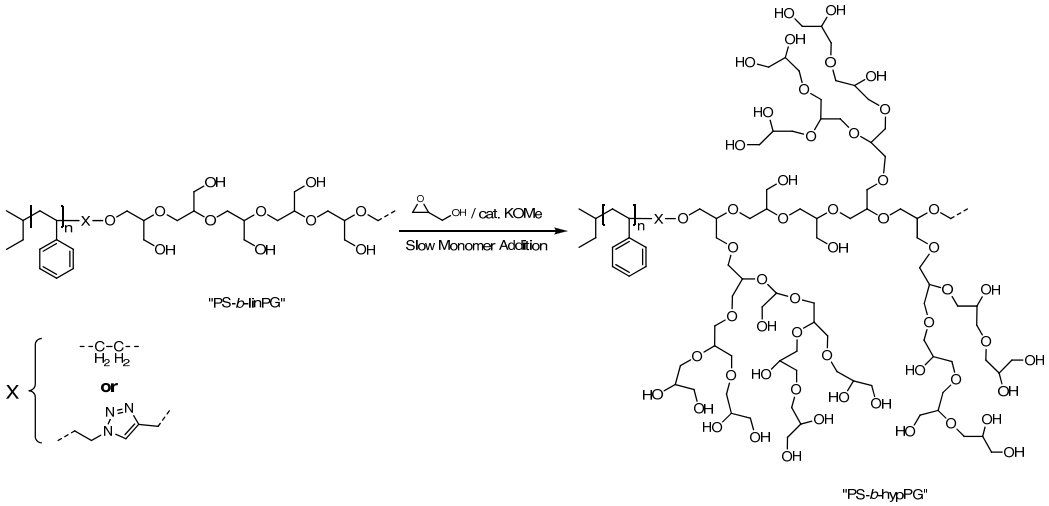

Figure 26 General scheme to linear-*b*-hyperbranched block copolymers via ROMBP.

Figure 26 shows the general scheme to linear-hyperbranched block copolymers via ROMBP. This strategy was applied for the **PS_{40}-*b*-linPG$_7$** and the **PS_{192}-*b*-linPG$_{24}$** block copolymer. Due to strong aggregation in non polar solvents for the **linPG$_{24}$-*b*-PS_{192}-*b*-linPG$_{24}$** copolymer, this technique could not be applied. The solubility of this block copolymer was rather low in apolar solvents, as it tended to form a gel. (*vide infra*).

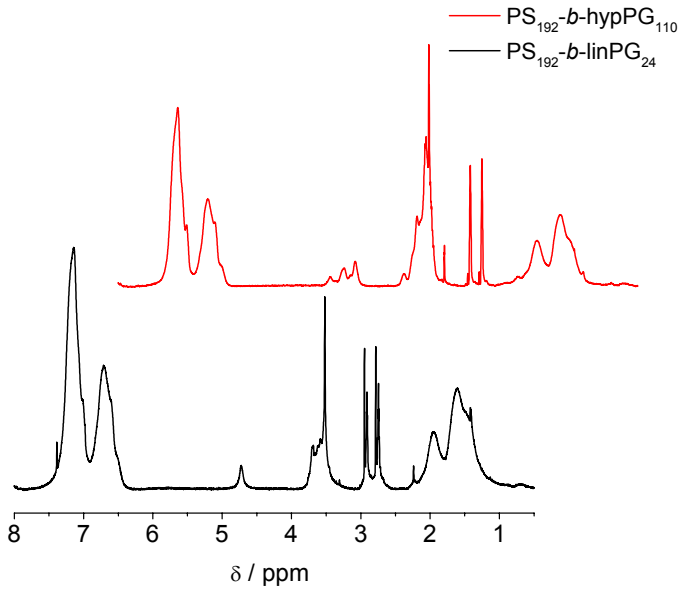

Figure 27 ^{1}H-NMR spectra of PS_{192}-*b*-linPG$_{24}$ vs. PS_{192}-*b*-hypPG$_{110}$ in DMF-d$_7$.

Based on the core : glycidol ratio the molecular weight of the hyperbranched block could be easily controlled. It was essential to introduce the glycidol monomer in the slow monomer addition mode to achieve the desired structures. The degree of polymerization could be calculated by ^{1}H-NMR. Figure 27 shows the ^{1}H-NMR spectra of **PS_{192}-*b*-linPG$_{24}$** versus **PS_{192}-*b*-hypPG$_{110}$** measured in DMF-d_7. DMF is a good solvent for both blocks, therefore aggregation is suppressed and both blocks can be analyzed together. For the sample **PS_{192}-*b*-linPG$_{24}$** beside the usual PS signals and the signals from the PG methylene groups also the hydroxyl protons were visible at 4.7 ppm. After the hyperbranching reaction this peak was split into several peaks. This can be easily explained by taking into account that a hyperbranched PG possesses different types of hydroxyl groups (e.g. secondary, primary) that may be situated more or less close to the core, which of course yields slightly different signals.

Table 2 General characteristics of the amphiphilic block copolymers obtained by SEC in $CHCl_3$.[a]

	NMR	SEC	
	wt.-% PG	M_n	PDI
PS_{40}-*b*-linPG$_7$	11.1	3 400	1.08
PS_{40}-*b*-hypPG$_{30}$	34.8	5 100	1.05
PS_{192}-*b*-linPG$_{24}$	8.2	22 600	1.03
PS_{192}-*b*-hypPG$_{110}$	29.0	22 400	1.04
linPG$_{24}$-*b*-PS_{250}-*b*-linPG$_{24}$	12.0	30 600	1.04

To enable a comparison concerning aggregation behavior for different topologies the weight fraction of PG for both linear and linear-hyperbranched copolymers should be similar (Table 2). The grafting efficiency was between 50 and 60 % in both cases.
All block copolymers used for the study of the aggregation behavior were well-defined concerning their polydispersity, which represented an important precondition. Figure 28 shows the proposed structures of a **PS_{20}-*b*-linPG$_{10}$** and a **PS_{20}-*b*-hypPG$_{40}$** copolymer. This model was obtained as energy-minimized structure by using the Spartan software. This model illustrates that linear-hyperbranched block copolymers contain (*vide supra*) also a globular, stiff structure rather than a flexible coil, similar to a linear-dendrimer block copolymer.

[a] Only nonaggregated. These values will be discussed in detail in chapter 4.3.

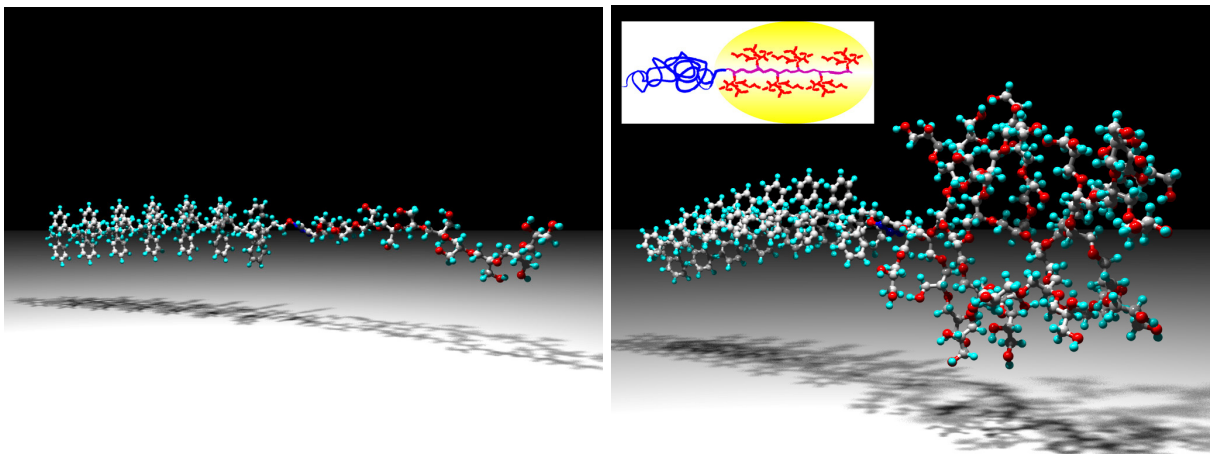

Figure 28 Proposed structure for a **PS_{20}-*b*-linPG$_{10}$** vs. **PS_{20}-*b*-hypPG$_{40}$**.

3.4. Conclusion

The objective of this chapter was the synthesis of linear-linear and linear-hyperbranched amphiphilic block copolymers. Following the work of a former group member (see chapter 1.3.3.), linear and hyperbranched polyglycerol blocks were targeted. The hydrophobic block used was polystyrene with polyglycerol as hydrophilic block. All materials prepared therefore are summarized in Table 3 below.

Table 3 General characteristics of the homopolymers and corresponding acetal-protected block copolymers.

	SEC	
	M_n	PDI
PS_{40}-OH	4 200	1.05
PS_{192}-Tos	20 600	1.06
PS_{192}-N_3	20 700	1.06
Tos-PS_{250}-Tos	25 300	1.04
N_3-PS_{250}-N_3	25 700	1.04
$PEEGE_{46}$	6 700	1.20
PS_{40}-*b*-linPEEGE$_7$	5 600	1.13
PS_{192}-*b*-linPEEGE$_{24}$	25 300	1.09
linPEEGE$_{24}$-*b*-PS_{250}-*b*-linPEEGE$_{24}$	35 700	1.13

Using these block copolymers as starting compounds yielded amphiphilic block copolymers of different sizes and architectures (Table 2, page 42).

Two methods were explored to generate well-defined block copolymers. Starting from activated hydroxyl functionalized polystyrene a protected glycidol monomer (EEGE) was added in a sequential anionic polymerization strategy, yielding a well-defined block copolymer. The macroinitiotor was synthesized by the classical anionic polymerization method to afford well-defined polymers with respect to polydispersity and end groups. Unfortunately, the size of the PEEGE block was limited, due to synthetic restrictions (P_n = 7).

Variations for the synthesis of the polystyrene homopolymer yielded ω and α,ω-azide functionalized polystyrenes that were coupled by a “Click” chemistry-based mechanism with alkyne-functionalized PEEGE homopolymers. Optimizing polymerization conditions, the homopolymerization of EEGE could be better controlled to yield well-defined and alkyne terminally functionalized PEEGEs.

All block copolymers synthesized by the sequential anionic polymerization or by “Click”-coupling possessed low polydispersity (Table 3). After cleavage of the protecting group, the desired linear amphiphilic block copolymers were obtained. Hypergrafting with glycidol afforded the corresponding linear-hyperbranched block copolymer with narrow polydispersity.

All results concerning the supramolecular organization of the materials in solution will be discussed in the following chapter 4.

3.5. Experimental Part

3.5.1. Materials

THF (Acros) for polymerizations was purified by cryo transfer from a purple K/benzophenone solution just prior to use. Cyclohexane (Acros) for polymerizations was purified by cryotransfer from a red, living polystyrene (PS) solution just prior to use. Styrene (Acros) was stored over CaH_2 until used. Methanol, chloroform, and other common solvents or reagents were purchased from Acros and used as received. *sec*-Butyllithium (1.6 m, Acros) was used as received. The concentration of the initiator was determined by the Gilman double titration method.[154] Ethylene oxide

(EO) (≥99.8 %, Aldrich) was used without further purification. All degassing and cryo transfer procedures were done using liquid Nitrogen if not otherwise mentioned.
Tosyl chloride, copper iodide, DBU, sodium azide, propargylbromide and other solvents and reagents were purchased from Acros and used as received.
For the synthesis of the hyperbranched block, potassium tert-butoxide was purchased by Acros. Glycidol (Degussa) was distilled prior to polymerization and kept under Argon.

3.5.2. Synthesis of Styrene Homopolymers

3.5.2.1. Hydroxy endfunctionalized PS[138-140]

A typical polymerization procedure is described below. The polymerization was performed in a 1 L glass reactor containing a 100 mL flask with living PS (closed by a Teflon tap), a magnetic glass stirrer, a rubber septum and a Teflon tap to remove the reactor under vaccum from the vaccum line. The glass reactor was connected to a high vacuum line (10^{-7} mbar) containing a graduated ampoule and the flasks with the solvents and reagents.
The reactor was evacuated (10^{-6} - 10^{-7} mbar) and removed from the vacuum line for rinsing with the living PS solution. Using cryo transfer procedures the living PS was removed back to the 100 mL flask including unwanted impurities. The reactor was connected again to the vacuum line and after establishing a vacuum of 10^{-6} - 10^{-7} mbar the graduated ampoule was flame dried with a heating gun. After cooling 20-25 mL of styrene were cryo-transferred into the graduated ampoule and after estimating the exact amount again cryo-transferred into the reactor. Afterwards the cyclohexane was cryo-transferred into the reactor. For a typical polymerization the amount of solvent was chosen such that the monomer concentration was ≈10 Vol%. Keeping the reactor under liquid nitrogen, the solvents in the reactor were again degassed, keeping a vacuum of 10^{-6} - 10^{-7} mbar for at least ½ h. The reactor was closed and heated to room temperature to melt the solvents, and then cooled again with an ice bath to 0 °C. The desired amount of *sec*-butyllithium was added via a gas tight Hamilton syringe. After 5-10 min the mixture was heated to 40 °C to start the polymerization and kept at this temperature for ≈12 h. After polymerization the

mixture is cooled down slowly to -10 °C. To the frozen solution were ≈25 mL of dried THF cryo-transferred. The solution was again cooled down to -10 °C. Approximately 5 mL (0.1 mol) of EO were cryotransfered to the graduated ampoule using a dry ice/acetone bath and then cryo-transferred to the reactor. The solution was heated to room temperature and kept after decolorizing for an additional ½ h stirring at this temperature. Approximately 5 mL of Methanol were added to finish the reaction. The solvent was removed under vacuum and the polymer was precipitated twice from THF/MeOH.

^{1}H-NMR ($CDCl_3$): δ, 7.30-6.20 (*PS aromatics*), 3.29 (PS-$\underline{CH_2}$-OH), 2.30-0.50 (*PS backbone*).

3.5.2.2. Tosylate-endfunctionalized PS

The procedure is analogous to the operations described above, except that 10 eq. of tosyl chloride were added to the lithium alkoxide mixture and stirred overnight before work-up.

^{1}H-NMR ($CDCl_3$): δ 7.61 (*tosylate aromatic unit*), 7.3-6.2 (*PS aromatic unit*), 3.78-3.58 (PS-$\underline{CH_2}$-Tos), 2.30-0.50 (*PS backbone, tosylate methyl*).

3.5.2.3. α,ω-tosylate endfunctionalized PS

The procedure is analogous to the steps described above except that lithium naphthalide was used as initiator and the end functionalization reaction with ethylene oxide was performed over night because of gelation of the reaction mixture.

^{1}H-NMR ($CDCl_3$): δ 7.61 (*tosylate aromatics*), 7.3-6.2 (*PS aromatics*), 3.78-3.58 (PS-$\underline{CH_2}$-Tos), 2.30-0.50 (*PS backbone, tosylate methyl*).

3.5.2.4. Azide functionalized PS

PS-Tos or Tos-PS-Tos and 8 eq. of sodium azide respective to the tosylate group were dissolved together in DMF and stirred for 2-3 h at 120 °C. The polymer was purified by repeated precipitation from THF/MeOH.

^{1}H-NMR ($CDCl_3$): δ 7.3-6.2 (*PS aromatics*), 2.83 (PS-$\underline{CH_2}$-N_3), 2.30-0.50 (*PS backbone*).

3.5.3. Synthesis of PEEGE Homopolymers

3.5.3.1 Synthesis of EEGE[143]

The procedure for the synthesis of acetal-protected glycidol was performed as described in literature. A typical procedure to obtain the ethyl ethoxy glycigyl ether is described in the following.

80 g glycidol and 400 mL ethyl vinyl ether were cooled to 0 °C. 2 g *p*-toluenesulfonic acid·H_2O was added in small quantities, keeping the temperature below 20 °C. After stirring for 3 hours at room temperature, 100 mL of a saturated $NaHCO_3$ solution was added. The organic layer was dried and distilled. The product fraction (5 mbar; 47 °C) yielded 183 g (97 %) of a clear colorless liquid.

^{1}H-NMR ($CDCl_3$): δ, 4.79-4.73 (m, 1H), 3.84-3.39 (m, 4H), 3.18-3.13 (m, 1H), 2.81 (t, 1H, ^3J = 4.6 Hz), 2.68-2.60 (m, 1H), 1.32 (t, 3H, ^3J = 5.2 Hz,), 1.20 (t, 3H, ^3J = 7.0 Hz).

3.5.3.1 Alkyne–functionalized PEEGE

To CsOH·H_2O (9 mmol), mechanically stirred in a reaction vessel equipped with argon and vacuum line, an equimolar amount of 1-methoxy-2-ethanol was added at 90 °C. After stirring for 1 h, the system was switched to the vacuum line for two more hours. After flushing the vessel with dry argon another 9 mmol of 1-methoxy-2-ethanol were added. The polymerization of the PEEGE block was started by adding the calculated amount of EEGE monomer to the fresh initiator mixture at 60 °C and stirred for 24 h. Afterwards were 10 eq. of propargyl bromide added with respect to the initiator amount and cooled slowly to room temperature. To remove excess propargyl bromide and other byproducts, the crude mixture was dialyzed using methanol as solvent and dialysis tubes with small porosities (cutoff ≈ 1000 g/mol). The dialysis was performed for 24 h in a special setup with continuous solvent exchange. Methanol was removed from the purified polymer solution on rotary evaporator and the polymer was obtained as colorless, viscous materials in 70-80 % yield.

^{1}H-NMR (C_6D_6): δ, 4.74 (*acetal*), 4.00-3.55, 3.50-3.30 (*methylene*), 2.20 (-C≡C-H), 1.40-1.10 (*methyl*).

3.5.4. Synthesis of Block Copolymers

3.5.4.1. PS-PEEGE by sequential anionic polymerization[147]

A PS-OH was dissolved in THF and deprotonated with an excess of potassium hydride under argon atmosphere. The mixture was kept stirring in a sealed flask with an argon-filled balloon for one day. Then it was filtered and placed in a reactor equipped with a mechanical stirrer and a dosing pump. The activated polystyrene was dissolved in diglyme, and heated up to 120 °C. THF was then distilled off from the reactor via a distillation bridge. The amount of macro-initiator was chosen according to the desired monomer/initiator ratio. Ethoxy ethyl glycidyl ether was dissolved in THF and was slowly added at 120 °C. After completion of the reaction the product was neutralized with a cationic-exchange resin (Lewatit K1131). Then the crude product was twice precipitated in cold methanol from a THF solution and dried for an extended period at 60 °C in vacuo. The polymer was obtained as colorless solid in 80-90 % yield.

^{1}H-NMR ($CDCl_3$): δ 7.3-6.2 (*PS aromatics*), 4.74-4.70 (*PEEGE acetal*), 3.85-3.35 (*PEEGE methylene*), 2.30-0.50 (*PS backbone, PEEGE methyl*).

3.5.4.2. PS-PEEGE by "Click"-coupling[99]

Alkyne functionalized PEEGE (3 eq.), azide functionalized PS (1 eq.) and CuI (0.05 eq.) were placed in a Schlenk tube which was fitted with a stopper, evacuated and back-filled with dry nitrogen. This procedure was repeated three times. After the evacuating cycles, tetrahydrofuran (final concentration ≈ 0.2 g/L) and DBU (20 eq.) were added and the reaction mixture was placed in a statically controlled oil bath at 50 °C for 18 hours. The polymer was precipitated in methanol yielding a slightly blue colored solid. The polymer was dissolved in dichloromethane and washed with a 0.065 M EDTA solution. The organic layer was dried with anhydrous magnesium sulfate and was concentrated *in vacuo*. The polymer was precipitated in methanol, yielding a white solid, which was dried under vacuum and gave the desired block copolymer in 80-90 % yield.

^{1}H-NMR ($CDCl_3$): δ 7.3-6.2 (*PS aromatics*), 4.74-4.70 (*PEEGE acetal*), 3.85-3.35 (*PEEGE methylene*), 2.30-0.50 (*PS backbone, PEEGE methyl*).

3.5.4.3. Cleavage of the acetal protecting groups in PEEGE

This is a general procedure for the cleavage of the acetal protecting groups in PEEGE in all block copolymers. The block copolymer was dissolved in THF to yield a concentration of ≈ 1 g/L. 6 mL of 35 % hydrochloric acid per 1.1 g of pure PEEGE were added to cleave the protecting groups. The mixture was stirred for 2 h at room temperature. The solution was concentrated *in vacuo* and diluted again with benzene. The benzene solution was concentrated again *in vacuo*. To remove residual acid and other byproducts was the raw mixture dialyzed using THF as solvent and dialysis tubes with small porosities (cutoff ≈ 1000 g/mol). The dialysis was performed for 24 h in a special setup including a continuos solvent exchange. The solvent was removed *in vacuo*. The final product was obtained as white solid after freeze-drying from a benzene solution in 80-90 % yield.

^{1}H-NMR (DMF-d_7): δ 7.6-6.3 (*PS aromatics*), 4.72 (PG-OH), 3.80-3.25 (*PG -CH_2-O-*), 2.40-0.90 (*PS backbone*).

3.5.4.4. Hypergrafting

Polymerizations were carried out in the same reactor as in 3.5.3.1. 10 % of the hydroxyl groups of the macroinitiator (**PS-linPG**) were deprotonated with potassium *tert*-butoxide. The activated macronitiator was dissolved in 20 ml Diglyme, heated up to 120 °C and placed in the reactor. The amount of macroinitiator was chosen according to the desired monomer/initiator ratio. Glycidol was dissolved in THF and was slowly added at 120 °C. After completion of the reaction the product was neutralized with a cationic-exchange resin. The final product was obtained as white solid after freeze drying from a benzene solution in 70-80 % yield.

^{1}H-NMR (DMF-d_7): δ 7.6-6.3 (*PS aromatics*), 4.72 (PG-OH), 3.80-3.25 (*PG -CH_2-O-*), 2.40-0.90 (*PS backbone*).

4. Amphiphilic Block Copolymers – Aggregation

4.1. Introduction

4.1.1. Principles of Light Scattering

Between 1864 and 1873, James Clerk Maxwell developed the theoretical description of electricity and magnetism. His results lead to the marvelous prediction that light is electromagnetic radiation propagating through free space in the form of orthogonal, oscillating electric and magnetic fields. Maxwell's description explains many of the important properties of light. For example, light is often linearly polarized. The polarization of light is determined by the direction of oscillation of the electric field.[155]
If the wavelength of light is much longer than the physical dimensions of a particle, light scattering occurs. The oscillating electric field of the light partially separates into positive and negative charges inside the particle, depending on its polarizability. The separated charges produce a dipole field. The oscillating electric field creates an oscillating dipole in the particle, which can then reradiate the light. The intensity of light scattered ($I_s(\theta)$) is typically small - only a fraction of a percent of the incident light (I_i). Several excellent textbooks deal with the theoretical background of light scattering in detail.[156,157]

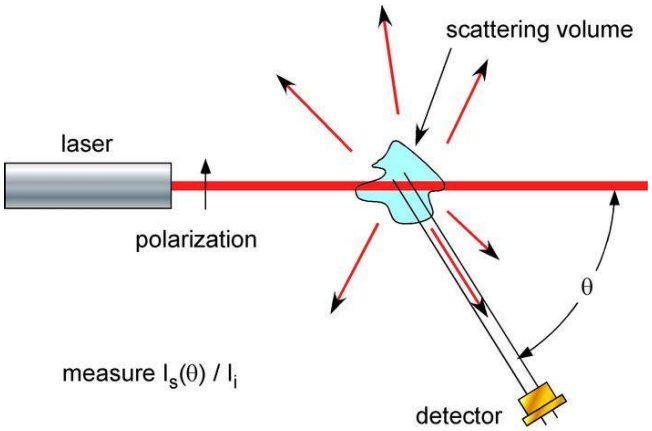

Figure 29 Schematic representation of a light scattering experiment

Figure 29 shows the general setup of a light scattering experiment. Light scattering is a technique that allows direct determination of some of the global properties of particles. In general there are two basic light scattering techniques: static light scattering

(SLS) and dynamic light scattering (DLS). Table 4 shows the parameters that can be determined by the different light scattering techniques.

Table 4 Molecular parameters and techniques for their determination

Parameter	Symbol	Technique
molar mass	M_w	SLS
radius of gyration	$R_g \equiv [<S^2>_z]^{½}$	SLS
second virial coefficient	A_2	SLS
translational diffusion coefficient	D_z	DLS
second cumulant	μ_2	DLS

SLS arises from fluctuations in materials around their mean values. Local fluctuation of the density and concentration of dilute solutions are the key parameters, which are measured. In SLS experiments the averaged scattering intensity at different angles is observed. A relationship for evaluation of these data from dilute solutions is given by the famous Zimm equation:[31,100]

$$\frac{Kc}{R_\theta} = \frac{1}{M_w}\left[\left(1+\frac{1}{3}\left\langle S^2\right\rangle_z q^2\right)+2A_2c\right] \qquad (4.1)$$

$$\left(qR_g < 2; \qquad A_2M_wc < 0.5\right)$$

In this equation, R_θ is the normalized scattering intensity (Rayleigh ratio) at the scattering angle θ, A_2 is the second virial coefficient, c is the concentration in g/cm^3, and q is the magnitude of the scattering vector that is related to the scattering angle

$$q = \left(\frac{4\pi n_0}{\lambda_0}\right)\sin\left(\frac{\theta}{2}\right) \qquad (4.2)$$

where λ_0 is the wavelength of the used light and n_0 the refractive index of the solvent. K is a contrast constant that is defined as

$$K = \frac{16\pi^2}{\lambda_0^4 N_A} n_0^2 \left(\frac{\partial n}{\partial c}\right)^2 \qquad (4.3)$$

in which here $\partial n/\partial c$ is the refractive index increment which, roughly speaking, is the difference in the refractive indices between a solution and the solvent divided by the concentration.

In contrast to SLS, in DLS the fluctuations are statistically analyzed in short time intervals.[31,100] Here a time correlation function (TCF) of the scattering intensity is measured that is given as

$$g_2(q,t) \equiv \frac{\langle i(0) \cdot i(t) \rangle}{\langle i(\infty) \rangle^2} \tag{4.4}$$

In this relationship *i*(0) and *i*(t) are the scattering intensities at the time zero and after a short delay time *t* respectively. Correspondingly *i*(∞) is the scattering intensity at delay time $t \rightarrow \infty$. The brackets < > denote the average over a large number of repetitions ($n > 10^5$). If the delay time is of the order of a relaxation time, the correlation function decreases from a value of about $g_2(q,0) = 2$ to a base line at $g_2(q,t \rightarrow \infty) = 1$. The intensity TCF $g_2(q,t)$ is related to the field TCF $g_1(q,t)$, that is accessible to theoretical derivations by the Siegert relationship

$$g_2(q,t) = 1 + \beta \left[g_1(q,t) \right]^2 \tag{4.5}$$

The coefficient $\beta<1$ depends on the quality of the instrumental set-up but takes a value close to unity when monomodal fibers are used. The field TCF can be calculated on the basis of Brownian motion theory. Its initial time dependence is in every case described by a single exponential decay

$$g_1(t) \cong \exp\left(-\Gamma(q)t\right) \qquad \Gamma(q) = q^2 D_{app}(q) \tag{4.6}$$

Here D_{app} is the apparent diffusion coefficient. Extrapolation of $q \rightarrow 0$ yields

$$\lim_{q \rightarrow 0} D_{app}(q) = D_z \tag{4.7}$$

D_z is the translation coefficient of the particle's center of mass, while the subscript indicates the *z*-average over the molar mass distribution.

The hydrodynamic radius can be calculated by the Stokes-Einstein relationship (4.8):

$$R_h = \left\langle \frac{1}{R_h} \right\rangle_z^{-1} = \frac{k_B T}{6\pi\eta D_z} \tag{4.8}$$

Equation (4.6) is only valid for particles of unique size. In general synthetic polymers have a size distribution and so it is necessary to make some approximations. For a system of polydisperse spheres this yields to

$$g_1(q,t) = \sum_j a_j(q) \exp\left(-D_j q^2 t\right) \tag{4.9}$$

with

$$a_j(q) = \frac{c_j M_j P_j(q)}{\sum_j c_j M_j P_j(q)} \tag{4.10}$$

where the subscript *j* refers to particles with molar mass M_j and particle scattering factor $P_j(q)$ which are present in the system with the concentration c_j. Equation (4.9) leads to some important conclusions. For a system of spheres with a size distribution the TCF becomes angular-dependent, if the particle scattering factors $P_j(q)$ deviates from unity.

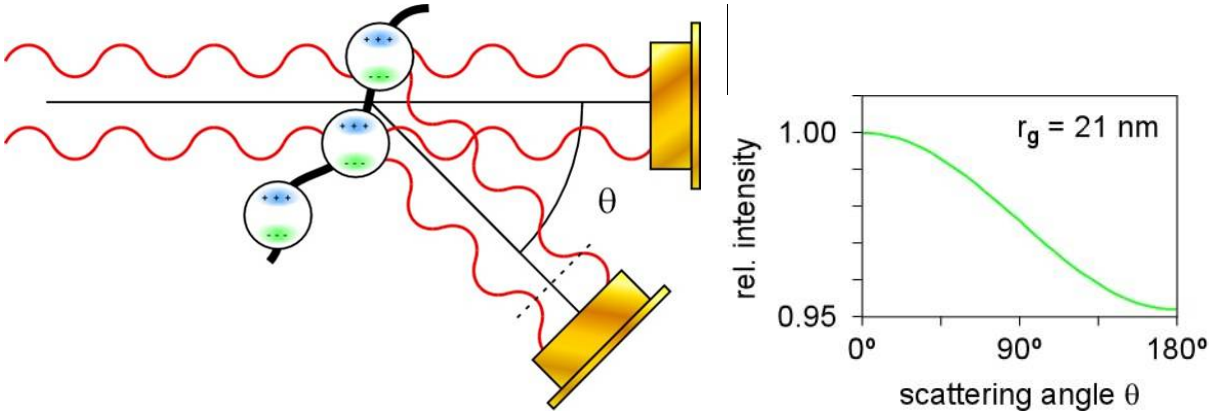

Figure 30 Left: intramolecular interference leads to a reduction in scattering intensity. Right: dependency of the scattering intensity with the scattering angle.

For particles much smaller than the wavelength of the incident light (< 10 nm for λ = 690 nm), the amount of radiation scattered into each angle is the same in the plane perpendicular to the polarization. In case of larger particles an intramolecular interference leads to a reduction in scattering intensity as the scattering angle increases (Figure 30). This behavior is described by the particle scattering factor $P_j(q)$. Roughly speaking, when small and large particles are mixed, the large particles seem to become invisible at higher scattering angles.

Another method to approximate the apparent diffusion coefficient is based on the method of the cumulants:[101,102]

$$\ln g_1(t) = -\Gamma t + \frac{\mu_2}{2!}\Gamma^2 t^2 - \frac{\mu_3}{3!}\Gamma^3 t^3 + \ldots \tag{4.11}$$

with μ_i as the *i*-th cumulant. The first cumulant (Γt) describes the average decay rate of the distribution and yields the hydrodynamic radius. The second moment corresponds to the variance, and the third moment provides a value for the asymmetry of the distribution. The first two cumulants have to be positive, but the third cumulant can also be negative. Values for the second cumulant below 0.05 are characteristic

for almost monodisperse particles. In contrast values above 0.1 are typical for polydisperse particles. In general the third cumulant is not determined.

A very useful architecture-dependent parameter can be obtained from the quotient of the radii that are measured by SLS and DLS, the so called ρ-ratio parameter:[158]

$$\rho = \frac{R_g}{R_h} \tag{4.12}$$

This parameter has been calculated for different architectures and polydispersities. Some of these values are summarized in Table 5.

Table 5 Selected ρ-ratios for some architectures.[100]

Architecture	ρ
Homogenous sphere	0.778
Random coil, monodisperse	
θ-conditions	1.50
good solvent	1.78
Random coil, polydisperse	
θ-conditions	1.73
good solvent	2.05
Regular stars	
θ-conditions, *f* = 4	1.33
θ-conditions, *f* >> 1	1.079
Rigid rod	
monodisperse	> 2.0
polydisperse	> 2.0

4.1.2. SEC with Triple Detection

By far the most popular and convenient method of determining the average molecular weight and the polydispersity of a polymer is size exclusion chromatography (SEC).[148] Typically, in less than 30 min, using standard high-performance liquid chromatography (HPLC), the complete molecular weight distribution of a polymer can be determined along with all of the statistical moments of the molecular weight distribution. SEC separates on the basis of molecular hydrodynamic volume or size,

rather than by enthalpic interactions with the stationary phase or packing surfaces. When compared to other modes of HPLC, the instrumentation requirements for SEC are somewhat simpler since mobile phase gradients are not used.

If the detection is only based on concentration detectors (RI, UV-vis) the columns have to be calibrated with polymer standards of known molecular weight. This classical SEC method is a *relative* method and not an absolute molecular weight technique. Recent developments have led to molecular weight sensitive detectors. For example a viscometer also measures a change in a physical property of the column effluent but also responds to the molecular weight as well as the concentration of the solute. Thus a viscometer is classified as a molecular weight sensitive detector. A light scattering detector is sensitive to both molecular weight and the concentration of the solute in the effluent and is also classified as a molecular weight sensitive detector. The combination of a classical SEC based on standard concentration detector(s) with an additional light scattering and viscometer detector is called a “Triple Detection” setup.

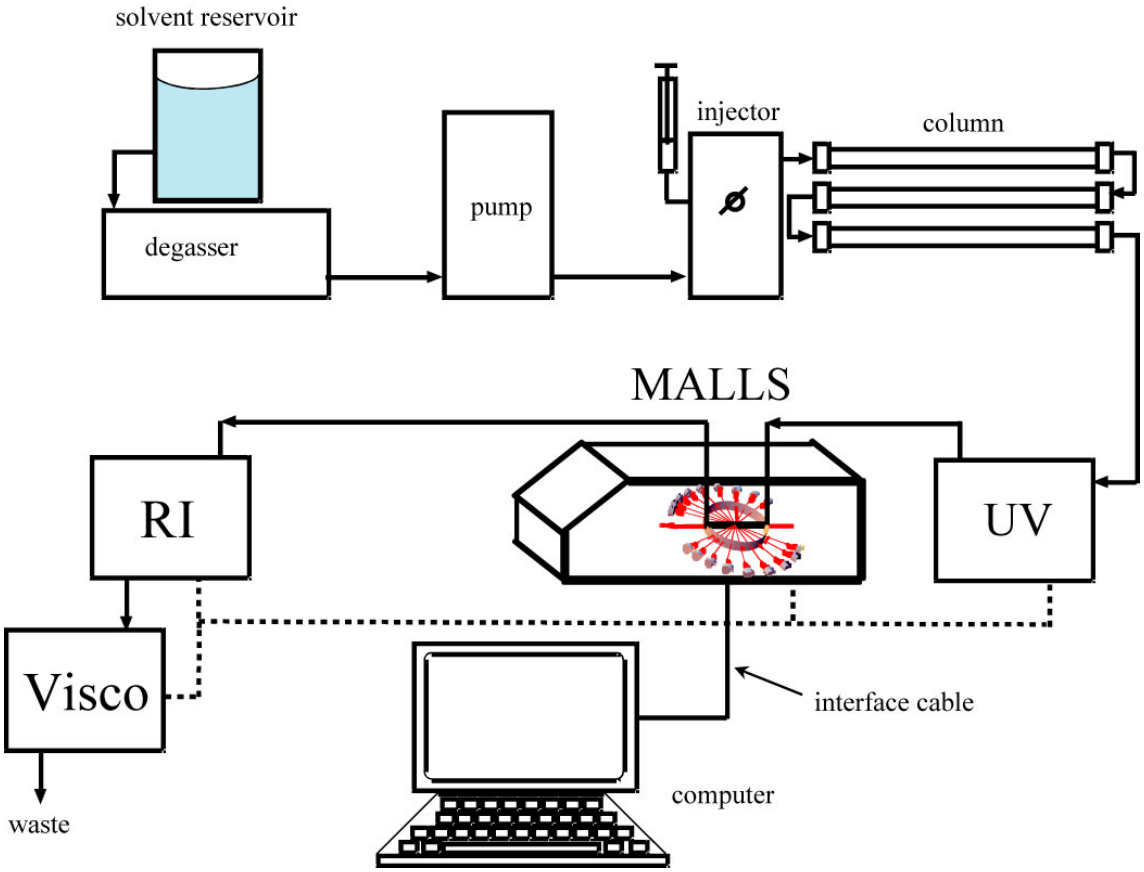

Figure 31 Schematic representation of the used triple detection setup.

For this work it was necessary to upgrade the classical SEC to a triple detection system (Figure 31).
The absolute molar masses were recorded by an online multi-angle static light scattering instrument (MALLS). SLS obviously yields M_w, but because SEC separates according to size, it is possible to calculate M_n and the PDI with SEC-LS. This becomes possible as the elugram is subdivided in small slices, into which the observed polymers are almost monodisperse ($M_w \approx M_n$).

To complete the triple detection setup a capillary viscometer was introduced. Because of the great dilution factor of this instrument it had to be placed at the end of the system. A schematic representation of the viscometer employed can be found in the appendix (Figure 141, page 184).
The viscosity of a solvent is increased, if macromolecules are dissolved in it. The specific viscosity η_{sp} of a diluted macromolecule in a solvent is defined by

$$\eta_{sp} = \frac{(\eta - \eta_0)}{\eta_0} \tag{4.13}$$

with η being the viscosity of the solution and η_0 the viscosity of the pure solvent. This viscosity depends on the concentration. The reduced viscosity is then defined by

$$\eta_{red} = \frac{\eta_{sp}}{c} \tag{4.14}$$

with *c* being the concentration of the macromolecules. To eliminate the concentration dependence completely, the data has to be extrapolated to concentration zero, yielding:

$$[\eta] = \lim_{c \to 0} \left(\frac{\eta_{sp}}{c} \right) \tag{4.15}$$

the intrinsic viscosity or Staudinger index. This value is, roughly spoken, a reciprocal density. The online viscometer measures pressure differences between a concentrated and a diluted polymer solution. The specific viscosity η_{sp} is calculated from the equation:

$$\eta_{sp} = \frac{4\Delta p}{p_i - 2\Delta p} \tag{4.16}$$

where Δp is the differential pressure across a capillary bridge and p_i is the inlet pressure of the flow through the bridge. The intrinsic viscosity [η] is then calculated from

equation (4.14), approximating that the concentration *c* is very low under SEC conditions. Initially, the viscometric radius of the molecule (R_η) is calculated from

$$R_\eta = \frac{\sqrt[3]{3[\eta]M_w}}{\sqrt[3]{10\pi N_A}} \tag{4.17}$$

where M_w is the molecular weight calculated from the light scattering detector.[59]

4.2. Dynamic and Static Light Scattering Measurements

4.2.1. Measurements in Chloroform

The newly prepared block copolymers described in chapter 3 were dissolved in chloroform and measurements were performed at different concentrations. For clarification, the solutions were passed through 0.2 µm pore size Millex LG filters into dust-free cylindrical cuvettes.

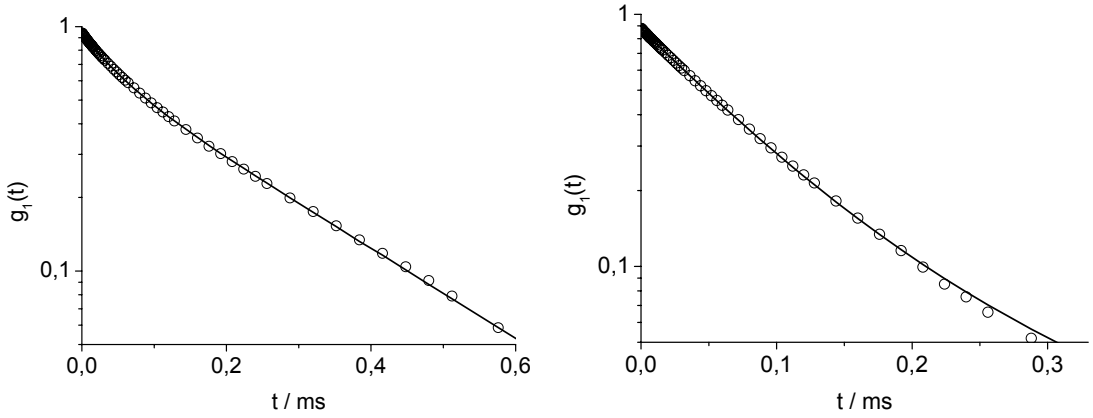

Figure 32 TCF for **PS_{192}-*b*-linPG$_{24}$** (left) and **linPG$_{24}$-*b*-PS_{250}-*b*-linPG$_{24}$** (right) measured at an angle of 90° in chloroform (20 °C).

In Figure 32 the TCFs for the linear copolymers **PS_{192}-*b*-linPG$_{24}$** and **linPG$_{24}$-*b*-PS_{250}-*b*-linPG$_{24}$** are plotted. Concerning equation (4.6) one would expect a linear function in case of monodispersely distributed aggregates. Especially **PS_{192}-*b*-linPG$_{24}$** seems to be very broadly distributed with at least two different exponential functions being visible. In comparison the plot obtained from **linPG$_{24}$-*b*-PS_{250}-*b*-linPG$_{24}$** copolymer exhibited a more linear decay. Another feature that can be used to distinguish both aggregates qualitatively is the correlation time itself. As the corre-

lation is related to the diffusion coefficient, one can directly conclude that larger particles will require longer time scales then smaller particles. The time scale for **PS$_{192}$-*b*-linPG$_{24}$** was twice as long as the time scale for the **linPG$_{24}$-*b*-PS$_{250}$-*b*-linPG$_{24}$** copolymer.

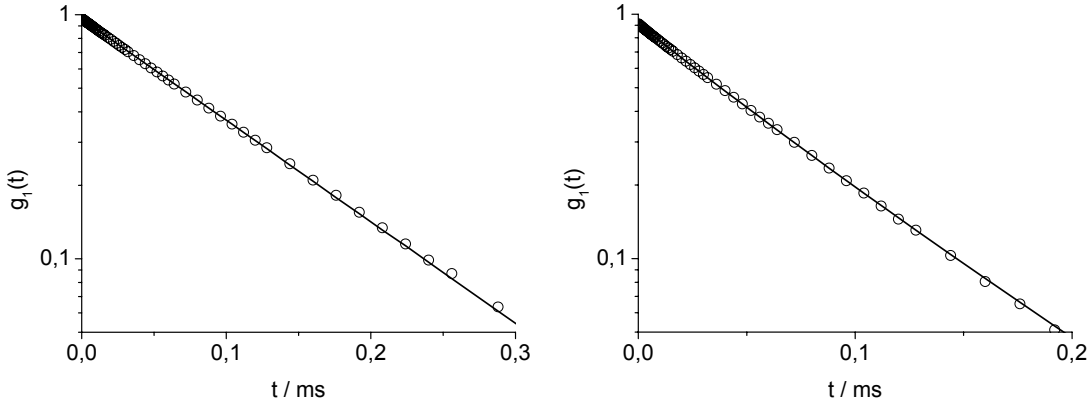

Figure 33 TCF for **PS$_{192}$-*b*-hypPG$_{110}$** (left) and **PS$_{40}$-*b*-hypPG$_{30}$** (right) measured at an angle of 90° in chloroform (20 °C).

In Figure 33 the TCFs for the samples **PS$_{192}$-*b*-hypPG$_{110}$** and **PS$_{40}$-*b*-hypPG$_{30}$** are shown. Both TCFs can be described by a linear function. Obviously, both linear-hyperbranched block copolymers formed aggregates that seemed to be monodispersely distributed in chloroform.

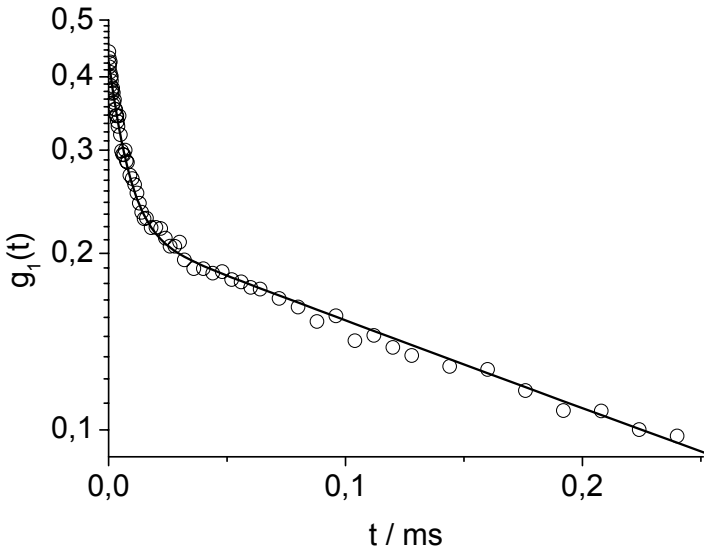

Figure 34 TCF for **PS$_{40}$-*b*-linPG$_{7}$** measured at an angle of 90° in chloroform (20 °C).

Figure 34 shows the TCF for the linear **PS$_{40}$-*b*-linPG$_{7}$** copolymer, which is completely different from the TCFs of all other block copolymers. The diffusion coefficient is obtained by the slope of the TCF. It is obvious that there are very small and very large particles present.

The TCFs then were evaluated by applying a biexponential fit function (equation (4.9) with *j* = 2). Two different diffusion coefficients were obtained and combined to an apparent diffusion coefficient by

$$D_{app} = \frac{a_1}{a_1 + a_2} D_1 + \frac{a_2}{a_1 + a_2} D_2 \tag{4.18}$$

At this point it should be mentioned that block copolymer **PS_{40}-*b*-$linPG_7$** formed mostly unimers, thus it will not be included in the following discussion.

Performing DLS at different scattering angles and plotting all apparent diffusion coefficients versus the scattering angle yields the translational diffusion coefficient by the extrapolation of q→0. Figure 35 shows that the diffusion coefficient for both linear-hyperbranched block copolymers were independent from the scattering angle. In contrast, the **$linPG_{24}$-*b*-PS_{250}-*b*-$linPG_{24}$** copolymer shows a slight dependency and the **PS_{192}-*b*-$linPG_{24}$** copolymer shows a strong dependency of the diffusion coefficient on the scattering angle. Taking equation (4.9) into consideration this has to be expected for polydisperse samples (*vide supra*). As expected, the diffusion coefficient increased with increasing scattering angle (fewer larger particles detected).

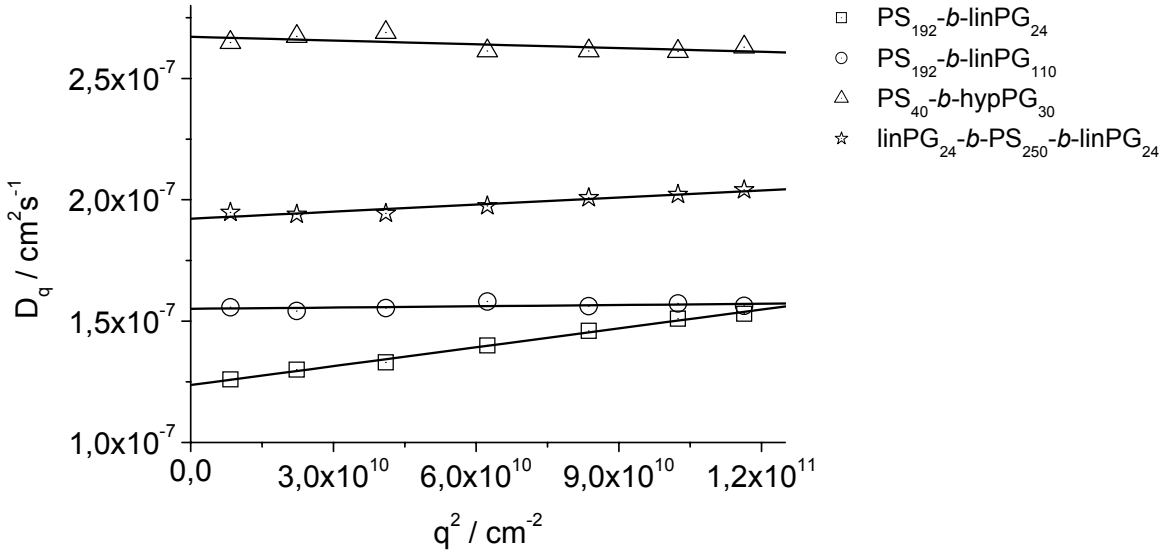

Figure 35 Plot of the apparent diffusion coefficient versus the scattering vector in chloroform (20 °C).

The diffusion coefficient was determined at different polymer concentrations to verify, if the aggregation was concentration dependent. Figure 36 shows the plot of the translational diffusion coefficient versus the polymer concentration in chloroform for different block copolymers.

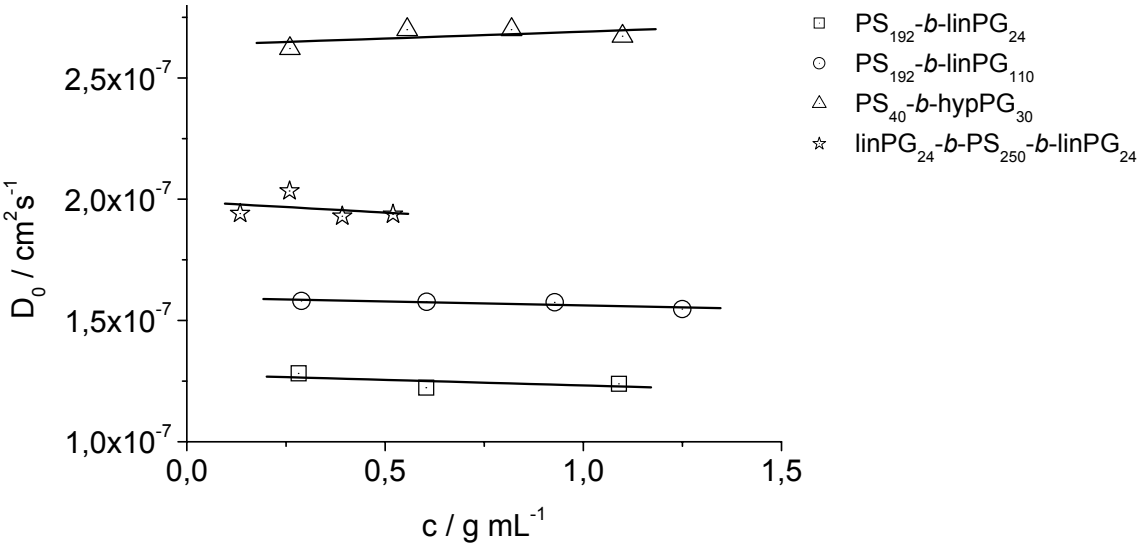

Figure 36 Plot of the translational diffusion coefficient versus the polymer concentration in chloroform (20 °C).

The particle size of the aggregates was independent on the concentration for all block copolymers. Nevertheless, it should be mentioned that the ABA type block copolymer could be measured only at concentrations below 0.5 g/mL, as it tended to form gels at higher concentrations (*vide infra*).

The polydispersity of the particles was then determined via the method of the cumulants (*vide supra*). Indeed, polydisperse particles yield narrower distributions at high scattering angles. Thus, the second cumulant is generally given at the scattering angle of 90°.

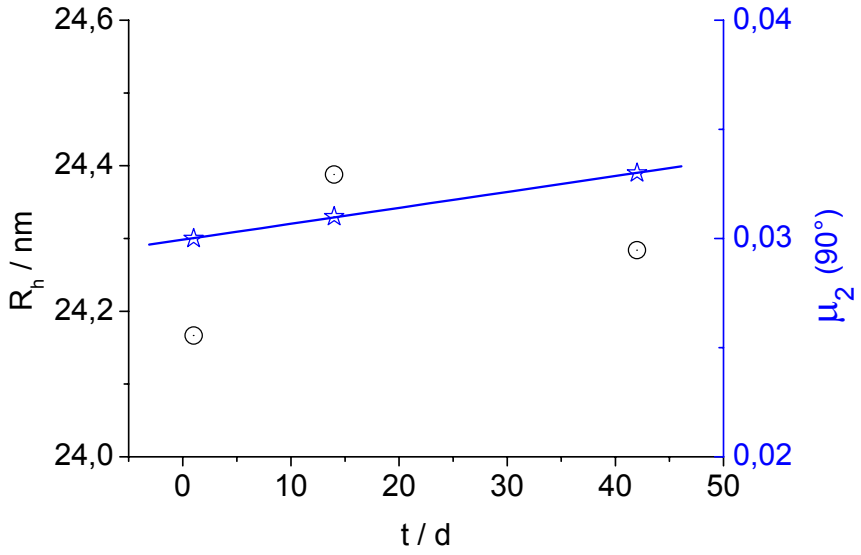

Figure 37 Supramolecular development for copolymer **PS_{192}-*b*-hypPG$_{110}$** in chloroform solution over a period of six weeks (20 °C).

Figure 37 shows the development of the aggregate size and polydispersity for the block copolymer **PS_{192}-*b*-$hypPG_{110}$** over a period of six weeks. Size and polydispersity were almost constant during the timescale of the experiment, proving the aggregates to be kinetically very stable.

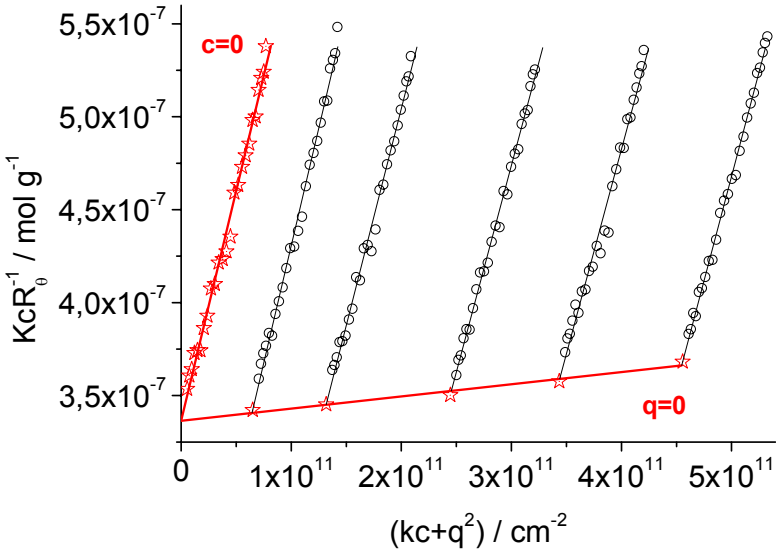

Figure 38 Zimm-plot of **PS_{192}-*b*-$linPG_{24}$** measured in chloroform (20 °C).

SLS measurements were performed to complete the data for the global properties of these block copolymers. Figure 38 shows a typical Zimm-plot. The extrapolated curves (c = 0 and q = 0) are plotted in red. Their intersection permits the calculation of the weight average molecular weight of the aggregates. The slopes give the radii of gyration and the second virial coefficient.

Table 6 SLS and DLS Data obtained in chloroform (20 °C).

	SLS				DLS		ρ
Copolymer	**M_w**	**Z**	**$R_g(z)$**	**A_2**	**$R_h(z)$**	**μ_2**	
PS_{192}-*b*-$linPG_{24}$	2 972 000	136	47.0	1.6 x 10^{-5}	30.4	0.21	1.55
PS_{192}-*b*-$hypPG_{110}$	3 851 000	137	17.3	-9.8 x 10^{-6}	24.0	0.02	0.72
PS_{40}-*b*-$linPG_7$ [b]	39 400	8	---	-1.5 x 10^{-7}	---	---	---
PS_{40}-*b*-$hypPG_{30}$	942 000	148	13.7	-2.4 x 10^{-5}	14.3	0.05	0.96
$linPG_{24}$-*b*-PS_{250}-*b*-$linPG_{24}$	1 131 000	38	28.0	-1.5 x 10^{-6}	19.6	0.12	1.49

M_w in g/mol; R_g oder R_h in nm; A_2 in mol*mL*g^{-2}

Table 6 summarizes the light scattering results obtained for the different block copolymers in chloroform. As mentioned before, the block copolymer **PS_{40}-*b*-$linPG_7$** did not form aggregates. Nevertheless, the weight average molar mass for these aggre-

[b] R_g and R_h are below 10 nm, resulting in high errors.

gates is higher than the mass of the block copolymer obtained by NMR techniques. This indicates at least the formation of small amounts of aggregates. Thus, the overall amount can be neglected as it is very low. Surprisingly all AB-type block copolymers formed micelles with an aggregation number of approximately 140. The ABA type block copolymer clearly deviates from this behavior. This will be explained in detail in chapter 4.4.

The radii of the **PS_{192}-*b*-linPG$_{24}$** copolymer are much higher than for the linear-hyperbranched block copolymers. Furthermore it features the highest polydispersity (μ_2). Radii by LS are always *z*-averaged, thus the radius of the **PS_{192}-*b*-linPG$_{24}$** copolymer predomently reflects the larger aggregates.

In contrast, the linear-hyperbranched block copolymers exhibit very low μ_2 values. These values are typical for almost monodisperse distributions. This finding is very important, because it demonstrates one very important advantage of the linear-hyperbranched block-copolymers.

Finally, the ρ-ratios yield some very interesting information concerning the structural manifestation. All linear block copolymers gave values around 1.5, which is typical for coiled polymers in solution or less defined aggregates. The linear-hyperbranched block copolymers on the other hand yielded values between 0.7 and 1.0, indicating well-defined spherical micelles.

4.2.2. Measurements in Toluene

The influence of the nature of the solvent on the aggregation was studied by performing the same light scattering experiments in another non-polar solvent. Toluene was chosen, since some very interesting features concerning aggregation behavior have been reported in the literature.[80,147] The sample preparation for LS measurements was the same as for measurements in chloroform. Unfortunately, the **linPG$_{24}$-*b*-PS_{250}-*b*-linPG$_{24}$** copolymer was even less soluble in toluene and no measurements could be carried out. Sonification of the solution for extended periods did not result in any improvement. Therefore this copolymer was not studied in toluene.

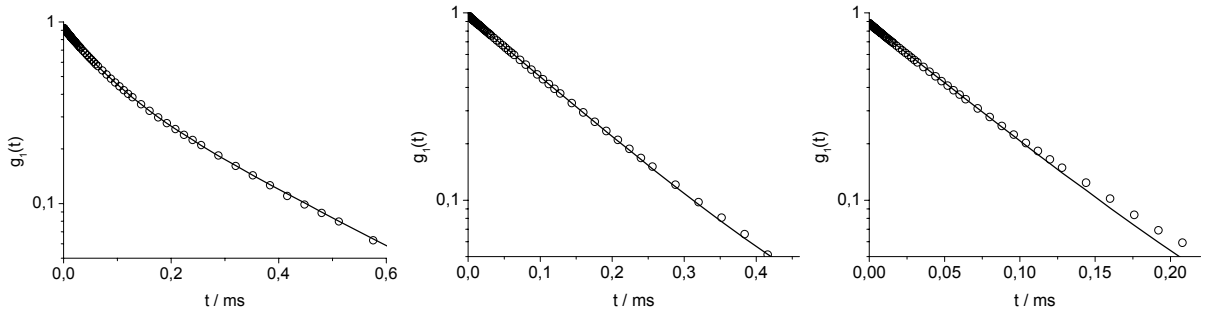

Figure 39 TCFs for **PS_{192}-*b*-linPG$_{24}$** (left), **PS_{192}-*b*-hypPG$_{110}$** (middle) and **PS_{40}-*b*-hypPG$_{30}$** (right) measured at an angle of 90° in toluene (20 °C).

The TCF obtained in toluene are analogous to the measurements in chloroform. The linear block copolymers exhibit a non-linear decay, while the linear-hyperbranched analogues show a linear decay, indicating a monodisperse distribution.

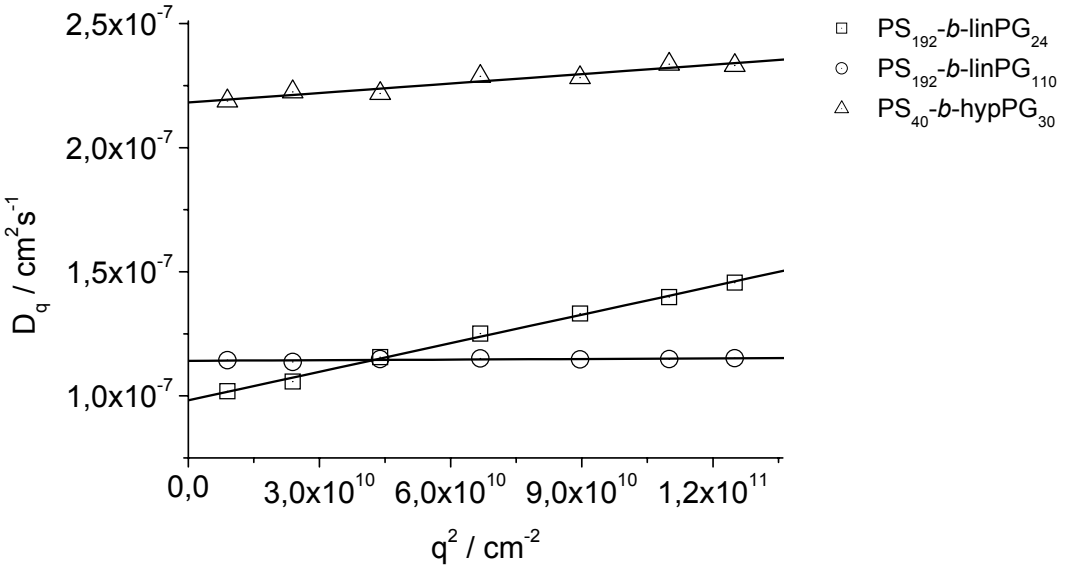

Figure 40 Plot of the apparent diffusion coefficient versus the scattering vector in toluene (20 °C).

It should be mentioned that the linear **PS_{40}-*b*-linPG$_7$** copolymer again did not form aggregates. The less polar solvent toluene did not induce the formation of aggregates.

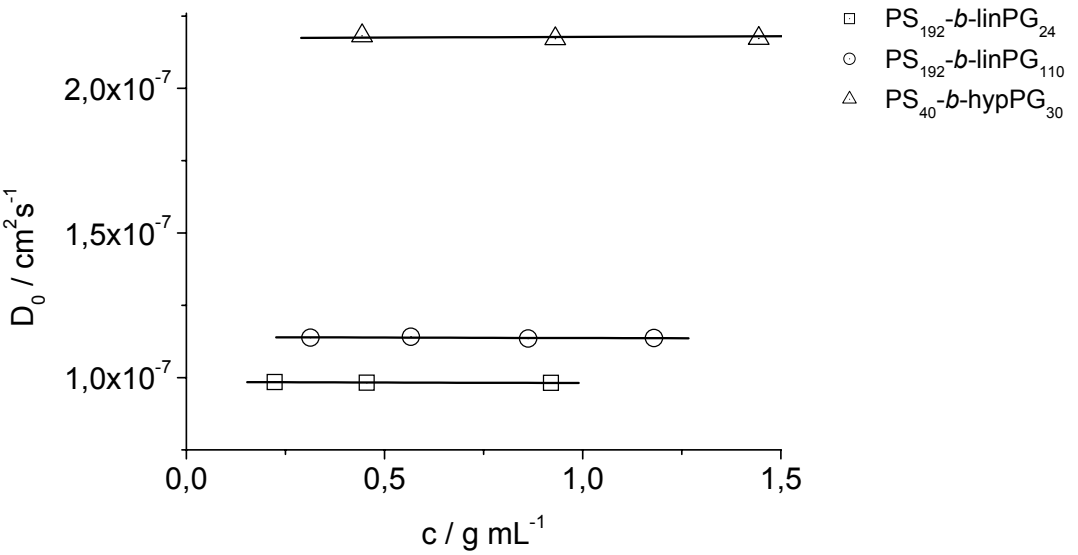

Figure 41 Plot of the translational diffusion coefficient versus polymer concentration in toluene (20 °C).

Figure 40 shows the plot of the apparent diffusion coefficient versus the scattering vector in toluene. This plot slightly differs from the diagram obtained for measurements in chloroform (Figure 35, page 59). The **PS_{192}-*b*-linPG$_{24}$** copolymer again shows a strong dependency of the diffusion coefficient on the scattering angle, as it was observed in chloroform as well. The linear-hyperbranched **PS_{40}-*b*-hypPG$_{30}$** copolymer shows a small dependency of the diffusion coefficient on the scattering angle, which is not the case in chloroform. However, the diffusion coefficient of the **PS_{192}-*b*-hypPG$_{110}$** copolymer is still independent on the scattering angle.

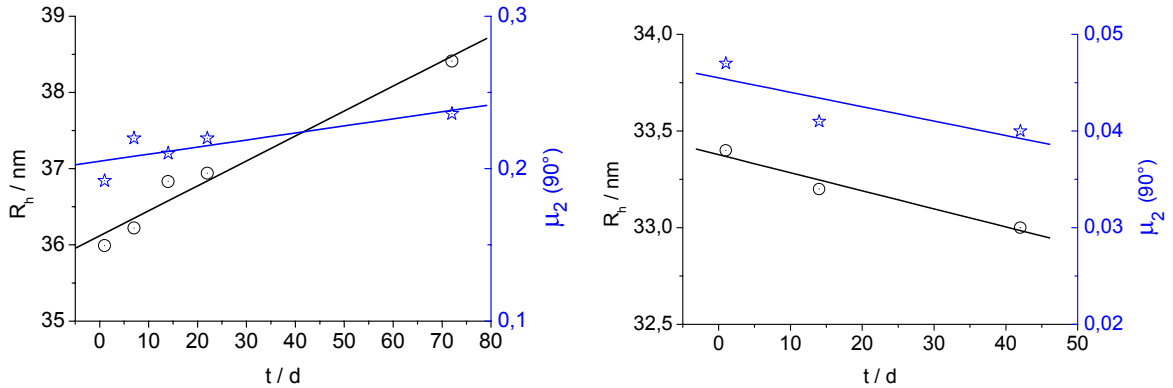

Figure 42 Supramolecular aggregation for copolymer **PS_{192}-*b*-linPG$_{24}$** (left) and **PS_{192}-*b*-hypPG$_{110}$** (right) in toluene solution over a period of several weeks (20 °C).

Figure 41 shows the plot of the translational diffusion coefficient versus polymer concentration in toluene. This plot is completely analogous to the plot obtained from measurements in chloroform (Figure 36, page 60), indicating that aggregation is not influenced by the polymer concentration.

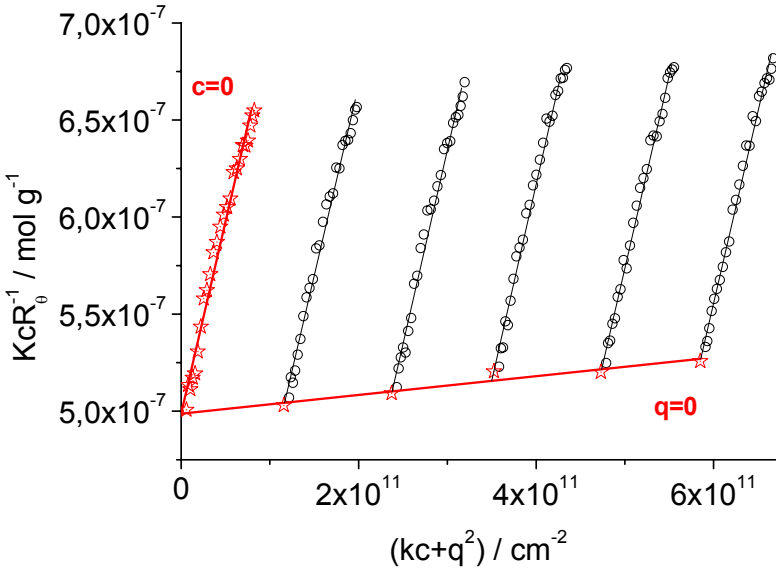

Figure 43 Zimm-plot of **PS_{192}-*b*-linPG$_{24}$** measured in toluene (20 °C).

Figure 42 shows the aggregation kinetics studied over an extended period of time. Unlike in chloroform, the aggregates in toluene changed slightly with time. Aggregates based on copolymer **PS_{192}-*b*-linPG$_{24}$** became larger and more polydisperse. In contrast the aggregates based on copolymer **PS_{192}-*b*-hypPG$_{110}$** became smaller and more narrowly dispersed. These results show that not only the direct morphology of the fresh aggregates is determined by the structure of the block copolymer, but also the equilibration kinetics is strongly influenced.

Table 7 SLS and DLS Data obtained in toluene (20 °C).

	SLS				DLS		ρ
Copolymer	**M_w**	**Z**	**R_g(z)**	**A_2**	**R_h(z)**	**μ_2**	
PS_{192}-*b*-linPG$_{24}$	2 005 000	92	34.5	1.2 x 10^{-5}	37.0	0.19	0.93
PS_{192}-*b*-hypPG$_{110}$	5 867 000	208	33.3	5.6 x 10^{-9}	31.7	0.04	1.05
PS_{40}-*b*-linPG$_7$	30 600	7	---	-2.1 x 10^{-5}	---	---	---
PS_{40}-*b*-hypPG$_{30}$	533 000	84	30.3	-7.4 x 10^{-8}	16.1	0.10	1.88

M_w in g/mol; R_g oder R_h in nm; A_2 in mol*mL*g^{-2}

Table 7 summarizes the results obtained from DLS and SLS in toluene. In analogy to the results in chloroform, the most polydisperse aggregates were formed by the **PS_{192}-*b*-linPG$_{24}$** copolymer (Table 6, page 61). Surprisingly, the aggregates formed by **PS_{40}-*b*-hypPG$_{30}$** were no longer monodisperse (but still narrowly distributed). Additionally this block copolymer did not form well-defined spherical aggregates anymore (ρ = 1.88). However, spherical aggregates were formed by the **PS_{192}-*b*-linPG$_{24}$**

copolymer now. These results emphasize the intricacy of predicting the structure of the aggregates based on the copolymer architecture.

4.3. SEC Measurements in Chloroform

Generally the analysis of supramolecular structures by SEC is not possible, because these structures are often destroyed or modified by shear forces on the column. However, these shear forces can be minimized by using columns with very large pore sizes. The setup used for this work (Figure 31, page 55) consisted of three styrene-divinylbenzene columns with diameters of 10^4, 10^5 and 10^6 Å. These values are not the actual pore sizes of the PS gels, but depict the extended chain lengths of a PS polymer, which elutes at the exclusion limit.[148] The product of the nominal porosity times 41.3 is approximately equal to the molecular weight of PS at the exclusion limit. Therefore the exclusion limits in our experiments varied from 400 000 to 40 millions!

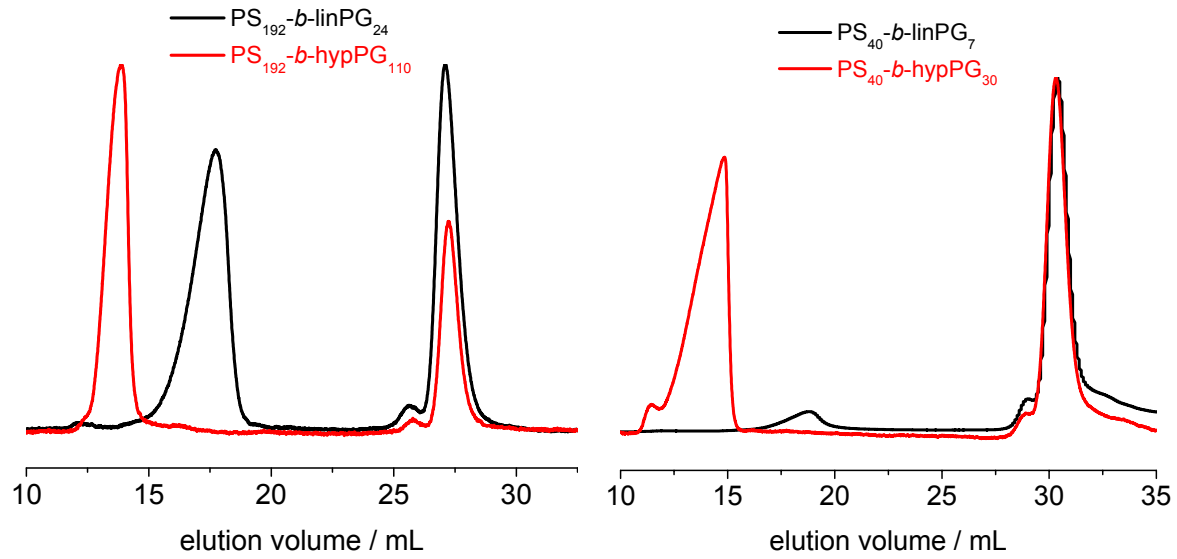

Figure 44 SEC of the AB-type block copolymers in chloroform (UV-detector, injected concentration = 0.5 g/L).

Figure 44 shows the SEC chromatograms of the different AB-type block copolymers. As already evidenced by light scattering the **PS_{40}-*b*-linPG$_7$** copolymer formed only a very low amount of aggregates. The block copolymer elutes almost entirely as a unimer. The larger **PS_{192}-*b*-linPG$_{24}$** forms higher amounts of similarly sized aggregates (same elution volume). This may be explained by the higher amphiphilic character of

the larger copolymer. This effect is well known for the phase separation of block copolymers in bulk.[84] Phase separation of immiscible blocks is induced above a certain polymer size and becomes also stronger with increasing size (keeping the block length ratios constant). The analogous linear-hyperbranched block copolymers formed larger aggregates. Interestingly the sample **PS$_{192}$-*b*-hypPG$_{110}$** appeared to form more narrowly dispersed aggregates as the corresponding **PS$_{40}$-*b*-hypPG$_{30}$**. It should be mentioned that according to the manufacturer all block copolymers still eluted below the upper exclusion limit. Thus, the narrow polydispersity was not an artifact. Unfortunately the columns were calibrated only in the range from 18.4 to 36.9 mL.[c] This made it impossible to calculate molar masses and polydispersities in relation to PS standards. The values for the unimers are given in chapter 3.3.

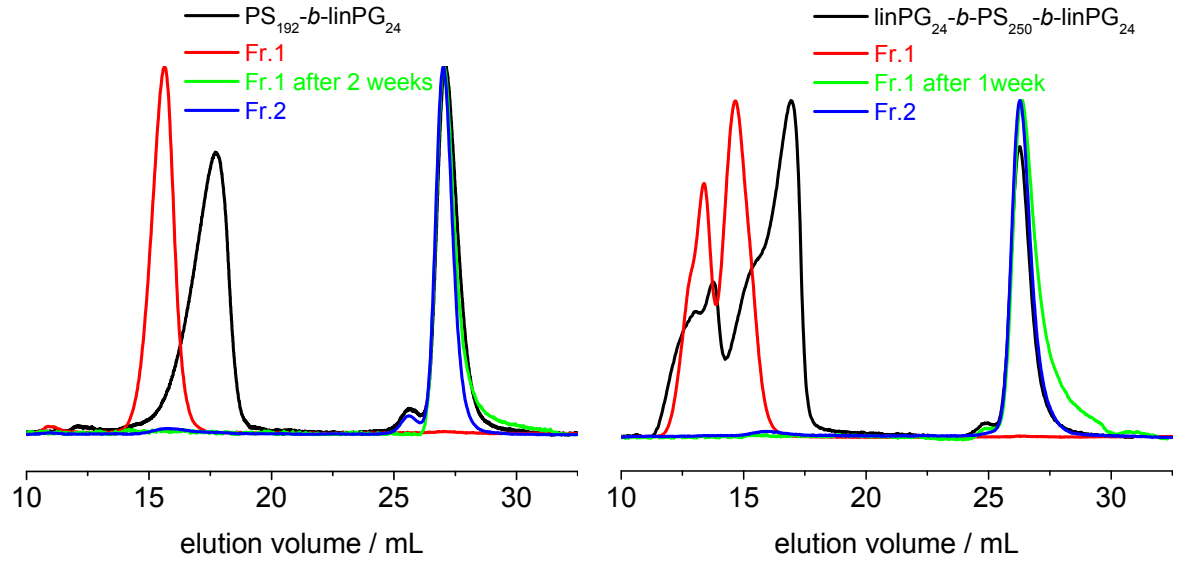

Figure 45 SEC fractionation results of **PS$_{192}$-*b*-linPG$_{24}$** (left) and **linPG$_{24}$-*b*-PS$_{192}$-*b*-linPG$_{24}$** (right) copolymer aggregates in chloroform (UV-detector). Fr.1 denotes the aggregate fraction and Fr.2 the unimer fraction.

In order to study the effect of the shear forces on the aggregates and to confirm the supramolecular nature of the high molecular weight distribution mode, the eluted aggregate and the unimer fraction were collected separately and injected a second time. Figure 45 shows the results for the pure linear block copolymers. In case of the **PS$_{192}$-*b*-linPG$_{24}$** it is apparent that the aggregate fraction did not contain unimers any more. The size of the particles seemed to become larger and more monodisperse. However, after two weeks storage of the solution, all aggregates in this fraction had disintegrated into unimers. It should be mentioned that the polymer concentration in the collected SEC fractions was very low ($c < 0.05$ g/L) and apparently below the

[c] 376 – 2 570 000 g/mol concerning PS standard

critical micelle concentration. Thus, after collection the unimer fraction did not form micelles again.

The aggregates formed by the **linPG$_{24}$-*b*-PS$_{192}$-*b*-linPG$_{24}$** copolymer showed a clearly bimodal distribution (Figure 45, right image). This may be explained by the formation of flower-like micelles (chapter 4.4, page 74). Furthermore, the same effects are found as for the **PS$_{192}$-*b*-linPG$_{24}$** copolymer micelles. The pure aggregate fraction is more monodisperse without unimers. After one week, SEC showed that these aggregates dissociated into unimers.

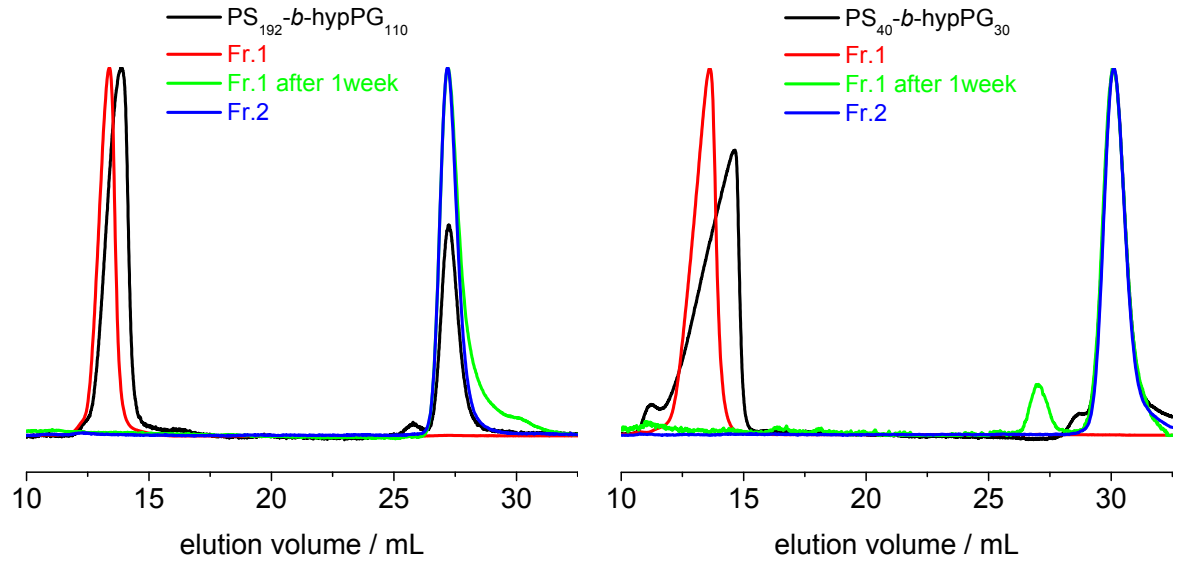

Figure 46 SEC fractionation results of **PS$_{192}$-*b*-hypPG$_{110}$** (left) and **PS$_{30}$-*b*-hypPG$_{40}$** (right) copolymer aggregates in chloroform (UV-detector). Fr.1 denotes the aggregate fraction and Fr.2 the unimer fraction.

Figure 46 shows the fractionation results for the linear-hyperbranched block copolymers. These results are consistent with the results for the non-associated linear block copolymer aggregates. The separated aggregates are free of unimers in the beginning and later disintegrate into the corresponding unimers. The aggregates also appear to be more narrow than the injected non-separated aggregates.

Table 8 DLS of fractionated and non-fractionated block copolymer aggregates in chloroform.

Copolymer	fractionated	R_h (z)	μ_2
PS$_{192}$-*b*-linPG$_{24}$	no	30.4 nm	0.224
	yes	14.4 nm	0.113
PS$_{192}$-*b*-hypPG$_{110}$	no	24.0 nm	0.020
	yes	24.5 nm	0.004

The SEC aggregates of the **PS_{192}-*b*-linPG$_{24}$** and **PS_{192}-*b*-hypPG$_{110}$** copolymers were collected for DLS measurements in order to confirm their narrow polydispersity. Table 8 presents the results of this investigation. Both block copolymers showed more narrow distributions after fractionation. In case of the **PS_{192}-*b*-hypPG$_{110}$** copolymer, the values for the second cumulant (μ_2) are typical for monodisperse aggregates. Surprisingly, the hydrodynamic radius decreased for **PS_{192}-*b*-linPG$_{24}$** to half the size of the non-fractionated aggregates. This result can be confirmed by SEC directly, because the apparently lower polydispersity influences the z-average of the hydrodynamic radius more strongly by DLS. The fractionated **PS_{192}-*b*-linPG$_{24}$** aggregates (Figure 45, left) are found at higher elution volumes than the **PS_{192}-*b*-hypPG$_{110}$** aggregates (Figure 46, left). Thus the **PS_{192}-*b*-hypPG$_{110}$** aggregates are obviously also larger, what was also found by DLS.

These results are very interesting, since a similar phenomenon is known from the extrusion of vesicles.[159,160] These extruded vesicles become smaller but also more narrow in size distribution. It is important to point out that the extrusion methods employed for vesicles are used for dimensions around 200 nm. The particles formed by this SEC-method are smaller by one order of magnitude.

A possible explanation for this phenomenon is that the SEC columns act as in the way of a template, forcing the aggregates to certain sizes. It is highly probable that this can be related to the pore size of the columns. Unfortunately, the limited time frame of this work did not allow for a further investigation of this observation.

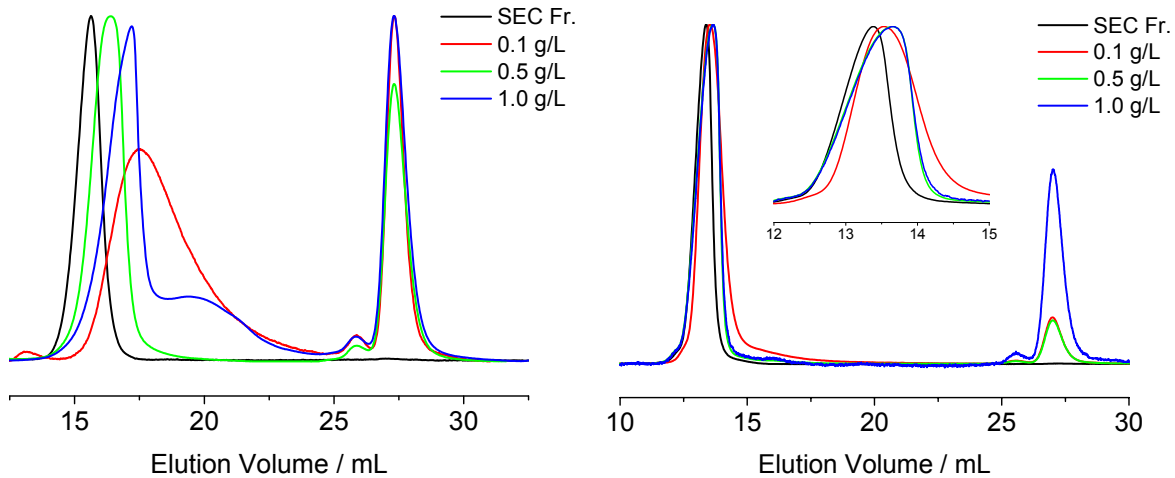

Figure 47 SEC for **PS_{192}-*b*-linPG$_{24}$** (left) and **PS_{192}-*b*-hypPG$_{110}$** (right) injected with different concentration solutions vs. the SEC fractionated aggregates.

In order to rule out the possibility that the formation of the well-defined aggregates on the SEC columns was caused by concentration effects, copolymer solutions of different concentrations have been injected and compared to the aggregates obtained

from fractionation (Figure 47). It was found that unimers were always present even at very low concentrations. **PS_{192}-*b*-linPG$_{24}$** copolymer aggregates were more affected by concentration than their linear-hyperbranched counterparts. In case of **PS_{192}-*b*-linPG$_{24}$** the aggregates varied significantly in polydispersity and size. At low or high concentrations, very broad distributions were found. In case of the **PS_{192}-*b*-hypPG$_{110}$** aggregates this effect was much less pronounced.

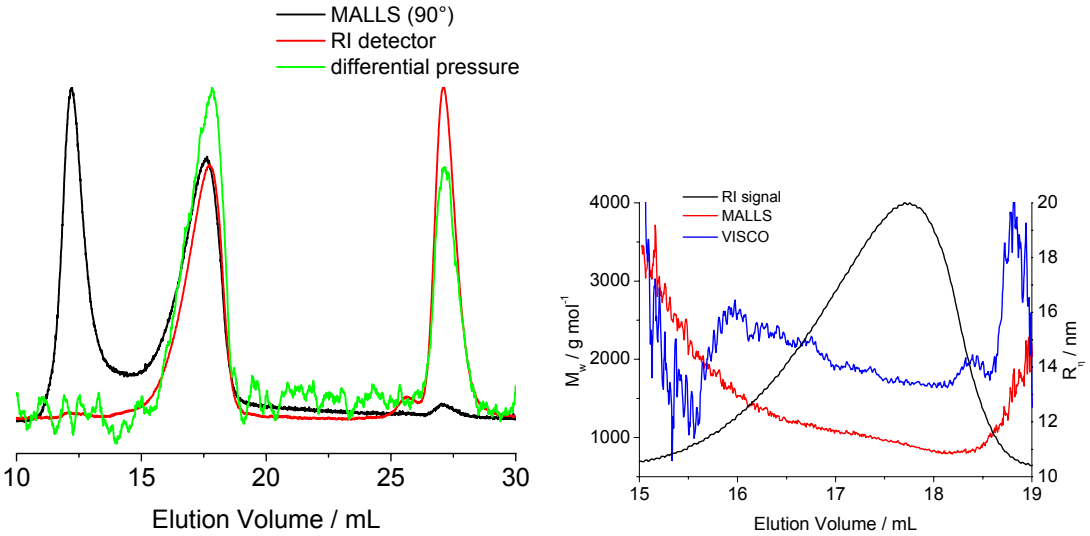

Figure 48 Results for triple detection SEC for **PS_{192}-*b*-linPG$_{24}$**. Left: raw detector signals. Right: M_w and R_η versus elution volume.

Another method to analyze the particles eluted from the SEC column is the application of SEC with triple detection (Figure 31, page 55). Figure 48 (left) shows the direct output of the detectors. It should be mentioned that all polymers synthesized exhibited a very strong light scattering peak at 12.5 mL. This peak has to belong to a very large mass, since the concentration detector (RI) shows no signal. The amount of this side product should be therefore below 1 %.

Table 9 Summary fort the results by triple detection (θ = 71 – 118°, 6 angles)

	M_n / g mol^{-1}	PDI	R_g (z) / nm	R_η (z) / nm
PS_{192}-*b*-linPG$_{24}$	1 018 000	1.07	18.9	14.1
PS_{192}-*b*-hypPG$_{110}$	7 904 000	1.04	13.7	21.5
PS_{40}-*b*-hypPG$_{30}$	4 878 000	1.12	17.4	14.8
linPG$_{24}$-*b*-PS_{250}-*b*-linPG$_{24}$ [d]	5 073 000	1.42	45.6	34.2
	1 111 000	1.10	11.5	15.5

[d] bimodal distribution, refer to chapter 4.4.

Table 9 summarizes the results obtained by the triple detection method. The molar masses significantly differ from the results obtained by a batch light scattering experiment (Table 6, page 61). However, respective radii match the DLS results obtained for the SEC aggregates (Table 8).

Generally in all SEC experiments the elution rates were set to 1.0 mL/min. In order to study the effect of the elution rate, the same experiment was performed at 0.5 mL/min.

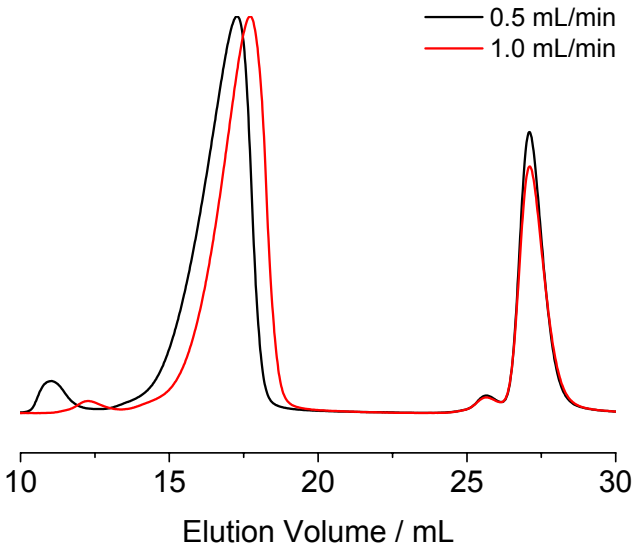

Figure 49 SEC chromatogram for **PS_{192}-*b*-linPG$_{24}$** at different elution rates.

Figure 49 shows the SEC chromatogram of the **PS_{192}-*b*-linPG$_{24}$** copolymer recorded at different elution rates. Apparently the aggregates become larger at lower elution rates.

Table 10 Triple detection results for copolymer **PS_{192}-*b*-linPG$_{24}$** in Figure 49.

Flow rate	M_n / g mol^{-1}	PDI	R_g (z) / nm	R_η (z) / nm
0.5 mL/min [1]	1 228 000	1.12	28.2	16.1
1.0 mL/min [2]	1 018 000	1.07	18.9	14.1

[1] θ = 71 – 118° (6 angles); [2] θ = 99.5 – 152.3° (6 angles)

This assumption is supported by the triple detection results shown in Table 10. The increasing size of the aggregates after decreasing the elution rate can be explained by the lower shear forces on the column.

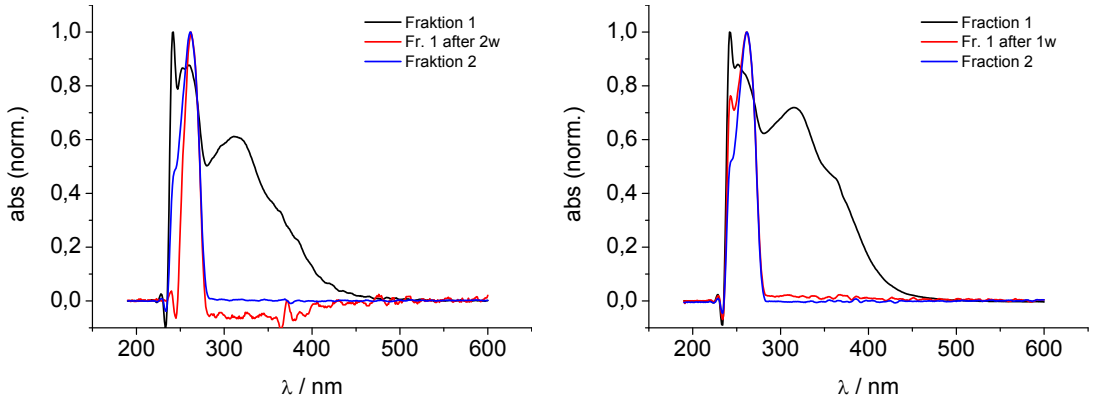

Figure 50 UV-vis spectra obtained by SEC for **PS_{192}-*b*-linPG$_{24}$** (left) **PS_{192}-*b*-hypPG$_{110}$** (right). Aggregate fraction (1) was compared with the unimer fraction (2) directly after fractionation and one or two weeks later.

Finally, the aggregates and unimers were characterized by UV-vis spectroscopy. The employed SEC setup permits measurement of a full UV-vis spectrum at each point of the elution chromatogram. Therefore UV-vis spectra were collected at each peak maximum. All block copolymers exhibited the same UV-vis spectrum. Figure 50 shows the spectra obtained from the copolymers **PS_{192}-*b*-linPG$_{24}$** and **PS_{192}-*b*-hypPG$_{110}$**. A single absorption band at approximately 254 nm for PS was expected. Surprisingly the aggregates exhibited a broad absorption band from 230 to 450 nm with three maxima at 240, 256 and 313 nm. This absorption spectrum was not found for the unimer fraction or for the aggregate fraction after disintegration into unimers. In that case the spectra matched expectation for PS. It should be mentioned that these peculiar aggregate spectra were only obtained after fractionation with the SEC columns. The SEC fractions were collected and measured on a conventional UV-vis spectrometer in order to rule out instrumental errors. The results were the same like those recorded by the online UV-vis spectrometer. Tentavely this can be explained by π-π interactions between styrene units at the core (more dense packing). No similar example was found in the literature. A satisfactory explanation for this observation has yet to be found and can not be part of this work.

4.4. Aggregate Structure in Nonpolar Solvents

Shape and size of the aggregates are determined by a variety of parameters that affect the balance between three major forces acting on the system: These forces are caused by

i the extent of constraints between the blocks forming the core (the blocks will be more or less stretched depending on the solvent).

ii interaction forces between chains forming the corona.

iii the interfacial energy between the solvent and the core of the micelle.

Possible structures are spherical micelles, non-spherical micelles, vesicles, bilayers and bicontinuous planes.[81]

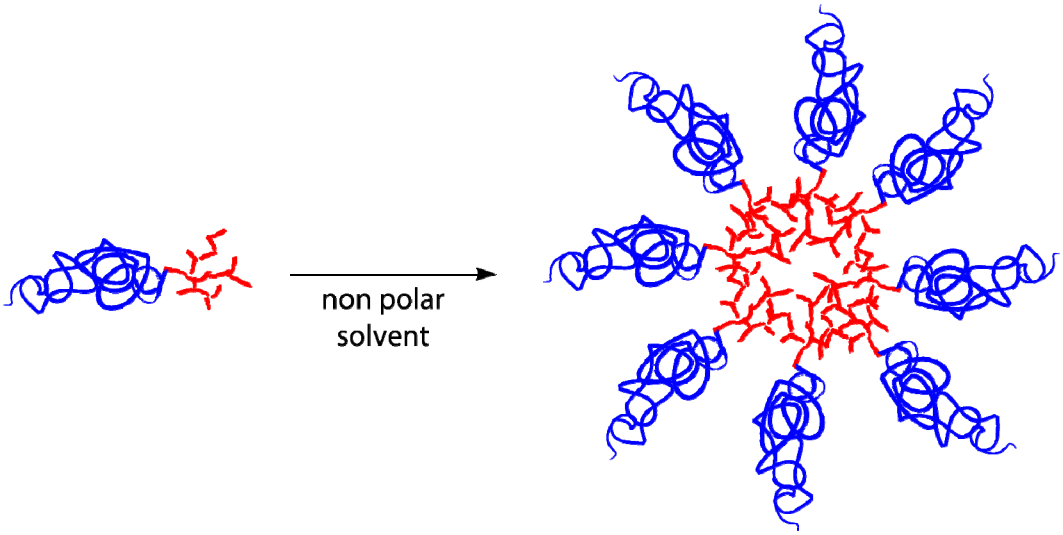

Figure 51 Schematic representation of a micelle formed by a linear-hyperbranbched block copolymer.

Based on the data summarized in chapters 4.1 to 4.3 it is possible to draw conclusions on the presence of such aggregates. When using non-polar solvents the micellar core is due to the solvent polarity the polyglycerol block. This is already evidenced by NMR experiments (see chapter 3, page 38). The size of all aggregates was in the range of 10 to 40 nm. This is a typical value for micelles; vesicles are generally larger (> 100 nm). A schematic representation of a micelle formed by a linear-hyperbranched block copolymer is shown in Figure 51.

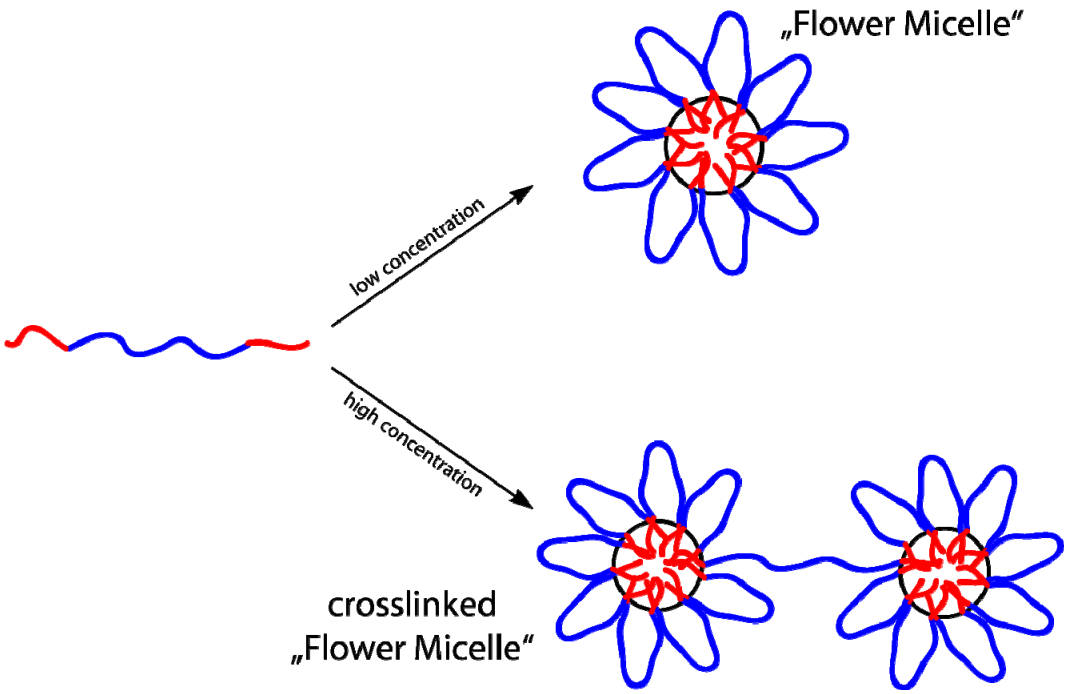

Figure 52 Schematic representation of a flower micelle formed by a **linPG$_{24}$-*b*-PS$_{192}$-*b*-linPG$_{24}$** copolymer.

In the case of ABA type block copolymers the situation is somewhat different. The core of the **linPG$_{24}$-*b*-PS$_{192}$-*b*-linPG$_{24}$** copolymer is still formed by the linear polyglycerol block, but there are two possibilities for the PS block to pack: At low concentrations the block copolymer will mainly form loops and the so-called flower micelles are formed (Figure 52). At higher concentrations the probability that these micelles are crosslinked by an ABA block copolymer is drastically increased. This also explains the bimodal SEC distribution of the aggregates (Figure 45, page 67). According to the SEC experiments with triple detection approximately five micelles were crosslinked (Table 9, page 70).

Transmission electron microscopy (TEM) and atomic force microscopy (AFM) measurements were performed to obtain a visual image of the block copolymers.
In TEM, electrons are accelerated to a few hundred keV. One single column of only a few atoms is sufficient to determine the positions and, in principle, also the types of atoms from the scattered electron wave.[161] A schematic representation of a TEM instrument is shown in the appendix (Figure 142, page 184)

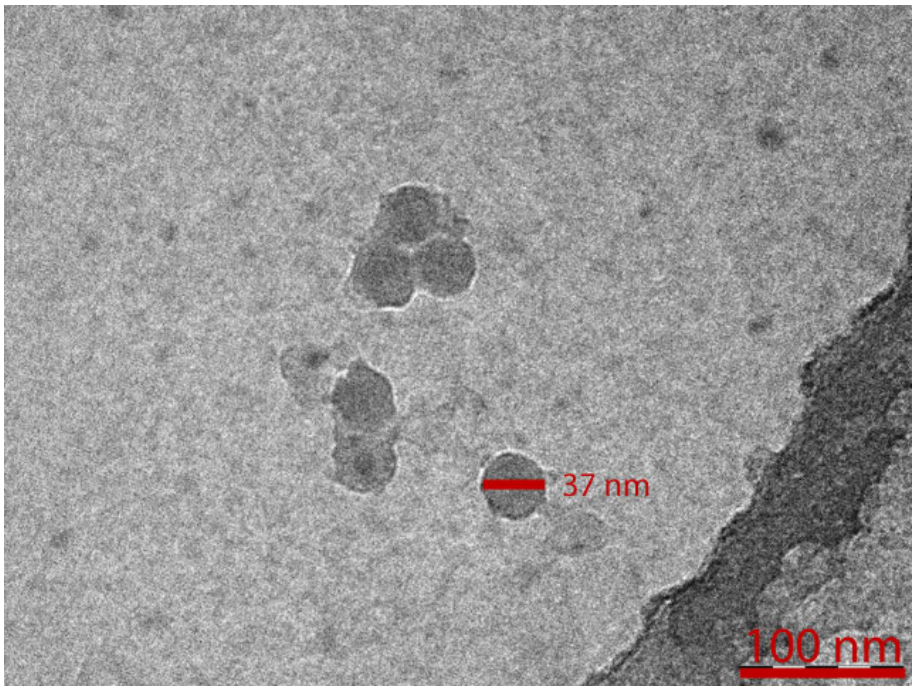

Figure 53 Cryo-TEM image of **PS_{192}-*b*-hypPG$_{110}$** measured in toluene (c=1.0 g/L).

The cryo-TEM variant is often employed to obtain structural information of particles in solution. To this end, the particles are frozen in a selected solvent and then directly analyzed by TEM. Figure 53 shows a cryo-TEM image of the aggregates formed by the **PS_{192}-*b*-hypPG$_{110}$** copolymer in toluene (concentration 1.0 g/L). The size distribution seems to be monodisperse and the shape confirms the formation of well-defined spherical aggregates as found by light scattering. However, the aggregates determined by dynamic and static LS were 60 nm in diameter. It has to be pointed out that LS gives real average values, while TEM only shows representation of small sections that may vary in their appearance depending also on the sample preparation.

Another very useful method to obtain an optical image in the atomic-scale is the atomic force microscopy (AFM). A universal tip-sample force interaction is employed for surface imaging in AFM. The simple optical lever method is used for the detection of small forces between the apex of a microfabricated tip (positioned at one end of a tiny cantilever) and a sample surface.[162] A schematic representation of this setup is shown in the appendix (Figure 143, page 185).

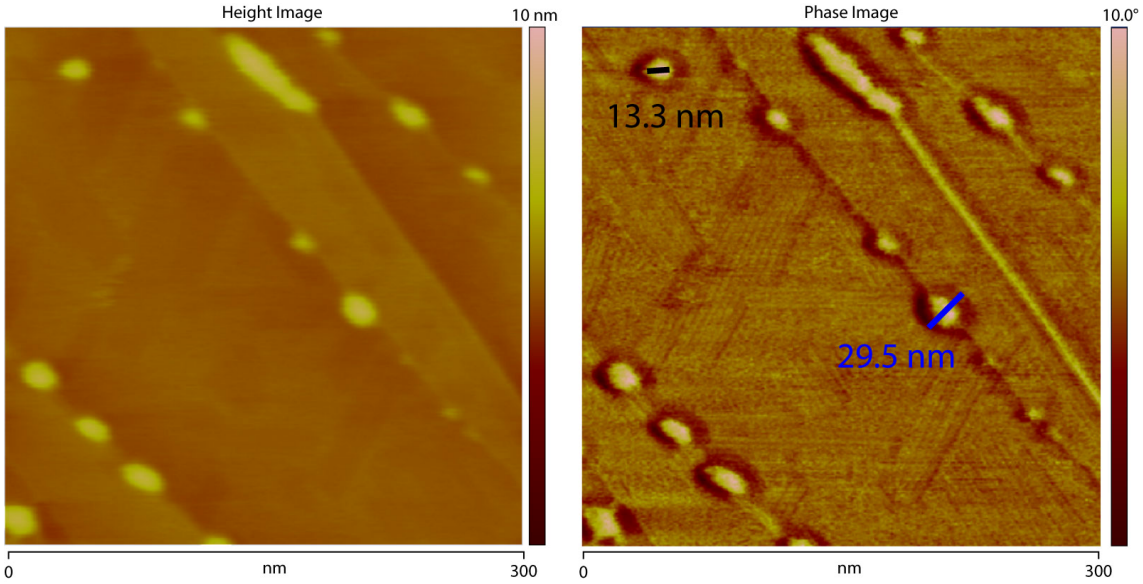

Figure 54 AFM image of **PS_{192}-*b*-hypPG$_{110}$** (c=0.5 g/L) spin coated from a toluene solution (c=0.5 g/L) onto HOPG.

Figure 54 shows an AFM-micrograph of the sample **PS_{192}-*b*-hypPG$_{110}$** spin coated from toluene solution onto graphite (HOPG). The solution concentration was set at 0.5 g/L in order to realize a homogeneous coverage on the surface of the substrate by the micellar structures.

As the aggregates are deposited on the surface, the spherical micelles adopt an open, flattened morphology. Such core-shell superstructures appear when one of the blocks is strongly adsorbed (here PS) and forms a tightly bound monomolecular layer on the surface, while the other block is incompatible with the surface and forms a morphology similar to a droplet. The dimensions obtained by AFM are half the size of the dimensions obtained from light scattering. This can be explained by the fact that the aggregates are measured in the dry state. Thus they may be collapsed in comparison to a solution where they are swollen. However, the micelles formed from **PS_{192}-*b*-hypPG$_{110}$** appear to be well-defined concerning their polydispersity. The phase image clearly shows that the micelle core is chemically different from the surrounding shell. In contrast micelles from the **PS_{192}-*b*-linPG$_{24}$** copolymer adopt a similar conformation but the polydispersity of the micellar size is larger (Figure 55).

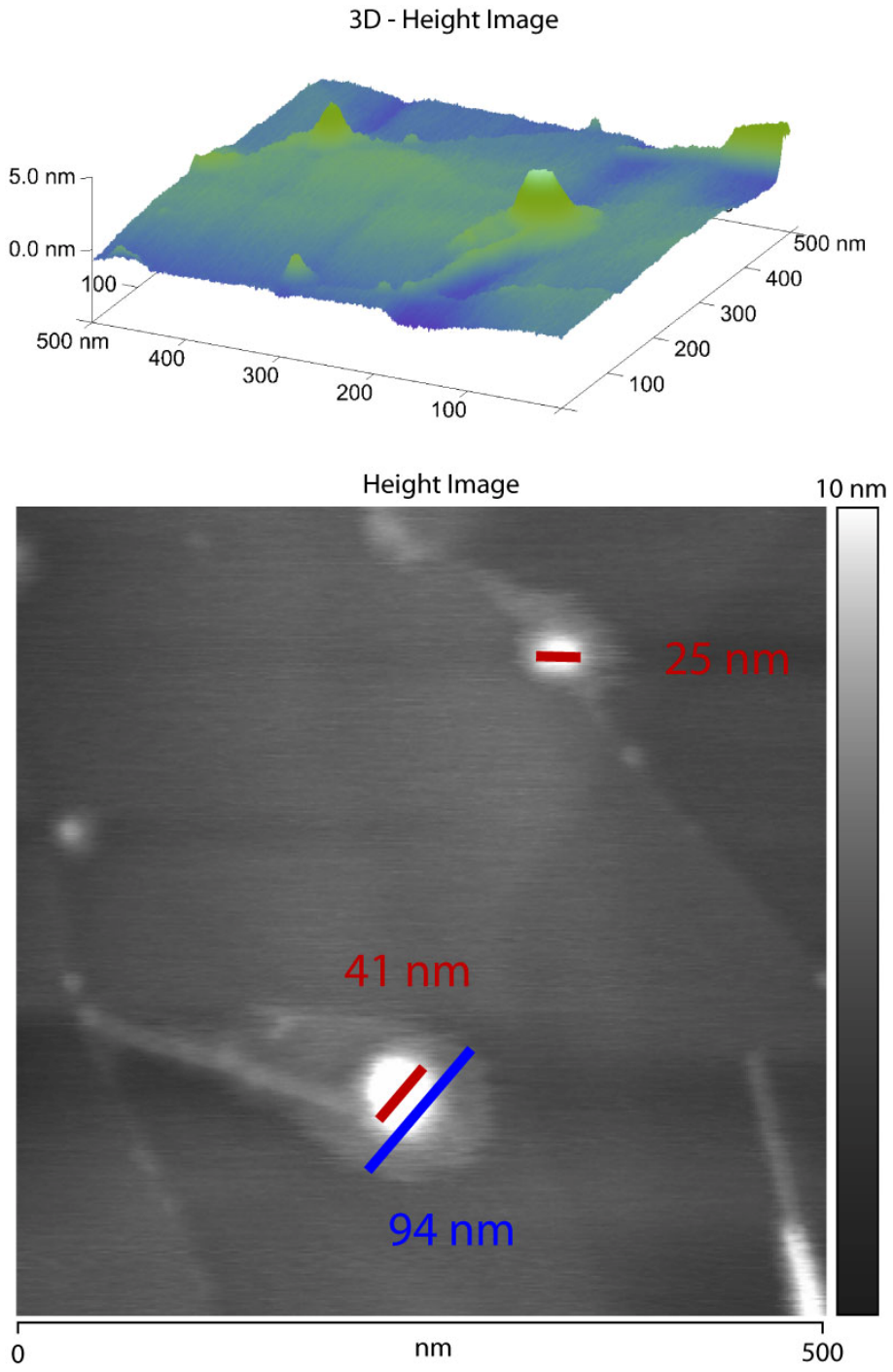

Figure 55 AFM image of **PS_{192}-*b*-linPG$_{24}$** spin-coated from a toluene solution (c=0.5 g/L) onto HOPG.

Similar surface patterns were first observed experimentally for linear block copolymers in thin films formed by adsorption of symmetrical polystyrene-*block*-poly(2-vinylpyridine) (PS-*b*-P2VP) copolymers from a dilute nonselective solvent onto a mica substrate.[163,164] For the copolymer PS_{300}-*b*-$P2VP_{300}$ a polystyrene core cluster with a height of 5 nm surrounded by a P2VP shell with a height of 1 nm was measured. Similar values for the height of the PG core and PS shell were found in this work as well as in previous studies.[80,147] A schematic representation of the aggregate mor-

phology after deposition onto graphite is shown in Figure 56. It is interesting to note that the elevated regions on the surface in this case are the polar, highly hydroxyl-functional polyglycerol blocks.

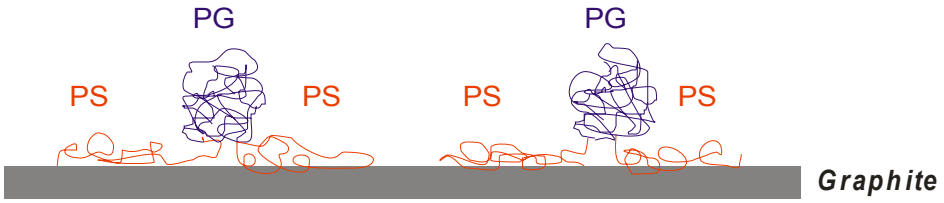

Figure 56 Schematic illustration of core-shell structures after deposition from toluene solution onto graphite.

4.5. Aggregation in Methanol

The micelle structures studied previously were constituted by the hydrophilic PG block as the core. In order to form the reverse micelles with PG in the shell, the polarity of the solvent had to be varied. For example methanol is a solvent that solubilizes PG and forces PS to precipitate. Therefore micelles from a PS-*b*-PG copolymer in methanol should incorporate PG in the shell and PS in the core. Unfortunately, none of the block copolymers could be directly dissolved in methanol. In such cases the slow exchange of a nonpolar solvent with the polar one is a possibility to access micelles with PG in the shell.

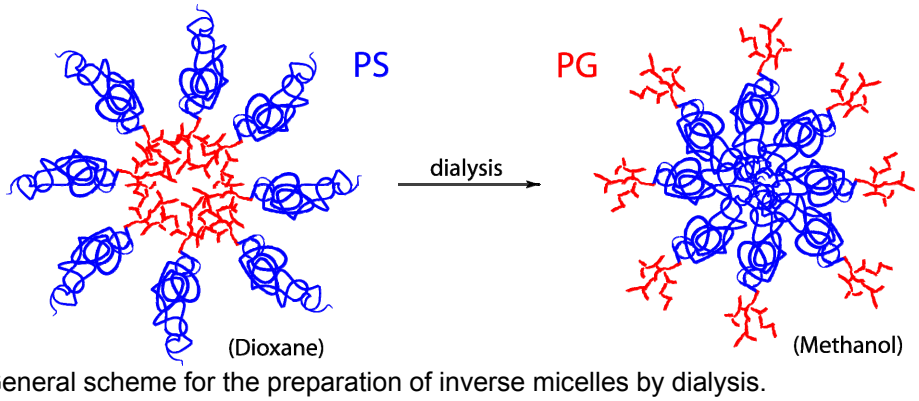

Figure 57 General scheme for the preparation of inverse micelles by dialysis.

Figure 57 shows the general scheme for the preparation. Dioxane was chosen as nonpolar solvent as it can be easily removed by dialysis with methanol. PG is not soluble in dioxane, thus it should form the core. Dialysis was performed for three days, changing the solvent twice a day. Surprisingly, not only the **PS_{40}-*b*-linPG$_7$**, but

also the **PS_{40}-*b*-hypPG$_{30}$** copolymer precipitated in the dialysis tube during this process. In these cases the PG block was simply too short and the amphiphilic character not sufficient to keep the block copolymer in solution.

Figure 58 Inverse micelles solutions: **PS_{192}-*b*-hypPG$_{110}$** (left) and **linPG$_{24}$-*b*-PS_{192}-*b*-linPG$_{24}$** (right).

Figure 58 shows the respective methanol solutions containing the inverse micelle structures of the **PS_{192}-*b*-hypPG$_{110}$** and **linPG$_{24}$-*b*-PS_{192}-*b*-linPG$_{24}$** copolymers. The dioxane solutions were not opaque; they became opaque after approximately one day of dialysis. The actual concentration after dialysis is unknown and can only be approximated (c ≈ 1 g/L). The opaque appearance is a strong indication for the formation of very large particles.

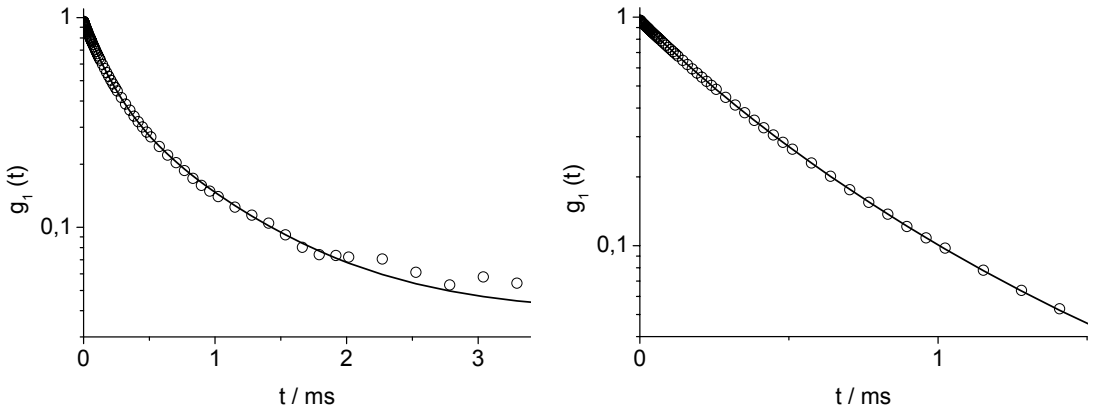

Figure 59 DLS data obtained from **PS_{192}-*b*-hypPG$_{110}$** (left) and **linPG$_{24}$-*b*-PS_{192}-*b*-linPG$_{24}$** (right) in methanol.

In order to gather more information about these particles, DLS and SLS measurements were performed. It was not possible to apply the same sample preparation as

for the aggregates in chloroform or toluene because of the large expected size of the particles. Filtration with filters with narrow pore sizes would possibly destroy the aggregates. On the other hand only a very small amount would be necessary for the measurement because of this large particle sizes. Thus only one unfiltered drop was diluted with very pure methanol that had been filtered through a Millex VV filter (0.1 μm pore size). The concentration after dilution was estimated to be approximately 3 mg/L, three orders of magnitude below the concentrations applied in nonpolar solvents.

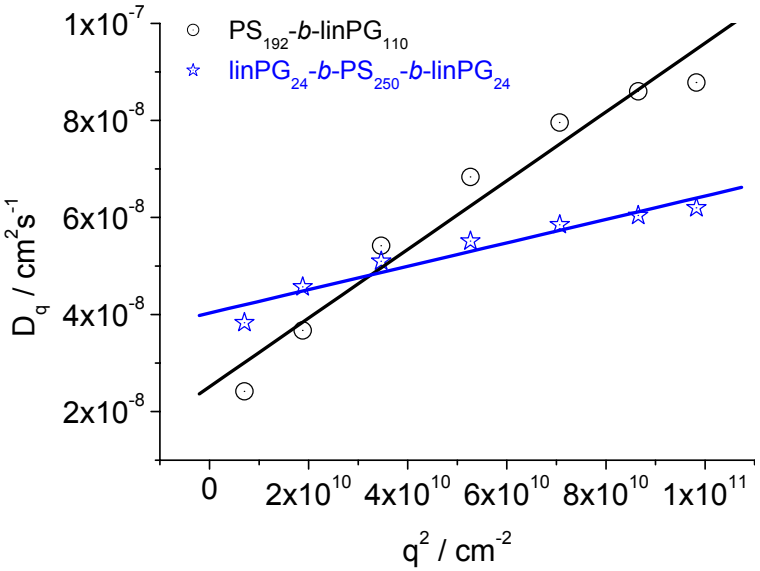

Figure 60 Plot of the apparent diffusion coefficient versus the scattering vector in methanol (20 °C).

Figure 59 shows the TCF obtained by DLS for the **PS$_{192}$-*b*-hypPG$_{110}$** copolymer. In case of DLS it is not necessary to know the actual concentration. Roughly speaking, the amount of correlating signals decreases but the relation of these signals is still the same.

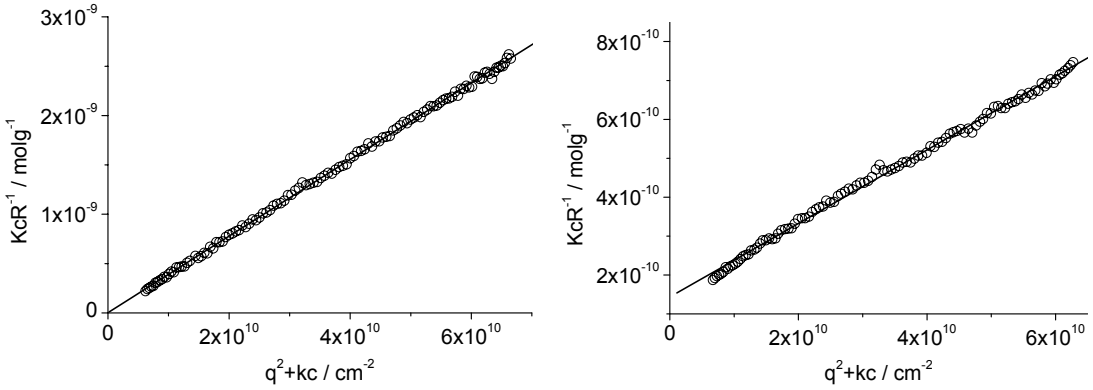

Figure 61 SLS data obtained from **PS$_{192}$-*b*-hypPG$_{110}$** (left) and **linPG$_{24}$-*b*-PS$_{192}$-*b*-linPG$_{24}$** (right) in methanol.

It is important to point out that the time scale of the TCF is ten times larger than for the aggregates in nonpolar solvents. Concerning the shape of the TCF, these aggregates seem to be more polydisperse than those in nonpolar solvents. The results for the **linPG$_{24}$-*b*-PS$_{192}$-*b*-linPG$_{24}$** copolymer are similar. However, these aggregates appear to be smaller (shorter correlation times) and more monodisperse (more linear function).

SLS was performed with these aggregates (Figure 61). Usually it is essential to know the exact concentration and the $\partial n/\partial c$ in SLS. Nevertheless, some information can still be obtained from measurements with an almost unknown concentration and $\partial n/\partial c$. The radius of gyration for example is independent on the concentration and the $\partial n/\partial c$. Relying on the Zimm-equation, only the intercept is influenced by the concentration and $\partial n/\partial c$, but not the slope, which means that it can be determined without additional approximations.

Table 11 SLS and DLS Data obtained in methanol (20 °C).

	SLS		DLS		ρ
Copolymer	**M_w (app.)**	**R_g(z)**	**R_h(z)**	**μ_2**	
PS$_{192}$-*b*-hypPG$_{110}$	2 x 10^{10}	431.9	145.5	0.15	3.0
linPG$_{24}$-*b*-PS$_{250}$-*b*-linPG$_{24}$	6 x 10^{9}	131.4	90.1	0.13	1.5
PS$_{192}$-*b*-linPG$_{24}$	non measurable				
PS$_{40}$-*b*-linPG$_{7}$	polymers precipitated during dialysis				
PS$_{40}$-*b*-hypPG$_{30}$					

Apparent M_w in g/mol; R_g(z) and R_h(z) in nm

The molar mass can be approximated under two assumptions. i) The concentration of 3 mg/L is so low that it can be treated as the extrapolated zero concentration (online-MALLS detectors make the same approximation). ii) $\partial n/\partial c$ is also unknown, but normally this value deviates only slightly from 0.1. With $\partial n/\partial c$ = 0.1, at least the correct order of magnitude of the molar mass can be estimated.

Table 11 shows the summary of the results obtained by DLS and SLS measurements. The **PS$_{192}$-*b*-linPG$_{24}$** copolymer gave an opaque but also more turbid solution making it impossible to perform light scattering measurements. As mentioned before, the **PS$_{40}$-*b*-linPG$_{7}$** and **PS$_{30}$-*b*-hypPG$_{30}$** copolymers yielded no aggregates in methanol. Only the samples **PS$_{192}$-*b*-hypPG$_{110}$** and **linPG$_{24}$-*b*-PS$_{192}$-*b*-linPG$_{24}$** could be measured. As expected the aggregates were very large (in the range of 6 to 20 billion (!) g/mol). These molar masses were only apparent, nevertheless the order of

magnitude is correct. The radii are very large (from 90 to 430 nm). In combination with the determined ρ-ratios, this indicates spherical or tube-like vesicles.

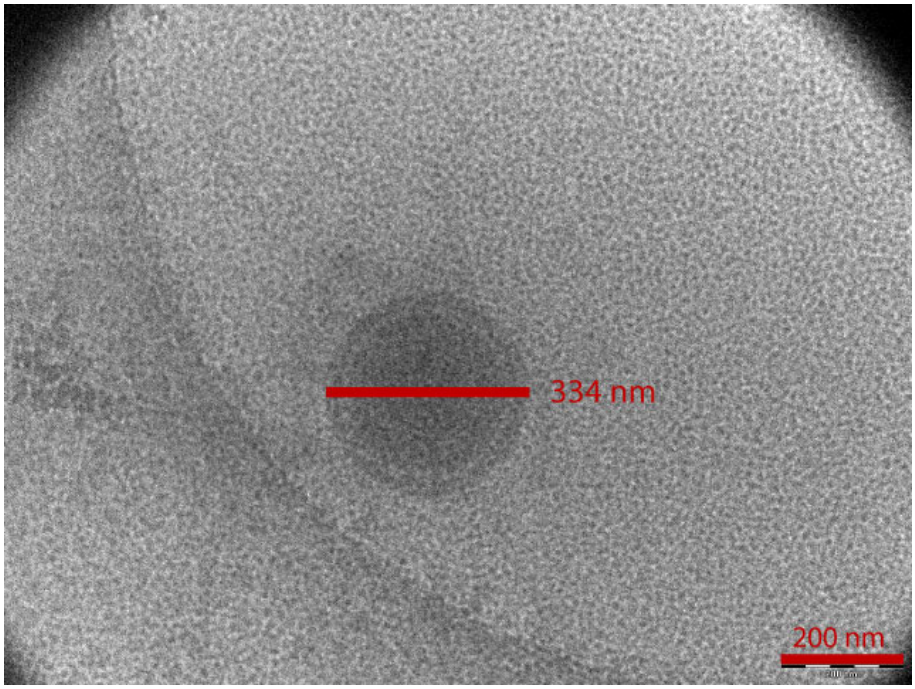

Figure 62 Cryo-TEM image of **PS_{192}-*b*-hypPG$_{110}$** measured in methanol (c≈1.0 g/L).

Figure 62 shows the cryo-TEM image of a **PS_{192}-*b*-hypPG$_{110}$** copolymer dissolved in methanol (c≈1.0 g/L). Visible ring like structure are characteristic for vesicles. The size is very similar to the hydrodynamic radius obtained from DLS. Hence it can be concluded that the block copolymers formed vesicle-like structures in methanol. Unfortunately the time frame of this work did not allow deeper experiments by variation of some parameters like the concentration. Thus these results have to be treated as very interesting but still preliminary results.

4.6. Conclusion

In chapter 3 new methods were presented for the synthesis of PS-*b*-linPG copolymers. These copolymers were well-defined concerning molecular weight and polydispersity. The hypergrafting strategy yielded the corresponding linear-hyperbranched block-copolymers that were also well-defined. The scope of this

chapter was to elucidate the consequences of hypergrafting and the resulting hyperbranched block on supramolecular association.

The data show that hypergrafting is a crucial step if well-defined, monodisperse aggregates are desired. The linear AB as well as the ABA structure were not able to form stable, well-defined superstructures. In case of the ABA structure, a strong gelation tendency additionally limited the possibilities concerning the studies in nonpolar solvents. On the other hand, further studies of the gels and a comparison with known bola-amphiphiles appear to be promising. In contrast the linear-hyperbranched block copolymers formed well-defined, almost monodisperse micellar structures. These micelle structures were very stable for extended periods of time.

It was furthermore found that the micellar size distribution could be improved dramatically by passing the aggregates through an SEC column with large pores. The SEC columns seemed to act like a template in which the aggregates adopt a more stable conformation. Surprisingly the aggregates synthesized under these conditions exhibited UV-vis spectra with multiple UV absorption bands. These “extruded” aggregate conformations were stable for several days even below the critical micelle concentration.

Additionally, the formation of aggregates with PG in the shell was explored. Methanol was identified as a suitable solvent. The aggregates in methanol were less defined in all cases (independent of the copolymer structure). In contrast to the aggregates in nonpolar solvents the aggregates in methanol were identified to represent very large spherical vesicles.

The results presented here are important, as they clearly evidence for the first time that linear-hyperbranched block copolymers are able to form ordered nanostructures in solution.

5. Branched Polydienes

5.1. Introduction

5.1.1. Branched Polymers Based on Common Monomers

Polymers with dendritic structure currently receive considerable attention by many research groups, since their globular structure combined with a high number of functional groups renders them promising for various aspects of materials science.[8] Unfortunately, the structurally perfect dendrimers are usually available in small quantities only, due to the inavoidable multi-step synthesis.[14]

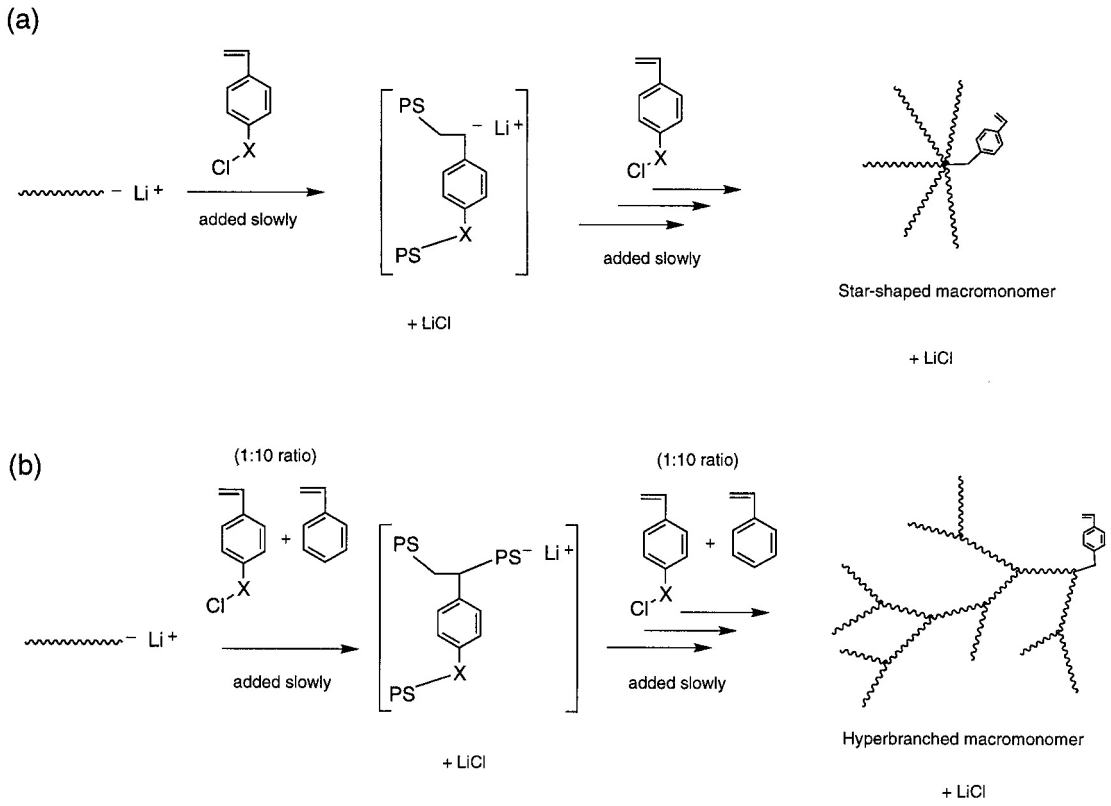

Figure 63 Synthesis of (a) star-shaped polystyrene macromonomer and (b) hyperbranched polystyrene macromonomer. X = $Si(CH_3)_2$ or CH_2.

Therefore, the long-known polycondensation of AB_2-monomers[18] affording branched or “hyperbranched” polymers attracts renewed interest, since these materials combine some of the advantages of dendrimers, i.e., globular structure and high func-

tionality with a synthesis that is straightforward and economical.[26] Improvements in the synthetic procedures for these macromolecules have led to branched polymers with low polydispersity and controlled molecular weights (see chapter 1).

Despite the numerous strategies developed for the preparation of branched polymers in recent years, there are still a limited number of simple synthetic strategies based on common vinyl monomers. Interesting work in this area has been performed by Baskaran[103] and Yan et al.[48] A particularly elegant route for the "convergent construction" of branched structures with narrow polydispersity based on anionic polymerization has been introduced by Knauss et al. (Figure 63).[165,166] The slow addition of a stoichiometric amount of either 4-(chlorodimethylsilyl)styrene or vinylbenzyl chloride as a coupling agent to living polystyryllithium yielded branched polystyrene macromonomers. Star-shaped macromonomers were produced by the addition of the coupling agent alone, and hyperbranched macromonomers resulted from the addition of the coupling agent along with styrene monomer.

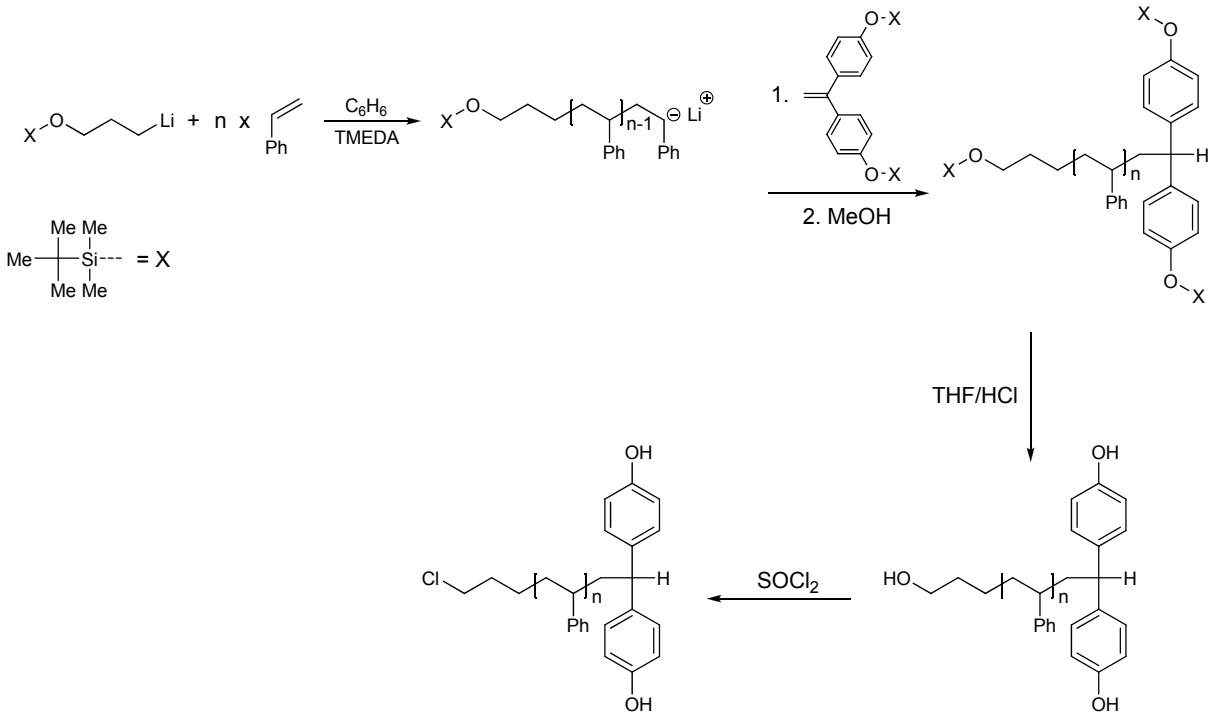

Figure 64 Synthesis of AB_2 Polystyrene macromonomer.

An innovative macromonomer route for branched polymer structures has been presented in a recent work by Hutchings et al.,[104,105] who exploited endcapping of an α-functional, anionically prepared polystyrene with suitable difunctional 1,1-diphenyl-(ethylene) units (Figure 64). In this manner, α,ω-functional AB_2-type macromonomers

were obtained that were converted to branched polystyrene by subsequent poly(benzyl ether) formation (Figure 65, left).

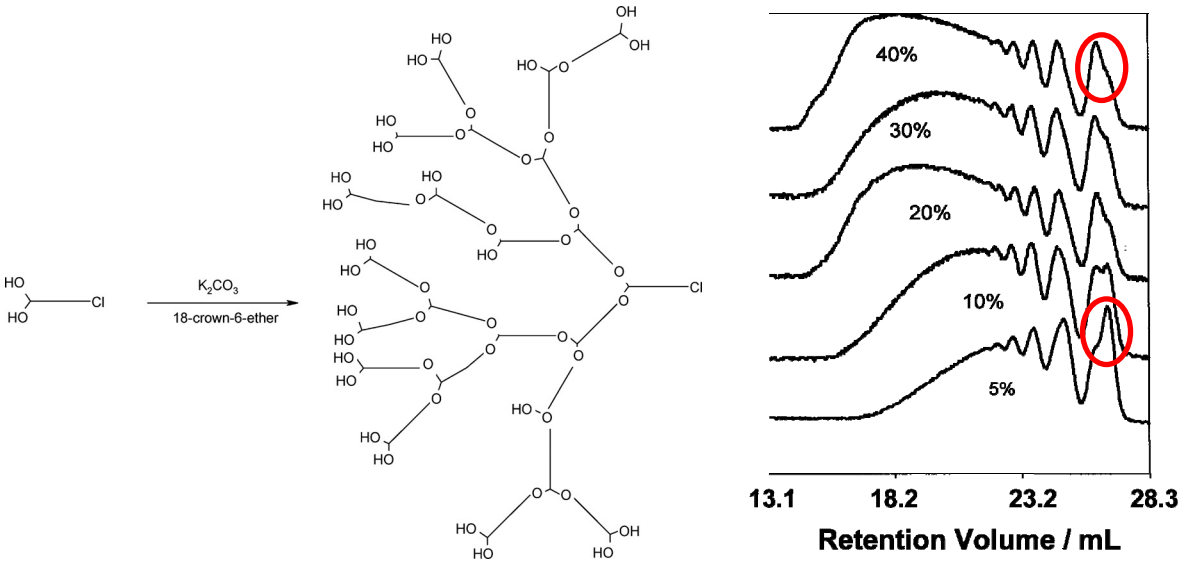

Figure 65 Left: Synthesis of HyperMac from Polystyrene AB_2 macromonomer. Right: SEC chromatograms showing affect of solution concentration w/v on extent of polycondensation and degree of cyclization. As the concentration of solution increases, the extent of polycondensation increases and the degree of cyclization decreases.

Being a very elegant route, it had still some large disadvantages. The conversion or polymerization degree was of course strongly dependent on the macromonomer concentration (Figure 65, right). At very low concentrations the macromonomer tended to form cycles. Concerning SEC the macromonomer peak was shifted to higher elution volumes.[e] At higher concentrations the intramolecular cyclization was strongly lowered, nevertheless the amount of macromonomer was still very high. Additional the synthesis of the macromonomers required already four polymer analogous synthetic steps requiring an expensive endcapping agent, what compensates the elagent route.

[e] The hydrodynamic radius of a cycle is smaller than for the linear analogue.

5.1.2. Metal Catalyzed Hydrosilylation

Hydrosilylation (or hydrosilation) is a term describing an addition reaction of organic and inorganic silicon hydrides to multiple bonds, particularly carboncarbon, carbon-oxygen and carbon-nitrogen. Hydrosilylation was first reported in 1947 by Sommer in the reaction between trichlorosilane and 1-octene in the presence of acetyl peroxide.[167] Later in 1957 Speier reported hexachloroplatinic acid as a very efficient catalyst;[168] this discovery prompted a wide and common application by both academic and industrial synthetic chemists. The next generation of platinum based catalyst was introduced in the late 70s by Karstedt.[169] His so called Karstedt's catalyst is today one of the most employed hydrosilylation catalysts (Figure 66).

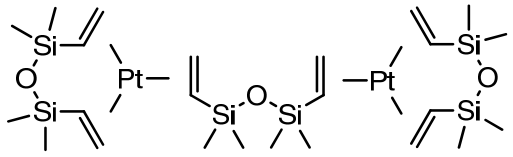

Figure 66 Structure of the Karstedt catalyst.

Two possibilities exist for the addition of a silane R_3SiH to a substituted alkene: namely, Markovnikov or anti-Markovnikov addition mechanism, which results in the formation of branched (α-adduct) and/or linear (β-adduct) products, respectively (Figure 67). It has been shown that the amount of each depends on the catalyst and the nature of the substituents on both the alkene and the silane, but generally the β-adduct tends to predominate.[170,171]

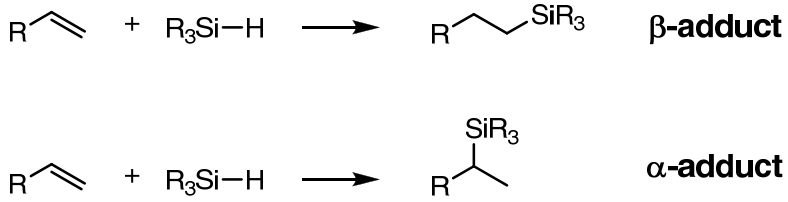

Figure 67 Possible adducts in the hydrosilylation reaction.

A mechanism of hydrosilylation catalyzed by transition metal complexes was proposed in 1965 by Chalk and Harrod (Figure 68).[172] This mechanism was derived originally from the studies of chloroplatinic acid and provided a rational qualitative generalization useful for other transition metal complexes. The mechanistic scheme presents a conventional oxidative addition/reductive elimination sequence to account for the hydrosilylation.

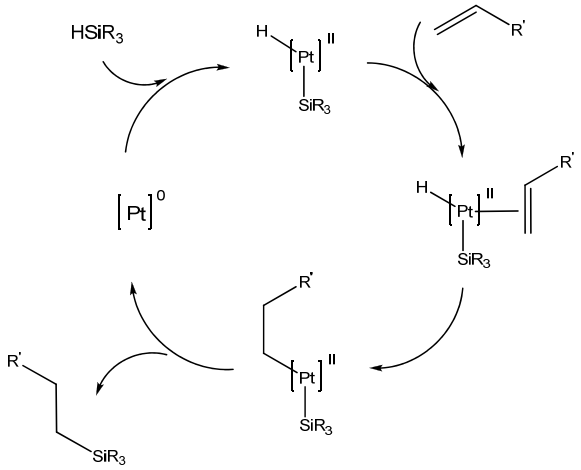

Figure 68 Chalk-Harrod mechanisms for the hydrosilylation of olefins.

The speed for a hydrosilylation reaction is influenced by both components: the olefin and the silane.

Generally electron-rich olefins react faster in a hydrosilylation reaction than electron-poor olefins.[173] The rate of hydrosilylation of haloalkenes is

$$H_2C{=}CH_2 > H_2C{=}F_2 > F_2C{=}CFCl > F_2C{=}F_2$$

The relative rate for alkylsilanes follows the trend:

$$R_3SiH > R_2SiH_2 > RSiH_3$$

Dialkylsilanes (R_2SiH_2) and monoalkylsilanes ($RSiH_3$) can “poison” platinum catalyst by forming chelates, which are more difficult to remove than monohydrides. This results in the observed slower reactions rates for di- and tri-hydrides.[172,174]

In general is the reaction rate for the hydrosilylation increased for silanes bearing electron-withdrawing groups.[173] The relative rates for the hydrosilylation of heptene were found to be

	$HSiCl_3$ >	$HSiEtCl_2$ >	$HSiEt_2Cl$ >	$HSiEt_3$
k_{rel}	3.00	2.64	1.94	1.00

5.2. Synthesis and Properties of Branched Polyisoprenes

In analogy to the work of Hutchings et al. (*vide supra*), yet simplifying the general approach further, a facile two-step synthesis for branched poly(isoprene)s is described here by the polycondensation of AB_n type macromonomers. The synthesis of the macromonomers was conducted in one step by conventional anionic polymerization of isoprene, leading to well-defined polymers with respect to molecular weight and polydispersity (Figure 69). Quantitative end-capping of the polymers was achieved with chlorodimethylsilane. In the resulting AB_n-macromonomers the silane Si-H end-group represents the single A-functionality, while the alkenyl groups of the PI chain represent the B-groups for the ensuing hydrosilylation-based polyaddition that leads to branched polymers.

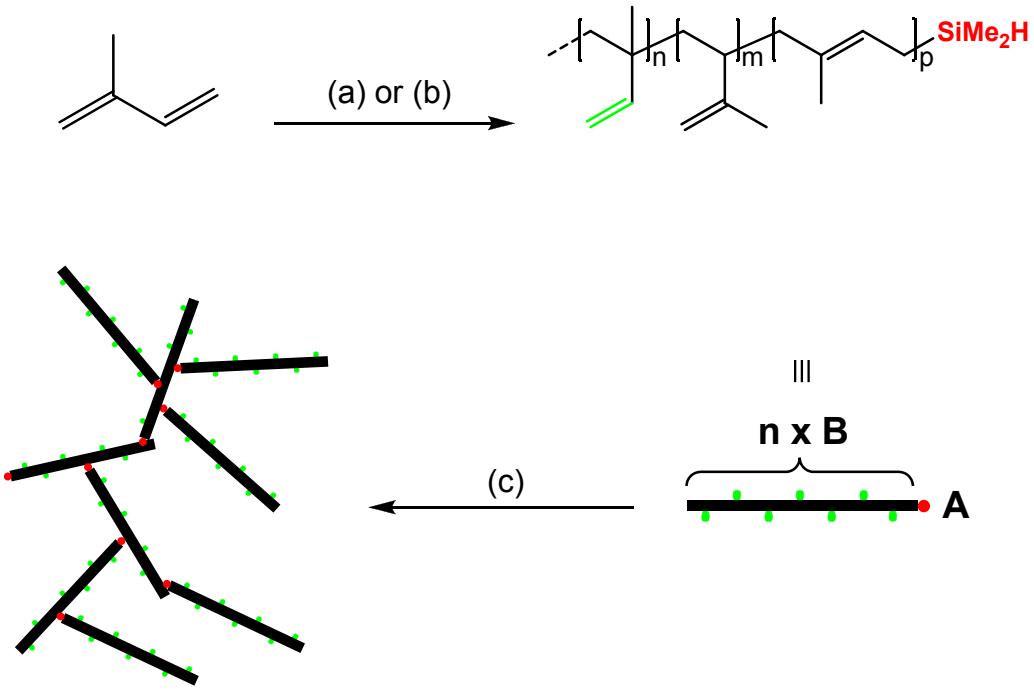

Figure 69 Synthesis and subsequent polycondensation of AB_n macromonomers. a) *s*-BuLi, $HSiMe_2Cl$, cyclohexane; b) *s*-BuLi, $HSiMe_2Cl$, THF; c) Karstedt's catalyst, 100 °C (for solution reactions in 50 wt% toluene).

The structure of polyisoprene (PI) was controlled by the choice of solvent and characterized using ^{1}H-NMR spectroscopy according to literature.[133,175] A series of linear macromonomers **M1-M7** (Table 12) has been prepared in this manner. Depending on the microstructure of PI, macromonomers containing internal (from 1,4- polymerization) or pending alkene groups (from 1,2- and/or 3,4-polymerization) can be obtained. According to Rempel et al., only primary-alkene moieties (resulting from a 1,2- and/or 3,4-polymerization) can react in a hydrosilylation reaction of diene-based poly-

mers.[176,177] Therefore, the microstructure of the PI samples is expected to determine the amount of polymerizable olefinic B-functionalities in the ensuing branching step.

Table 12 Molecular weights, polydispersity, microstructure and viscometry data for macromonomers (**M**) and polymers (**P**), synthesized according to Figure 69.

	SEC[a]		MALLS	NMR[b]					Viscometry[c]			
	M_n gmol^{-1}	PDI	M_n gmol^{-1}	M_n gmol^{-1}	P_n	1,2 m[d]	3,4 n[d]	1,4 p[d]	$\eta_{30°C}$ mLg^{-1}	α	K mLg^{-1}	g'
M1	5 300	1.07	3 600	3 500	51	0	3	48	---	---	---	---
P1-*b*	6 200	1.60	4 100	---	51	0	3	47	---	---	---	---
P1-*s*	5 800	1.26	4 100	---	51	0	3	47	---	---	---	---
M2	1 800	1.07	1 700	1 200	18	5	10	2	3.9	---	---	---
P2-*b*	4 400	2.21	5 600	---	18	6	8	3	5.6	0.29	0.55	0.66
P2-*s*	3 400	2.02	3 200	---	18	5	10	2	4.9	0.33	0.38	0.83
M3	2 400	1.10	2 000	2 100	31	9	18	4	4.3	---	---	---
P3-*b*	6 600	2.63	6 600	---	31	9	16	4	6.6	0.35	0.31	0.70
P3-*s*	4 800	2.11	4 300	---	31	9	16	5	6.9	0.35	0.31	0.97
M4	7 800	1.17	6 400	7 200	106	35	56	14	9.3	---	---	---
P4-*s*	12 000	1.62	10 900	---	106	36	55	14	11.8	0.39	0.31	0.91
M5	17 800	1.08	13 900	12 100	178	71	88	19	14.9	---	---	---
M6	20 700	1.08	16 000	14 400	211	85	109	17	16.6	---	---	---
M7	27 300	1.10	22 100	24 600	361	142	182	37	20.7	---	---	---

[a] vs. polystyrene standards
[b] M_n and P_n are the number averages of the molecular weight and the degree of polymerization determined by end-group analysis.
[c] Mark-Houwink parameters for the linear macromonomers **M2-M7** are α=0.647 & K=0.0317 and were calculated using the molar masses from MALLS (Figure 145, page 185). g' values are average values, including the macromonomer impurity.
[d] For branched polymers these values have to be treated as average values concerning the silane groups.

AB_n-macromonomers with varying amount of B-groups have been prepared. The amount of 1,2-, 1,4- and 3,4- structures in the chains, as determined from ^{1}H-NMR-spectra, is summarized in Table 12. As can be seen, macromonomer **M1** shows an almost exclusive 1,4-microstructure. Thus, macromonomer **M1** consists on average of 3 terminal and 48 internal double bonds and therefore in fact represents an AB_3 macromonomer. In contrast to the microstructure of **M1**, macromonomers **M2-M7** consist mainly of reactive (1,2- and/or 3,4-) double bonds for the hydrosilylation reaction. The microstructure was controlled by solvent variation, i.e., in cyclohexane preferential 1,4-addition was obtained, whereas in THF 1,2- and 3,4-addition predominated.[133]

The synthesis of the branched polymers was carried out by a simple one pot hydrosilylation procedure. Because of the low T_g and low viscosity of the PIs[178] the reaction can be performed in bulk (for low molecular weight PIs) or in solution (hydrosilylation polymerization products are denoted **P-*s*** and **P-*b*** for solution and bulk

polymerizations, respectively). Characterization of the resulting polymers was carried out using SEC, SEC-MALLS, SEC-viscometry and ^{1}H-NMR-spectroscopy. We expected to obtain polymers in which the coiled PI-chains are connected via silane linkages, as exemplified in Figure 69. Using ^{1}H-NMR spectroscopy it was possible to analyze the microstructure of the macromonomers in detail (Figure 144, page 185).[175]

Macromonomer **M1** was not suitable for the polymerisation via hydrosilylation in bulk or in solution. As can be seen in Table 12 (polymers **P1-*s*** and **P1-*b***), the conversion was very low in both cases and led merely to a dimerization product (**P1-*s*** = 18 % and **P1-*b*** = 26 %), which is explained by the low effective B-functionality. The SEC-diagram of **M1** and the corresponding hydrosilylation product is shown in Figure 70 (left). According to ^{1}H-NMR the average pending vinyl functionality is 3 (cf. Table 12). The low conversion is explained on one hand by the unreactive 1,4-microstructure of the polymer, leading to a very low number of B-groups (*vide infra*). In addition, chelation of the Pt-catalyst by the internal double bonds of the macromonomer may contribute to the inactivation observed.

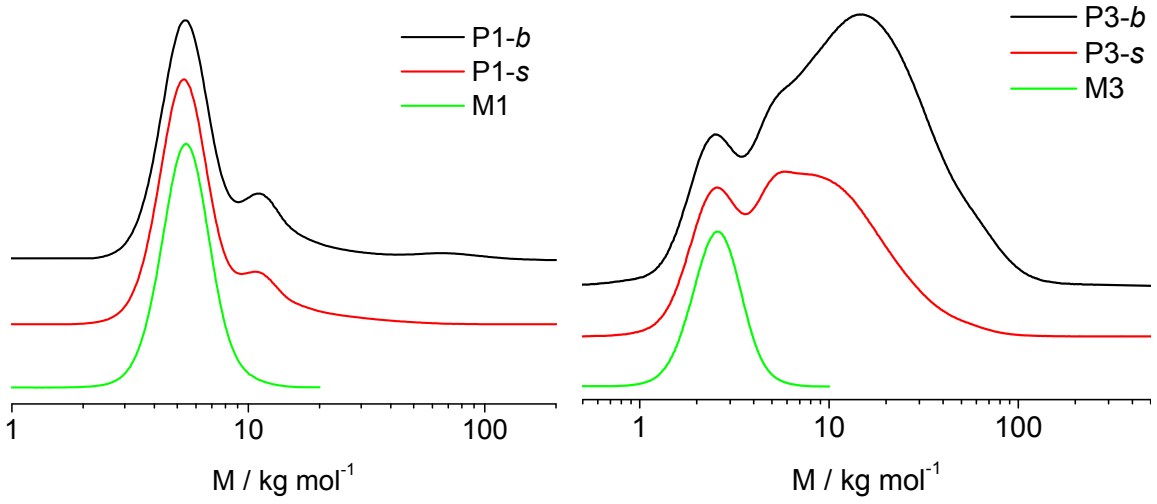

Figure 70 Left: SEC chromatograms of macromonomer **M1** with the corresponding branched poly(isoprene)s prepared in solution (*s*) or bulk (*b*). Right: SEC chromatograms of macromonomer **M3** with the corresponding branched poly(isoprene)s prepared in solution (*s*) or bulk (*b*).

Macromonomers **M2-M4** containing considerably larger amounts of alkenyl moieties than **M1** afforded high molecular weight materials upon hydrosilylation polymerization, as can be seen in Table 12. The SEC-results for polymers **P2-*s*, P2-*b*, P3-*s*, P3-*b*** as well as **P4-*s*** show reasonable conversion to the branched polymers (Figure 71).

Figure 70 (right) exemplifies the SEC-diagrams of **M3** as well as the corresponding branched polymers. Clearly, polymerization of **M3** leads to high molecular weight branched polymers. From SEC a rough estimate of the yield of the Pt-catalyzed hydrosilylation can be obtained, resulting in values of 80% and 85% for **P2-*b*** and **P3-*b***, respectively, but only 25% for **P1-*b***. It is interesting to note that the conversion in solution is always 5-10% lower than in bulk. This effect can be ascribed to the pronounced intramolecular cyclization in solution, leading to the disappearance of the single Si-H functionality.

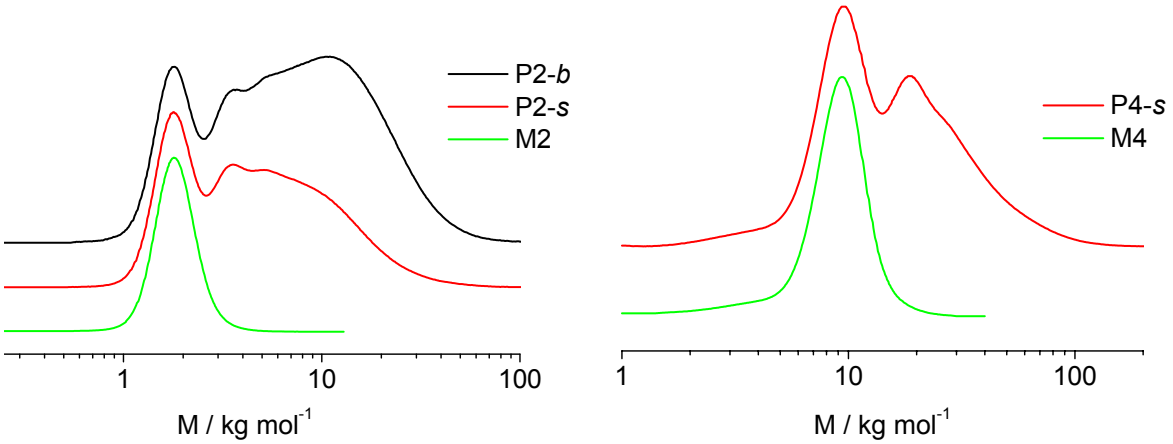

Figure 71 Left: SEC chromatograms of macromonomer **M2** with the corresponding branched poly(isoprene)s prepared in solution (*s*) or bulk (*b*). Right: SEC chromatograms of macromonomer **M4** with the corresponding branched poly(isoprene)s prepared in solution (*s*).

It is important to note that a certain fraction of the macromonomer is still present in all samples, as it is obvious from SEC-analysis. This is in agreement with the above-mentioned results of Hutchings et al.[104] However, on the base of our data we are unable to conclude, whether this mode is due to unreacted or cyclized macromonomer structures in our system. For our materials SEC analysis does not show a shift of the macromonomer peak to lower apparent molar masses, caused by ring closure as reported by Hutchings et al. for branched polystyrenes.[104] ^{1}H-NMR-analysis does not reveal the presence of unreacted silanes that would permit to compare the conversion estimated from SEC with values obtained from NMR. Polymers **P2-*b*** and **P3-*b*** show apparent PDIs close to 2 (SEC). Macromonomer **M4**, which could not be bulk-polymerized due to its high viscosity, led to branched polymer **P4-*s*** with the lowest PDI (1.62), which is most likely a result of its limited conversion of approximately 50%.

In addition to the structure, the molar mass of the macromonomers also had a strong influence on the conversion and consequently on the molecular weights of the result-

ing branched polymers. High molecular weight macromonomers like **M4** led to low conversion, which can be explained by shielding of the single Si-H end-group by the polymer coil. In addition, it is likely that larger coils impede intermolecular reaction and favor an intramolecular ring closure. Macromonomer **M2**, which was the lowest molecular weight structure employed in this study, led to lower conversion compared to **M3**, presumably due to the presence of a lower number of vinyl groups than for the higher molecular weight macromonomers. The relationship of the conversion and the molar mass is nonlinear and may well show an optimum at moderate chain lengths. The decrease of conversion with increasing molar mass is ascribed to the enhanced viscosity in such systems and might be optimized by further variation of the hydrosilylation conditions.

It is a well known fact that the intrinsic viscosities of branched polymers are lower in comparison to their linear analogues.[14,179] This is attributed to the higher compactness of the structure. Thus, a branched polymer elutes later in a SEC measurement than its linear analogue because of the lower hydrodynamic radius.

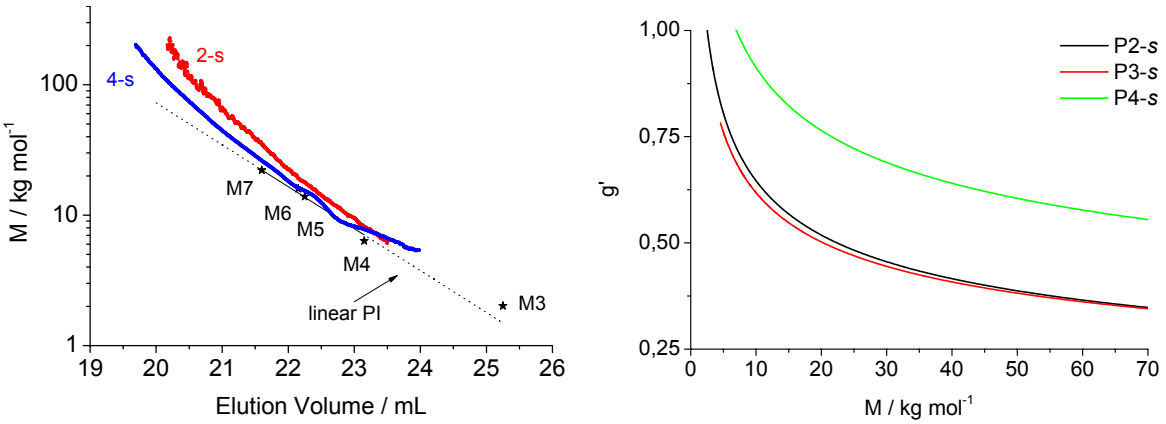

Figure 72 Left: molar mass vs. elution volume as calculated by SEC with MALLS detection for macromonomers **M3-M6** (stars) and branched analogues **P2-*s*** and **P4-*s*** (solid lines). A linear least square fit was performed for macromonomers **M4-M7**. Right: branching ratio dependence on the molar mass of the branched PIs **P2-*s*** to **P4-*s*** based on equation (5.3).

Figure 72 (left) shows the SEC calibration curve for the linear polymers **M4-M7**. The lower molecular weight samples **M2** and **M3** were not used for the calibration, because the SEC-columns only exhibit a linear dependence between 5 000 and 100 000 g/mol (approximately). A MALLS detector renders it possible to obtain absolute molar masses of polymers for each point of the elugram. It is obvious that at equal elution volume the branched polymers possess higher molar mass. This already represents evidence for the branched structure of the poly(isoprene)s pre-

pared. Furthermore, the branched materials obtained from lower molecular weight macromonomers (**2-*s***) exhibit higher apparent molecular weights at the same elution times than the branched polymers based on higher molecular weight macromonomers (**4-*s***). This is in line with expectation, since the branched polymer **4-*s*** contains more linear segments than polymer **2-*s*** with the same molecular weight.

To obtain further confirmation for these conclusions regarding the branching pattern, online SEC-viscometry measurements have been performed for all materials (except **M1**, **P1-*b*** and **P1-*s***). With the so called "Triple Detection Method" it is possible to obtain the intrinsic viscosities of the polymers during elution and correlate them to the corresponding molar masses obtained by MALLS.[f] According to Burchard et al. one can quantify the extent of branching by comparison of the intrinsic viscosities, leading to the so called g' parameter, as shown in equation (5.1):[31]

$$g' = \left(\frac{[\eta]_{br}}{[\eta]_{lin}} \right)_M \tag{5.1}$$

The average g' parameters (Table 12) demonstrate that with increasing macromonomer size the obtained branched structures become less compact, as already qualitatively observed (*vide supra*). The deviation from this trend observed for **P4-*s*** can be explained by the high amount of macromonomer in the respective polymer mixture. Generally, the comparison of the bulk reactions with reactions using a solvent shows that the obtained branching ratios are lower under bulk conditions. This also supports the assumption that under bulk conditions the amount of cyclization should be lower, leading to higher conversion and increasingly dense structures.

A plot of the molar mass versus the g' parameter (Figure 72, right) shows that even at low degrees of polymerization low values are obtained. This finding is of particular interest, since the synthesis of branched high molecular weight polymers is not in all cases trivial and/or straightforward. From this plot also polymer **P4-*s*** can be clearly identified as being less branched in comparison to the other branched materials obtained.

Another possibility to give a qualitative assessment concerning the extent of branching is the comparison of the α-parameter of the Mark-Houwink Equation (5.2) of the branched polymers with the respective linear analogue, as shown by Müller et al.[180]

$$[\eta] = KM^{\alpha} \tag{5.2}$$

[f] More detailed information can be found in chapters 1.3.3. and 4.1.

In this case, branched polymers show α-parameters below 0.5 because of their compact structure.[g] The Mark-Houwink-Parameters obtained for the branched PI-samples are summarized in Table 12 and are clearly lower than the α-parameter for the linear analogue (α = 0.647). These results are in line with the trend for the g' parameters. Interestingly, branched polymers based on the macromonomers **M2** and **M3** exhibit α values that are similar to those reported for hyperbranched polymers based on AB_2-monomers.

5.3. Olefin Reactivity of Polyisoprenes

As mentioned above the overall conversions for the polymerization of the polyisoprene macromonomers was rather low. As described in chapter 5.1.2. it is useful to use electron-rich olefins for hydrosilylations.

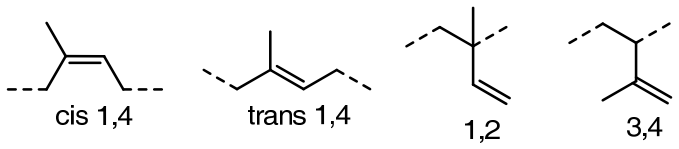

Figure 73 Structural units in polyisoprene.

In polyisoprene are four structural units found (Figure 73), whereby the relative distribution is adjustable concerning the reaction conditions (*vide supra*). Concerning a hydrosilylation only the 1,2 or 3,4 units were suitable. Concerning literature the 3,4 unit should be more reactive as the electron density should be there higher.

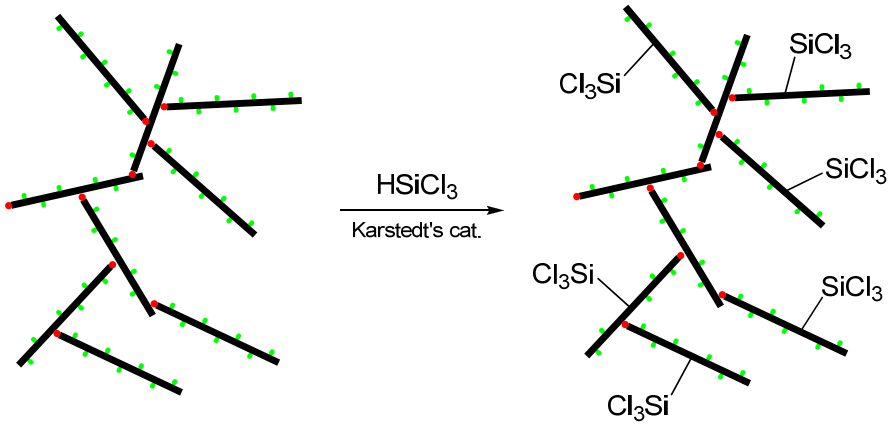

Figure 74 Functionalization of branched PI with trichlorosilane.

[g] In the appendix a Mark-Houwink plot for the branched polymers can be found (Figure 146, page 186)

To prove whether the 1,2 or 3,4 units were more reactive it was tried to functionalize a branched polyisoprene with trichlorosilane (Figure 74).

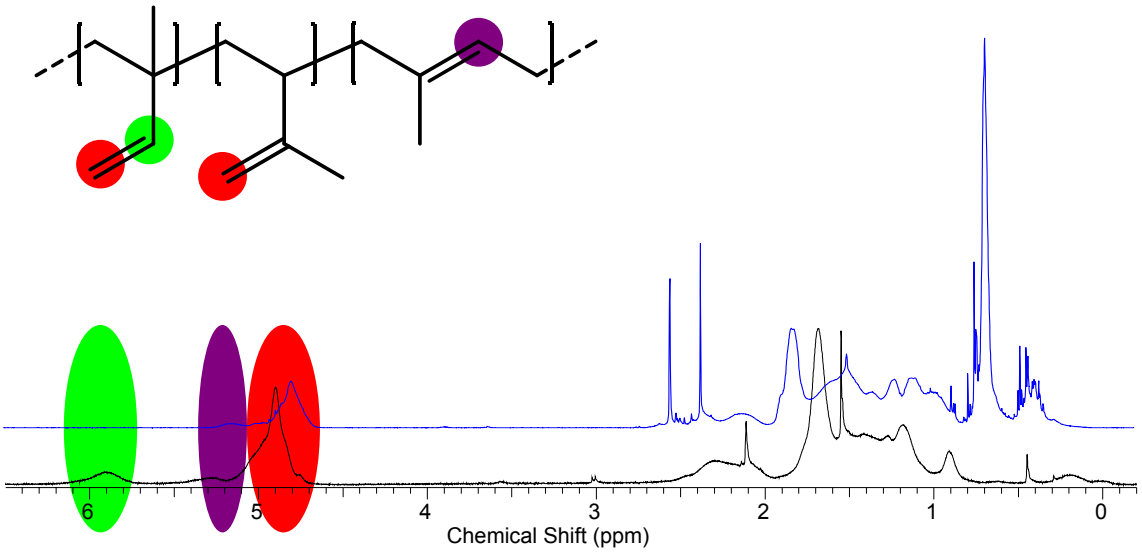

Figure 75 ^{1}H-NMR spectrum of a branched PI (black line) and a trichlorosilane functionalized branched PI (blue line).

Figure 75 shows the ^{1}H-NMR spectrum of a branched PI (black line) and a trichlorosilane functionalized branched PI (blue line). Even with high excess of trichlorosilane the 3,4 units were untouched. Only the 1,2 units seem to be suitable for a hydrosilylation. Concerning literature the addition to the 3,4 unit should be possible.[173] Nevertheless, it could be possible that the Karstedt's catalyst is more easily trapped in the branched structure of PI, reducing thereby the activity. However, this special feature could not be investigated in more detail in the timescale of this work.

As conclusion of this experiment the macromonomer route studied in chapter 5.2. was applied for polybutadiene macromonomers.

5.4. Synthesis and Properties of Branched Polybutadienes

The synthesis of the macromonomers was conducted in one step by conventional anionic polymerization of 1,3-butadiene in analogy to the synthesis of polyisoprene (*vide supra*), leading to well-defined polymers with respect to molecular weight and polydispersity.[181] The reaction conditions were chosen in such a way that 90% of the

monomers were incorporated in 1,2-addition mode, i.e., THF was used as solvent for the reaction.[133,175]

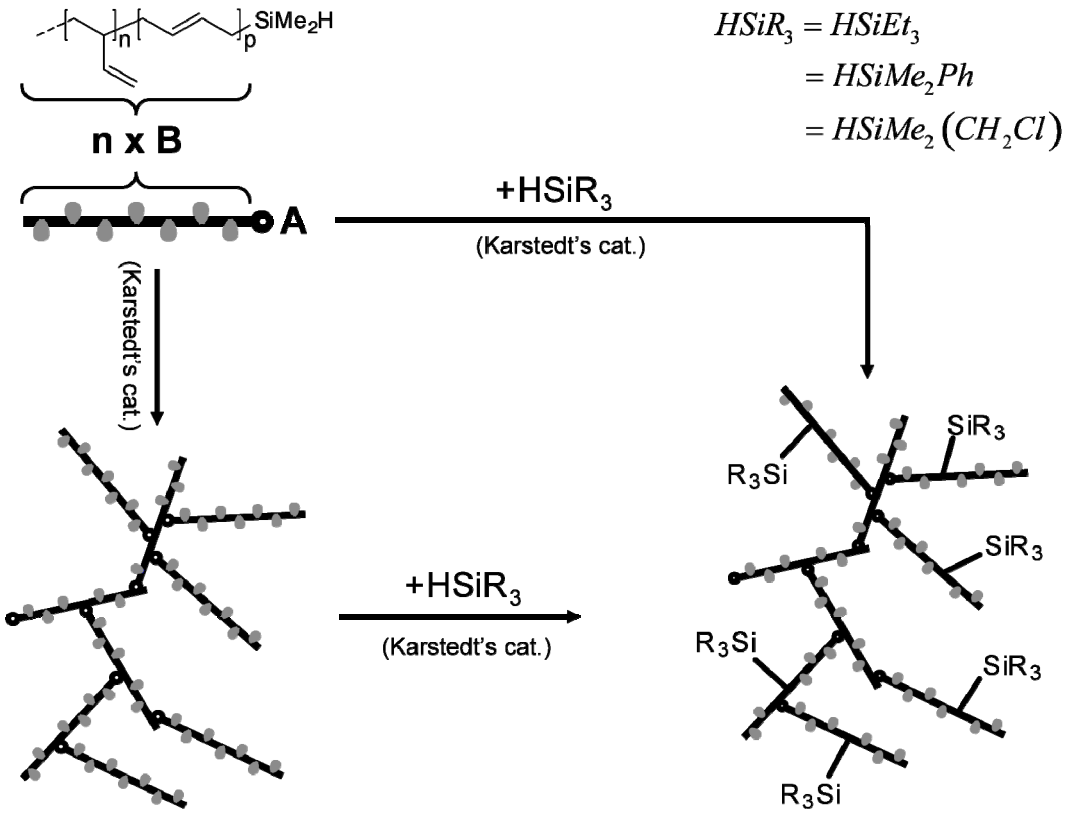

Figure 76 Possible pathways to functional branched polybutadienes.

Quantitative endcapping of the polymers was achieved using chlorodimethylsilane. Figure 76 shows the general strategy to obtain polybutadiene-based branched polymers. In the resulting AB_n-macromonomers the silane endgroup represents the single A-functionality, while the pendant vinyl groups of the polybutadiene chain represent the B-groups for the ensuing hydrosilylation-based polyaddition that leads to the targeted branched polymers. The hydrosilylation polyaddition was carried out via the convenient one-pot procedure mentioned above. Because of the low T_g and viscosity of the polybutadienes it was possible to perform the reactions under bulk conditions, reducing the probability for intramolecular reactions dramatically.[104,178] Using polybutadiene in comparison to polyisoprene also had the important advantage of a much higher amount of reactive double bonds. This advantage was used to introduce large amounts of functional silanes into the branched polybutadiene structure via a "pseudo copolymerization" approach.

Figure 77 (left) shows the ^{1}H-NMR of the macromonomer and the branched final product.

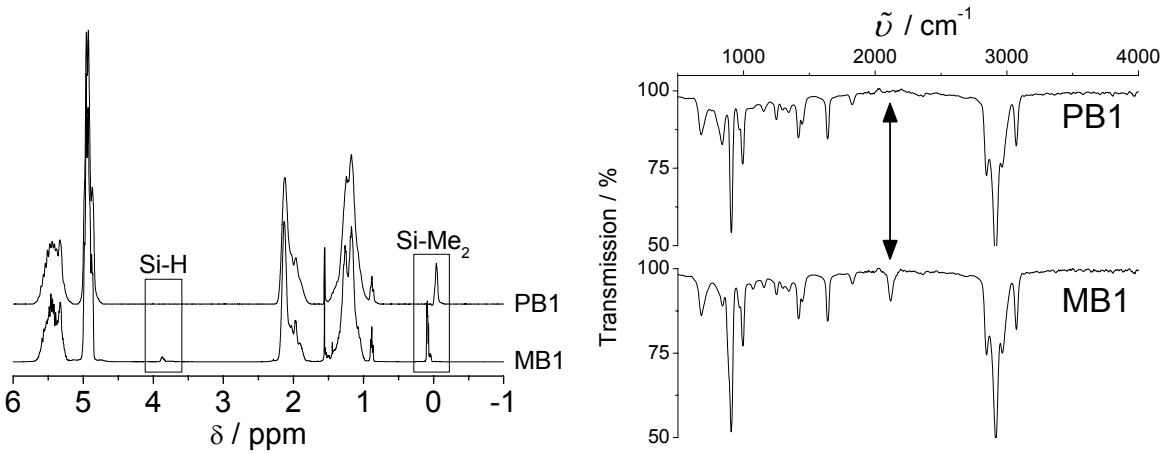

Figure 77 ^{1}H-NMR in $CDCl_3$ (left) and IR spectra (right) of the macromonomer **MB1** and the corresponding branched polymer **PB1**.

There are two resonances that can be monitored to confirm completion of the reaction. At 3.87 ppm the silane proton of the macromonomer can be observed. After the hydrosilylation polymerization this signal disappears. Concerning signal intensity the signals of the two methyl groups are much stronger; thus these six protons were also used to calculate the molar mass. From this signal it could be observed that the signal of the macromonomer was shifted to higher field from 0.09 ppm to -0.04 ppm.

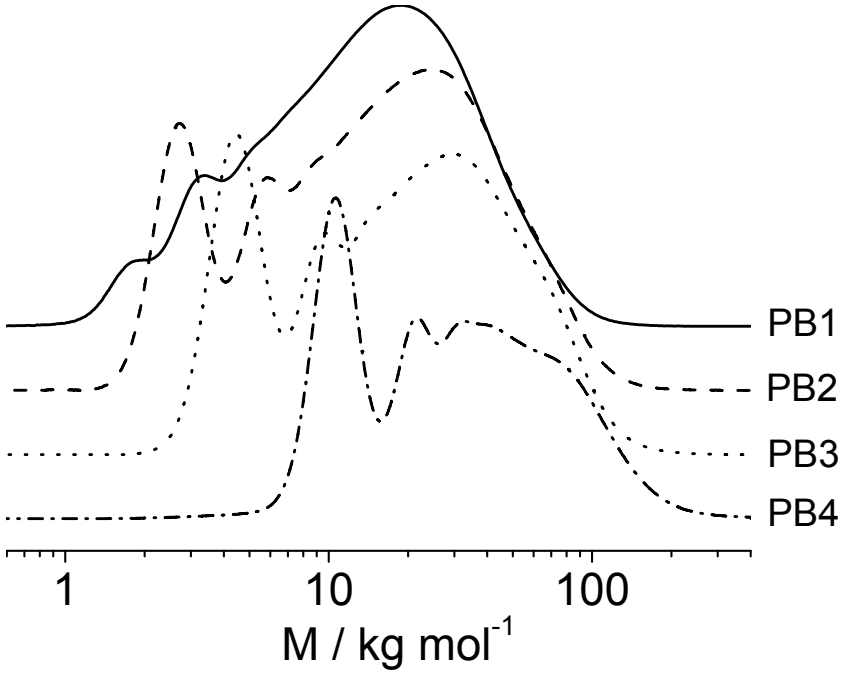

Figure 78 SEC chromatogram of branched polybutadienes prepared from different macromonomers.

This can be explained by the inductive effect of the additional alkyl substituent on the silicon atom after hydrosilylation. Because the branched polymer possesses no characteristic endgroups, the molar masses can not be calculated anymore (analogous to PI based branched polymers). Unfortunately it is not possible to distinguish between

intra- or intermolecular reactions by NMR techniques. In this case an SEC experiment was used in order to obtain qualitative information concerning the regioselectivity of the hydrosilylation. Additionally an IR experiment (Figure 77, right) proved full conversion of all hydrosilanes by the lack of a Si-H resonance after reaction.

Figure 78 displays the SEC chromatograms of branched polybutadienes formed from macromonomers with different molecular weights. The molecular weight of the macromonomer was increased from **PB1** to **PB4**. It is obvious that the fraction of the low molecular weight shoulder increases upon using higher molar mass macromonomer. When looking at polyadditions of AB_n–type macromonomers, cyclization is always observed. Of course, this undesired side reaction lowers the amount of polyaddition in general. It may be mentioned that the smallest macromonomer (M_n=1 300 g/mol) shows almost no cyclization, while the largest macromonomer with M_n=6 500 g/mol shows ca. 38% of cyclized polymer, as calculated from the respective SEC elugrams. Obviously, by increasing the number of B-functionalities in comparison to the A-functionality the probability for intramolecular hydrosilylation increases strongly. In the SEC analysis the materials do not show a shift of the macromonomer peak to lower apparent molar masses, caused by ring closure as reported by Hutchings et al. for branched polystyrenes.[104] Therefore the formation of rather small cycles that do not change the hydrodynamic radii of the polymer extensively was assumed.

By coupling of the SEC system with a multi angle laser light scattering (MALLS) detector it was possible to determine the absolute molar mass for every point of the elution curve. In general, branched macromolecules exhibit a more compact structure than their linear analogues, which enables one to compare the branched macromolecules with the corresponding linear ones. Linear polybutadienes (macromonomers **MB1** to **MB5**) were used to compare the elution volume with the branched polybutadiene (**PB3**) (Figure 79). The branched polybutadienes show significantly higher molecular weights than their linear analogues. This is clear evidence for the more compact structure.

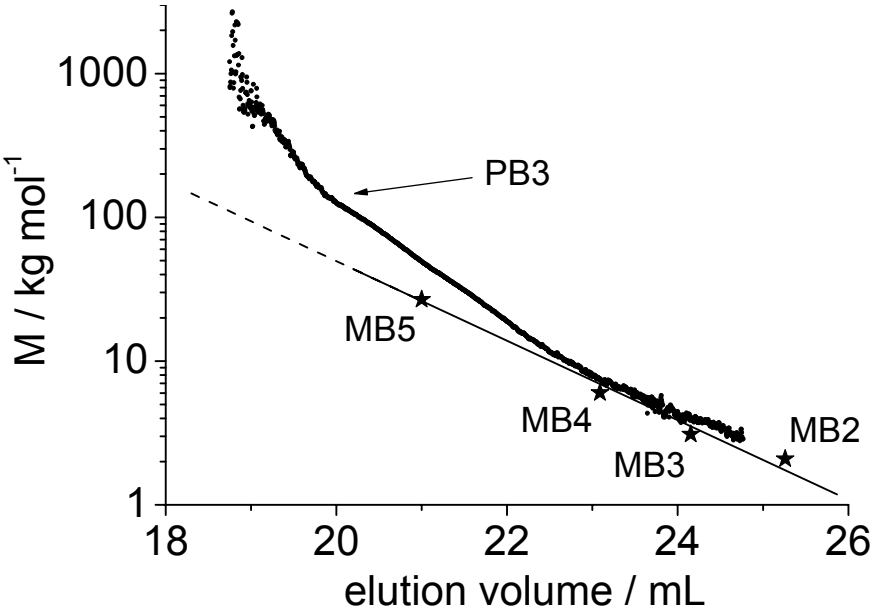

Figure 79 Molar mass versus elution volume obtained by SEC/MALLS.

Table 13 shows the molar masses determined in this manner. The degree of polymerization is highest for **PB1** and drops with increasing macromonomer length. Related to the high amount of monocyclic macromonomer it appears that low degrees of polymerization are obtained, especially for **PB4**. Calculating the molar masses without the macromonomeric species emphasizes the branched character of the high molecular weight fraction (marked by an asterisk).

Table 13 Molecular weight, polydispersity, and Intrinsic viscosity data for branched polybutadiene synthesized from the respective macromonomers

	SEC[a]			**NMR**[b]	**MALLS**[c]		**Viscosimetry**[d]			**DSC**[e]
#	M_n	PDI	Cycl.	M_n	M_n	P_n	[η]	α	g'	T_g
MB1	1 600	1.11	---	1300	1 300	---	3.6	---	---	
PB1	8 100	2.35	6%	---	9 100	7.0	6.9	0.30	0.53	-34
MB2	2 400	1.07	---	1800	1 800	---	4.5	---	---	
PB2	8 100	2.26	17%	---	8 600	4.7	8.9	0.30	0.72	-27
PB2*	14 200	1.85	---	---	14 500	8.1	8.9	0.28	0.51	---
MB3	4 700	1.06	---	2400	2 300	---	6.5	---	---	
PB3	10 900	2.46	24%	---	8 600	3.7	9.0	0.33	0.72	-21
PB3*	18 500	1.74	---	---	19 600	8.5	13.1	0.29	0.62	---
MB4	9 900	1.06	---	6700	6 500	---	10.2	---	---	
PB4	20 000	2.04	38%	---	13 000	2.0	15.0	0.38	0.93	-17
PB4*	33 500	1.53	---	---	34 200	5.3	20.3	0.31	0.68	---
MB5	33 300	1.06	---	---	26 800	---	25.5	---	---	

* Excluding the macromonomer peak. [a] In g/mol vs. polystyrene standards. Degree of cyclization. [b] M_n (g/mol) and P_n determined via endgroup analysis from ^{1}H-NMR. [c] polymers were measured using dn/dc = 0.108. M_n in g/mol. P_n concerning macromonomer. [d] [η] in mL/g. α and g' by applying equations (1) and (3). [e] T_g in °C

By excluding the cyclic "macromonomer impurity" the degree of polymerization rises slowly from 7.0 to 8.5 with macromonomer mass and then drops to 5.3 for the largest macromonomer. This finding is in agreement with observations in literature.[181] Of

course parameters like chain length and viscosity are very important with respect to the degree of polymerization. In case of very large macromonomers the polymerization terminates sooner because of the higher viscosity. In this case, the amount of cyclic sideproducts is particularly high.

To obtain further confirmation for our structural conclusions, additionally online SEC-viscosimetry measurements have been performed for all polymers. With the so-called "triple detection method" it was possible to obtain the intrinsic viscosities of the polymers during SEC and correlate them to the corresponding molar masses obtained by MALLS. In this manner a qualitative assessment concerning the extent of branching by comparison of the α-parameter of the Mark-Houwink equation (*vide supra*) In general the values for α are significantly lower than 0.5, which is characteristic for branched architectures because of their more compact structure (*vide supra*).

Figure 80 shows the KMH-plot for the macromonomers **MB1** to **MB4**. Calculated KMH-parameters from this plot (K = 0.04297 mL/g, α = 0.627) were in agreement with the literature.[182] The Mark-Houwink-Parameters measured for the branched polymers are lower than 0.5, supporting a branched structure (Table 13). Also here the obtained α-parameters were similar to the values from hyperbranched polymers based on AB_2 monomers (*vide supra*).[182]

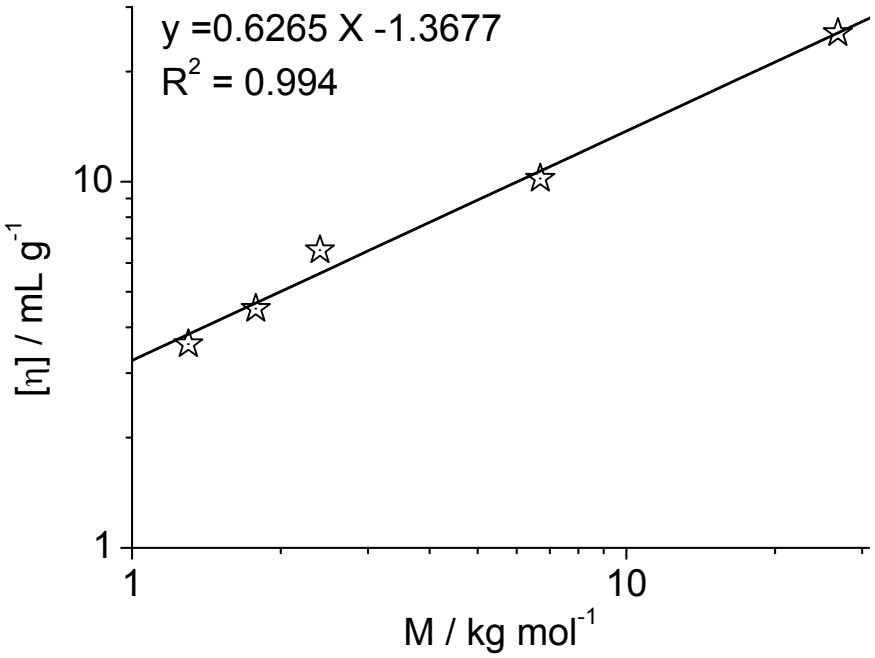

Figure 80 KMH plot of the macromonomers (**MB1** to **MB4**)

The values were all in the range from 0.3 to 0.4 without being strongly influenced by residual macromonomer impurities. However, the α–parameter is very sensitive to

branching and even a very low amount of branched material reduces its value drastically (*vide infra*). Thus, this parameter gives only an indication concerning the extent of branching.

The g' parameter yields more precise information about the extent of branching (*vide supra*). The values obtained from equation (5.1) are lower than 1, because branched polymers generally exhibit lower viscosities than their linear analogues (*vide supra*). Combination of (5.1) and (5.2) yields:

$$g' = \left(\frac{[\eta]_{br}}{K \cdot M^{\alpha}} \right)_M \tag{5.3}$$

where *K* and α are the values obtained from the macromonomers. The same trends were found for the α parameters (Table 13). Nevertheless the g'-parameter is influenced much stronger by residual macromonomer. It is obvious that with increasing size of the macromonomer also the g'-parameter increases. This is in agreement with expectation, because branched polymers synthesized from larger macromonomers possess longer linear segments than branched polymers with the same molecular weight prepared via polymerization of lower molecular weight macromonomers. The plot in Figure 81 shows the evolution of the g'-parameter with respect to molar mass for the branched polymers **PB1** and **PB4**. This plot also shows that polymers based on smaller macromonomers have higher degrees of branching.

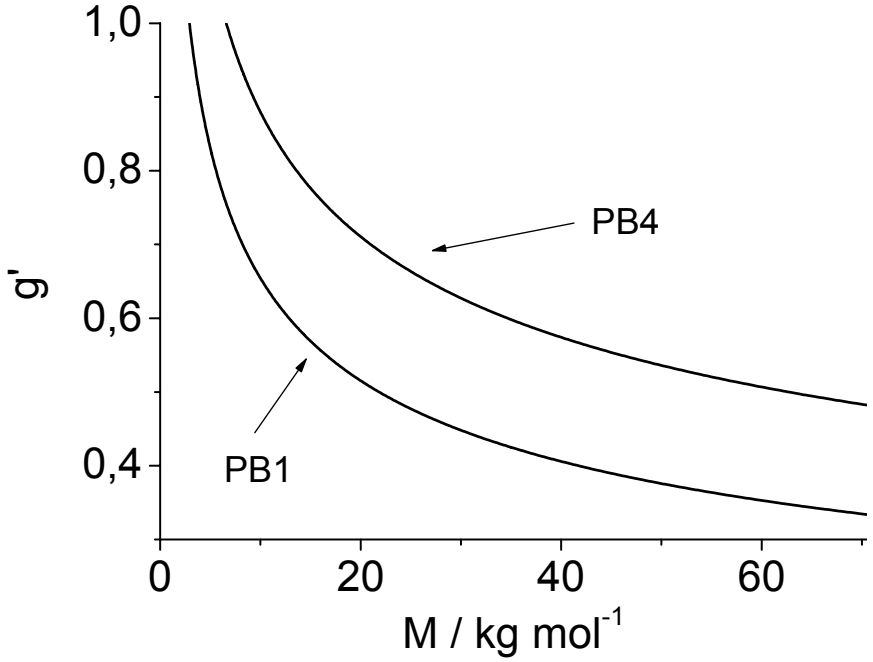

Figure 81 Plot g' versus molar mass.

To obtain more information about the branching reaction a kinetic study was performed to optimize the reaction conditions. Crucial information on the rate of the branching reaction was obtained. Usually polymerizations based on hydrosilylation reactions are very slow, and even at elevated temperatures they may require more than 24 hours to proceed to completion.[19] It is well known that catalysts such as the Karstedt catalyst can decompose at elevated temperatures when using prolonged reaction times.

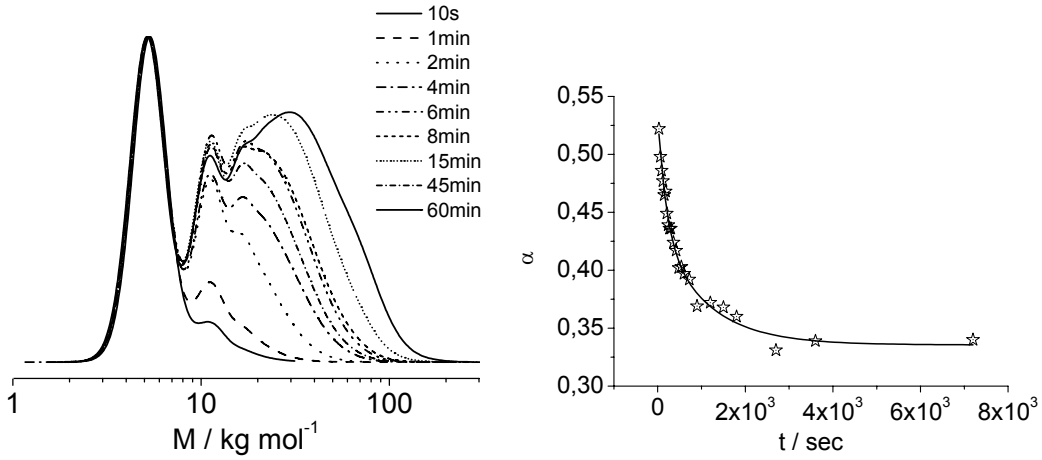

Figure 82 SEC elugrams after different time intervals during polymerization of **MB3** (left) and evolution of the KMH parameter α with time (right)

Figure 82 (left) shows the SEC elugrams after various time intervals during polymerization of **MB3**. Reaction times exceeding 60 minutes did not enhance the degree of polymerization according to SEC. On the other hand, decomposition of Karstedt's catalyst is likely after 60 min at these conditions. However, experiments showed that the polymerization did not continue after the addition of small aliquots of Karstedt's catalyst. Viscosity measurements show an exponential decay for the Mark-Houwink-parameter α during the reaction (Figure 82, right), reaching a plateau at α = 0.33. The large fraction of vinyl groups may be an important factor for this strong decrease in polymerization time in comparison to other hydrosilylation reactions.

The results on the degree of branching obtained by viscometry are supported by differential scanning calometry (DSC) measurements. Table 13 shows that with increasing macromonomer length the glass transition temperature (T_g) increases to higher values. This phenomenon is known in literature for brush- or bottlebrush-type polymers synthesized by a macromonomer approach.[30] In this case, the T_g is predominantly determined by the excess free volume effect of end group per unit MW. Generally, the T_g was found to decrease with decrease of the molecular weight of the

macromonomer and also that of polymacromonomers. Another possible explanation was obtained by Frey et al. from linear poly(L-lactide)/branched poly(L-lactide) co-polyester blends. For these materials the T_g is lowered with increasing degree of branching.[183] The simultaneous decrease of the glass transition temperature and the molar mass of the macromonomer could be a sign for an overall lower degree of entanglement.

5.5. Functionalized Polybutadienes Based on Common Silanes

The branched polybutadienes still bear many reactive vinyl groups, which renders them interesting for further investigation and modification. To increase the range of possible applications for the materials, various functional groups have been introduced by the use of commercially available functional silanes. There are two possible pathways for the introduction of functional groups (Figure 76); the “classical” route is the synthesis of the branched polymer at first and subsequent modification. This route clearly possesses the disadvantage that the polymer has to be worked up twice, and also the expensive platinum catalyst has to be used in both reactions. The second route is based on a concurrent “pseudo-copolymerization” of the macromonomers with the functional low molecular weight silane, formally an AB_x + A´ type polymerization. Employing this method, a complete step can be economized.

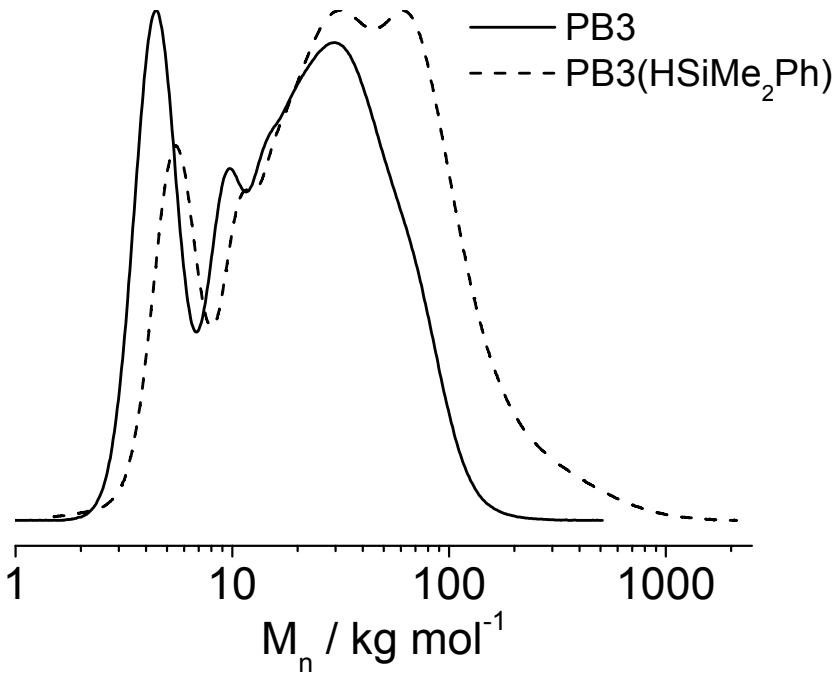

Figure 83 SEC-elugrams for a PB3 before and after functionalization with dimethylphenylsilane.

Using the “classical” two step route at first, as expected polymers with a very broad molecular weight distribution were formed. Figure 83 shows the SEC-elugrams for a branched polybutadiene before and after modification with dimethylphenylsilane. It is obvious that the molecular weight increased, but polydispersity increased as well (from 2.4 to 3.2).

The direct route via the “pseudo-copolymerization” method was more convenient (Figure 76). Interestingly even a relatively large amount of monofunctional silane $HSiR_3$ (up to 50 wt.-%) did not disturb the polyaddition process with respect to the degree of branching and molecular weight. Employing more than 50 wt.-% silane led only to low-molecular weight cyclization of the macromonomers. In summary, modified branched polybutadienes were very easily accessible by the concurrent polyaddition of (functional) silanes and the AB_n-type macromonomers.

Three different silanes were chosen as model compounds to study copolymerization. Modification with triethylsilane affords a polymer similar to a polycarbosilane. High degrees of functionalization could yield a material with low T_g and good chemical resistance.[173] In pronounced contrast, chlorodimethylsilane introduces a second functional group to the branched polybutadienes, making it possible to perform a variety of modifications based on nucleophilic substitution reactions. Finally, dimethylphenylsilane was a model compound for bulky silanes containing aromatic groups.

The degree of functionalization could be easily controlled by the stoichiometric addition of the silane into the reaction mixture. Even a relatively high amount of new silicon-carbon bonds could be achieved in this manner. The resulting polymers combined characteristics of a polydiene and the respective polycarbosilane.

The degrees of functionalization could be determined by ^{1}H-NMR spectroscopy to obtain the number of functional units per macromonomer. Figure 84 shows the ^{1}H-NMR spectrum of **MB2** copolymerized with different amounts of dimethylphenylsilane. The incorporated fraction of the silane could be determined by integration of the proton signals of the methyl protons from the macromonomer-silane at -0.04 ppm and the new methyl groups introduced by the dimethylphenylsilane at 0.27 ppm.

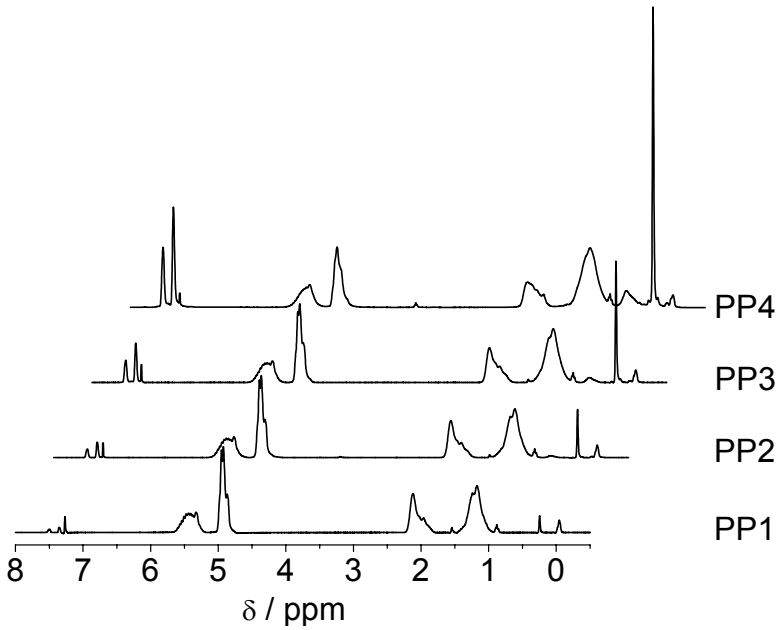

Figure 84 ^{1}H-NMR spectrum of **MB2** copolymerized with different amounts of dimethylphenylsilane.

Table 14 shows the data for simultaneous modification during the branching reaction for macromonomer **MB2** with triethylsilane, dimethylphenylsilane and (chloromethyl)dimethylsilane. Simultaneous functionalizations were carried out using the same conditions as for the branching reaction alone. In case of triethylsilane, the reaction temperature was reduced to refluxing conditions because of its low boiling point.

Table 14 Molecular weights, polydispersity, and viscosimetry data for functionalized branched polybutadienes synthesized using macromonomer **MB2**

	NMR[a]		SEC[b]		MALLS	VISCO[c]	DSC[d]
#	eqv.	wt.-%	M_n	PDI	M_n	α	T_g
PE1	0.5	2.4	8 600	2.29	8 740	0.36	-24
PE2	4.5	17.9	12 500	2.07	9 300	0.38	-24
PE3	12	36.8	8 500	1.96	11 900	0.36	-24
PE4	27	56.7	11 400	1.66	10 400	0.40	-24
PP1	1.0	5.4	11 000	2.06	8 800	0.39	-19
PP2	5.0	10.2	11 000	2.07	7 200	0.41	-19
PP3	10	20.4	11 100	2.12	7 300	0.40	-17
PP4	20	47.4	12 000	2.24	11 000	0.41	-21
PC1	5	18.5	7 000	2.02	8 250	0.35	-26
PC2	15	40.4	8 500	1.91	10 200	0.35	-29

[a] Equivalents and weight percent silane incorporated per macromonomer. [b] In g/mol vs. polystyrene standards. [c] α by applying equation (1). [d] T_g in °C

The molecular weights obtained were in the same range as for **MB2** alone. For all cases in this study the degree of polymerization was not affected by the presence of monofunctional silanes up to 50 weight percent of the polymer. Relying on the α-parameter, all polymers were still branched. Nevertheless all values were slightly higher than in the non-functionalized polymers. Copolymerization of the silane component may have reduced the degree of branching slightly as expected when working under solution conditions.[181]

Branched polybutadienes containing triethylsilane or (chloromethyl)dimethylsilane did not modify the T_g in comparison to **PB2** significantly. This is probably due to the chemical similarity of these structures with the backbone. In case of dimethylphenylsilane the T_g was enhanced slightly. This is explained by the lower mobility caused by the more bulky aromatic phenyl groups.

5.6. Functionalized Polyisoprenes Based on Common Silanes

In contrast to the branched polybutadienes, it was not possible to introduce functional silanes via a postfunctionalization reaction. One exception was the highly reactive trichlorosilane in chapter 5.3.

Table 15 Molecular weights, polydispersity, and viscosimetry data for functionalized branched polyisoprenes synthesized using isoprene based macromonomers (**IE**: triethylsilane functionalized, **IP**: dimethylphenylsilane functionalized, **IC**: (chloromethyl)dimethylsilane functionalized).[h]

	NMR[a]		SEC[b]		MALLS	VISCO[c]	DSC[d]
#	eqv.	wt.-%	M_n	PDI	M_n	α	T_g
IE1	5	25.5	5 900	2.0	7200	0.34	-17
IE2	15	35.4	6 400	2.4	7900	0.38	-17
IP1	2.2	7.5	8 500	2.1	21 100	0.34	-5
IP2	5.4	16.6	7 300	1.7	21 800	0.38	---
IP3	12.5	31.6	6 500	1.6	19 900	0.41	0
IC1	5	24.2	5 200	2.0	7100	0.35	-16
IC2	8	33.2	5 200	2.2	7200	0.38	-9

[a] Equivalents and weight percent silane incorporated per macromonomer. [b] In g/mol vs. polystyrene standards. [c] α by applying equation (1). [d] T_g in °C

Table 15 shows the overview of the functionalized isoprene polymers. **IE** denote triethylsilane functionalized polymers, **IP** denote dimethylphenylsilane functionalized polymers and **IC** denote (chloromethyl)dimethylsilane functionalized polymers.

Pseudocopolymerizations with functional silanes were performed analogous to chapter 5.5. yielding functionalized isoprenes with similar results to the functionalized polybutadienes. The degrees of functionalization were determined analogous by NMR techniques. All polymers exhibited α-values below 0.5 proving the branched nature of the polymer.

The T_gs have been similar modified for the isoprene based polymers as the corresponding polybutadiene based polymers. As expected the amount of triethylsilane incorporated did not affect the T_g significantly. In case of dimethylphenylsilane or (chloromethyl)dimethylsilane it was slightly enhanced. These results emphasize that the developed pseudocopolymerization could be applied to macromonomers of less reactivity without any limitation.

[h] PI macronomer: M_n=1 700 g/mol and PDI=1.07 (**IE** and **IC**) and M_n=3 700 g/mol and PDI=1.06 (**IP**).

5.7. Ferrocenyl Functionalized Polydienes

5.7.1. Functional Dienes based on the $HSiMe_2Fc$ group

Analogous to the simultaneous functionalizations mentioned above, were functionalizations also performed with ferrocenyldimethylsilane.[i] Currently ferrocenyl containing compounds are receiving increased attention. In particular, poly(ferrocenyl)-based macromolecules have been demonstrated to possess useful applications for the chemical modification of electrodes and also as electrode mediators and electrochemical sensors (see chapter 7).[184-189]

For this study a butadiene based (M_n = 3 200, PDI = 1.07) and an isoprene based (M_n = 2 200, PDI = 1.09) macromonomer were employed. The synthesis was performed analogous to the pseudo-copolymerizations mentioned above. In contrast to the functionalizations with the common silanes the viscosity increased here very fast. Thus toluene had to be added to ensure homogeneous reaction conditions. A reduced activity by the bulky ferrocene was not observed and therefore very high amounts of incorporated ferrocene could be obtained.

Table 16 Amount of incorporated $HSiMe_2Fc$ concerning NMR and UV-vis.

#	wt.-% $HSiMe_2Fc$ (NMR)	wt.-% $HSiMe_2Fc$ (UV-vis)
BF1	25.8	26.9
BF2	52.0	52.8
BF3	60.4	62.2
IF1	33.0	35.4
IF2	56.0	58.0

Table 16 shows the amount of incorporated ferrocenylsilane determined via ^{1}H-NMR and UV-vis spectroscopy.[j] **BF** denote butadiene based polymers and **IF** denote isoprene based polymers. As expected both methods yielded almost the same values. It has to be emphasized that the highest modified polymers contained more than 50 weight percent ferrocene. In case of ferrocene based applications this is a very interesting feature.

[i] Synthesis and properties of this ferrocenylsilane will be discussed in chapter 7 in detail.
[j] UV-vis spectra (Figure 147) and a calibration plot (Figure 148, page 186) for the $HSiMe_2Fc$ unit can be found in the appendix.

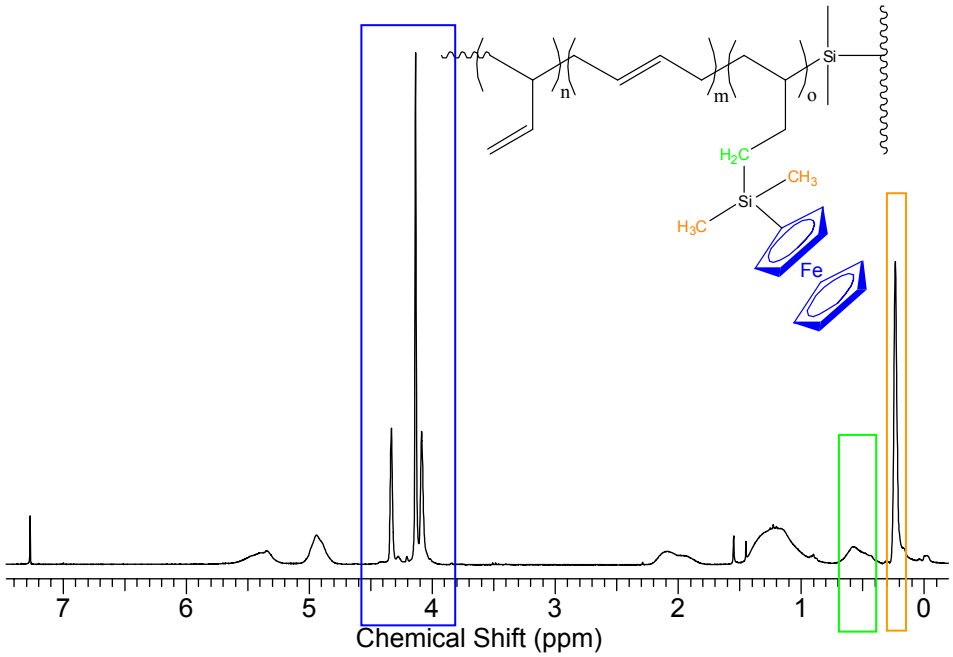

Figure 85 ^{1}H-NMR (in $CDCl_3$) of a branched PB functionalized with the $HSiMe_2Fc$ unit.

Figure 85 shows the ^{1}H-NMR spectrum of a branched PB functionalized with the $HSiMe_2Fc$ group. The degree of functionalization could be easily determined by the comparison of the methyl (orange box) or the methylene (green box) protons from the ferrocenylsilane with the methylene protons from the macromonomer (found at zero ppm).

Table 17 Overview of the $HSiMe_2Fc$ functionalized diene polymers.

#	Equivalents $HSiMe_2Fc$ employed	NMR[a]		SEC (THF)		SEC - Triple Detection	
		F	% of DB	M_n	PDI	M_n	α
BF1	5	4.5	9.6	12 200	2.3	12 800	0.39
BF2	10	10	21.3	15 200	2.9	38 900	0.39
BF3 [k]	20	20	42.6	25 500	2.9	43 800	0.54
IF1	5	5	50	10 200	2.8	12 000	0.40
IF2	15	10	100	7 200	1.7	11 200	0.49

[a] Amount of ferrocenylsilane incorporated per macromonomer and fraction of reactive double bonds.

Table 17 shows the overview of the $HSiMe_2Fc$ functionalized diene polymers. Obviously the calculated degrees of functionalization corresponded to the determined. Of course the amount of suitable olefins for a hydrosilylation is lower for a polyisoprene polymer. Nevertheless, all 3,4-double bonds could be functionalized. In case of butadiene based polymers this was not possible since the addition of high amounts of

[k] **BDF3** was formed by another butadiene based macromonomer (M_n = 3 200, PDI = 1.07).

silane yielded in higher cyclization. Under these conditions very large polymers could be obtained. SEC with triple detection proved the branching of the polymers by observing α-values for the Mark-Houwink parameters below 0.5.

5.7.2. Functional Dienes based on the $HSiMeFc_2$ group

Functionalizations based on the $HSiMeFc_2$ group were performed analogous to the $HSiMe_2Fc$ group. For this study butadiene based (M_n = 2 400, PDI = 1.06)[k] and an isoprene based (M_n = 1 700, PDI = 1.09) macromonomers employed. Unfortunately the $HSiMeFc_2$ group is a solid in contrast to all other employed silanes up to now. Therefore all reactions had to be performed with toluene as solvent to ensure miscibility. As mentioned above the addition of solvents increases of course the tendency for cyclization. Nevertheless, the properties of this ferrocenylsilane are very interesting. Silane bridged ferrocenes are able to interact with each other concerning electrochemistry (*vide infra*). This feature allows special applications that are less or even impossible with the $HSiMe_2Fc$ group.[l]

Table 18 Amount of incorporated $HSiMeFc_2$ concerning NMR and UV-vis.

#	wt.-% $HSiMeFc_2$ (NMR)	wt.-% $HSiMeFc_2$ (UV-vis)
BDF1	7.9	7.2
BDF2	35.8	38.9
BDF3	42.0	38.8
BDF4	65.3	60.9
IDF1	19.5	17.2
IDF2	59.0	56.1
IDF3	71.0	68.4

Table 18 shows the amount of incorporated ferrocenylsilane determined via ^{1}H-NMR and UV-vis spectroscopy. **BDF** denote butadiene based polymers and **IDF** denote isoprene based polymers. The $HSiMeFc_2$ group is larger than the $HSiMe_2Fc$ group. This was no hindrance to achieve very high amounts of ferrocenes incorporated into the polymer (will be discussed in chapter 7). In contrast the possible incorporated amounts of ferrocene were higher than for the $HSiMe_2Fc$ group (Table 16).

[l] Synthesis and properties of this ferrocenylsilane will be discussed in chapter 7 in detail.

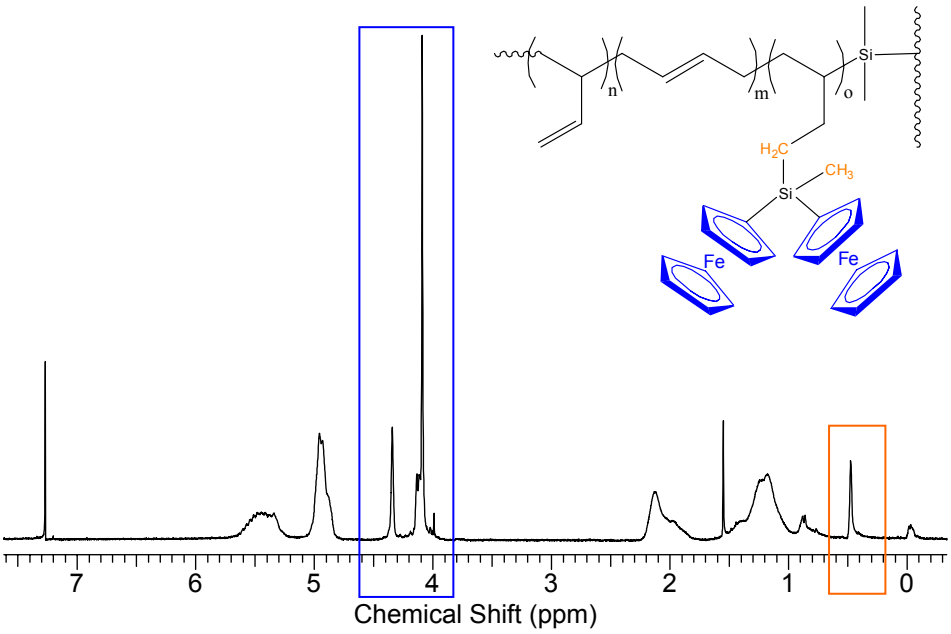

Figure 86 ^{1}H-NMR (in $CDCl_3$) of a branched PB functionalized with the $HSiMe_2Fc$ unit.

Figure 86 shows the ^{1}H-NMR spectrum of a branched PB functionalized with the $HSiMeFc_2$ unit. The degrees of functionalization were determined analogous as for the $HSiMe_2Fc$ group.

Table 19 Overview of the $HSiMeFc_2$ functionalized diene polymers.

#	Equivalents $HSiMeFc_2$ employed	NMR[a]		SEC (THF)		SEC - Triple Detection	
		F	% of DB	M_n	PDI	M_n	α
BDF1	1	0.5	1.3	12 100	2.3	10 700	0.34
BDF2	5	5	12.8	11 000	2.1	11 500	0.43
BDF3	10	4.3	9.1	12 100	2.7	15 600	0.36
BDF4	20	12.5	32.1	12 200	2.2	16 500	0.36
IDF1	1	1	12.5	6 600	2.4	15 400	0.34
IDF2	5	6	75.0	6 500	2.1	14 500	0.36
IDF3	15	10	100	7 700	1.8	26 000	0.45

[a] Amount of ferrocenylsilane incorporated per macromonomer and fraction of reactive double bonds.

Table 17 shows the overview of the $HSiMeFc_2$ functionalized diene polymers. In contrast to the $HSiMe_2Fc$ group the desired degrees of functionalization were not always reached for butadiene based polymers. Pseodo-copolymerizations with more than five equivalents of ferrocenylsilane resulted in an incomplete incorporation. This may be influenced partly by sterical reasons as the $HSiMeFc_2$ group is similar to a small dendron making it more difficult to obtain high degrees of functionalization with post-functionalization methods.[77,78] In case of the PI based polymer all reactive olefins

could be functionalized. Of course, the amount of the suitable 3,4 microstructure for hydrosilylations is rather low (*vide supra*). Apparently, the molar masses are lower than for the $HSiMe_2Fc$ based polymers. As mentioned above it was necessary to add toluene to the reaction mixture because the $HSiMeFc_2$ group is a solid. Especially in case of a high functionilization degree large amounts were necessary. This yielded a dramatically decreased degree of polymerization. However, SEC with triple detection proved the branching of the polymers by observing α-values for the Mark-Houwink parameters below 0.5. In fact, the observed values were lower than for the $HSiMe_2Fc$ based polymers. It can be concluded that these polymers achieved a more branched structure.

5.7.3. Electrochemistry of the Ferrocenyl Functionalized Polydienes

The functionalization with ferrocene groups introduced electrochemical properties into the polymer. The electrochemical properties were analyzed by cyclic voltammetry (CV). The power of CV results from its ability to rapidly provide considerable information on the thermodynamics of redox processes, on the kinetics of heterogeneous electron-transfer reactions and on coupled chemical reactions or adsorption processes.[m]

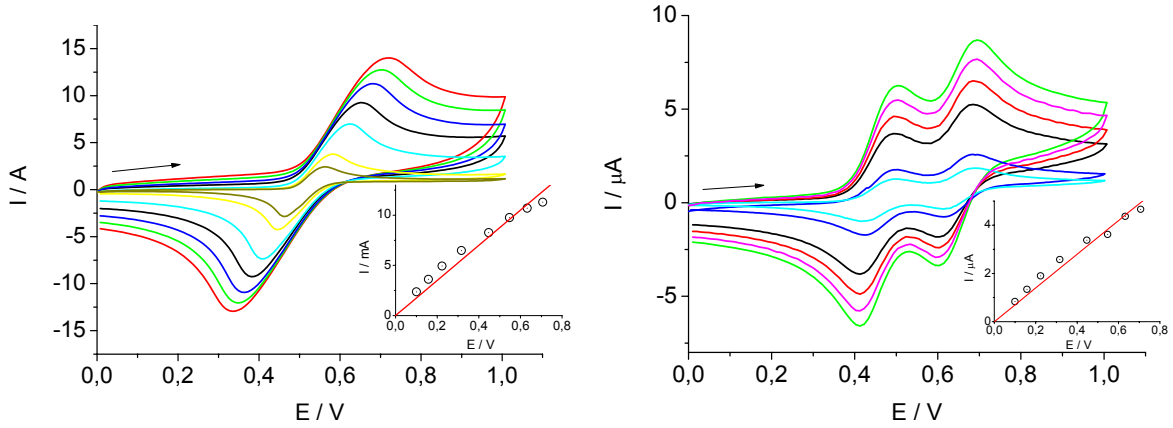

Figure 87 CVs at a Pt disk electrode obtained in CH_2Cl_2 (TBAH) solution for **BF2** (left) and **BDF1** (right) (scan rates: 0.01; 0.025; 0.05; 0.1; 0.2; 0.3; 0.4; 0.5 V/s). Inset: scan rate dependence of the first anodic peak current.

The redox properties of the studied polymers vary primarily with the nature of the silane unit attached. The $HSiMeFc_2$ group contains ferrocenes that are bridged by a

[m] Chapter 6 contains a detailed introduction on cyclic voltammetry

silane. In this case the ferrocenes affect each other, leading to two different formal potentials, as demonstrated in Figure 87 (right) for polymer **BDF1** that was measured in a dichloromethane solution. Ferrocenes in the polymers based on the $HSiMe_2Fc$ group are so far away from each other that this kind of interaction is impossible, leading to a single formal potential (**BF2**, Figure 87, left). Independently concerning kind and size of the macromonomers were the observed formal potentials. In case of $HSiMe_2Fc$ based polymers a formal potential ($E_{½}$)of 0.52 V was observed. Because of the interaction of the ferrocenes in the $HSiMeFc_2$ group two formal potentials were obtained at $E_{½}$ (1) = 0.46 V and $E_{½}$ (2) = 0.64 V.

To prove that the ferrocenyl functionalized polymers gave stable electrochemical reactions CVs at different scan rates were recorded. Based on the Randless-Sevcic equation this can be proved when a linear dependency of the square root of the scan rate versus the peak current is observed.[n] This relation was found for all polymers independently from the ferrocenylsilane. The insets in Figure 87 show that the linear relationship was fulfilled for scan rates in the range from 10 to 500 mV/s ($R^2 \geq 0.993$).

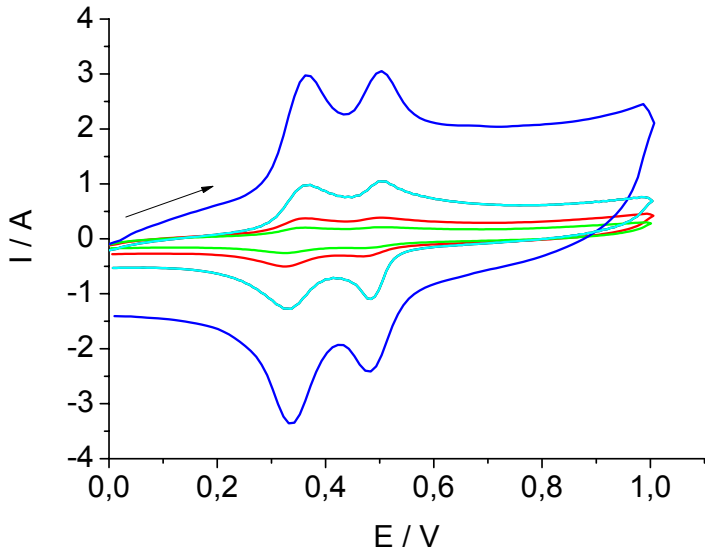

Figure 88 CVs of copolymer platinum electrodes **BDF4** measured in CH_2Cl_2 (TBAH) (scan rates: 0.1; 0.2; 0.3; 0.5 V/s).

One advantage of ferrocenes covalently linked to a polymer is the possibility to be immobilized on electrode surfaces.[n] The time frame of this work only allowed preliminary studies concerning this. It was found that all polymers could be immobilized on electrodes by performing several consecutive cycles (>20) or by applying a fixed potential of 0.7 V for several minutes. Figure 88 shows the response of a platinum electrode modified with polymer **BDF4** recorded at different scan rates. Obviously the

[n] For more details refer to chapter 6 and/or 7.

peak separation between oxidation and reduction is almost zero. This behavior is related to a monolayer-like film thickness which is especially for catalytic reactions in biosensors of great importance.

5.7.4. DSC Measurements of Ferrocenyl Functionalized Polydienes

In contrast to the other functional silanes employed, functionalizations with a ferrocenylsilane had a deep impact on the T_g. Table 20 summarizes the results obtained for the ferrocenyl functionalized branched polydienes. Obviously with increasingly ferrocenyl content the T_g is raised strongly. Materials containing more than 50 wt.-% silane at room temperature are hard solids. This can be related to thermal properties of the ferrocene. With increasing amounts of the large and bulky ferrocenes the mobility of the polymer segments is strongly reduced, yielding increased T_g's.

Table 20 Summary of the T_g's found for the ferrocenyl functionalized branched polydienes.

#	wt.-% silane	T_g / °C	#	wt.-% silane	T_g / °C
BF1	25.8	-15	**BDF1**	7.9%	-18
BF2	52.0	-9	**BDF2**	35.8%	-8
BF3	60.4	23	**BDF3**	42.0%	-6
IF1	33.0	2	**BDF4**	65.3%	29
IF2	56.0	25	**IDF1**	19.5%	-5
			IDF2	59.0%	21
			IDF3	71.0%	37

5.7.5. TGA Measurements of Ferrocenyl Functionalized Polydienes

Ferrocene containing polymers exhibit generally very good thermal stability.[107] To study whether the thermal properties of the polymers were enhanced or not, TGA studies were performed. The measurements were performed under inert conditions (N_2 atmosphere) and the temperature was raised until no more decomposition could be detected.

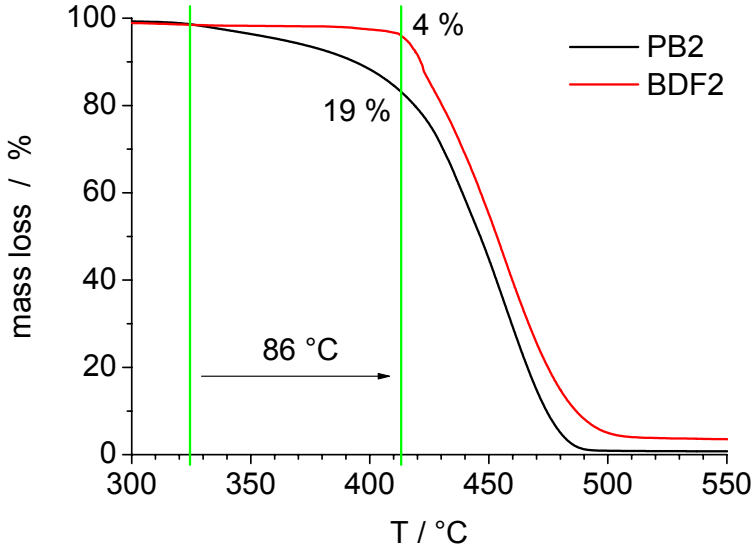

Figure 89 TGA plots for the branched **PB2** and the $HSiMeFc_2$ functionalized **BDF2**.

Figure 89 shows the TGA plots for the branched PB2 and the $HSiMeFc_2$ functionalized BDF2. The plot of the ferrocenyl functionalized polymer starts approximately 86 °C later to decompose in comparison to the pure butadiene polymer. At 413 °C **PB2** has lost already 19 % of the mass in contrast to **BDF2** with 4 %. Nevertheless, both copolymers decompose similar at temperatures higher than 430 °C. It should be mentioned in case of lower degrees of functionalization this behavior was also found but less pronounced. This increased thermal stability could be of interest for high temperature applications.

5.8. Conclusion

In summary, a very convenient route to branched polydienes was demonstrated, using macromonomers bearing a silyl-hydride endgroup. Using SEC/MALLS/viscometry it was confirmed that branched structures were obtained after polymerization of the AB_n-type macromonomers. Kinetic studies have shown that the reaction proceeded faster as expected comparing to carbosilane-based polymerizations. Hereby the large fraction of vinyl groups may be an important factor. Polymers based on polybutadiene yielded slightly larger branched polymers. The resulting branched materials are based on standard monomers and thus offer interesting potential for application,

e.g. as viscosity- or rheology-modifiers for processing. Additionally the possibility to obtain functionalized polymers by applying a pseudo-copolymerization with monofunctionalized silanes was an attractive feature of this approach. Postfunctionalization was found to be only possible with branched polybutadienes but not with the analogous polyisoprenes. It was found that this was related to a much lower fraction of double bonds that were for hydrosilylation suitable.

Simultaneous functionalizations were carried out using commercial silanes and the same conditions as for the branching reaction alone. For all cases in this study the degree of polymerization was not affected by the presence of monofunctional silanes up to 50 weight percent of the polymer. Relying on the α-parameter, all polymers were still branched. Additional to the commercial silanes employed above also special ferrocenylsilanes were employed to introduce electrochemical properties into the polymers that renders them afterwards suitable for biosensoric applications.

In common hydrosilylation chemistry offers further intriguing possibilities for modification of the branched polybutadienes, which are currently under investigation.[190]

5.9. Experimental Part

5.9.1. Materials

THF (Acros) for polymerizations was purified by cryo-transfer from a living polystyrene solution solution just prior to use. Butadiene ≥99.5% (Aldrich) was used without further purification. Isoprene (Acros) was stored over CaH_2 until use. Methanol, chloroform, and other solvents and reagents were purchased from Acros and used as received. *n*-Butyllithium (2.5 m, Acros) was used as received. The concentration of the initiator was determined by the Gilman double titration method.[154] Chlorodimethylsilane (Acros) was dried over CaH_2 and cryo-transferred into an ampoule until used. CaH_2 was purchased from Fluka and used as received. Karstedt's catalyst in xylene (2.1 – 2.4 % Pt), triethylsilane, dimethylphenylsilane and (chloromethyl)dimethylsilane was purchased from ABCR GmbH & Co. KG and used as received. The synthesis of $HSiMeFc_2$ and $HSiMe_2Fc$ is described in Chapter 7. All de-

gassing and cryo-transfer procedures were carried out using liquid nitrogen as cooling agent, if not otherwise mentioned. Deuterated chloroform-d_1 was purchased from Deutero GmbH and used as received.

5.9.1. Synthesis of the Macromonomers

A typical polymerization procedure is described below. The polymerization was performed in a 1 L glass reactor containing a 100 mL flask with living PS (closed by a Teflon tap), a magnetic glass stirrer, a rubber septum and a Teflon tap to remove the reactor under vacuum from the vacuum line. The glass reactor was connected to a high vacuum line (10^{-2} mbar) containing a graduated ampoule and the flasks with the solvents and reagents.

The reactor was evacuated and removed from the vacuum line for rinsing with the living PS solution. Using cryo-transfer procedures, the living PS was removed back to the 100 mL flask including unwanted impurities. The reactor was transferred again to the vacuum line. After establishing a vacuum of 10^{-2} mbar, the graduated ampoule was dried with a heat gun. After cooling, 20-25 mL of butadiene (or isoprene) were transferred into the graduated ampoule and after determination of the exact amount cryo-transferred into the reactor. Afterwards, THF or was cryo-transferred into the reactor. For a typical polymerization the amount of solvent was chosen such that the monomer concentration was approx. 10 vol.-%. The monomer solution was degassed by one further freeze-thaw cycle. The reactor was closed and heated to room temperature to melt the solvents. It was then cooled with an acetone/liquid nitrogen bath to approximately -95°C and the desired amount of *n*-BuLi was added via a gas-tight syringe (Hamilton). The mixture was stirred and allowed to warm slowly over a period of approx. 5 h to -10 °C. Afterwards, ca. 10 eq. of chlorodimethylsilane were cryo-transferred to the reactor. The solution was heated to room temperature and was stirred after decolorizing for an additional ½ h at this temperature. The solvent was removed under vacuum and the polymer precipitated in THF/methanol (5 times).

5.9.2. Synthesis of Branched (Functionalized) Polydienes

All catalytic reactions were conducted in parallel using Radley's 12-placed reaction carousel. 1 g of the PB-$SiMe_2H$ polymer was placed in the reaction tube and evacuated for 1h (10^{-2} mbar). The tube was heated to 100 °C and then filled with dry Ar-gas. In case of pseudocopolymerizations was the silane added in the desired amount. For polymerizations under solution conditions was dry toluene added to the reaction mixture. 50 μL Karstedt's catalyst (≈2.3 x 10^{-6} mol) were added and the mixture was stirred at 100°C for 18 h (in case of triethylsilane under reflux). The polymer was purified by precipitation from THF/methanol (5 x).

6. Ferrocenyl-Functionalized Hyperbranched Polyglycerols

6.1. Introduction

6.1.1. Ferrocene Containing Polymers

Currently ferrocene-containing compounds are receiving increased attention. Particularly the high chemical and thermal stability in combination with the electrochemical properties of the ferrocene group are very attractive.[106] The range of possible applications ranges from military hardware development to the development of anticancer drugs.[107] During the last decade a large number of research groups has investigated different polymer systems with respect to ferrocene-containing structures. Different types of polymers have been developed that contain the ferrocene units as part of the backbone or as side groups of linear chains.[116-122] Unfortunately most polymers adopt a coiled conformation, minimizing the amount of catalytically active ferrocene. With respect to electrochemical reactions, this undesired shielding effect can be very pronounced.[191] Considering applications based on the electrochemical properties, the number of ferrocenes that are actually involved in an electrochemical process is crucial for the sensitivity of the sensor. Dendrimers were believed to overcome these problems, since the structure of dendrimers permits the regular placement of functional groups at their molecular periphery. Encouraged by the rapid advances in this field of chemistry, a large number of materials scientists have focused their research on functional dendrimers, with some of them involving interactions with biological molecules.[11,14,16,17,108] The development of ferrocenyl-functionalized dendrimers was therefore soon investigated and numerous examples are now known in the literature.[109-115] A major drawback of the dendrimer concept lies in the fact that structurally perfect dendrimers are usually available in small quantities only, due to the unavoidable multi-step synthesis. Therefore, the long-known polycondensation of AB_2-monomers resulting in “hyperbranched polymers” attracts renewed interest, since these materials combine some of the advantages of dendrimers, i.e., globular structure and high functionality with a synthesis that is straightforward and economical.[18] Improvements in the synthetic procedures have led to hyperbranched polymers with low polydispersity, controlled molecular weights and high degrees of branch-

ing.[46,47,56,192] Interestingly, to date hyperbranched polymers have rarely been combined with ferrocene moieties.[193,194]

In this context, the development of ferrocenyl-containing block copolymers has been also an important challenge. The corresponding methods developed by Nuyken et al. and Frey et al. are based on the controlled anionic and radical polymerization and were successfully applied for the copolymerization of vinylferrocene with styrene or other olefinic monomers.[123,124] Subsequently, Balsara et al. have shown that a poly(vinylferrocene)-*b*-poly(isoprene) block copolymer could be successfully applied as heterogeneous catalyst for Michael additions.[125] Intensive research performed by Manners et al. has led to a wide range of examples concerning block copolymers with a well-defined ferrocene-containing block. This group combined polyferrocenylsilane polymers with a second block like polystyrene, polydimethylsiloxane or polypeptides and demonstrated very interesting properties in solution as well as in the bulk state.[195-197]

6.1.2. Cyclic Voltammetry

Cyclic voltammetry is the most widely used technique for acquiring qualitative information about electrochemical reactions. The power of cyclic voltammetry results from its ability to rapidly provide considerable information on the thermodynamics of redox processes, on the kinetics of heterogeneous electron-transfer reactions, and on coupled chemical reactions or adsorption processes.[198-200]

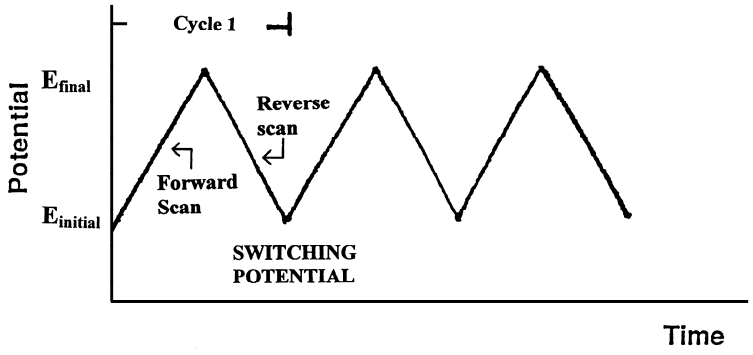

Figure 90 Potential-time excitation signal in cyclic voltammetric experiment.

Cyclic voltammetry consists of scanning linearly the potential of a stationary working electrode (in an unstirred solution) using a triangular potential waveform (Figure 90).

During the potential sweep, the potentiostat measures the current resulting from the applied potential. The resulting plot of current versus potential is termed a *cyclic voltammogram.*

Figure 91 illustrates the expected response of a reversible redox couple during a single potential cycle. It is assumed that only the oxidized form O is present initially. Thus, a negative-going potential scan is chosen for the first half-cycle, starting from a value where no reduction occurs. As the applied potential approaches the characteristic *E°* for the redox process, a cathodic current begins to increase, until a peak is reached. After traversing the potential region in which the reduction process takes place (at least 90/*n* mV beyond the peak), the direction of the potential sweep is reversed. During the reverse scan, R molecules (generated in the forward half cycle, and accumulated near the surface) are reoxidized back to O and an anodic peak results.

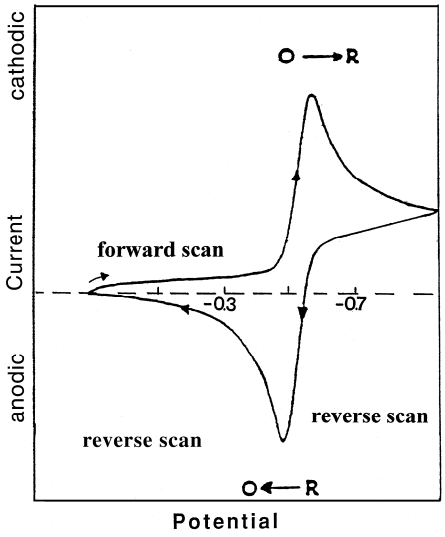

Figure 91 Typical cyclic voltammogram for a reversible $\mathrm{O} + ne^- \rightleftharpoons \mathrm{R}$ redox process

The characteristic peaks in the cyclic voltammogram are caused by the formation of the diffusion layer near the electrode surface. The resulting current peaks thus reflect the continuous change of a concentration gradient with the time. Hence, the increase to the peak current corresponds to the achievement of diffusion control, while the current drop (beyond the peak) exhibits a $t^{-½}$ dependence (independent of the applied potential). For the above reasons, the reversal current has the same shape as the forward one.

In the early 60s Nicholson and Shain developed the diagnostics for analyzing the cyclic voltammetric response.[201] One of the most famous relations is the *Randles-*

Sevcik equation. It defines the peak current for a reversible couple (at 25 °C) and is given by

$$I_p = \left(2.69 \times 10^5\right) n^{3/2} A c D^{1/2} \upsilon^{1/2} \quad (6.1)$$

where *n* is the number of electrons, *A* is the electrode area (in cm^2), *c* is the concentration (in mol cm^{-3}), *D* is the diffusion coefficient (in $cm^2\ s^{-1}$), and ν is the scan rate (in $V\ s^{-1}$). Accordingly, the current is directly proportional to concentration and increases with the square root of the scan rate. The ratio of the reverse-to-forward peak currents, $I_{p,r}/I_{p,f}$ is unity for a simple reversible couple. This peak ratio can be strongly affected by chemical reactions coupled to the redox process. The current peaks are commonly measured by extrapolating the preceding baseline current. The position of the peaks on the potential axis (E_p) is related to the formal potential of the redox process. The formal potential for a reversible couple is centered between $E_{p,a}$ and $E_{p,c}$:

$$E° = \frac{E_{p,a} + E_{p,c}}{2} \quad (6.2)$$

The separation between the peak potentials (for a reversible couple) is given by

$$\Delta E_p = E_{p,a} - E_{p,c} = \frac{0.059}{n} V \quad (6.2)$$

Thus, the peak separation can be used to determine the number of electrons transferred, and as a criterion for a Nernstian behavior.

Cyclic voltammetry can also be used for evaluating the interfacial behavior of electroactive compounds. Both the reactant and the product can be involved in an adsorption-desorption process. Such interfacial behavior can occur in studies of numerous organic compounds, as well as of metal complexes. Especially in biosensoric applications the formation of monolayer films of a catalytic active substance is crucial.[186,187] In case of monolayers an ideal Nernstian behavior of surface-confined nonreacting species is observed with symmetrical cyclic voltammetric peaks ($\Delta E_p = 0$), and a peak half-width of 90.6/*n* mV (Figure 92).

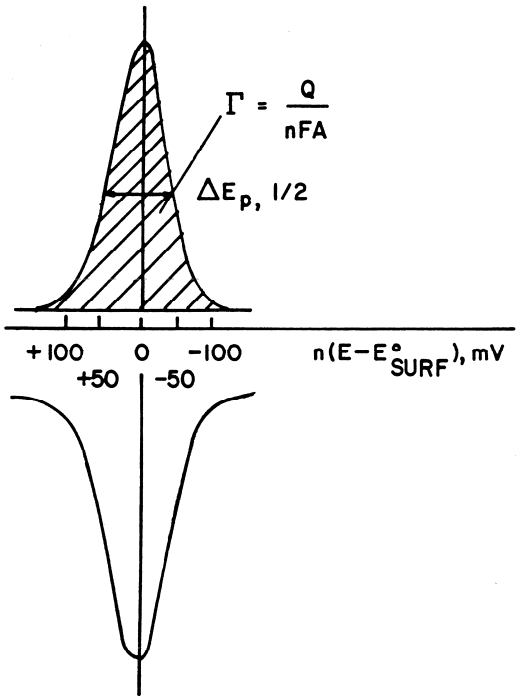

Figure 92 Ideal cyclic voltammetric behavior for a surface layer on an electrode. The surface coverage, Γ, can be obtained from the area under the peak.[200]

The peak current is directly proportional to the surface coverage (Γ) and potential scan rate:

$$I_p = \frac{n^2 F^2 \Gamma A \upsilon}{4RT} \tag{6.3}$$

with F the Faraday constant, R the gas constant and T the temperature. Γ is defined by

$$\Gamma = \frac{Q}{nFA} \tag{6.4}$$

6.2. Synthesis and characterization of PG-Fc Polymers

The experience with PG renders this material attractive as an alternative to dendrimers. Applying the “ring-opening-multibranching polymerization“ (ROMBP)[56] it was possible to prepare a highly branched system with a low polydispersity and a high amount of reactive hydroxyl groups on a more or less globular structure. The functionalization of the PG with ferrocene-monocarboxylic acid was performed applying a method introduced by Stupp et al.[202]

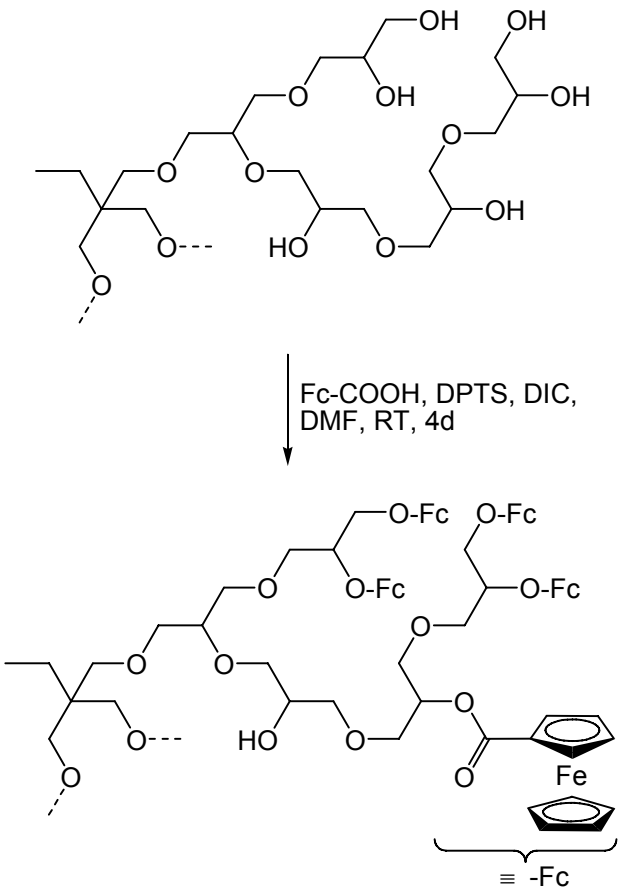

Figure 93 Reaction scheme to ferrocenyl functionalized PG.

Figure 93 outlines the very convenient synthesis of the ferrocenyl functionalized PG. The synthesis of the PG precursor in different molecular weights was performed in a single step. For our investigation we have chosen PGs built of 7, 15 and 30 monomer units. The functionalization of PG was performed in a second step. For the esterification using DIC as esterification agent, DPTS was added as an additive. DPTS enhances the activity of DIC and lowers at the same time the formation of side products. Purification of the crude material was performed by dissolving it in THF (urea-insoluble) and precipitation in diethyl ether (ferrocene monocarboxylic acid soluble). After several cycles the polymer was free of undesired side products.

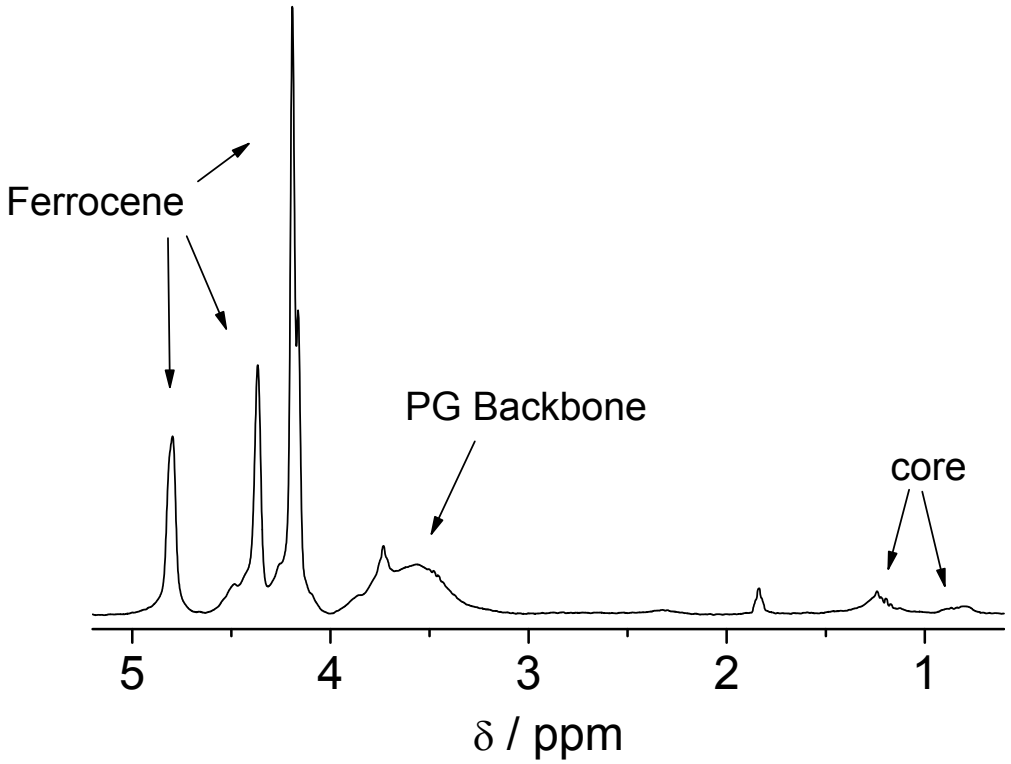

Figure 94 ^{1}H-NMR spectrum of PG_7-Fc_{10} in $CDCl_3$

Figure 94 shows the ^{1}H-NMR spectrum of PG_7-Fc_{10} in $CDCl_3$. Besides the signal of the PG backbone one can observe the three characteristic resonances for monofunctionalized ferrocenes in a ratio of 2:2:5. The TMP core protons were used to calculate the molar mass and the degree of functionalization. It is noteworthy to mention that the unfunctionalized PG is insoluble in chloroform. Table 21 shows the obtained degrees of functionalization in weight % of ferrocene in the final polymers. In all cases materials with high amount of ferrocene were obtained, with degrees of functionalization ranging from almost quantitative for PG_7 and PG_{15} to approximately 55% for the sample PG_{30}.

Table 21 Functionalization data of the Polymers: number of hydroxyl groups per macromolecule, degree of functionalization and main products found by MALDI-ToF.

Polymer	NMR # OH/pol.	$Fc_{wt\%}$	MALDI-ToF
PG_7-Fc_{10}	0	67	PG_x-Fc_{x+2} PG_x-Fc_{x+1}
PG_{15}-Fc_{16}	2	64	PG_x-Fc_{x+1} PG_x-Fc_x
PG_{30}-Fc_{18}	15	54	PG_x-$Fc_{0.25x}$ - PG_x-$Fc_{0.5x}$

More information concerning the chemical composition was obtained by MALDI-ToF analysis. Figure 95 shows the MALDI-TOF mass spectra of the hyperbranched PG_7-Fc_{10} and PG_{30}-Fc_{18}. Depending on the degree of functionalization, different kinds of

matrices were chosen. Dithranol was used in the case of PG_7-Fc_{10} and PG_{15}-Fc_{16}. Distilled THF was used as solvent without other additives (e.g. stabilizers) and the PG_xFc_y were detected as radical molecular ions.[203] It was possible to obtain a detailed composition analysis, but because of the broad polydispersity, the spectra are also affected by mass discrimination effects.

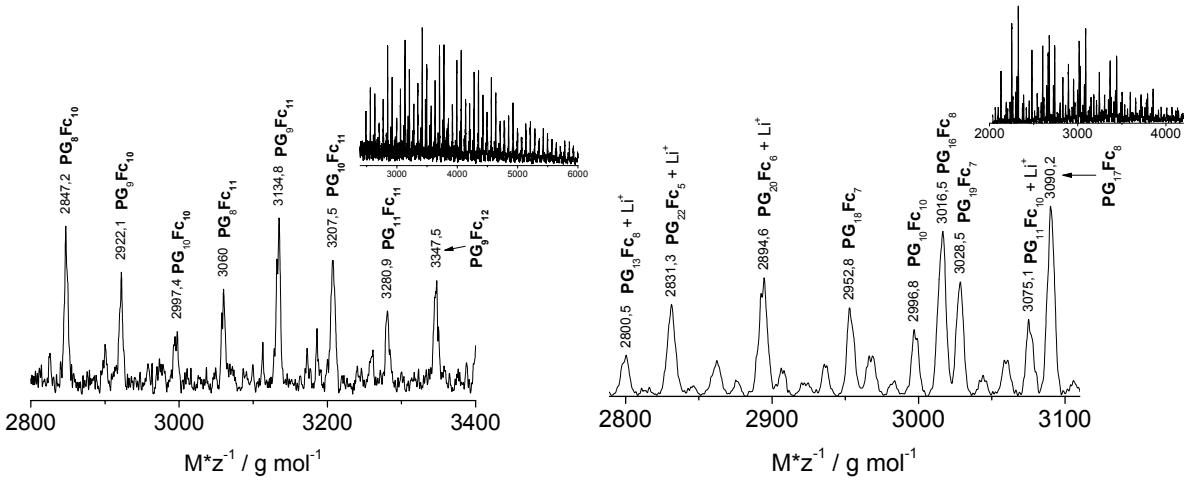

Figure 95 MALDI-TOF spectra of PG_7Fc_{10} (left) and PG_{30}-Fc_{18} (right).

It is possible to calculate the numbers of the repeating units of PG and of the ferrocenyl moiety that correspond to every signal in the spectra. One can calculate a combination PG_x-Fc_y calculated as [TMP (131.15)] + x[glycidol unit (74.078)] + y[ferrocenemonocarboxy unit (213.00)] for every signal. In the case of complete functionalization y will be (x +3) because the number of the hydroxyl groups is equal to the number of glycerol monomer units + 3.

The MALDI-Tof analysis shows a high degree of functionalization of the hyperbranched polyglycerol in the case of the lower molecular weight PG. A particular combination of PG_xFc_y is found in the spectra of PG_7-Fc_{10} (Figure 95, left): all peaks can be assigned to a specific composition yielding mainly PG_x-Fc_{x+2} and PG_x-Fc_{x+1} as main products. In the spectra of PG_{15}-Fc_{16}, PG_x-Fc_{x+1} and PG_x-Fc_x are found as main distribution. The apparently lower degree of functionalization compared to PG_7-Fc_{10} was confirmed by NMR spectroscopy (Table 21). Because of the mass discrimination effect, the limited resolution and the different capacity of vaporization and ionization of the different molecular species, it is impossible to obtain a complete picture of all species that are present in the samples.

In the case of PG_{30}-Fc_{18} with a PG core with 30 monomer units and a lower degree of functionalization, α-cyano-4-hydroxy cinnamic acid was used as matrix and LiCl was

added as additive. PG_x-Fc_y was detected as the radical species, or as Li adduct. From the analysis of the spectrum the degree of functionalization appears to be lower than expected from the NMR analysis. In this case the spectra does not show the regular pattern found in the case of PG_7-Fc_{10} and PG_{15}-Fc_{16} but a more random combination (PG_x-$Fc_{0.25x}$ to PG_x-$Fc_{0.5x}$). Because of the mass discrimination effect it is possible to elucidate the species present in the spectra up to ca. 3500 Da (Figure 95, right). For species with higher mass the resolution was not sufficient to perform an acceptable analysis.

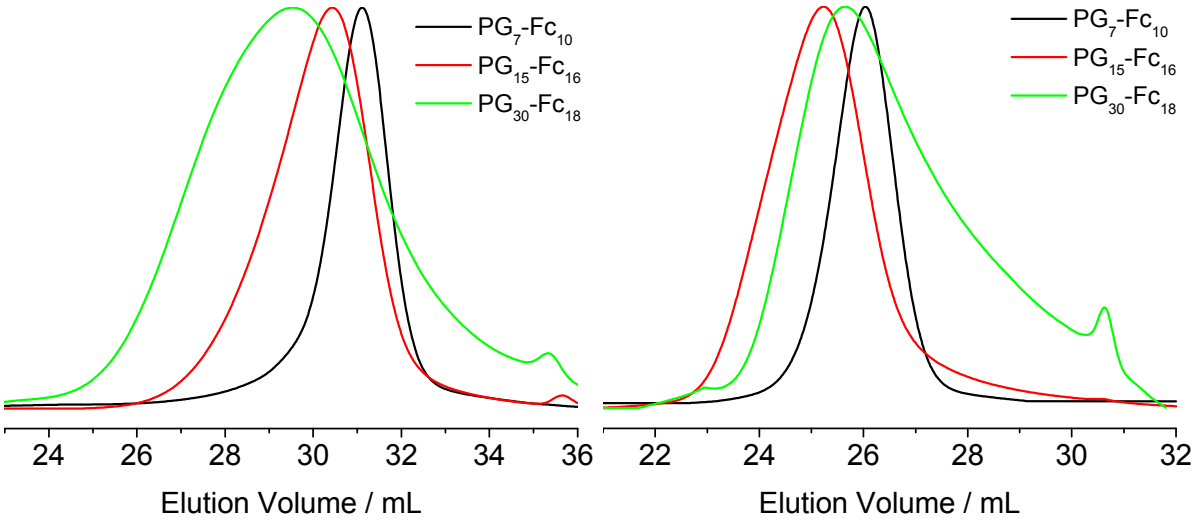

Figure 96 SEC diagrams of ferrocene-substituted samples obtained from DMF (left) and THF (right) using the UV detector.

Figure 96 shows the SEC elugrams for the different polymers in DMF and THF. In DMF the peak maximum is shifted to smaller elution volumes with increasing molar mass of PG, as expected. Nevertheless in THF the peak maximum for PG_{30}-Fc_{18} is between PG_7-Fc_{10} and PG_{15}-Fc_{16}.

Table 22 Summary of the SEC results vs. NMR

	SEC (DMF)		SEC (THF)		NMR
Polymer	M_n	PDI	M_n	PDI	M_n
PG_7	610	1.5	---	---	630
PG_7-Fc_{10}	1890	1.2	1910	1.2	2760
PG_{15}	1160	1.7	---	---	1220
PG_{15}-Fc_{16}	3100	1.3	2590	1.4	4630
PG_{30}	2000	2.0	---	---	2380
PG_{30}-Fc_{18}	2150	3.6	650	3.3	6210

Molar masses in $gmol^{-1}$

Table 22 shows the different results obtained from SEC in comparison to the results from NMR for the polymers. It is important to point out that the unfunctionalized PG is very poorly soluble in THF. SEC measurements for non-functionalized PGs with DMF as eluent, using defined polystyrenes as standard yielded molar masses very close to the results by NMR. However the molar masses for the ferrocenyl-functionalized PGs are strongly underestimated. The dimension of PG_{30}-Fc_{18} appears to be significantly underestimated by SEC. Especially in THF this effect is very pronounced, this could be related to the structure of the hyperbranched polymer and is strongly influenced by the number of residual hydroxyl groups. Table 21 shows that for PG_7-Fc_{10} and PG_{15}-Fc_{16} the amount of remaining hydroxyl groups is negligible. In case of the PG_{30}-Fc_{18} half of the hydroxyl groups still remains in the hyperbranched polymer.

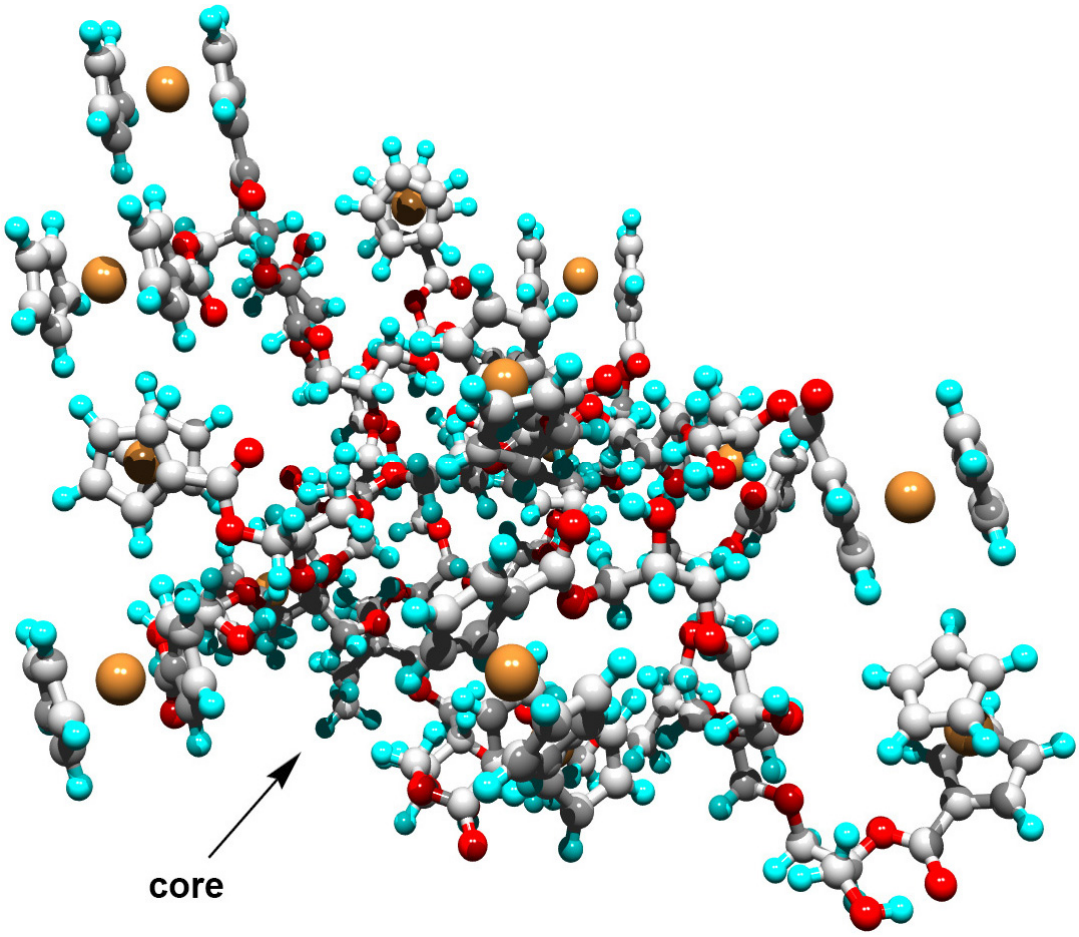

Figure 97 A space-filling molecular model of $PG_{30}Fc_{18}$. The three-dimensional image was obtained by modeling with Spartan.

Figure 97 shows a computed model for the energy-minimized structure of $PG_{30}Fc_{18}$ in the gas phase. It shows the globular structure of the hyperbranched ferrocenyl-functionalized polymer. The polymer adopts a core-shell like structure, wherein the

bulky ferrocenes are located in the shell and the residual hydroxyl groups are located in proximity of the core. Due to the very crowded surface of $PG_{30}Fc_{18}$ the realization of higher degrees of functionalization becomes very difficult, because of the very bulky ferrocene group. In solvents of high polarity (DMF: dielectric constant = 36.7 at 20°C) where the draining of the ferrocene shell and the PG core is high, this polymer shows a high hydrodynamic radius (Figure 96, left). In less polar solvents (THF: dielectric constant = 7.6 at 20°C) hydrogen bonding between free hydroxyl groups becomes much stronger, yielding a collapsed core-structure with the shell keeping the structure dissolved, explaining the peak shift to larger elution volumes in THF (Figure 96, right).

As it is also shown by MALDI-TOF, the functionalized PG_{30} does not yield a preferred combination, what explains partly the higher polydispersity in comparison to PG_7-Fc_{10} and PG_{15}-Fc_{16}. In addition it has to be taken into account that the different degrees of functionalization may yield very different, strongly collapsed structures in solution because of the different amount of free hydroxyl groups.

6.3. Electrochemical properties of PG-Fc Polymers

Functionalization with ferrocene groups introduces redox properties in the polymer. It was of particular interest to in study the influence of the molecular weight and the degree of functionalization of PG on the overall electrochemical response of the macromolecules. The electrochemical properties were characterized by cyclic voltammetry. The power of cyclic voltammetry lies in its ability to rapidly provide detailed information on the thermodynamics of redox processes, on the kinetics of heterogeneous electron-transfer reactions and on coupled chemical reactions or adsorption processes.

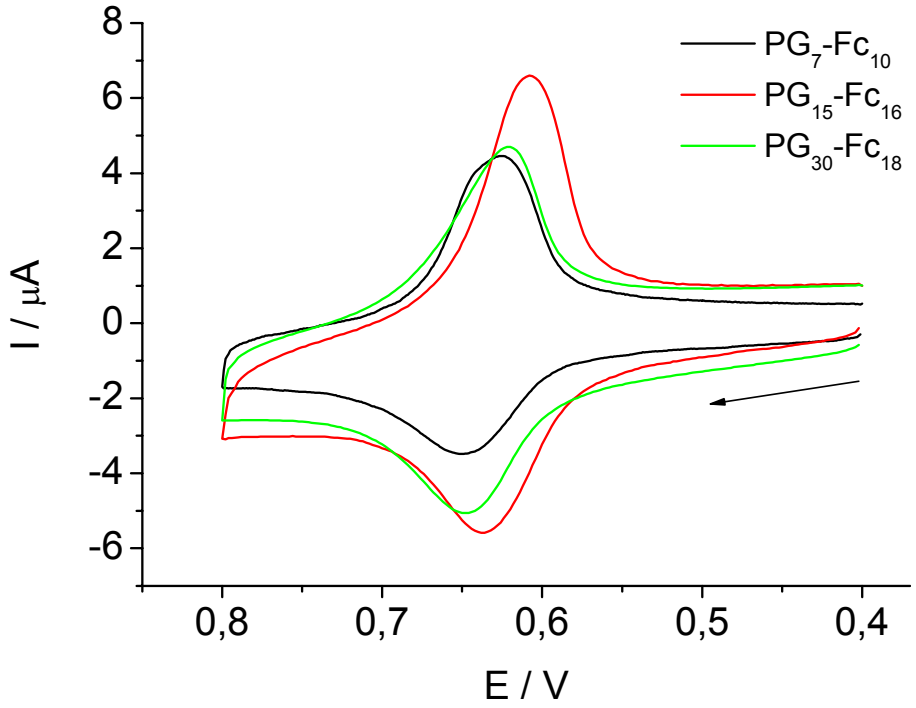

Figure 98 Response of 0.1 mmol PG_7-Fc_{10}, PG_{15}-Fc_{16} and PG_{30}-Fc_{18} in CH_2Cl_2; HOPG electrode.

Figure 98 shows the cyclic voltammograms for the different polymers dissolved in CH_2Cl_2, using TBAH as supporting electrolyte. Table 23 summarizes the results for the electrochemical properties measured in solution. The formal potentials of all polymers were always at 0.63 V, and well above the formal potential of ferrocene ($E° = 0.426$ V in CH_2Cl_2), this is attributed to the electron-withdrawing ester group attached to the ferrocene moiety.

Table 23 Summary of the electrochemical properties of PG_x-Fc_y solutions.

Polymer	PG_7-Fc_{10}	PG_{15}-Fc_{16}	PG_{30}-Fc_{18}
$E_{½}$ / V	0.64	0.62	0.63
I_{ox} / µA	-2.4	-3.8	-2.9
I_{red} / µA	4.5	6.3	4.2

The large difference between the peak currents for the oxidation and reduction wave is an indication of precipitation, when the second wave (here the cathodic one) yields a higher current. It also shows that the electrochemical reactions are fully reversible.
In our case the formation of polymeric films on the electrodes could be achieved by cycling several times or by applying a fixed potential of 0.7 V. Under these conditions the ferrocenyl-functionalized polymer is deposited as ferricenium species. This technique possesses the advantage that the thickness of the deposited films can be very

well controlled. It is known from theory that the peak current for an immobilized species is linearly dependent on the scan rate [200].

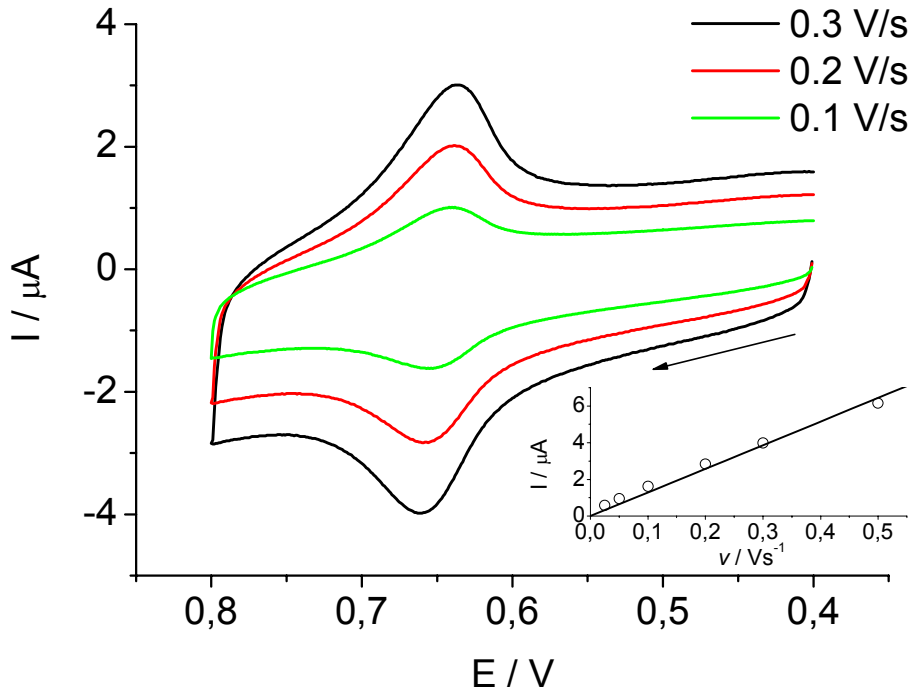

Figure 99 Response of a modified PG_{15}-Fc_{16} glassy carbon -electrode in CH_2Cl_2 at different scan rates. Inlay: oxidation peak currents versus the corresponding scan rates.

Figure 99 exemplifies the response of a glassy carbon electrode modified with a thin film of PG_{15}-Fc_{16} measured at different scan rates. The inlay shows the peak current for the oxidation wave measured at different scan rates. The applied linear fit function had an error below 0.1 %. The thickness of the polymer film can be calculated by the equation 6.4 (*vide supra*). Materials with high weight fractions of ferrocene (50% ≤ *w*) and with Γ values around 10^{-10} mol_{Fc} x cm^{-2} are usually present as a monolayer film on the electrode. [200]

Table 24 Summary of the electrochemical properties of a polymer modified glassy carbon electrode using CH_2Cl_2 as solvent 0.1 M TBAH (0.1 V/s) with PG_x-Fc_y polymers.

Polymer	PG_7-Fc_{10}	PG_{15}-Fc_{16}	PG_{30}-Fc_{18}
$E_{½}$ / V	0.61	0.65	0.62
ΔE_p / V	0.013	0.011	0.027
ΔE_{FWHM} / V	0.069	0.067	0.067
I_{ox} / µA	-0.23	-0.63	-5.3
I_{red} / µA	0.22	0.64	5.4
Γ / mol_{Fc} cm^{-2}	$9.8x10^{-11}$	$7.4x10^{-11}$	$5.8x10^{-10}$

Table 24 summarizes the results for the electrodes modified with PG_x-Fc_y. The coverage of the modified electrodes for the samples PG_7-Fc_{10} and PG_{15}-Fc_{16} were close to 10^{-10} mol_{Fc} x cm^{-2}. We can also observe a small peak to peak separation (ΔE_p), as expected for monolayers. In case of the sample $PG_{30}Fc_{18}$, the thickness of the film was slightly higher, which resulted in higher ΔE values. Also an important value is given at the full width at half maximum (FWHM) for the corresponding waves. Values around 0.096 V for single electron species are representative of non-interacting neighbors. [200] Larger values are found for repulsive interactions and smaller values for attractive or stabilizing interactions. In our case the FWHM values were independent with the molar mass of the macromolecules, the film thickness or the degree of functionalization. With values around 0.067 V they were also slightly below the theoretical value of 0.096 V, indicating small attractive interactions. It has to be emphasized that glycidol monomers are not spatially demanding, i.e., PG has the reactive groups in close proximity (see Figure 97), this leads to interaction between the ferrocene units.

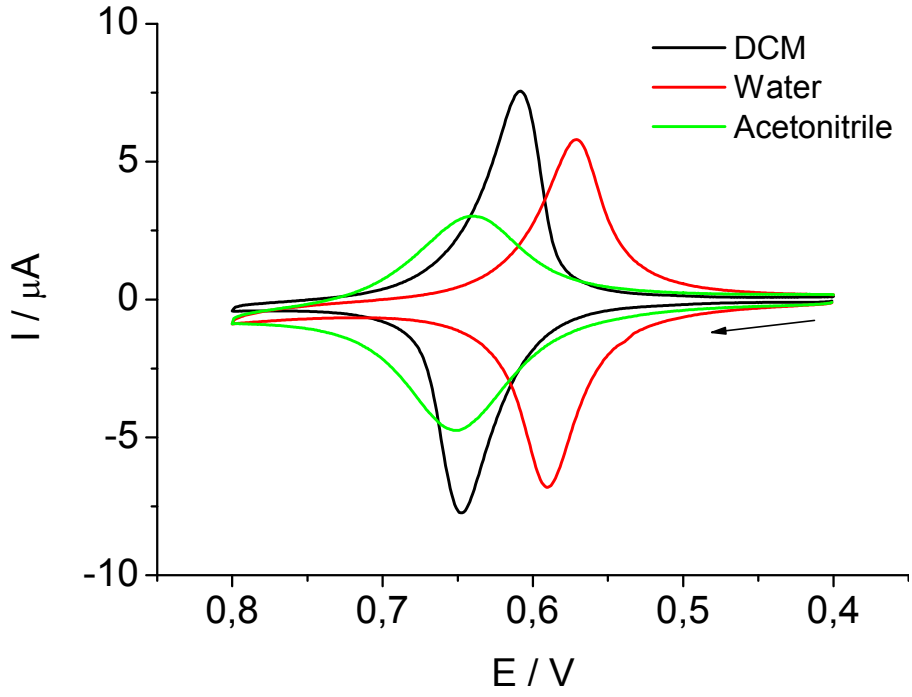

Figure 100 Response of Pt-Electrode modified with PG_{15}-Fc_{16} in different solvents.

The compatibility of electrodes modified with PG_x-Fc_y towards different solvents is of interest for various electrochemical purposes. It was found that nicely resolved signals could be obtained in nonpolar solvents like CH_2Cl_2, as well as in very polar solvents like acetonitrile and water.

6.4. Conclusion

A facile two step synthesis of ferrocene-functionalized hyperbranched PG was presented. The polymeric materials have been characterized with respect to their molecular structure applying NMR and MALDI-ToF. As expected, higher molecular weight PGs present more difficulties for functionalization with the very bulky ferrocene monocarboxylic acid. This is attributed to the proximity of the hydroxyl groups. In case of the sample $PG_{30}Fc_{18}$ a material that obviously possessed a core-shell structure with different polarities was obtained.

Furthermore, the electrochemical properties of the materials have been analyzed. Reversible electrochemical properties have been observed for almost all samples studied. The fabrication of thin polymer films on electrodes could be conveniently realized and thin polymer films that were compatible with almost all common solvents in their electrochemical behavior were formed.

The compatibility of this material concerning different solvents, especially water, renders this material promising for biosensoric applications. It is very important to point out that most enzymatic reactions used in biosensoric applications are performed in an aqueous environment.

6.6. Experimental Part

6.6.1. Materials

Dried DMF (stored over molecular sieves) was purchased from Fluka, and used without further purification. Diisopropylcarbodiimide (DIC) was purchased from Acros and used as received. All other standard solvents were purchased from Acros in p.a. quality and used as received. Ferrocenemonocarboxylic acid was synthesized according to a literature procedure.[204] 4-(Dimethylamino)pyridinium 4-toluenesulfonate (DPTS) was prepared according to a literature procedure. [202] Polyglycerol PG_7 (M_n = 630, M_w/M_n = 1.5), PG_{15} (M_n = 1220, M_w/M_n = 1.7) and PG_{30} (M_n = 2380, M_w/M_n = 2.0) were prepared as reported previously [56], using trishydroxymethylpropane (TMP)

as initiator. Tetrabutylammonium hexafluorophosphate (TBAH) and lithium perchlorate ($LiClO_4$) were purchased from Aldrich (electrochemical grade).

6.6.2. Synthesis of ferrocenyl-functionalized polyglycerols

For a typical reaction 1 g PG was dissolved in 2.5 mL of dried DMF. Afterwards 1 equivalent of ferrocene monocarboxylic acid, 1.4 equivalents of DIC and 0.21 equivalents of DPTS were added according to the amount of hydroxyl groups of PG. The mixture was stirred under inert gas (Argon) for 4 days. The resulting white urea precipitate was filtered from the reaction mixture. To remove residual urea and other side products the polymer was dissolved in 10 mL of THF. The insoluble urea was removed by filtration and the polymer was then precipitated in 100 mL of diethyl ether. This procedure was repeated at least three times. The resulting slurry precipitate was dried in vacuum at 40°C over night, leading to a gold-colored solid powder. The yields for PG_{15}-Fc_{16} and PG_{30}-Fc_{18} were between 75 % and 95 %. PG_7-Fc_{10} could only be obtained in 20 % yield.

6.6.3. MALDI-TOF characterization

Dithranol or α-cyanohydroxycinnamic acid were used as matrix. Samples were prepared by dissolving the polymer in THF at a concentration of 10 g/L. A 10 μL aliquot of this solution was added to 10 μL of a 10 g/L matrix solution and in some cases LiCl dissolved in methanol was added as cationizing agent. A 1 μL aliquot of the resulting mixture was applied to a multistage target to evaporate the THF or methanol and create a thin matrix/analyte film. The samples were measured in positive linear mode.

6.6.4. Electrochemical characterization

Electrochemical measurements were performed using a BAS CV-50W. All experiments were carried out in a conventional three-electrode cell at 20-21°C. A glassy carbon-disk of 7 mm^2 diameter served as working electrode, a Pt wire as auxiliary electrode, and a saturated Calomel reference electrode (SCE) was employed.

Voltammetric measurements in non-aqueous solution were performed in CH_3CN or CH_2Cl_2, using TBAH as supporting electrolyte in 0.1 M concentration. In aqueous solution $LiClO_4$ was used as supporting electrolyte in 0.1 M concentration. A conventional sample cell operating under an atmosphere of prepurified nitrogen was used for CV. The electrodes were polished prior to use with either 1 μm diamond paste (Buehler) or 0.05 mm alumina/oligo(ethylene glycol) slurry and rinsed with purified water and acetone. All solutions were deoxygenated by bubbling high-purity nitrogen for at least 15 min.

Polymer films were deposited on glassy carbon electrodes from an electrolyte bath containing approximately 0.1 mM Fc and 0.1M TBAH in dichloromethane, by controlled potential electrolysis at 0.7 V versus SCE. Alternatively it was also possible to deposit the polymer films by consecutive cycling. The amount of electroactive material electrodeposited can be controlled with the charge passed during the electrodeposition. The coated electrodes were rinsed with dichloromethane. The surface coverage of electroactive ferrocenyl sites in the film, Γ, was determined from the integrated charge of the cyclic voltammetric waves.[200]

7. Ferrocenyl-Functionalized PS-*b*-PB Copolymers

7.1. Introduction

7.1.1. Biosensors

The need for disposable systems or tools for environmental monitoring has encouraged the development of new technologies and more suitable methodologies. The ability to monitor the increasing number of analytes in clinical, environmental, and food samples as quickly and as cheaply as possible is a very important nowadays. In this respect, biosensors have demonstrated a great potential in recent years and thus arise as proposed analytical tools for effective monitoring in these programs.

Table 25 Biosensor types classified according to the method of signal transduction and according to the biorecognition element

Signal transduction	
Electrochemical	amperometric conductimetric impedimetric potentiometric
Optical	absorption fluorescence/phosphorescence bio/chemiluminescence reflectance raman scattering refractive index
Mass sensitive	surface acoustic wave biosensors cantilever biosensors
Thermometric	
Biorecognition element	
Antibodies (Immunosensors)	monoclonal policlonal
Protein Receptors	metabotropic receptors ionotropic receptors
Whole Cells	microbial sensors mammalian cells tissue
Nucleic Acids	hybridization low weight compound interaction
Enzymes	

A biosensor is defined as a self-contained (all parts being packaged together), usually small, integrated device, which is capable of providing specific quantitative or

semi-quantitative analytical information using a biological recognition element which is retained in direct spatial contact with a transduction element which converts the biological recognition event into a useable output signal.[205]

Biosensors can be classified according to the method of signal transduction or according to the biorecognition element. Table 25 gathers together all biosensors types considering both perspectives.[206,207] Most of the biosensors described in the literature are electrochemical biosensors. Electrochemistry offers high sensitivity, compatibility with modern microfabrication technologies, portability, low cost and minimal power requirements.[208]

7.1.2. Enzyme-Based Electrodes

Enzymes are proteins that catalyze chemical reactions in living systems. Such catalysts are not only efficient but are also extremely selective. Hence, enzymes combine the recognition and amplification steps, as needed for many sensing applications.

Enzyme electrodes are based on the coupling of a layer of an enzyme with an appropriate electrode. Such electrodes combine the specificity of the enzyme for its substrate with the analytical power of electrochemical devices.[209]

In this context the glucose sensor is one of the most famous examples. The determination of glucose in blood plays a crucial role in the diagnosis and therapy of diabetes. Electrochemical biosensors for glucose play a key role in this direction. The glucose amperometric sensor, developed by Updike and Hicks, represents the first reported use of an enzyme electrode.[210]

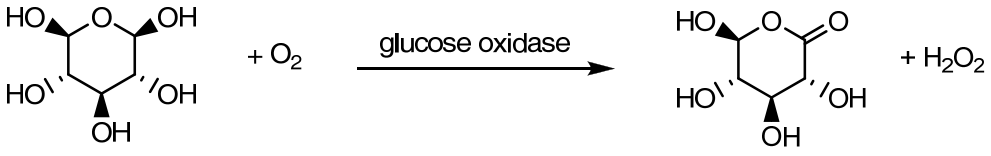

Figure 101 Basic enzymatic reaction for a glucose sensor based on the glucose oxidase enzyme.

As enzyme often the glucose oxidase (GOX) is employed that oxidizes glucose to the corresponding lactone (Figure 101). The electrode is commonly based on the entrapment of the enzyme between polyurethane and permselective membranes on a platinum working electrode (Figure 102).

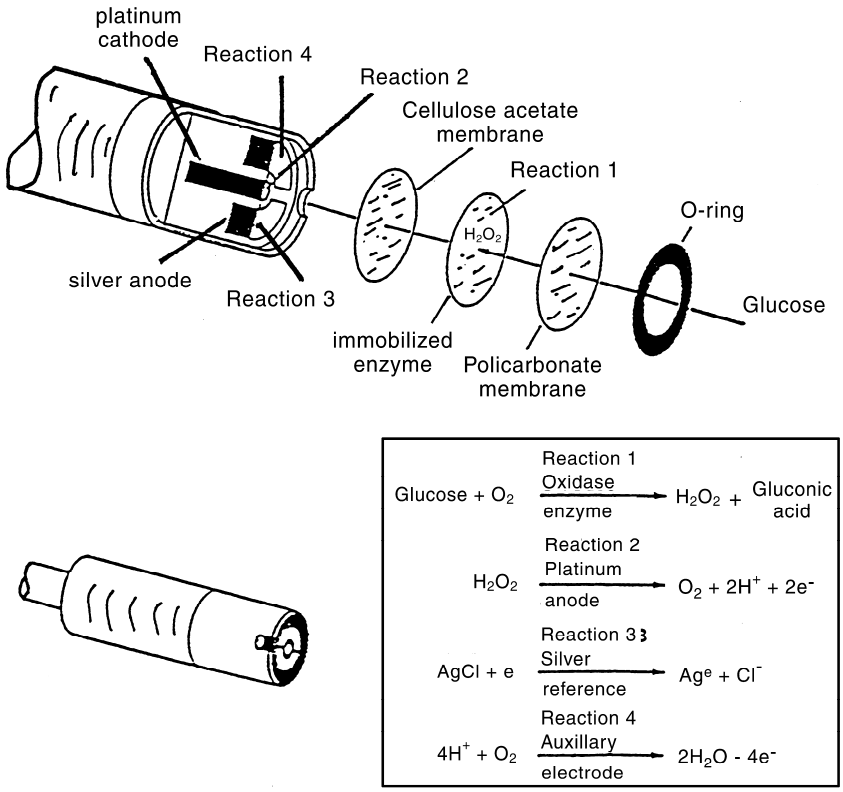

Figure 102 Schematic representation of a "first-generation" glucose biosensor (based on a probe manufactured by YSI Inc.).

The liberation of hydrogen peroxide in the enzymatic reaction can be monitored amperometically at the platinum surface:

$$H_2O_2 \xrightarrow{electrode} O_2 + 2H^+ + 2e^- \qquad (7.1)$$

Generally in enzymes, the cofactor is buried within the enzyme structure forming an insulating layer between an electrode and the redox-cofactor of the enzyme bound to the electrode surface. Therefore the direct electron transfer of the enzyme with the electrode is not possible. Using a mediator between electrode and enzyme could be a possibility to increase the sensibility in biosensors. Especially ferrocenes seem to be very useful concerning this because of their favorably formal potential regarding to enzyme redox chemistry.[211]

As a result of using artificial (diffusional) electron-carrying mediators, measurements become insensitive to oxygen fluctuations and can be carried out at lower potentials that do not provoke interfering reactions from coexisting electroactive species (Figure 103). Therefore a mediator improves the peroxide detection (aerobe conditions) or replaces the oxygen for regenerating the enzyme completely (anaerobe conditions).

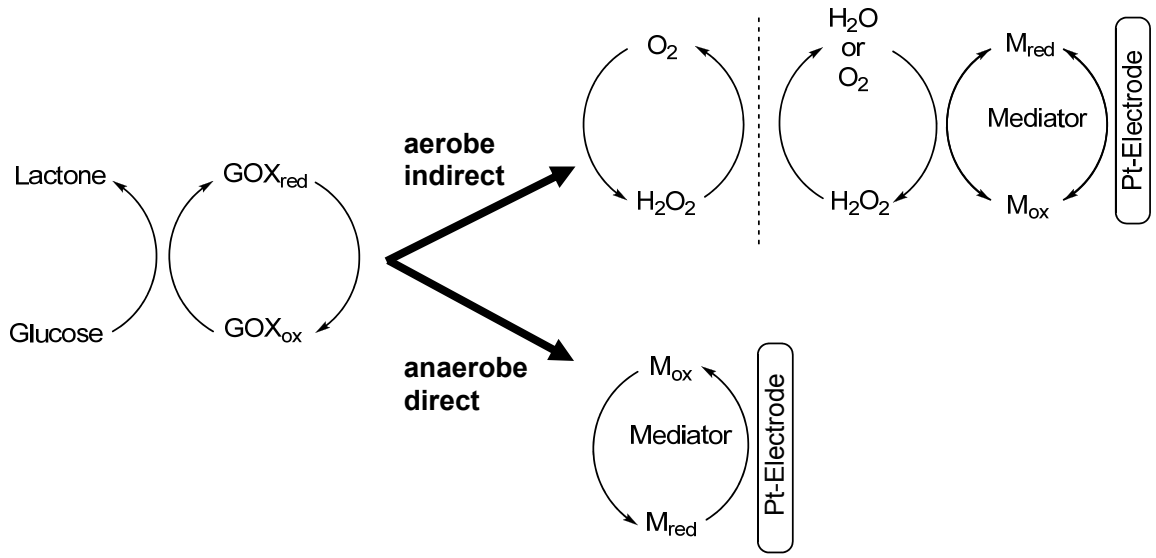

Figure 103 "Second-generation" enzyme electrode: sequence of events that occur in a mediated system under aerobe or anaerobe conditions.

This chemistry has led to the development of a pen-sized meter for personal glucose monitoring in a single drop of blood. Such rapid (~ 30 s) self-testing assays commonly rely on a chronoamperometric operation. The single-use disposable strips used with this device are made of poly(vinyl chloride) and a screen-printed carbon electrode containing a mixture of glucose oxidase and the mediator (Figure 104).

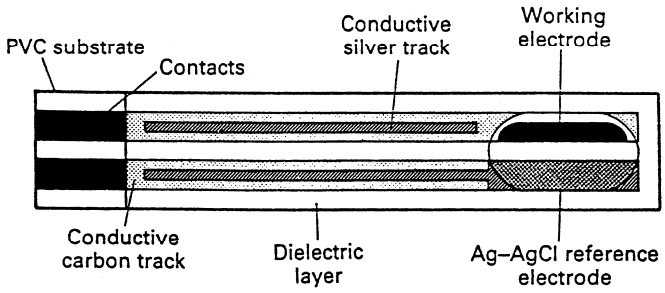

Figure 104 Schematic representation of a disposable glucose sensor strip.[212]

The cofactor nicotinamide-adenine dinucleotide (NADH) is another enzyme that is very frequently used in combination with electrochemical biosensors. Figure 105 shows the pathway for the ferrocene mediated oxidation of NADH to NAD^+.[107] Electron transfer between Fc^+ and NADH generates Fc and $NADH^{\bullet+}$. In the presence of base, this radical cation continues to react, giving the free radical $NAD^{\bullet}$. A second electron transfer step, involving another molecule of Fc^+, affords the end product of the overall NADH oxidation sequence, the pyridinium derivative NAD^+, and a second molecule of the neutral ferrocene is generated.

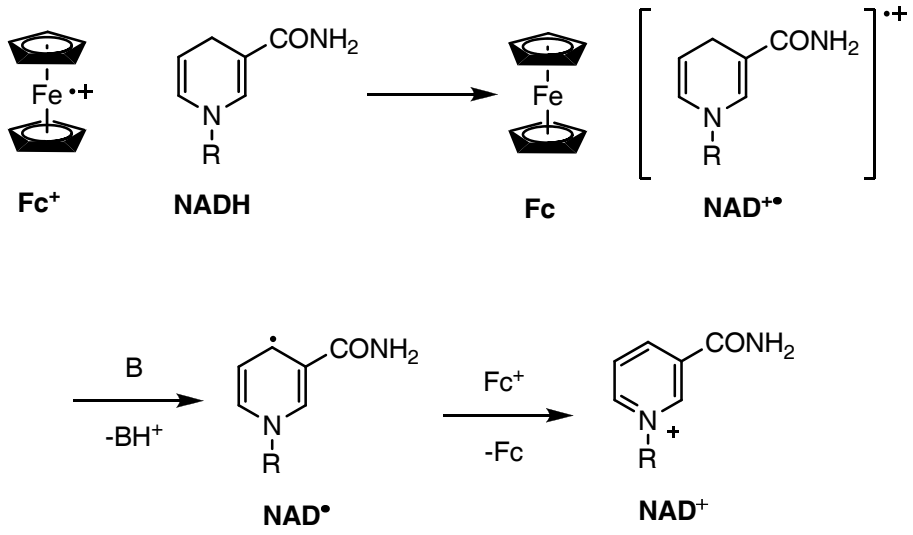

Figure 105 Ferricenium reduction by NADH (R = Adenosine diphosphoribosyl).

A particular application for this mediator/enzyme combination is found in ethanol electrodes. The reliable sensing of ethanol is of great significance in various disciplines. The enzymatic reaction of ethanol with NADH, in the presence of alcohol dehydrogenase (ADH) serves as a basis of amperometric sensors for ethanol.[213] Reagentless devices based on the coimmobilization of ADH and NAD^+ to various carbon or platinum anodes are employed (e.g., Figure 106). NAD^+ is regenerated electrochemically by oxidation of the NADH, and the resulting anodic current is measured.

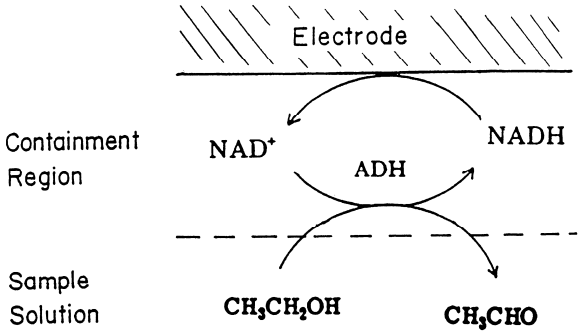

Figure 106 Reagentless ethanol bioelectrode.

As last example for a ferrocene based mediator/enzyme combination will be the tyrosinase enzyme given. Biosensors based on the tyrosinase enzyme can be used in a vide range of applications. Phenolic compounds are important contaminants in ground and surface waters.[214] Recently, a considerable amount of attention has been focused on the so-called endocrine-disrupting compounds (EDCs), which constitute a wide group of environmental pollutants that are able to mimic or antagonize

the effects of endogenous hormones, such as estrogens and androgens, or to disrupt synthesis and metabolism of endogenous hormones and hormone receptors.[215]

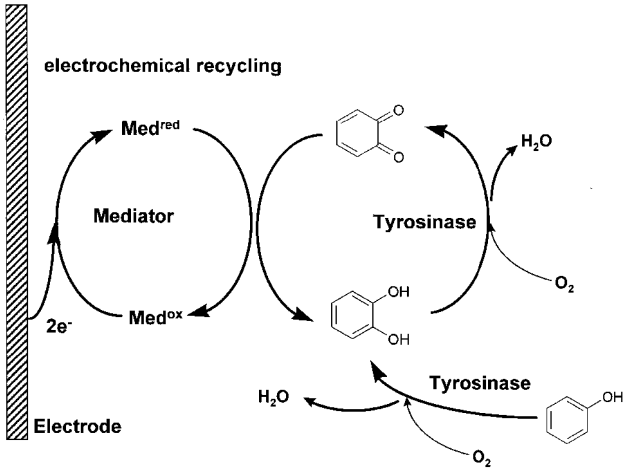

Figure 107 Reaction sequence for catechol detection used in amperometric tyrosinase lectrodes.

Tyrosinase is a copper-containing tetrameric enzyme. It catalyzes the oxidation of phenolic compounds in two steps: in the first step, ortho-hydroxylation of a phenol using molecular oxygen is producing catechols (hydroxylase activity of tyrosinase) and, in a subsequent dehydrogenation step (catecholase activity) the primarily formed catechol is converted to the related *o*-quinone as the final reaction products.[216] During the second step tyrosinase is concomitantly reduced to its original form (Figure 107). The enzymatically produced *o*-quinone can be electrochemically re-reduced to catechol at potentials lower than -50mV (vs. Ag/AgCl) at a suitable electrode surface leading to electrochemical recycling of the intermediate product catechol which may be again used as substrate of the enzyme. Thus, this regeneration implies an amplification of the signal response and hence leads to an improved detection limit based on the number of possible enzymatic conversion cycles.[217,218]

7.2. Preparation of Ferrocenylsilanes

Polymer functionalization is useful to obtain different functional polymers from the same starting material. Three different PS-*b*-PB copolymers were prepared with different ratios of styrene and butadiene, using the well known sequential anionic polymerization.[219] The ferrocene units were then introduced via hydrosilylation reaction of ferrocene-containing silanes. This permits to study the influence of different block

length on the redox properties. To this end, suitable silanes had to be synthesized at first.

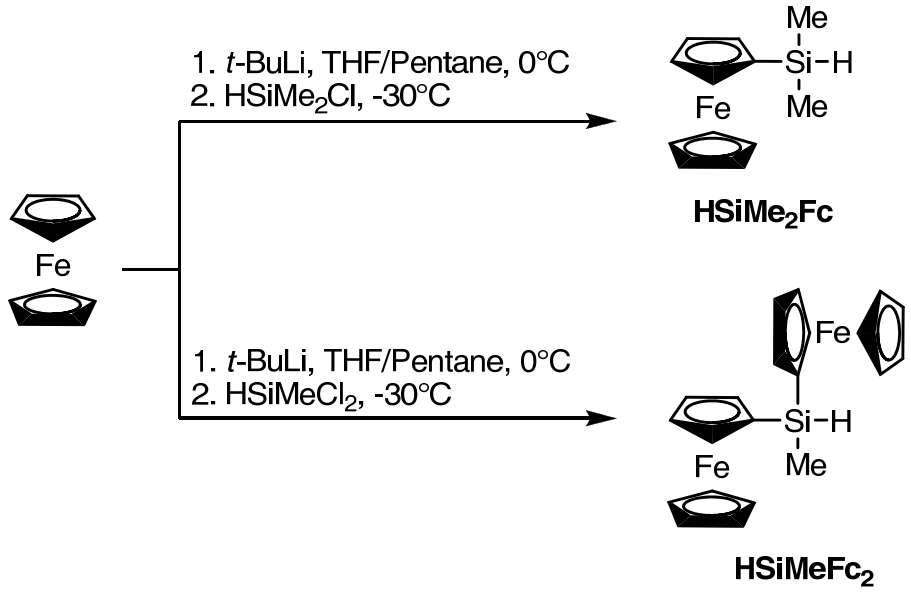

Figure 108 Synthesis of ferrocenyl-functionalized silanes

Figure 108 shows the synthesis for this purpose newly designed ferrocenyl-functionalized silanes. The two silanes prepared offered different electrochemical properties (*vide infra*). The synthesis is based on the controlled preparation of mono-lithioferrocene[220] and subsequent coupling with chlorodimethylsilane or dichloro-methylsilane. The resulting ferrocenyldimethylsilane ($HSiMe_2Fc$) or diferrocenyl-methylsilane ($HSiMeFc_2$) were analyzed by NMR, FD-MS and in case of $HSiMeFc_2$ also by X-Ray diffraction analysis. After purification the targeted $HSiMe_2Fc$ was obtained as a dark red liquid and $HSiMeFc_2$ as an orange crystalline solid.

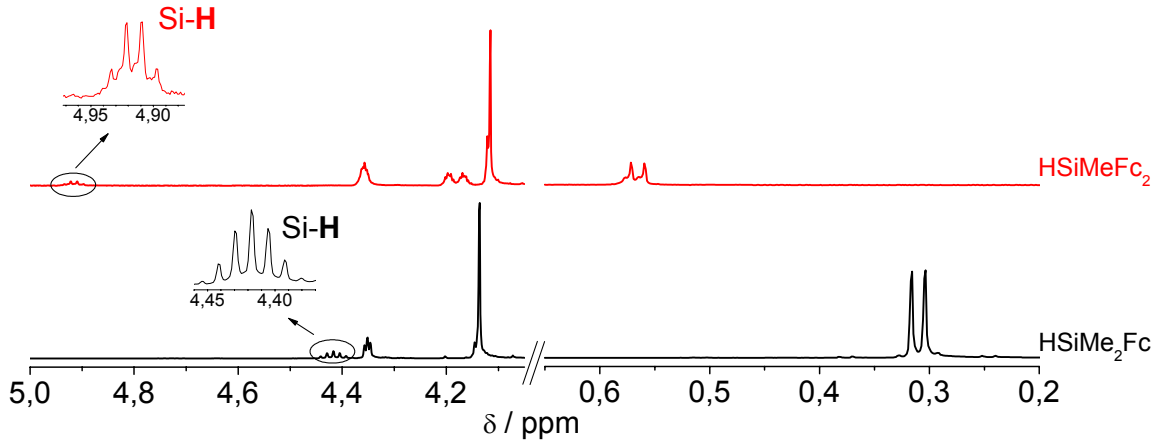

Figure 109 ^{1}H-NMR spactra of ferrocenyl-functionalized silanes in $CDCl_3$

In Figure 109 the ^{1}H-NMR spectra of the ferrocenyl-functionalized silanes are depicted. Coupling of the proton adjacent to the silane with the methylic protons gives

rise to a sevenfold split signal in case of the $HSiMe_2Fc$ and a quartet in case of the $HSiMeFc_2$, as anticipated. The silane proton for $HSiMeFc_2$ is strongly shifted to lower field in comparison with $HSiMe_2Fc$, which is based on the cumulative effect of both electron withdrawing ferrocene groups. This effect was very favorable in our case, since a lower reactivity of the sterically more demanding molecule is balanced by the fact that stronger electron withdrawing groups generally increase the hydrosilylation reactivity in the subsequent attachment step.[173]

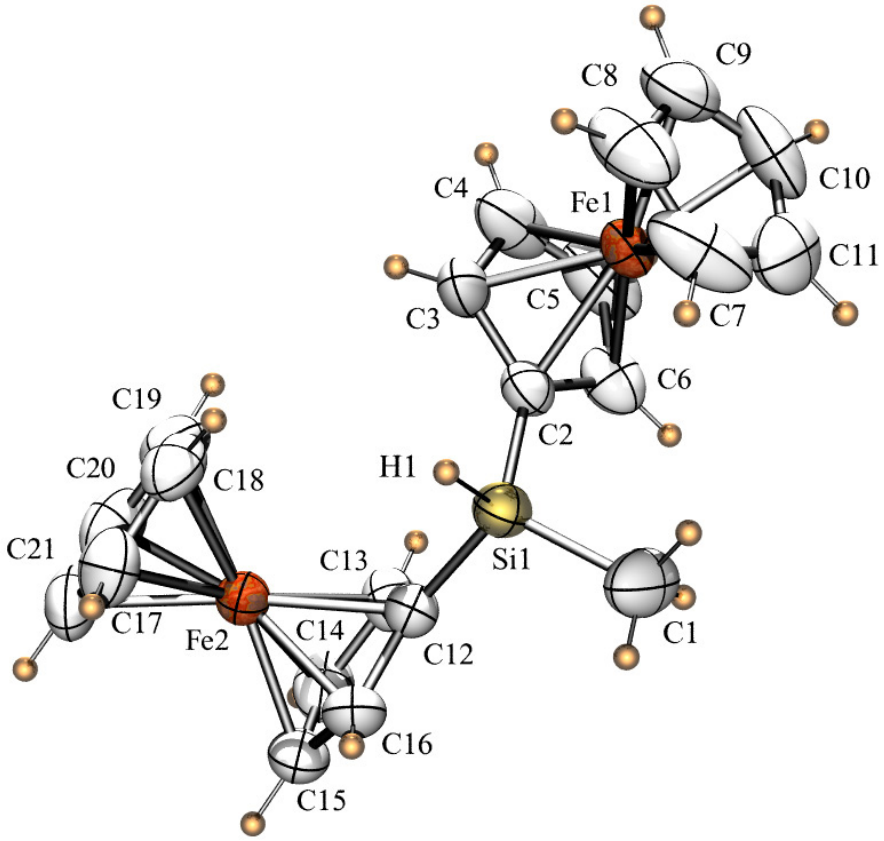

Figure 110 X-Ray crystallographic structure of $HSiMeFc_2$

In Figure 110 the X-Ray diffractogram of the newly prepared compound $HSiMeFc_2$ is shown. Because of the large ferrocene groups the tetrahedral configuration present at the silicon is slightly distorted. The angle C2-Si1-C12 formed by the two ferrocenes and the silane is slightly smaller (107.41°) than the tetrahedral angle (109.47°). This may be explained by the repulsive interaction of the ferrocene (Fe1) with the methyl group (C1) leading to an angle of 111.35° for C2-Si1-C1. The molecular structure also shows that the ferrocenyl groups are oriented at ca. 90° relative to one another. The crystallographic results obtained are in general quite similar to those obtained for the diferrocenylmethylvinylsilane published before.[221]

7.3. Preparation of Ferrocenyl-functionalized Blockcopolymers

The functionalization of the PS-*b*-PB copolymers was performed by the Pt-catalyzed hydrosilylation using Karstedt's catalyst (Figure 111).

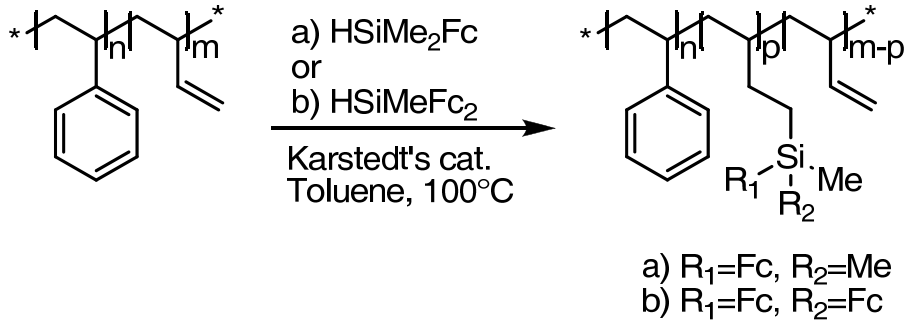

Figure 111 Synthesis of ferrocenyl-functionalized PS-*b*-PB copolymers

Starting with three different block copolymers, six different ferrocene-substituted block copolymers have been obtained after functionalization with the respective ferrocenyl silanes. The degree of functionalization can be monitored conveniently by standard ^{1}H-NMR techniques.

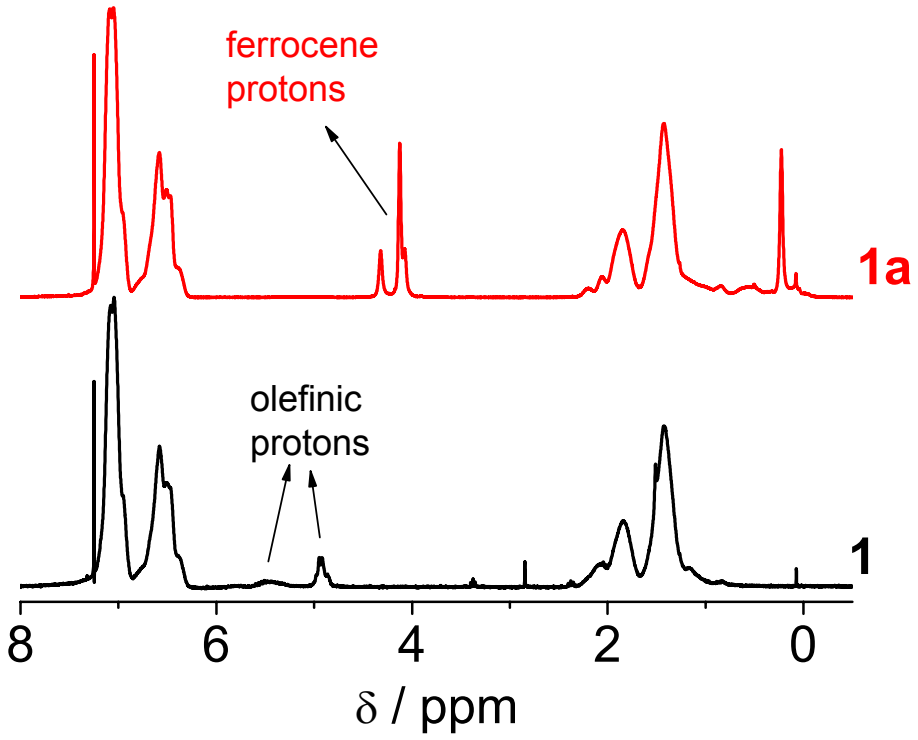

Figure 112 ^{1}H-NMR for polymers before (**1**) and after functionalization (**1a**) in $CDCl_3$

In Figure 112 the ^{1}H-NMR spectra of one of the blockcopolymers are depicted before and after functionalization with $HSiMeFc_2$. Both spectra show the aromatic protons of PS between 6.3 and 7.3 ppm and between 0.8 and 2.4 ppm the backbone protons.

Before the functionalization the olefinic protons of the PB block are visible at 5.45 and 4.94 ppm with an integral ratio of 1:2. After functionalization these signals disappear almost completely. New signals emerge between 4.00 and 4.40 ppm and at 0.23 ppm, which belong to the aromatic ferrocene protons and the methylic protons next to the silicon atom.

Table 26 Characterization of Ferrocenyl-functionalized Polymers

	w_{PB} [a]	w_{Fc} [a]	F_{Fc} [b]
1	4.3	---	---
1a	---	9.8	79.2
1b	---	17.2	73.6
2	11.3	---	---
2a	---	19.2	67.4
2b	---	36.8	82.6
3	18.9	---	---
3a	---	29.1	74.5
3b	---	48.3	83.3

[a] Mass fraction butadiene or ferrocene by ^{1}H-NMR in %
[b] Degree of olefin groups functionalized by ^{1}H-NMR in %

Table 26 shows the information gathered from ^{1}H-NMR spectra from which the relative weight content of polybutadiene in the starting block copolymer was obtained. It was found to be between 4 and 20 %, leading to relative PS:PB block length ratios of 10:1, 4:1 and 2:1. After functionalization block copolymers with weight fractions of ferrocene in the range of 10 to nearly 50 wt% of ferrocene were obtained. This corresponds to a degree of functionalization of 67 to 83 %, which is high, if taking into account that especially the $HSiMeFc_2$ group is sterically very demanding.

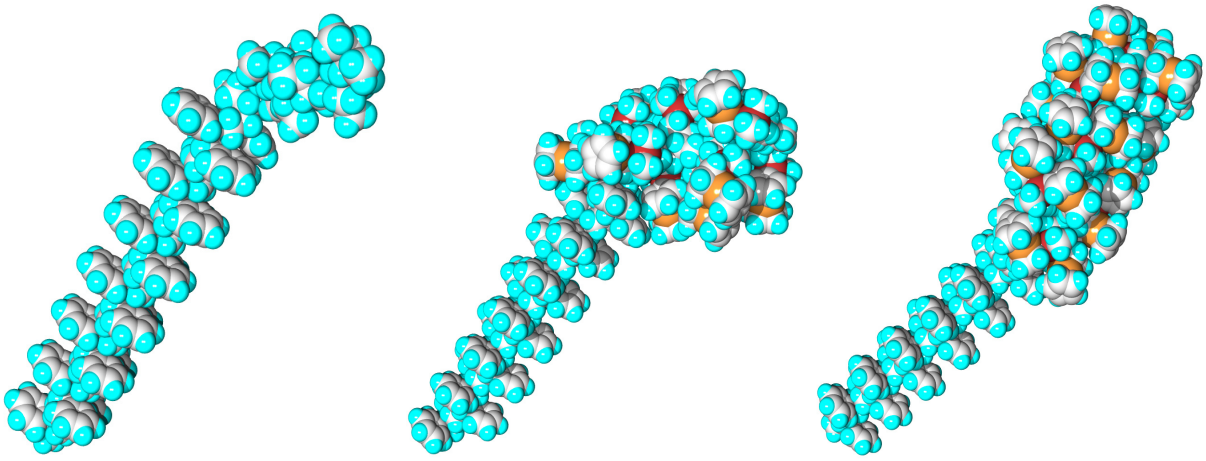

Figure 113 Stretched structure for PS_{20}-*b*-PB_{10} (left), PS_{20}-*b*-$PB_{10}(HSiMe_2Fc)_{10}$ (middle) and PS_{20}-*b*-$PB_{10}(HSiMeFc_2)_{10}$ (right) (calculated by GAMESS).

Figure 113 shows the computed stretched structures of a PS_{20}-*b*-PB_{10} before and after functionalization with the ferrocenylsilanes. It has to be pointed out that the attachment of the $HSiMeFc_2$ group forces the polybutadiene block into a more stretched structure than with the $HSiMe_2Fc$ group. The effect observed here is already very well-known for dendronized polymers. The attachment of small dendrons to polymers does not change the hydrodynamic radii significantly, even if the molar mass is strongly increased, as reviewed by Schlüter et al. for dendronized polymers.[77,222]

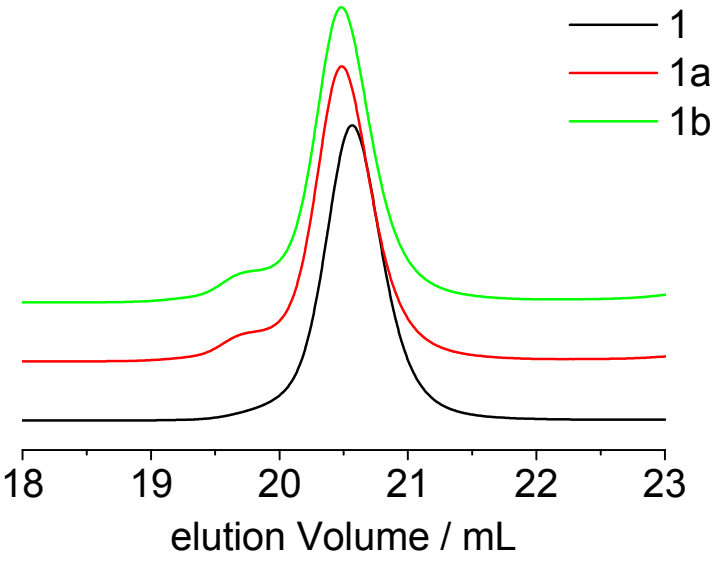

Figure 114 SEC chromatograms for polymers **1**, **1a** and **1b** in THF

Figure 114 shows the SEC chromatograms measured in THF. The peak maximum after functionalization is only slightly shifted to lower elution volumes, as expected (*vide supra*). We can observe that after functionalization a shoulder at lower elution volumes appears. There are two reasons for the formation of this high molecular weight side product. On the one hand, small amounts of a PB-*b*-PS-*b*-PB block copolymer are formed as an unavoidable side product in the anionic polymerization procedure.[79] On the other hand the Karstedt catalyst tends to form cross linked side products, especially at elevated temperatures and higher catalyst concentrations.[19] The formation of insoluble, crosslinked byproducts was not observed in our case. The block copolymers seemed to be linked mainly to a dimeric species (Figure 114). Unfortunately at lower temperatures and/or lower catalyst concentrations only poor degrees of functionalization could be obtained. The amount of dimer formed from the starting copolymer **1** was below five percent for both ferrocenylsilanes. Copolymers **2** and **3** were in the range of 5-10 percent.

Table 27 SEC/MALLS/Viscometry data of ferrocenyl-functionalized Polymers

		M_n[a]	PDI[a]	R_η[b]
1	PS_{615}-PB_{53}	66.9	1.02	6.2
1a	PS_{615}-$PB_{53}(HSiMe_2Fc)_{42}$	87.1	1.04	6.1
1b	PS_{615}-$PB_{53}(HSiMeFc_2)_{39}$	98.6	1.04	6.6
2	PS_{375}-PB_{92}	44.1	1.07	5.1
2a	PS_{375}-$PB_{92}(HSiMe_2Fc)_{62}$	83.7	1.17	5.7
2b	PS_{375}-$PB_{92}(HSiMeFc_2)_{76}$	97.4	1.11	5.5
3	PS_{455}-PB_{204}	58.4	1.02	5.7
3a	PS_{455}-$PB_{204}(HSiMe_2Fc)_{152}$	151.9	1.24	7.2
3b	PS_{455}-$PB_{204}(HSiMeFc_2)_{170}$	157.0	1.10	6.5

[a] Calculated by the combination of SEC/MALLS (x 10^3 $gmol^{-1}$)
[b] Calculated by the combination of SEC/Viscometry (x 10^3 $gmol^{-1}$)

Concerning SEC analysis all polymers were still quite narrowly distributed after functionalization, which is indicative of very well-defined polymer structures (Table 27). By coupling SEC/MALLS and NMR the relative ratio of the different blocks can be calculated. It was found that block copolymers contained between 42 and 340 ferrocene units.

7.4. Electrochemical Properties of Ferrocenyl-functionalized Block-copolymers

Figure 115 shows the cyclic voltammograms (CVs) for the ferrocenyl-functionalized polymers **2a** and **2b** measured in CH_2Cl_2. The most interesting characteristic observed are the two redox steps for the $HSiMeFc_2$ group in contrast to the $HSiMe_2Fc$ group.

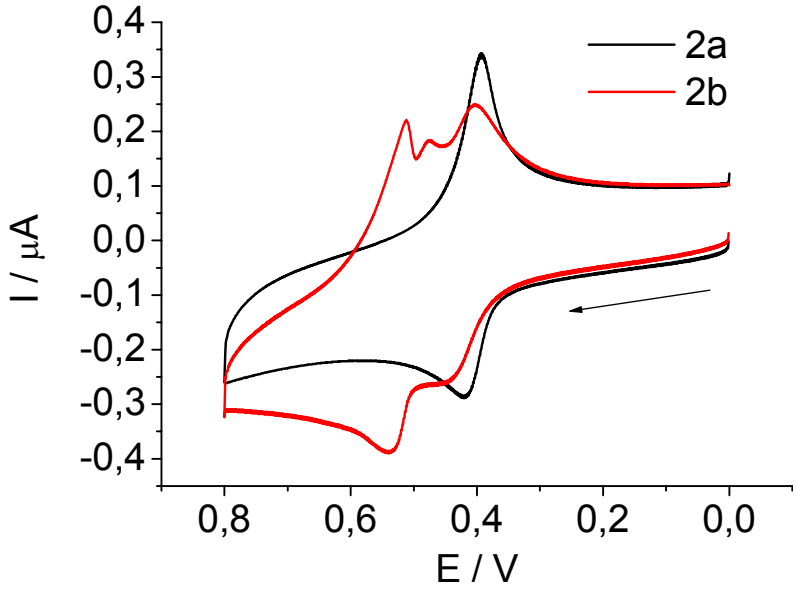

Figure 115 CVs at a Pt disk electrode in CH_2Cl_2 (TBAH) solution for copolymers **2a** and **2b** (scan rate 0.1 V/s).

This behavior was expected, since polysiloxanes modified with diferrocenylmethylvinylsilanes have been shown to behave similarly.[118] Also Manners et al. have reported that polyferrocenylsilanes exhibited two well-separated redox potentials.[223] Adjacent ferrocenyl units bridged by a silicon atom can interact with each other. The first oxidation wave corresponds to nonadjacent ferrocenes in the polymer. It is more difficult to oxidize the adjacent ferrocene, because of the neighboring positive charge of the already oxidized one. The CVs of **2a** and **2b** also illustrate that the reverse scan leads to a higher peak current. The visible difference between the peak currents is firm evidence for a precipitation process of the polymer on the electrode, leading also to shoulders in case of **2b**. When the ferrocenes are oxidized, they become insoluble in a solvent of low polarity and the polymers tend to precipitate onto the electrode. In the backward scan the signal is sharper in this case, because the mass transport is no longer diffusion-controlled.[212]

The influence of the polymer block length ratios on the electrochemical response of the attached ferrocenyl units was investigated by cyclic voltammetry. One could expect that the formation of a more or less coiled conformation of the ferrocenyl-containing block has a strong impact on the amount of ferrocenes participating in the electron transfer reaction. A comparison of the theoretical peak currents with the experimental values yields a very good approximation concerning this.[191] The peak current in a CV experiment can be theoretically evaluated from the Randles-Sevcik equation:[199,200]

$$I_p = \left(2.69 \times 10^5\right) n^{3/2} A c D^{1/2} \upsilon^{1/2} \quad (7.2)$$

With I_p as peak current, and n being the number of electrons transferred per molecule, A the electrode surface, D the diffusion coefficient, υ the scan rate, and c the polymer concentration. Dynamic light scattering (DLS) is a technique that yields the diffusion coefficients independent of electrochemical properties. These diffusion coefficients can be used to calculate the theoretical peak currents via the Randles-Sevcik equation (7.2). The value for the first oxidation peak obtained from a clean electrode was used for evaluation.

Table 28 Dimensions, diffusion coefficient, and electrochemical properties of ferrocenyl-functionalized polymers in CH_2Cl_2 solution

	D^a	$R_h{}^a$	$I_{th}{}^b$ / µA	I_{exp} / µA	I_{exp} / I_{th}
1a	0.65	7.6	1.00	0.20	0.22
2a	0.62	8.0	0.97	0.19	0.18
3a	0.62	8.0	0.97	0.24	0.14
1b	0.61	8.1	0.97	0.13	0.34
2b	0.52	9.5	0.89	0.14	0.26
3b	0.55	8.9	0.92	0.15	0.18

[a] Determined via DLS (D x 10^{-6} cm^2s^{-1}, R_h x nm).
[b] Applying Randles-Sevcik: $I_p = (2.69 \times 10^5) n^{3/2} A D^{1/2} v^{1/2} C$.

Table 28 shows the diffusion coefficients obtained by dynamic light scattering. The Stokes-Einstein equation (*vide supra*) yields the hydrodynamic radii of the polymers in CH_2Cl_2. The values are slightly higher than those obtained by online viscometry in THF (Table 27). This is explained by a different swelling behavior of the block copolymer in different solvents. These diffusion coefficients were then used to calculate the corresponding theoretical peak currents. The ferrocene concentration was set to 0.1 mmol/L in all experiments. Since the molecular weight of the polymers is similar, one would expect approximately always the same peak currents. However, in all cases much smaller currents were measured than expected. The ratio between practical and theoretical peak currents is due to the electroactive ferrocenes in solution. Polymers based on the $HSiMeFc_2$ group achieved always higher ratios. This phenomenon is related to the structure, like for dendronized polymers.[77,222] An increasing dendron size yields more stretched backbones (*vide supra*). Thus, in our case the number of ferrocenes on the electrode surface is increased. Additionally we found for both types of polymers (**a** and **b**) a decreasing fraction of electroactive units with increasing butadiene content. This again can be attributed to the coiled conformation of

the block copolymer. Larger ferrocenyl block will lead to a lower amount of ferrocenes on the surface, as expected for spherical objects.

To prove that our ferrocenyl-functionalized polymers lead to stable electrochemical reactions we recorded CVs at different scan rates. To a solution of 0.1 mmol/L ferrocene units in dichloromethane, acetonitrile was added dropwise until no further precipitation was observed in a CV experiment. In this solvent mixture the ferrocene as well as the oxidized ferricinium component are soluble.

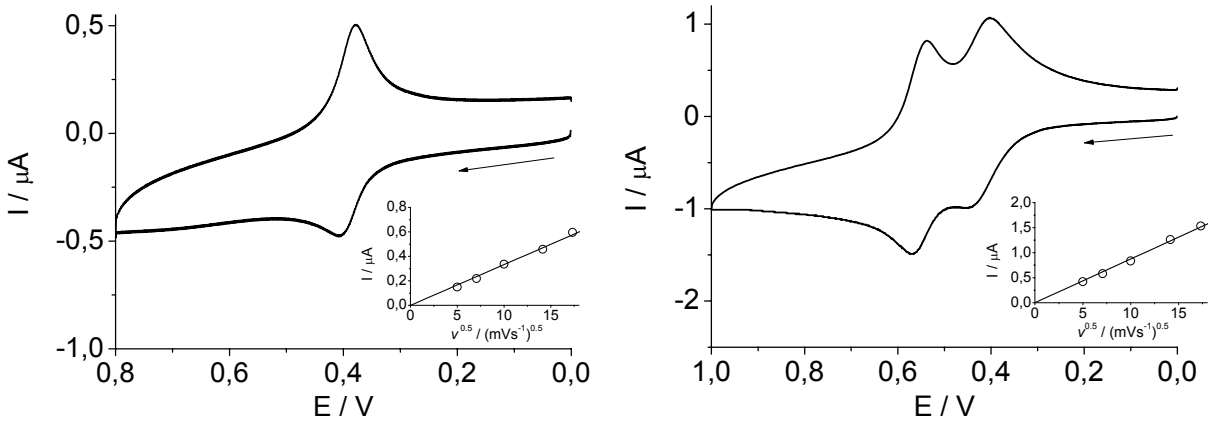

Figure 116 CVs at a Pt disk electrode obtained in CH_2Cl_2/CH_3CN (TBAH) solution for copolymer **2a** (left) and **2b** (right) (scan rate 0.1 V/s). Inset: scan rate dependence of the first anodic peak current.

Figure 116 shows the CVs measured in mixtures of dichloromethane and acetonitrile for the polymers **2a** and **2b**. The inset shows the corresponding plots of the peak current versus the square root of the scan rate for the oxidation wave. The linear dependence is evidence for diffusion-controlled redox processes.

Concerning applications, thin films (or monolayers) of an electroactive catalyst species deposited on an electrode are often preferred. The amount of catalyst required is minimized and the catalytic activity maximized because of the direct attachment onto the electrode. In our case we could obtain polymer films with controllable thickness by performing a certain number of consecutive cycles or by applying a fixed potential at 0.7 V. Using these methods we could obtain very thin polymer films.

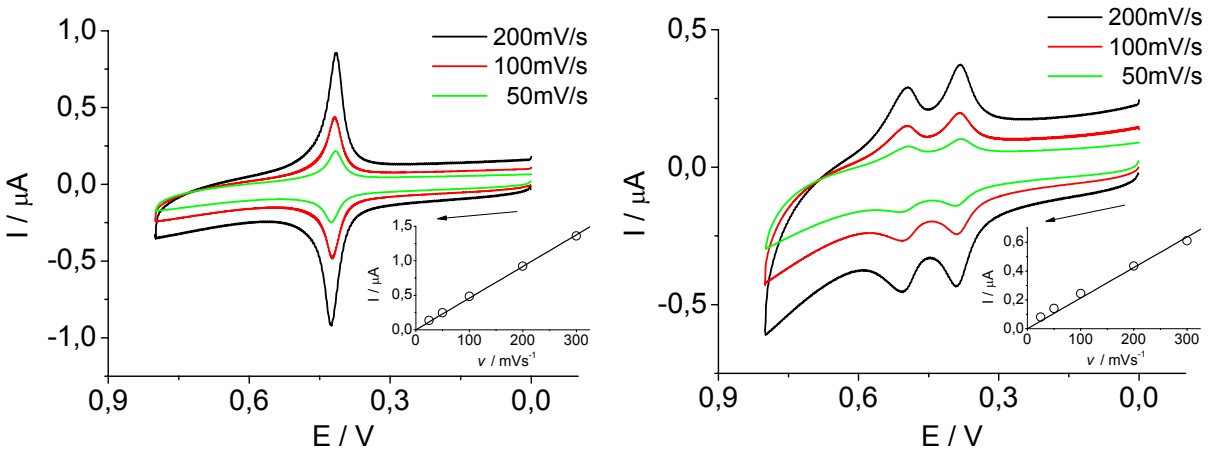

Figure 117 CVs of copolymer-coated platinum electrodes **3a** (left) and **3b** (right) measured in CH_2Cl_2 (TBAH). Inset: scan rate dependence of the first anodic peak current.

In Figure 117 the CV diagrams are depicted for the immobilized polymers **3a** and **3b** measured in CH_2Cl_2. The surface coverage of electroactive ferrocenyl sites in the film, Γ, was determined from the integrated charge of the cyclic voltammetric waves. For all polymers prepared we could obtain values for Γ in the range of 1.2 to 1.9×10^{-10} mol ferrocene per cm^2. This values are typical for monolayers of redox active species.[200] According to the theory for surface-immobilized redox centers the peak current can be described by the following equation:[224]

$$I_p = \frac{n^2 F^2 \Gamma \upsilon}{4RT} \quad with \quad \Gamma = \frac{Q}{nFA} \tag{7.3}$$

with *F* the Faraday constant, *R* the gas constant, *T* the temperature and *Q* the transferred charges. From this it follows that the peak current will be linearly dependent on the scan rate. Deviations from this dependency are an indication for a diffusional behavior of the electrons mainly caused by thicker films. In the range between 25 mV/s and 300 mV/s a linear behavior was observed (Figure 117, insets). This characterized the block copolymer films as being analogous to monolayers concerning their thickness. In general, electrodes modified with copolymers bearing the $HSiMe_2Fc$ group showed one formal potential at 0.41 V. In case of copolymers based on the $HSiMeFc_2$ group, two formal potentials were observed at 0.39 and 0.50 V. The formal potential of pure ferrocene was found to be 0.43 V with our setup. Obviously, substituents did not modify the redox potential of polymer-supported monoferrocenylsilanes in comparison to the unmodified ferrocene significantly. In contrast, for the case of diferrocenylsilanes one potential is slightly lower and the other considerably higher (*vide supra*).

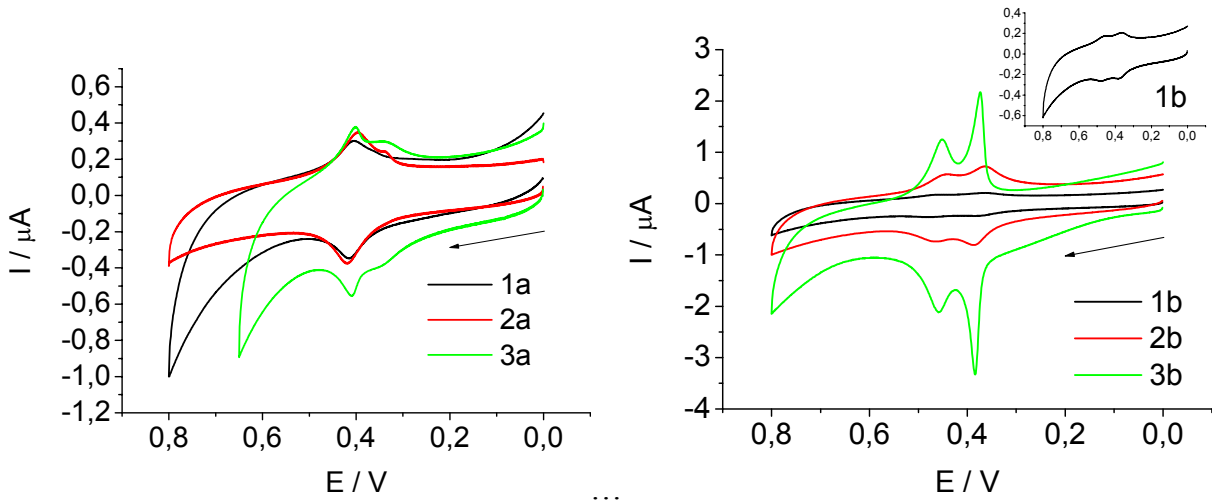

Figure 118 CVs of copolymer-modified platinum electrodes substituted with the $HSiMe_2Fc$ group (left) or on the $HSiMeFc_2$ group (right) measured in H_2O ($LiClO_4$) (scan rate 0.1 V/s).

Figure 118 shows the CV-diagram of the polymer-modified electrodes, when used in an aqueous environment. It is noteworthy that the materials behaved very stable under aqueous conditions and a film loss between two consecutive cycles could not be detected. The formal potential for all polymers was essentially the same as for measurements in CH_2Cl_2. The responses of electrodes modified with polymers **1ab**, **2ab** and **3a**, respectively, are very similar in water and CH_2Cl_2. In contrast, the features of the CV of a Pt disk electrode modified with copolymer **3b** deviates from this behavior. This copolymer with the highest ferrocene concentration exhibited similar features in CH_2Cl_2 as the other copolymers. However, in aqueous solution much sharper signals are observed. The wave shape is also characteristic of surface-confined redox couples, with the expected linear relationship of peak current with potential scan rate and peak-to-peak separation values of ΔE_{p1} = 10 mV and ΔE_{p2} = 4 mV at a scan rate of 100 mV/s. However the value of the full width at half maximum of the first redox wave (ΔE_{FWHM} = 22 mV at 100 mV/s) is smaller than 90.6/n (n = number of electrons transferred per redox center), which is the expected value for surface-confined redox species. This narrow wave can be attributed to attractive interactions between the electroactive centers within the film. This might be an indication of a special type of order on the electrode leading to a better stabilization of the oxidized polymer.[200] It is well known that polymers tend to phase separate in the bulk, if both blocks are immiscible, leading to a rich variety of morphologies (*vide supra*). A more detailed study concerning the relationship between the block length ratio and the precipitated bulk morphology on the electrode is in progress.

7.5. Application as Mediators in Biosensors

7.5.1. Peroxide Biosensor

Polymers containing ferrocene as functional group may be used in a wide range of applications (*vide supra*). Biosensoric applications represent an important target area. In general most biosensors are combined with enzymes, when employed in aqueous media.[209] Generally in enzymes, the cofactor is buried within the enzyme structure, forming an insulating layer between an electrode and the redox-cofactor of the enzyme bound to the electrode surface. Using a mediator between electrode and enzyme may represent a possibility to increase the sensibility in biosensors. Particularly ferrocenes have been proven to be very useful in this regard, because of their favorable formal potential regarding enzyme redox chemistry.[211] Unfortunately, the oxidized ferricinium species is soluble in aqueous media, which leads to undesired dissolution of the film. The hydrophobic nature of polystyrene can impede solubilization of even very ferrocene-rich polymer films (*vide supra*). Preliminary results concerning enzyme-based biosensors were very promising.[225] However, a detailed discussion for enzyme based biosensoric applications was not possible to establish in the time frame of this work.

The peroxide detector as one of the classical biosensors will be discussed in the following. Determination of hydrogen peroxide is of practical importance in clinical and environmental fields. Furthermore, the measurement of hydrogen peroxide is necessary for the development of many oxidase-based enzyme sensors.[226] A commonly used experimental principle is the electrochemical detection of hydrogen peroxide by its oxidation at a variety of electrodes. However, the major limitation of these techniques is the high operating potential required for detecting H_2O_2, which renders these devices susceptible to interfering substances.[227] Previous with siloxane based ferrocenyl-functionalized polymers and analogous dendrimers made an approach based on ferrocenyl-functionalized block copolymers very promising.[185,186] Especially the high stability under aqueous conditions were of great importance in this context (*vide supra*).

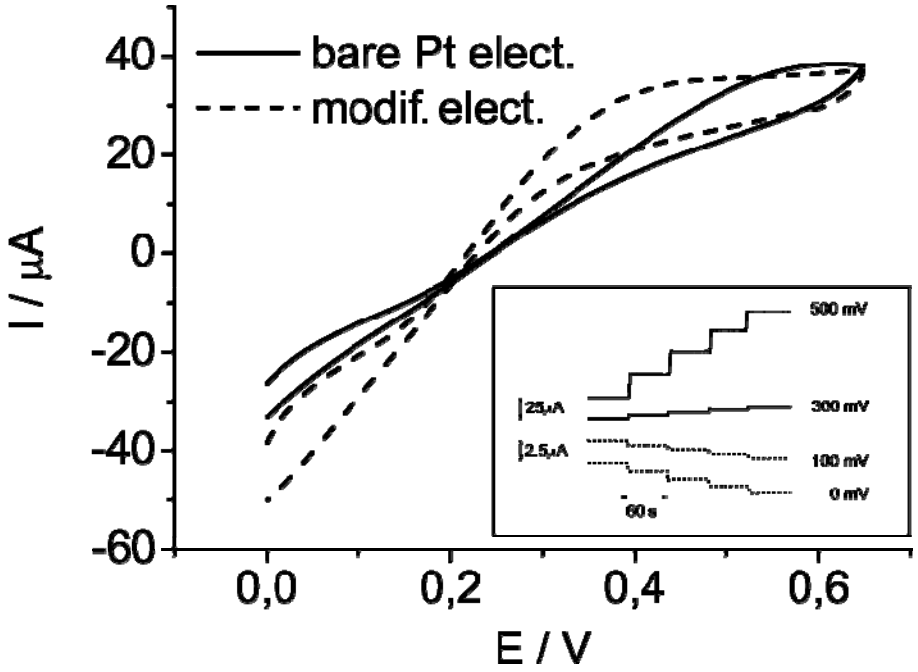

Figure 119 CVs for copolymer platinum electrode **2b** and a bare platinum electrode in aqueous 0.5mmol/L H_2O_2 ($NaClO_4$) solution (scan rate 25 mV/s). Inset: Response of copolymer platinum electrode **2b** to the batch addition of 0.5 mmol/L hydrogen peroxide aliquots at several applied potentials in H_2O.

Figure 119 shows the CVs for the copolymer platinum electrode **2b** and a bare platinum electrode in an aqueous 0.5 mmol/L H_2O_2 solution. In comparison to the bare platinum electrode the modified electrode was able to lower the potential for the catalytic oxidation of peroxides down to 0.3 V in comparison to the platinum electrode (≈0.5 V). This is clear evidence for a lowered activation energy concerning the catalytic oxidation of H_2O_2. The electrode reaction can then be expressed by:

$H_2O_2 + 2\text{Pol-Fc}^+ \rightarrow O_2 + 2\text{Pol-Fc} + 2H^+$

The range for the reduction was not increased like for the oxidation. However the voltammogram in Figure 119 also shows an enhancement of the current in the cathodic response of the modified electrode. These results are indicative of electrocatalytic behavior. The electrocatalytic activity observed can be related to the possibility of the modified electrodes to carry out multielectronic transfers. The interaction of a substrate molecule, H_2O_2, concurrent with two redox groups in the polymer is favored by the cooperative effects of short distance and electronic communication between adjacent ferrocenyl groups within the film. This fact must facilitate the simultaneous transfer of the two electrons required for the oxidation of H_2O_2.

The stepwise addition of small aliquots of hydrogen peroxide (Figure 119, inset) shows that the electrode equilibrates very fast. Figure 120 represents the plots for hydrogen peroxide, using an electrode modified with block copolymer **2b** and meas-

uring at several fixed potentials. At potentials of 300 mV and higher catalytic oxidation of the peroxide is observed. Potentials of 100 mV and lower show the reduction of the peroxide. At potentials of about 200 mV no catalytic activity could be observed.

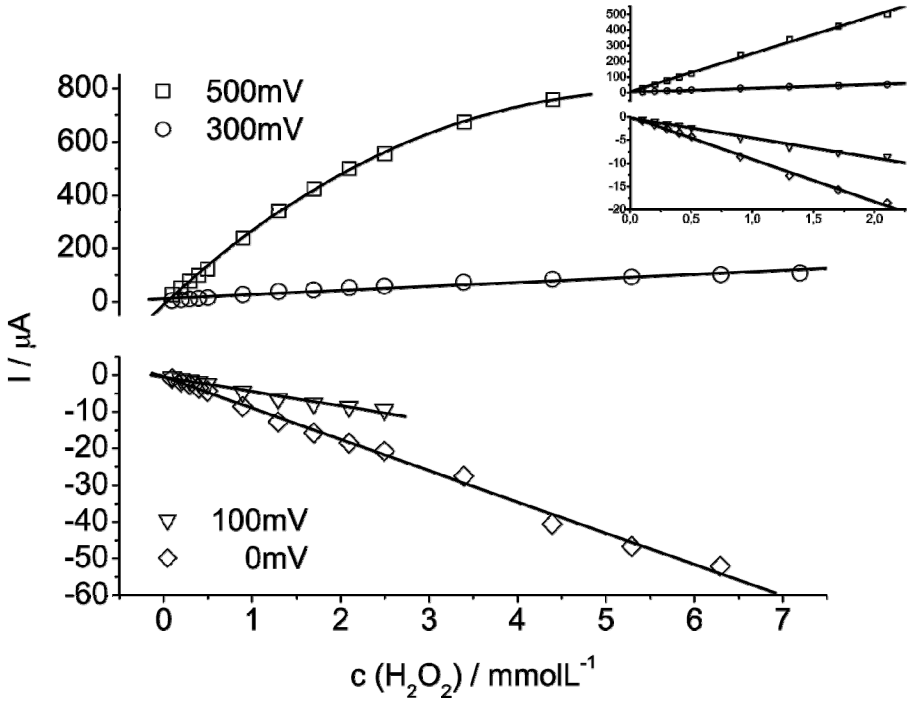

Figure 120 Hydrogen peroxide calibration plots from 0 to 500 mV copolymer platinum electrode **2b**.

These plots indicate linearity up to a concentration of 2 mmol/L for all potentials. A linear dependence between electrode response and substrate concentration could indicate that the chemical reduction of ferricinium sites in the polymer layer by H_2O_2 is the rate-determining step. This process is slower than the electrochemical oxidation of the reduced ferrocene groups.[228,229] Nevertheless, the range before reaching a saturation was very different for the studied potentials. At 500 and 100 mV the saturation was reached very fast at concentrations about 2 mmol/L peroxide. At 300 and 0 mV the linearity was kept up to concentrations of 7 mmol/L peroxide.

However, it has to be emphasized that the results presented here concerning biosensor applications are still of an exploratory nature. The effect of block length ratio of the block copolymers, nature of the ferrocenyl silane employed, pH of the solution, film thickness, etc. concerning peroxide sensors could not be investigated in the timescale of this work.

7.5.2. Enzyme Based Biosensor

The following results represent only preliminary results concerning the capabilities of the block copolymers to interact with different enzymes. All measurements were performed with the same Pt-electrode modified with block copolymer **2b** containing a surface coverage of 2.4×10^{-10} mol ferrocene per cm^2. Thus all enzyme reactions were performed with the enzyme in solution. Of course, the simultaneous immobilization of the mediator together with the enzyme yields in general better results. These experiments were not possible to be investigated in the time scale of this work. Nevertheless, these studies will be continued by coworkers as the following results were very promising.

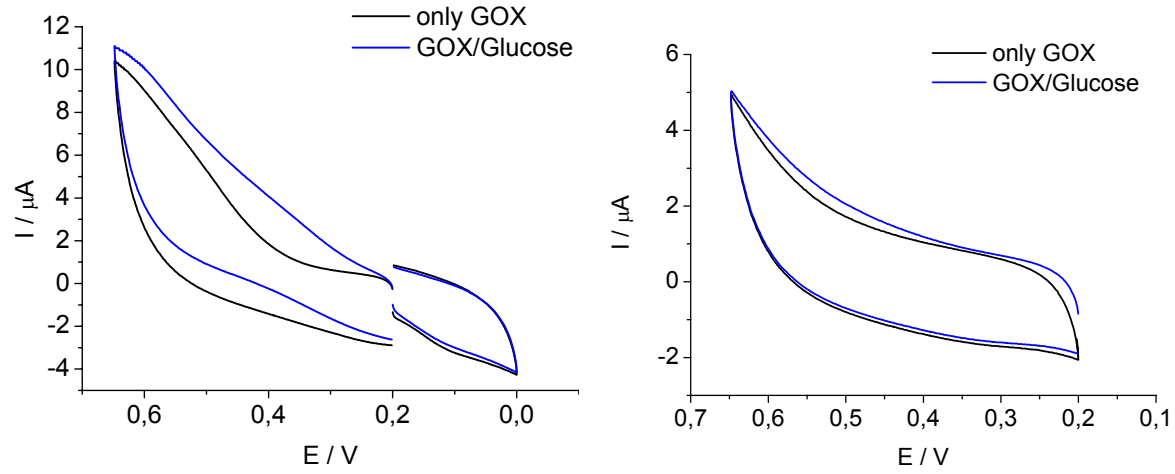

Figure 121 Cyclic voltammograms of **2b**/GOX enzyme sensor in absence and presence of 5 mM glucose in 0.1 M phosphate buffer (pH 6.65) and excess GOX in solution. Scan rate: 5 mV/s. Left: aerobe. Right: anaerobe.

As mentioned in the beginning the glucose biosensor is probably the oldest biosensor. It can be used under two particular different ways (Figure 103, page 140). On the one hand it is possible to perform the detection under aerobe conditions. In this case the GOX is regenerated by the oxygen in the water under formation of hydrogen peroxide. Thus the glucose is detected indirectly by the formed hydrogen peroxide. Figure 121 (left) shows the CV for aerobe measurements of a copolymer modified electrode in water containing the GOX enzyme with and without glucose. Obviously the formed peroxide could be detected by oxidation (0.2-0.6 V) but not by reduction (0.0-0.2 V). This is based in the worse signal strength for the reduction of peroxides (*vide supra*). On the other hand the glucose can be detected by the direct electron transfer of the GOX to the electrode via the mediator. Figure 121 (left) shows a CV obtained under anaerobe conditions. It is obvious that after the addition of the glu-

cose the current increased slightly. Generally it is very difficult to perform measurements in these concentrations without immobilization of the enzyme. Thus, these results are still very good by having this in mind.

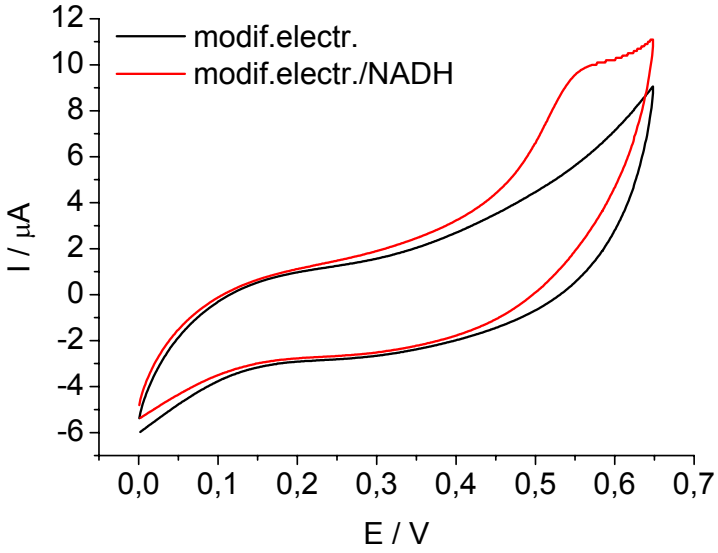

Figure 122 Cyclic voltammograms of **2b**/NADH enzyme sensor in absence and presence of NADH in 0.1 M phosphate buffer (pH 6.65). Scan rate: 10 mV/s.

The second enzyme employed in this preliminary study was the NADH. As the oxidation of NADH requires two electrons it was expected two obtain at least for the polymers based on the $HSiMeFc_2$ group good results (Figure 105, page 141). The interaction of the ferrocenes by the bridging silicon should enhance reactions based on two electron mechanism. Figure 122 shows the CV of a Pt/**2b** electrode in a buffered water solution with and without NADH. Apparently after the addition of NADH the current is increased for potentials above 0.5 V. This is a clear signal for the oxidation of the NADH by the electrode/mediator combination.

The last enzyme studied was the tyrosinase enzyme for the detection of phenol. In this case the mediator does not interact with the enzyme directly (Figure 107, page 142). The enzyme oxidizes the phenol first to an *o*-catechol and then to the corresponding *o*-quinone. The mediator reduces the *o*-quinone to back to *o*-catechol so that the enzyme has to oxidize it a second time, and so fort. Because of these cycles the sensibility is highly enhanced for the detection of phenols. All catalytic and electrochemical reactions are based on a two electron transfer mechanism.[218] Thus single electron mediators would yield only poor results.

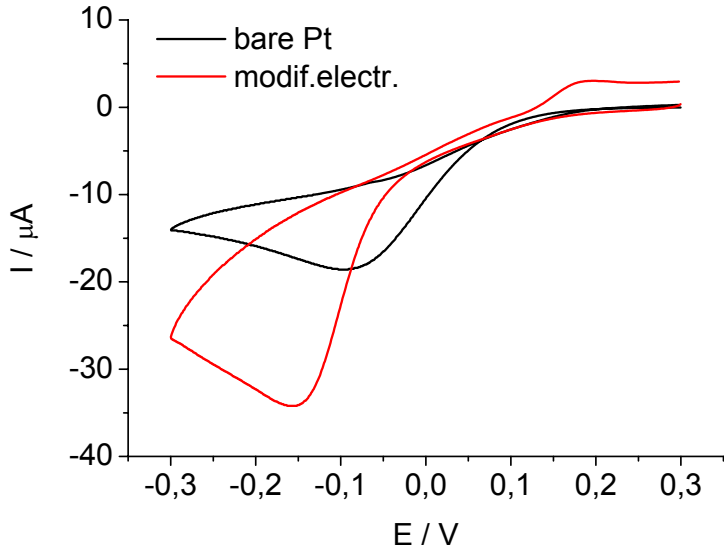

Figure 123 Cyclic voltammograms of phenol/tyrosinase enzyme sensor in absence and presence of **2b** on the electrode in 0.1 M phosphate buffer (pH 6.65). Scan rate: 50 mV/s.

Figure 123 shows the result for CV measurements of phenol with tyrosinase in buffered water with a bare Pt- and a Pt/**2b**-electrode. It is obvious that the peak current for the Pt/**2b** combination is much stronger than for the Pt-electrode alone. In contrast to the NADH biosensor the signal is here at negative potentials because the mediator acts as reducing agent.

7.6. Conclusion

The synthesis of a series of ferrocene-containing block copolymers with variable ferrocene fraction by attachment of ferrocene-bearing silane units was developped. To modify the polystyrene-polybutadiene blockcopolymers a hydrosilylation based route was chosen. Thus new literature unknown ferrocenylsilanes had to be prepared. This synthetic approach may be viewed as a modular approach, permitting to vary both block lengths as well as the fraction and nature of the electroactive ferrocene-based moiety.

The polymers exhibited different electrochemical behavior according to the structure of the functional units and the block length ratio. Polymers containing ferrocenes bridged by a silicon atom exhibited two formal potentials instead of one for the unbridged ferrocenes. It was furthermore observed that the presence of a higher frac-

tion of ferrocene lead to a lower fraction of electroactive ferrocene. The modified electrodes gave clear and stable signals for measurements under aqueous conditions. First experiments on use of the polymers as peroxide or enzyme biosensors were successful and very promising. In comparison to the ferrocenyl functionalized polymers presented in chapter 6, these polymers have the advantage to be stronger bound to the electrode because of the nonpolar polystyrene block.

7.7. Experimental Part

7.7.1. Reagents

Karstedt's catalyst in xylene (2.1 – 2.4 % Pt) was purchased from ABCR GmbH & Co. KG and used as received. PS_x-*b*-PB_y with a 100% 1,2-PB content was prepared in 20 g amounts via a simplified anionic polymerization procedure according to Gronski et al.,[219] using a specially constructed reactor system suitable for working under high vacuum and overpressure. Methanol, dichloromethane and other solvents and reagents were purchased from Acros and used as received or dried as described in the literature. *Sec*- and *tert*-butyllithium were purchased from Acros (1.5M solution in pentane) and the exact concentration was determined according to a literature procedure.[154]

7.7.2. Synthesis of Diferrocenylmethylsilane ($HSiMeFc_2$)

Ferrocene (4.4 g, 24 mmol) was dissolved under an inert atmosphere in a mixture of 15 mL dried THF and 15 mL dried pentane. After cooling the solution to 0 °C 20 mmol of *t*-BuLi were added slowly to the solution. The mixture was stirred for 30 min at 0 °C and then cooled down to -30 °C. Dichloromethylsilane (1.66 g, 14.4 mmol) was added slowly to the mixture. After complete addition the reactants were stirred for 30 minutes at -30 °C. Then the mixture was allowed to warm to room temperature. Solvents were removed under vacuum, the crude product was dissolved in pentane and LiCl was removed by filtration. The solvent was again removed under vacuum and the crude product was purified by flash chromatography

over silica gel using a mixture of petrol ether and dichloromethane (10:1). After purification the product was obtained in form of dark orange crystals in 39 % yield.
^{1}H-NMR ($CDCl_3$) δ: 4.92 (q, 1H, ^{3}J = 3.4 Hz), 4.38-4.33 (m, 4H), 4.22-4.15 (m, 4H), 4.11 (s, 10H), 0.57 (d, 3H, ^{3}J = 3.7 Hz). ^{13}C NMR ($CDCl_3$) δ: 73.38, 71.10, 71.01, 68.42, -4.33. FD-MS: 414.0 (calc. 414.0). Crystal data: M_r = 414.18, 0.10 x 0.06 x 0.02 mm dark yellow block; crystal system monoclinic; space group P $2_1/c$; z = 4; a = 9.8776(3), b = 12.0035(4), c = 15.5669(5) Å; β = 92.127(2)°; V = 1844.43(10) Å^3; ρ_{calc} = 1.492 g/cm^3.

7.7.3. Synthesis of Ferrocenyldimethylsilane ($HSiMe_2Fc$)

The procedure is analogous to the synthesis described above. However, 28.8 mmol of chlorodimethylsilane were added to the monolithioferrocene solution and purification was performed by vacuum distillation (10^{-2} mbar). After purification the product was obtained as a dark orange oil in 41 % yield.
Bp = 63 °C (1.2 x 10^{-2} mbar). ^{1}H-NMR ($CDCl_3$) δ: 4.42 (hept, 2H, ^{3}J = 3.7 Hz), 4.35 (t, 1H, ^{3}J = 1.7 Hz), 4.15-4.14 (m, 7H), 0.31 (d, 3H, ^{3}J = 3.7 Hz). ^{13}C NMR ($CDCl_3$) δ: 73.38, 71.05, 68.34, 68.04, -3.15. FD-MS: 244.1 (calc. 244.0).

7.7.4. Synthesis of Ferrocenyldimethylsilane ($HSiMe_2Fc$)

All catalytic reactions were conducted in parallel using Radley's 12-placed reaction carousel under inert gas (N_2). 200 mg of polymer and an equimolar amount of the above synthesized silanes according to the double bonds were dissolved in 5 mL of dried toluene and heated to 100 °C. 50 μL Karstedt's catalyst were added and the mixture was stirred at 100 °C for 3 days. The polymer was purified by repeated precipitation from THF/methanol (5 x). Yields obtained were in the range from 60 to 80 %.
^{1}H-NMR ($CDCl_3$) δ: 7.48-6.22 (aromatic PS protons), 4.49-3.93 (aromatic ferrocene protons), 2.40-0.41(aliphatic backbone protons), 0.23 (s, methylic ferrocene protons)

8. Summary and Conclusions

8.1. Amphiphilic Block Copolymers

The scope of this work was to study the influence of block copolymer architectures on the various global properties of aggregates formed. In this context, in chapter 3 a suitable synthesis for linear-linear and linear-hyperbranched structures based on polystyrene and polyglycerol are described. Two strategies were examined. One strategy was based on the classical sequential anionic polymerization; the second strategy was based on a “Click-Chemistry” approach. For both ways in the ensuing step glycidol was hypergrafted on these block copolymers by applying the hypergrafting strategy. Block copolymers of varying molecular weight were synthesized for a detailed comparison.

Table 29 General characteristics of the amphiphilic block copolymers.

	NMR	SEC	
	wt.-% PG	M_n	PDI
PS_{40}-*b*-linPG_7	11.1	3 400	1.08
PS_{40}-*b*-hypPG_{30}	34.8	5 100	1.05
PS_{192}-*b*-linPG_{24}	8.2	22 600	1.03
PS_{192}-*b*-hypPG_{110}	29.0	22 400	1.04
linPG_{24}-*b*-PS_{250}-*b*-linPG_{24}	12.0	30 600	1.04

All block copolymers used for the study of the aggregation behavior were well-defined concerning their polydispersity (Table 29).

In chapter 4 the global properties with respect to aggregation in solution were studied. Numerous of techniques like DLS, SLS, SEC/MALLS/Viscometry, AFM and Cryo TEM measurements were performed to obtain a visual image from the appearance of the aggregates.

Based on the results from DLS linear-linear PS-*b*-PG copolymers yielded in nonpolar solvents like toluene or chloroform polydisperse aggregates, while linear-hyperbranched analogues yielded well-defined aggregates. The aggregates based on the linear-hyperbranched structure were very stable and their size and polydisper-

sity was almost constant for longer periods of time. In case of the linear-linear structures they became only slightly larger and more polydispers.

Table 30 SLS and DLS Data obtained in chloroform (black) and toluene (blue).

	SLS				DLS		ρ
Copolymer	**M_w**	**Z**	**R_g(z)**	**A_2**	**R_h(z)**	**μ_2**	
PS_{192}-*b*-linPG$_{24}$	2 972 000	136	47.0	1.6×10^{-5}	30.4	0.21	1.55
PS_{192}-*b*-hypPG$_{110}$	3 851 000	137	17.3	-9.8×10^{-6}	24.0	0.02	0.72
PS_{40}-*b*-linPG$_7$	39 400	8	---	-1.5×10^{-7}	---	---	---
PS_{40}-*b*-hypPG$_{30}$	942 000	148	13.7	-2.4×10^{-5}	14.3	0.05	0.96
linPG$_{24}$-*b*-PS_{250}-*b*-linPG$_{24}$	1 131 000	38	28.0	-1.5×10^{-6}	19.6	0.12	1.49
PS_{192}-*b*-linPG$_{24}$	2 005 000	92	34.5	1.2×10^{-5}	37.0	0.19	0.93
PS_{192}-*b*-hypPG$_{110}$	5 867 000	208	33.3	5.6×10^{-9}	31.7	0.04	1.05
PS_{40}-*b*-linPG$_7$	30 600	7	---	-2.1×10^{-5}	---	---	---
PS_{40}-*b*-hypPG$_{30}$	533 000	84	30.3	-7.4×10^{-8}	16.1	0.10	1.88

M_w in g/mol; R_g oder R_h in nm; A_2 in mol*mL*g^{-2}

Table 30 shows the results from batch DLS and SLS measurements in toluene and chloroform. The linear-hyperbranched block copolymers achieved very low μ_2 values that are typical for almost monodisperse distributions. This result was very important because it demonstrates one very important advantage of the linear-hyperbranched block-copolymers in comparison to the linear-linear analogues. Surprisingly the smallest block copolymer (**PS_{40}-*b*-linPG$_7$**) did form hardly any aggregates, which can be explained by the lower amphiphilic character. Concerning the ρ-ratios all polymers were of approximately spherical shape (more or less defined). Especially the largest block copolymer based on a linear-hyperbranched structure (**PS_{192}-*b*-hypPG$_{110}$**) formed always very well defined aggregates similar to a homogeneous sphere.

Using SEC columns with large pore sizes it was possible to analyze the aggregates formed in chloroform by SEC. Surprisingly it was found that by passing the aggregates through a SEC column the polydispersity was greatly reduced. Because of the shear forces on the SEC columns the aggregates disintegrated always partly into the corresponding unimer fraction.

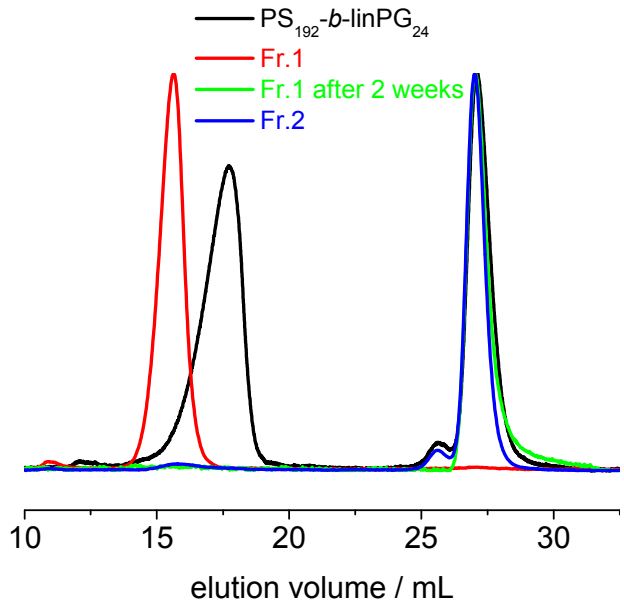

Figure 124 SEC fractionation results of **PS_{192}-*b*-linPG$_{24}$** copolymer aggregates in chloroform (UV-detector). Fr.1 denotes the aggregate fraction and Fr.2 the unimer fraction.

Figure 124 shows the results for the pure linear block copolymer **PS_{192}-*b*-linPG$_{24}$**. It was apparent that the aggregate fraction did not contain unimers any more. The size of the particles appeared to become larger and more monodisperse. After waiting for two weeks, all aggregates in this fraction were disintegrated into unimers. Because of the very low concentration ($c < 0.05$ g/L = below the critical micelle concentration), the unimer fraction never formed micelles again. For the other copolymers similar results were found. The **linPG$_{24}$-*b*-PS_{192}-*b*-linPG$_{24}$** copolymer showed a bimodal distribution in comparison to the other block copolymers, which was attributed to the formation of flower-like micelles. The much lower polydispersity was evident from DLS measurements (Table 31).

Table 31 DLS from fractionated and non fractionated block copolymer aggregates in chloroform.

Copolymer	fractionated	R_h (z)	μ_2
PS_{192}-*b*-linPG$_{24}$	no	30.4 nm	0.224
	yes	14.4 nm	0.113
PS_{192}-*b*-hypPG$_{110}$	no	24.0 nm	0.020
	yes	24.5 nm	0.004

The **PS_{192}-*b*-linPG$_{24}$** and **PS_{192}-*b*-hypPG$_{110}$** yielded a less polydisperse structure. In the case of the **PS_{192}-*b*-hypPG$_{110}$** copolymer, almost monodisperse aggregates were formed.

UV-vis spectra recorded during elution showed a very surprising behavior. The aggregates exhibited a broad absorption from 230 to 450 nm with three maxima at 240, 256 and 313 nm. This absorption spectrum was not obtained for the unimer fraction or for the aggregate fraction after disintegration into unimers (Figure 125).

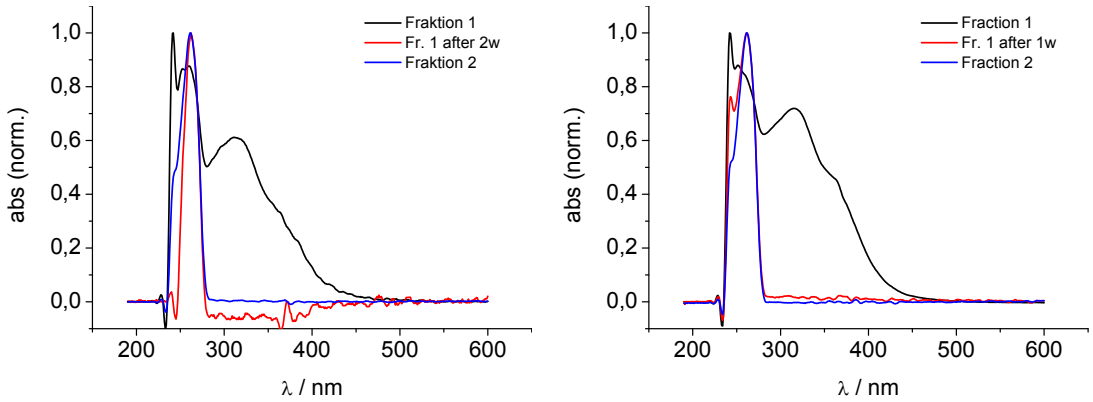

Figure 125 UV-vis spectra obtained during SEC for **PS_{192}-*b*-linPG$_{24}$** (left) **PS_{192}-*b*-hypPG$_{110}$** (right)

No similar example was found in literature. A possible explanation may be based on π-π interactions between styrene units near the core (more dense alignment). The observation will have to be explained in follow-up work. TEM and AFM microscopies confirmed the results from DLS and SLS concerning shape and polydispersity of the particles.

Finally the aggregation behavior in methanol was studied. This solvent forms micelles of inverse structure in comparison to nonpolar solvents.

Table 32 SLS and DLS Data obtained in methanol (20 °C).

	SLS		DLS		ρ
Copolymer	**M_w (app.)**	**R_g(z)**	**R_h(z)**	**μ_2**	
PS_{192}-*b*-hypPG$_{110}$	2 x 10^{10}	431.9	145.5	0.15	3.0
linPG$_{24}$-*b*-PS_{250}-*b*-linPG$_{24}$	6 x 10^{9}	131.4	90.1	0.13	1.5
PS_{192}-*b*-linPG$_{24}$	non measurable				
PS_{40}-*b*-linPG$_7$	polymers precipitated during dialysis				
PS_{40}-*b*-hypPG$_{30}$					

Apparent M_w in g/mol; R_g(z) and R_h(z) in nm

Table 32 shows the obtained data from DLS and SLS measurements for the inverse micellar structures. Surprisingly, not only the sample **PS_{40}-*b*-linPG$_7$**, but also the **PS_{30}-*b*-hypPG$_{30}$** copolymer was incapable of forming stable inverse micelles. The sizes of the other aggregates were very large. These in combination with the deter-

mined ρ-ratios were a strong indication for vesicles. Cryo-TEM measurements finally supported the formation of spherical vesicles.

It was concluded that hypergrafting to linear-hyperbranched copolymers was a crucial step, if well-defined, monodisperse aggregates were required. The linear AB as well as the ABA structure was not capable of forming well-defined superstructures. These results are important, as they clearly prove that linear-hyperbranched polymers offer advantages for the preparation of ordered nanoarrays.
Unfortunately the synthesis of larger linear polyglycerols was not trivial. Future projects in this area should deal with this problem to answer the question, if longer linear polyglycerol segments improve the polydispersity of the suprastructures.

8.2. Branched Polydienes

The target of this part of the thesis was the development of a new pathway to branched polydienes based on common vinyl monomers. The synthesis of the macromonomers was conducted in one step by conventional anionic polymerization of isoprene or butadiene, leading to well-defined polymers with respect to molecular weight and polydispersity (Figure 126).

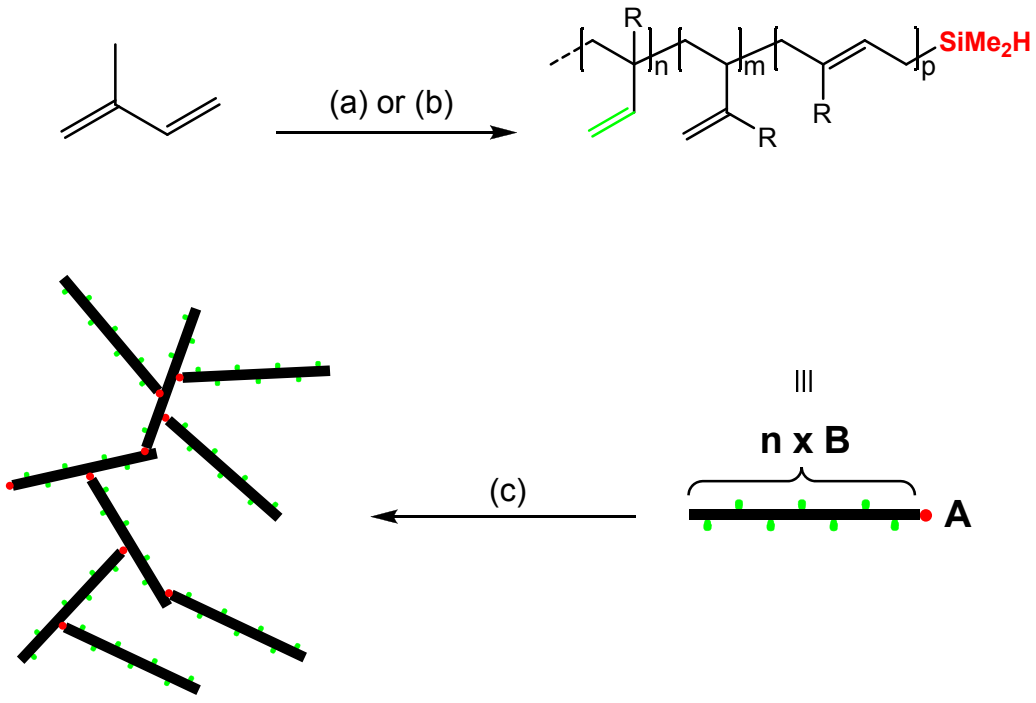

Figure 126 Synthesis and subsequent polycondensation of AB_n macromonomers (with R=H or CH_3). a) *s*-BuLi, $HSiMe_2Cl$, cyclohexane; b) *s*-BuLi, $HSiMe_2Cl$, THF; c) Karstedt's catalyst, 100 °C (for solution reactions in 50 wt% toluene).

Quantitative end-capping of the polymers was achieved with chlorodimethylsilane. In the resulting AB_n-macromonomers the silane Si-H end-group represented the single A-functionality, while the alkenyl groups of the PI/PB chain represented the B-groups for the ensuing hydrosilylation-based polyaddition that leads to branched polymers.

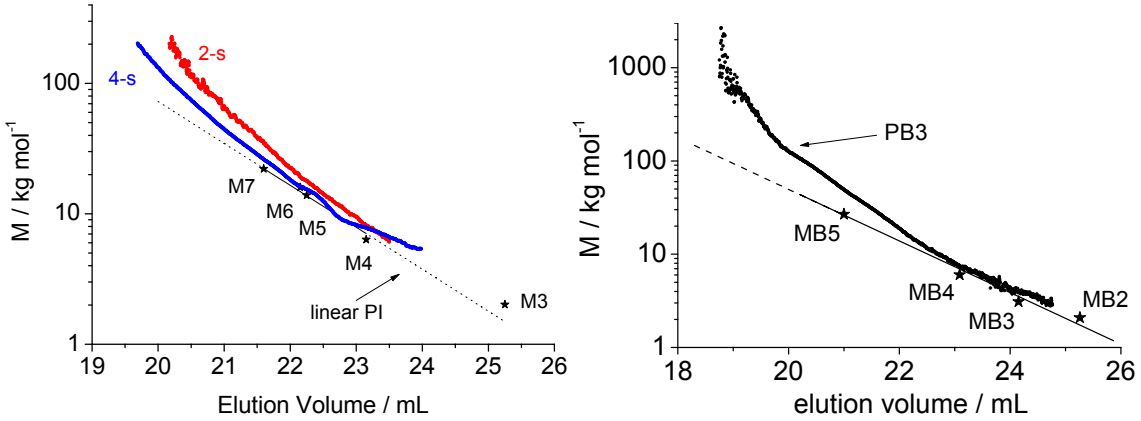

Figure 127 Molar mass vs. elution volume as calculated by SEC with MALLS detection for PI-based polymers (left) and PB based polymers (right). A linear least square fit was performed for the macromonomers.

Using a MALLS detector combined with SEC, it was possible to obtain absolute molar masses of polymers at each point of the elugram (Figure 127). It was obvious that at equal elution volume the branched polymers possess higher molar mass than the corresponding linear analogues. This already represented evidence for the branched structure of the polydienes prepared.

With the so called "triple detection method" it was possible to obtain the intrinsic viscosities of the polymers during SEC and correlate them to the corresponding molar masses obtained by MALLS. In this manner a qualitative assessment of the extent of branching by determination of the α-parameter of the Mark-Houwink equation for the branched polymers could be obtained. This parameter was lower than 0.5 for all branched polymers, supporting the branched structure (Table 33). Interestingly the obtained α-parameters were all similar to the values published for hyperbranched polymers based on AB_2 monomers in recent years. In addition the g'-parameter was determined, since it gives more precise values concerning the extent of branching. The results were almost analogous to the data from the α-parameters (Table 33).

Table 33 Molecular weight, polydispersity, and viscometry data for branched polyisoprenes (black) and polybutadienes (blue) synthesized from the respective macromonomers.

	SEC		MALLS	Viscometry	
	M_n / gmol^{-1}	PDI	M_n / gmol^{-1}	α	g'
M2	1 800	1.07	1 700	---	---
P2-*b*	4 400	2.21	5 600	0.29	0.66
P2-*s*	3 400	2.02	3 200	0.33	0.83
M3	2 400	1.10	2 000	---	---
P3-*b*	6 600	2.63	6 600	0.35	0.70
P3-*s*	4 800	2.11	4 300	0.35	0.97
M4	7 800	1.17	6 400	---	---
P4-*s*	12 000	1.62	10 900	0.39	0.91
MB1	1 600	1.11	1 300	---	---
PB1	8 100	2.35	9 100	0.30	0.53
MB2	2 400	1.07	1 800	---	---
PB2	8 100	2.26	8 600	0.30	0.72
PB2*	14 200	1.85	14 500	0.28	0.51
MB3	4 700	1.06	2 300	---	---
PB3	10 900	2.46	8 600	0.33	0.72
PB3*	18 500	1.74	19 600	0.29	0.62
MB4	9 900	1.06	6 500	---	---
PB4	20 000	2.04	13 000	0.38	0.93
PB4*	33 500	1.53	34 200	0.31	0.68

* Excluding the macromonomer peak.

Viscosity measurements show an exponential decay for the Mark-Houwink-parameter α during the reaction (Figure 82), reaching a plateau at α = 0.33. Kinetic studies showed rapid polymerization. The large fraction of vinyl groups may be an important factor for this enormous decrease in polymerization time in comparison to other hydrosilylation reactions.

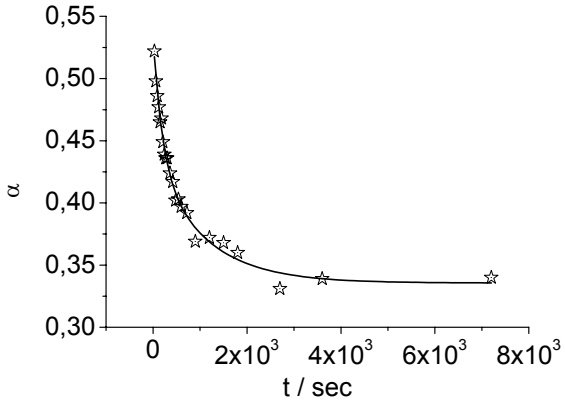

Figure 128 Evolution of the KMH parameter α with time (right)

The structure of the branched polymers is also reminiscent of an unsymmetrical star (Figure 129).

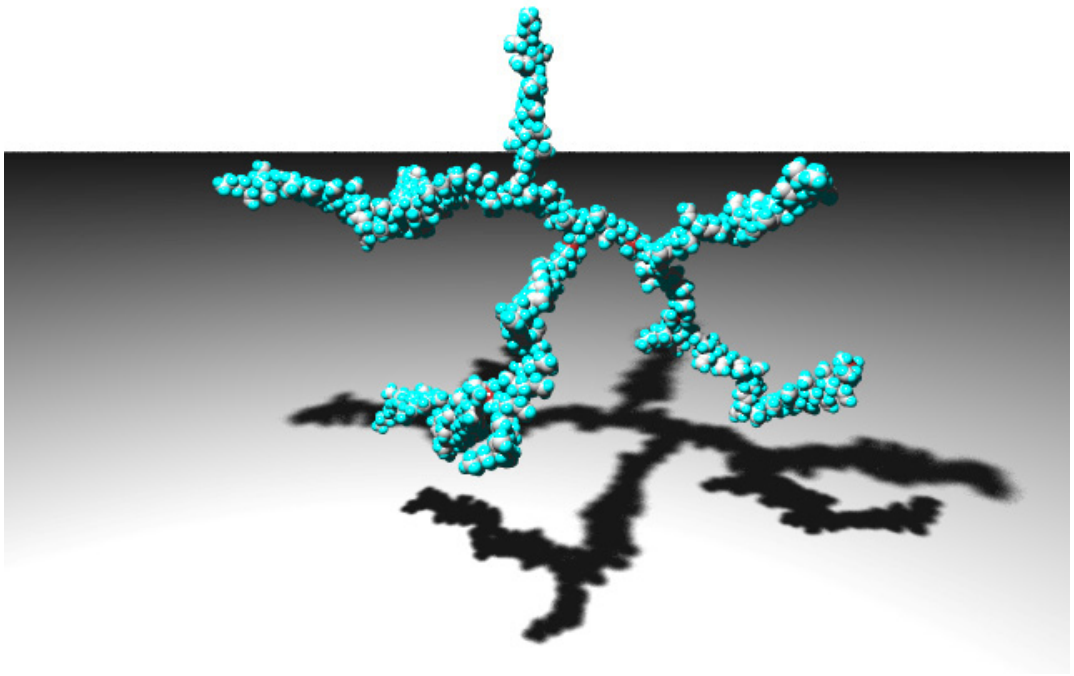

Figure 129 Proposed structure for **PB1** using the Spartan software.

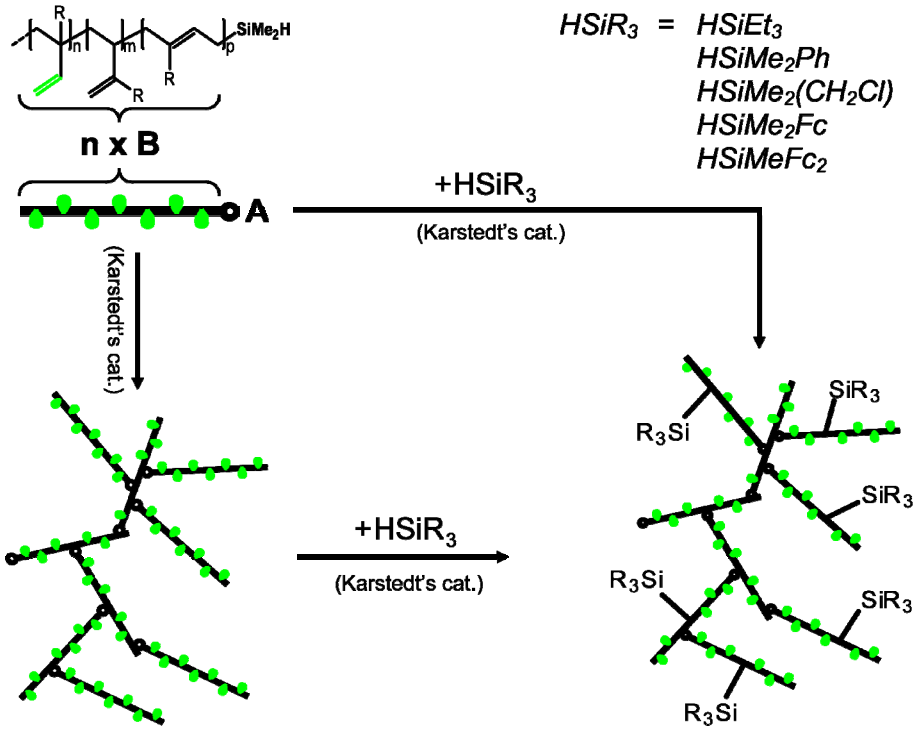

Figure 130 Possible pathways to functional branched polydienes.

To increase the range of possible applications for the materials, functionalities by the use of commercially available functional silanes and special designed ferrocenylsilanes have also been introduced. Two pathways for the introduction of functional

groups were studied (Figure 130); the “classical” route was the synthesis of the branched polymer at first and subsequent modification. The “classical” route could be only applied to polybutadienes and the functional polymers obtained had a very broad molecular weight distribution. The second route was based on a concurrent “pseudo-copolymerization” of the macromonomers with the functional low molecular weight silane. This route could be employed to polybutadiene as well as polyisoprene-based macromonomers.

Table 34 Molecular weights, polydispersity, and viscometry data for functionalized branched polybutadienes (**PE**: triethylsilane functionalized, **PP**: dimethylphenylsilane functionalized, **PC**: (chloromethyl)dimethylsilane functionalized) and for functionalized branched polyisoprenes (**IE**: triethylsilane functionalized, **IP**: dimethylphenylsilane functionalized, **IC**: (chloromethyl)dimethylsilane functionalized).

	NMR[a]		SEC[b]		MALLS	VISCO[c]	DSC[d]
#	eqv.	wt.-%	M_n	PDI	M_n	α	T_g
PE1	0.5	2.4	8 600	2.29	8 740	0.36	-24
PE2	4.5	17.9	12 500	2.07	9 300	0.38	-24
PE3	12	36.8	8 500	1.96	11 900	0.36	-24
PE4	27	56.7	11 400	1.66	10 400	0.40	-24
PP1	1.0	5.4	11 000	2.06	8 800	0.39	-19
PP2	5.0	10.2	11 000	2.07	7 200	0.41	-19
PP3	10	20.4	11 100	2.12	7 300	0.40	-17
PP4	20	47.4	12 000	2.24	11 000	0.41	-21
PC1	5	18.5	7 000	2.02	8 250	0.35	-26
PC2	15	40.4	8 500	1.91	10 200	0.35	-29
IE1	5	25.5	5 900	2.0	7200	0.34	-17
IE2	15	35.4	6 400	2.4	7900	0.38	-17
IP1	2.2	7.5	8 500	2.1	21 100	0.34	-5
IP2	5.4	16.6	7 300	1.7	21 800	0.38	---
IP3	12.5	31.6	6 500	1.6	19 900	0.41	0
IC1	5	24.2	5 200	2.0	7100	0.35	-16
IC2	8	33.2	5 200	2.2	7200	0.38	-9

[a] Equivalents and weight percent silane incorporated per macromonomer. [b] In g/mol vs. polystyrene standards. [c] by applying the Mark-Houwink eqn. [d] T_g in °C

Table 34 shows the data for simultaneous modification during the branching reaction for macromonomers based on polybutadiene or polyisoprene with triethylsilane, dimethylphenylsilane and (chloromethyl)dimethylsilane. Simultaneous functionalizations were carried out using the same conditions as for the branching reaction alone. For all cases in this study the degree of polymerization was not affected by the presence of monofunctional silanes up to 50 weight percent of the polymer. Relying on the α-parameter, all polymers were still branched.

In addition to the commercial silanes employed above, also special ferrocenylsilanes were employed to introduce electrochemical properties into the polymers that render them suitable for biosensoric applications.

Table 35 Overview of the $HSiMe_2Fc$ (black) and $HSiMeFc_2$ (blue) functionalized diene polymers. **BF** and **BDF** denote butadiene based **IF** and **IDF** denote isoprene based polymers.

#	Equivalents $HSiMe_2Fc$ employed	NMR[a]		SEC (THF)		SEC - Triple Detection	
		F	% of DB	M_n	PDI	M_n	α
BF1	5	4.5	9.6	12 200	2.3	12 800	0.39
BF2	10	10	21.3	15 200	2.9	38 900	0.39
BF3	20	20	42.6	25 500	2.9	43 800	0.54
IF1	5	5	50	10 200	2.8	12 000	0.40
IF2	15	10	100	7 200	1.7	11 200	0.49
BDF1	1	0.5	1.3	12 100	2.3	10 700	0.34
BDF2	5	5	12.8	11 000	2.1	11 500	0.43
BDF3	10	4.3	9.1	12 100	2.7	15 600	0.36
BDF4	20	12.5	32.1	12 200	2.2	16 500	0.36
IDF1	1	1	12.5	6 600	2.4	15 400	0.34
IDF2	5	6	75.0	6 500	2.1	14 500	0.36
IDF3	15	10	100	7 700	1.8	26 000	0.45

[a] Amount of ferrocenylsilane incorporated per macromonomer and fraction of reactive double bonds.

Table 35 summarizes the results for all ferrocenyl-functionalized polymers. Both ferrocenyl silanes could be incorporated in very high yields into the polymers, yielding weight fractions of ferrocene over 50 %. The incorporation of the $HSiMe_2Fc$ unit was more facile than for the $HSiMeFc_2$ unit. In case of very high amounts of incorporated ferrocenes the observed degrees of functionalization were lower than the calculated values in case of polybutadiene-based polymers.

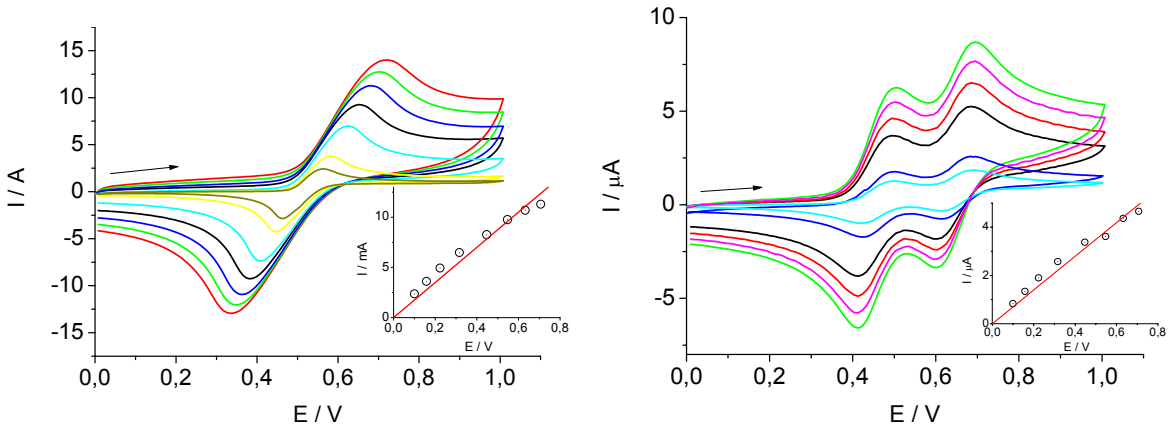

Figure 131 CVs at a Pt disk electrode obtained in CH_2Cl_2 (TBAH) solution for **BF2** (left) and **BDF1** (right) (scan rates: 0.01; 0.025; 0.05; 0.1; 0.2; 0.3; 0.4; 0.5 V/s). Inset: scan rate dependence of the first anodic peak current.

The obtained branched and ferrocenyl functionalized polymers gave stable electrochemical signals (Figure 131). In addition the incorporated ferrocenes enhanced thermal stabilities of the diene based polymers considerably (Figure 132).

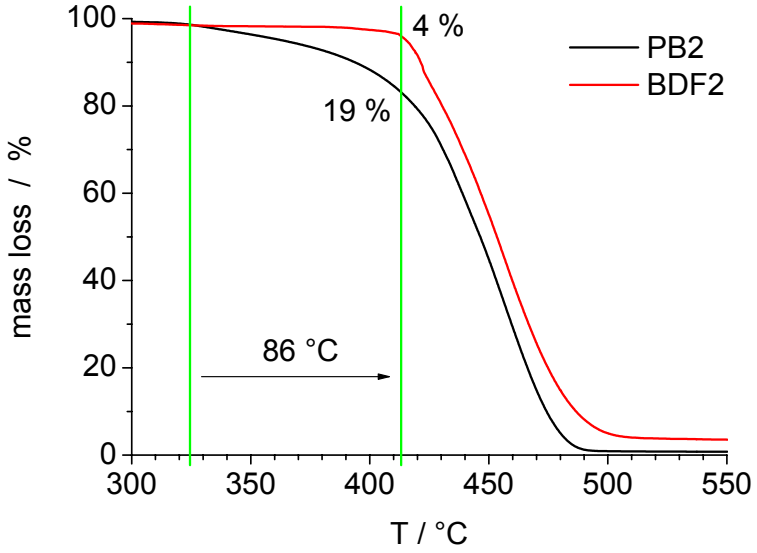

Figure 132 TGA plots for the branched **PB2** and the $HSiMeFc_2$ functionalized **BDF2**.

The resulting branched polyolefins are based on standard monomers and thus offer interesting potential for industrial application, e.g., for example as viscosity- or rheology-modifiers for processing. In combination with the very convenient functionalization route a broad range of possible applications can be discussed.

8.3. Ferrocenyl-Functionalized Hyperbranched Polyglycerols

Ferrocenyl-functionalized hyperbranched polyglycerols (PG) have been studied. Esterification of PGs of different molecular weight, using ferrocenemonocarboxylic acid gave the ferrocenyl functionalized polymers in high yields (Figure 133). The polymeric materials could be very well characterized applying NMR and MALDI-TOF techniques (Table 36). It was found that higher molecular weight PGs present more difficulties for functionalization by the bulky ferrocenemonocarboxylic acid than low molecular weight materials. This was attributed to the close proximity of the hydroxyl groups, making it more difficult to access two ferrocene units in direct neighborhood.

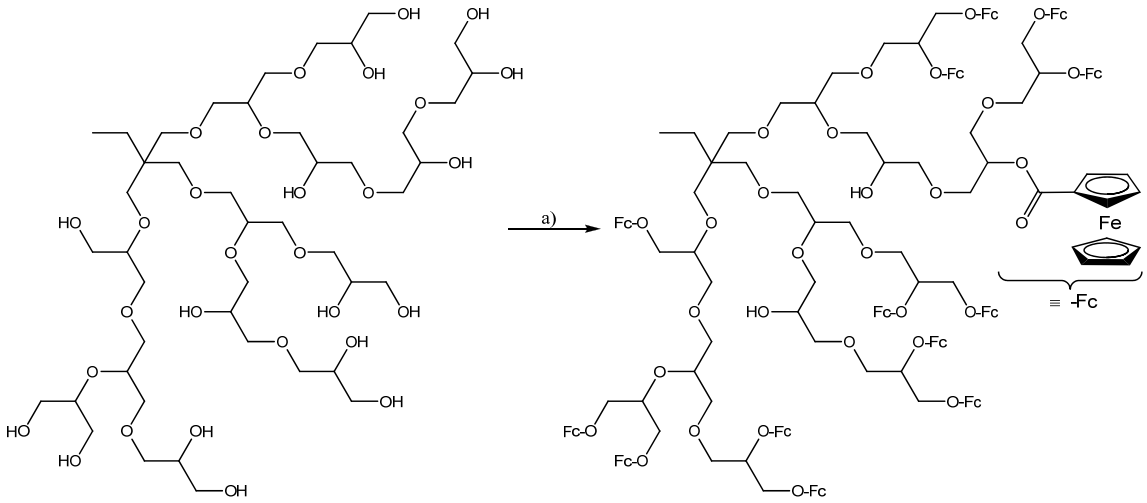

Figure 133 Reaction scheme for ferrocenyl functionalized PG. a) Fc-COOH, DPTS, DIC, DMF, RT, 4d.

In case of the $PG_{30}Fc_{18}$ we obtained a material that had a core shell structure with different polarities. This was evidenced by comparison of the SEC properties in different solvents.

Table 36 Functionalization data for the ferrocenyl functionalized hyperbranched polyglycerols.

	NMR		
Polymer	**# OH/pol.**	**$Fc_{wt\%}$**	**MALDI-ToF**
PG_7-Fc_{10}	0	67	PG_x-Fc_{x+2} & PG_x-Fc_{x+1}
PG_{15}-Fc_{16}	2	64	PG_x-Fc_{x+1} & PG_x-Fc_x
PG_{30}-Fc_{18}	15	54	PG_x-$Fc_{0.25x}$ - PG_x-$Fc_{0.5x}$

All polymers showed reversible electrochemical properties. The formation of thin polymer films was achieved and a high compatibility for electrochemical reactions was found in different solvents (Figure 134).

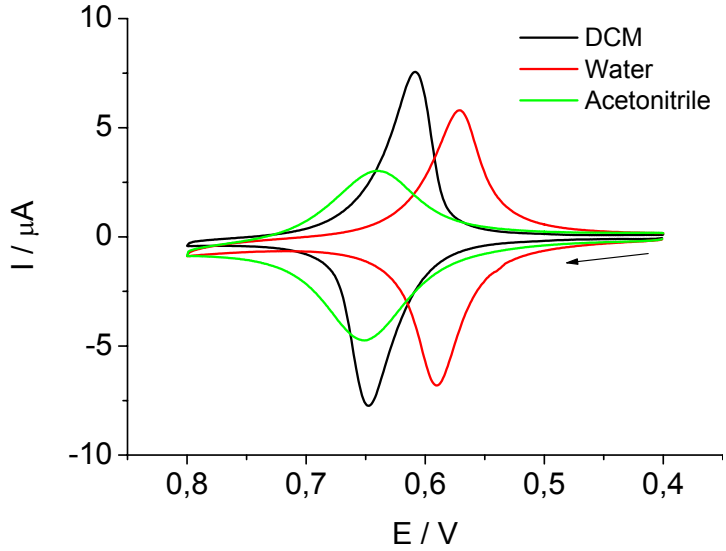

Figure 134 Response of Pt-Electrode modified with **PG_{15}-Fc_{16}** in different solvents.

The high compatibility of this material concerning different solvents, especially water, renders it a promising component for biosensoric applications. It is very important to point out that most enzymatic reactions used in biosensoric applications are performed in an aqueous environment.

8.4. Ferrocenyl-Functionalized PS-*b*-PB *Copolymers*

Two novel ferrocenylsilanes were prepared, bearing one ($HSiMe_2Fc$) or two ($HSiMeFc_2$) ferrocene units. The synthesis was based on the coupling of suitable chloromethylsilanes with monolithioferrocene. The formation of the ferrocenylsilanes was confirmed by NMR, FD-MS and X-Ray crystallographic analysis (Figure 135).

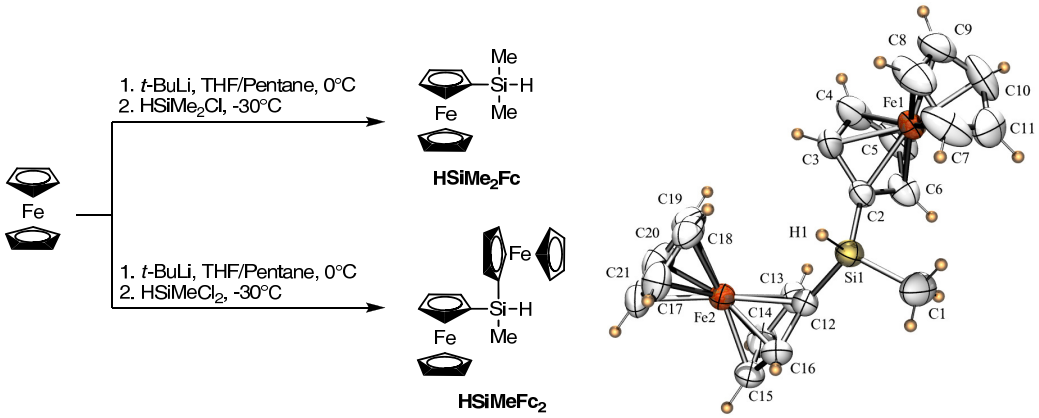

Figure 135 Synthesis of ferrocenyl-functionalized silanes (left) and X-Ray crystallographic structure of $HSiMeFc_2$ (right).

Three different block copolymers were prepared with different ratios of styrene to butadiene units (10:1, 4:1, 2:1). The double bonds of the 1,2-PB block were hydrosilylated using the novel ferrocenylsilanes (Figure 136).

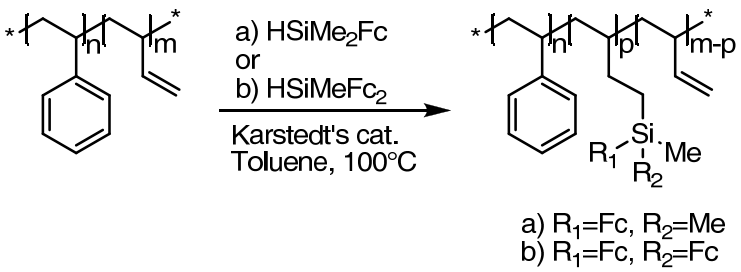

Figure 136 Synthesis of ferrocenyl functionalized PS-*b*-PB copolymers

In this manner six different ferrocenyl-rich block copolymers with different fractions of ferrocene were prepared and analyzed, employing NMR-spectroscopy, SEC, SEC/MALLS/viscosimetry, DLS and cyclic voltammetry.

The degrees of functionalization could be determined conveniently by standard ^{1}H-NMR techniques. High degrees of functionalization were obtained (up to 83 %). SEC analysis showed that all polymers were narrowly distributed after functionalization (Table 37). By combining SEC/MALLS and NMR it was possible to calculate the relative ratio of the different blocks. The block copolymers contained between 42 and 340 ferrocene units.

Table 37 SEC/MALLS/VISCO Data of Ferrocenyl Functionalized Polymers

		M_n[a]	PDI[a]	R_η[b]
1	PS_{615}-PB_{53}	66.9	1.02	6.2
1a	PS_{615}-$PB_{53}(HSiMe_2Fc)_{42}$	87.1	1.04	6.1
1b	PS_{615}-$PB_{53}(HSiMeFc_2)_{39}$	98.6	1.04	6.6
2	PS_{375}-PB_{92}	44.1	1.07	5.1
2a	PS_{375}-$PB_{92}(HSiMe_2Fc)_{62}$	83.7	1.17	5.7
2b	PS_{375}-$PB_{92}(HSiMeFc_2)_{76}$	97.4	1.11	5.5
3	PS_{455}-PB_{204}	58.4	1.02	5.7
3a	PS_{455}-$PB_{204}(HSiMe_2Fc)_{152}$	151.9	1.24	7.2
3b	PS_{455}-$PB_{204}(HSiMeFc_2)_{170}$	157.0	1.10	6.5

[a] Calculated by the combination of SEC/MALLS (x 10^3 $gmol^{-1}$)
[b] Calculated by the combination of SEC/Viscometry (x 10^3 $gmol^{-1}$)

The redox properties of the polymers in solution varied according to the block length ratio of the block copolymers. To estimate the amount of ferrocene units involved in a redox cycle the theoretical peak currents were calculated according to the Randles-Sevcik equation based on the diffusion coefficients determined by DLS. Comparing these results to the data obtained under experimental conditions it became clear that only a small fraction of the ferrocenes was active during a cycle (Table 37). Unexpectedly, with increasing block length of the ferrocenyl block the fraction of active ferrocenes decreased. This can be attributed to the coiled conformation of the block copolymer. The longer the coil segment, the smaller the relative amount of active groups on the coil surface. Additional polymers based on the $HSiMeFc_2$ group achieved always higher ratios. This phenomenon is related to the dendronized polymers. For such polymers an increasing dendron size yields more stretched backbones with more ferrocenes on the surface.

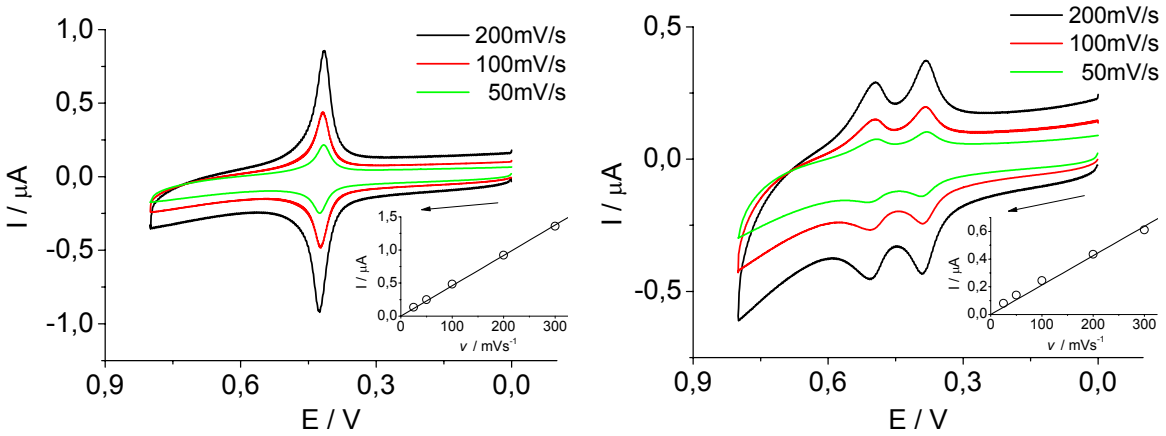

Figure 137 CVs of copolymer platinum electrodes **3a** (left) and **3b** (right) measured in CH_2Cl_2 (TBAH) (scan rate 0.1 V/s). Inset: scan rate dependence of the first anodic peak current.

Polymer films with controllable thickness were obtained by performing a certain number of consecutive cycles or by applying a fixed potential at 0.7 V. In Figure 137 the CV are depicted for the polymers **3a** and **3b** measured in CH_2Cl_2. In the range between 25 mV/s and 300 mV/s linear behavior was observed (Figure 137, insets). Thus, the films behaved like monolayers concerning their thickness. The materials were very stable under aqueous conditions and a film loss between two consecutive cycles could not be detected.

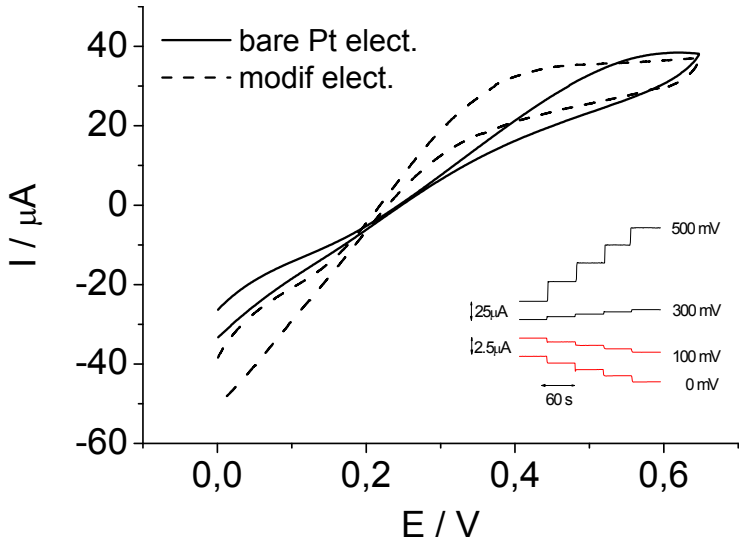

Figure 138 CVs for copolymer platinum electrode **2b** and a bare platinum electrode in aqueous 0.5mmol/L H_2O_2 ($NaClO_4$) solution (scan rate 25 mV/s). Inset: Response of copolymer platinum electrode **2b** to the batch addition of 0.5 mmol/L hydrogen peroxide aliquots at several applied potentials in H_2O.

In Figure 138 the CVs for the copolymer platinum electrode **2b** and a bare platinum electrode in an aqueous 0.5 mmol/L H_2O_2 solution are depicted. In comparison to the bare platinum electrode the modified electrode was able to lower the potential for the catalytic oxidation of the peroxide down to 0.3 V in comparison to the bare platinum

electrode (≈0.5 V). These experiments from one of the ferrocenyl-functionalized block copolymers as peroxide biosensor were very promising. These results can be of general importance for the design of polymers used in biosensing devices. Preliminary experiments using these polymers in combination with enzymes for the detection of glucose, NADH and phenol were also very promising. In comparison to the ferrocenyl functionalized polymers presented in chapter 6, these polymers possess the advantage of stronger bonding to the electrode because of the nonpolar polystyrene block. Future projects in this area will deal with a more detailed study concerning the relationship between the block length ratio and the precipitated bulk morphology on the electrode and the resulting influence for biosensoric applications.

9. Methods and Instrumentation

Atomic force microscopy (AFM)

AFM measurements were carried out on a Dimension 3100 instrument equipped with a Nanoscope IV Controller or a MultiMode connected to a NanoScope IIIa Controller using an E scanner. For SFM measurements, a standard solution (1 gL/1) was prepared and subsequently filtered through a 0.45 μm polytetrafluoroethylene (PTFE) syringe filter. This solution was diluted as required. Samples were prepared by drop-casting or spin-coating the dilute solution (5 mgL/1) onto freshly cleaved mica. Both film-casting techniques gave identical results. To achieve an equilibrium state, solutions were prepared at least 12 h before casting. Olympus tapping-mode silicon cantilevers (OMCL-AC160 TS-W2, R_{Tip}<10 nm opening angle, spring constant K_F=42 N/m, F_{res}=300 kHz) were used for measurements. All cantilevers were cleaned with Ar plasma immediately prior to use. Cantilever functionalization was carried out according to a general procedure: decalin, carbon tetrachloride, and chloroform were mixed in a 7:2:1 ratio and 1 vol% trimethylsilyl chloride was added. The solution was placed in a closed desiccator, and the plasmacleaned SiO2 cantilevers were placed in the gas phase above the solution for four days. Contact-angle measurements on the chip support were used to prove functionalization.

Cyclic voltammetry (CV)

Experiments were performed using a BAS CV-50W potentiostat using dichloromethane or water under an inert atmosphere (N_2). The supporting electrolyte was lithium perchlorate ($LiClO_4$) in H_2O or tetra-n-butylammonium hexafluorophosphate (TBAH) in CH_2Cl_2. The supporting electrolyte concentration was typically 0.1 M. All experiments were performed at 25 °C, in a conventional three-electrode cell using a platinum working electrode (A=0.02 cm^2). All potentials are referred to a saturated calomel reference electrode (SCE). A coiled platinum wire was used as counter electrode.

In case of the electrochemical measurements concerning the application as peroxide biosensor an Ecochemie BV Autolab PGSTAT 12 potentiostat and a larger Pt disk electrode (A=0.07 cm^2) were used instead. In steady-state measurements, a Metrohm 628-10 rotating electrode was used. Measurements under aqueous condi-

tions were performed in 0.1 M phosphate buffer (pH = 6.65) with 0.1 M sodium perchlorate ($NaClO_4$) as supporting electrolyte. The solutions were deoxygenated by bubbling high-purity nitrogen in all peroxide sensors measurements.

Differential scanning calorimetry (DSC)

DSC measurements were carried out on a Perkin-Elmer 7 series thermal analysis system in the temperature range from –70 to 150 °C at heating rates of 10 $K \cdot min^{-1}$ under nitrogen.

Electron spray ionization (ESI) mass spectrometry

ESI mass spectra were recorded on a Micromass Q-TOF Ultima 3 from 1 $g \cdot l^{-1}$ solutions.

Field desorption (FD) mass spectrometry

FD mass spectra were measured on a Finnigan MAT 95.

Infra-red (IR) spectrometry

FT-IR spectra were recorded on a Nicolet SDXC FT-IR spectrometer equipped with an ATR unit.

Light scattering (LS)

Static light scattering (SLS) was performed with equipment composed of an ALV SP-86 goniometer, a Spectra Physics 2011-s Kr ion laser (647.1 nm wavelength, 500 mW output power) and an ALV-3000 correlator. Dynamic light scattering (DLS) was performed with an argon ion laser (Stabilite 2060-04, λ 514 nm, Spectra-Physics), a SP-125 goniometer, and an ALV-5000 multiple-tau digital correlator. The temperature was kept constant at 293 K for light scattering measurements.

Matrix assisted laser desorption ionization - time of flight (MALDI-Tof)

Measurements were performed with a Shimadzu Axima CFR MALDI-TOF (matrix-assisted laser desorption and ionization time-of-flight) mass spectrometer, equipped

with a nitrogen laser delivering 3 ns laser pulses at 337 nm. Dithranol or α-cyanohydroxycinnamic acid were used as matrix. Samples were prepared by dissolving the polymer in THF at a concentration of 10 g/L. A 10 μL aliquot of this solution was added to 10 μL of a 10 g/L matrix solution and in some cases LiCl solved in methanol was added as cationizing agent. A 1 μL aliquot of the resulting mixture was applied to a multistage target to evaporate the THF or methanol and create a thin matrix/analyte film. The samples were measured in positive linear mode.

Nuclear magnetic resonance spectroscopy (NMR)

^{1}H-NMR spectra were recorded in d_1-$CDCl_3$, d_3-Methanol and d_6-DMF at concentrations of 100 $g \cdot l^{-1}$ on Bruker ARX 300 spectrometer or a Bruker ARX 400 spectrometer, operating at 400 MHz.

^{13}C-NMR spectra were recorded on a Bruker ARX 400 spectrometer, operated at 75.4 MHz.

Size exclusion chromatography (SEC)

SETUP 1: Measurements were performed on an instrument consisting of a Waters 717 plus autosampler, a TSP Spectra Series P 100 pump and three sets with three different columns each:

- 3 PSS-SDV 5μ columns with 100, 1 000 and 10 000 Å porosity for THF
- 3 MZ-SDV 5μ columns with 50, 1 000 and 10 000 Å porosity for $CHCl_3$
- 3 PSS-SDV 5μ columns with 10×10^4, 10×10^5 and 10×10^6 Å porosity for $CHCl_3$

The eluent was used at 30 °C and at a flow rate of 1 mL min^{-1}. UV absorption was detected by a SpectraSYSTEM UV2000. The specific refractive index increment (dn/dc) was measured at 30 °C on an Optilab DSP interferometric refractometer (also RI detector) and determined with the Wyatt ASTRA IV software (Version 4.90.08). Online-SEC static light scattering measurements were performed on a multi-angle laser light scattering detector (MALLS) DAWN EOS laser photometer (Wyatt Technology Co.) equipped with a GaAs laser emitting at a wavelength of 685 nm. Molar masses were calculated during SEC measurements using the Wyatt ASTRA IV software (Version 4.90.08) & ASTRA V (Version 5.1.9.1). Masses were calculated in

0.25 s intervals using the Zimm equation. Viscosity measurements were carried out online during SEC using a Dr. Bures ETA-2010 at 30°C.

SETUP 2: For measurements in DMF (containing 1 g/L of lithium bromide as an additive) an Agilent 1100 Series was used as an integrated instrument including a PSS Gral column ($10^4/10^4/10^2$ Å porosity), a UV (275 nm) and a RI detector. Calibration was done using poly(styrene) standards provided by Polymer Standards Service.

Thermogravimetry Analysis (TGA)

TGA measurements were on a Perkin Elmer Pyris 6 TGA performed.

Transmission electron microscopy (TEM)

High-resolution TEM studies were conducted on a Philips Tecnai F30 analytical TEM at an operating voltage of 300 kV and on a TEM EM420 electron microscope at an operating voltage of 120 kV.

Ultra violet-visible spectroscopy (UV-vis)

UV-*vis* spectra were recorded on a PERKIN-ELMER Lambda 2 UV/VIS spectrophotometer.

X-ray Crystal structures

were determined on a Bruker SMART6000 CCD-based X-ray diffractometer with a monochromatic radiation source (λ = 1.54178 Å). A suitable orange crystal of **$HSiMeFc_2$** with the dimensions 0.10 x 0.06 x 0.02 mm was located and mounted on a glass fiber with silicone cement in air and placed on the diffractometer. Data were collected at 296 K using continuous ω-2*B* scans. A total of 3368 independent reflections (R_{int} = 0.0359) were collected in the range 4.92° < 2Θ < 140.86°. The stability of the crystal was tested every 50s with three check reflections that showed only random fluctuations in intensity during data collection. The intensities were corrected for Lorentz and polarization effects. Scattering factors and corrections for anomalous dispersion were taken from a standard source.[230] Calculations were performed using Bruker SHELXTL for NT, version 6.10, a system of programs refining on F^2. The structure was solved by direct methods, and there were no unusual features in this

refinement. The hydrogen atom positions were calculated with fixed isotropic contributions at their calculated positions determined by molecular geometry. An absorption correction using an empirical model (SADABS V2.03) was applied. All non-hydrogen atoms were refined with anisotropic thermal parameters.

10. Appendix

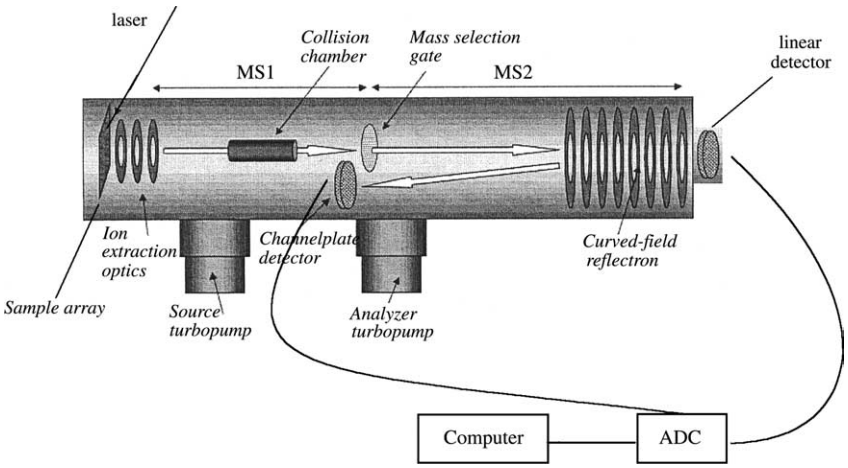

Figure 139 Scheme of a MALDI-ToF mass spectrometer showing the location of the collision chamber, the mass selection point for the first mass analyzer, and the second mass analyzer with a curved field reflectron.[141]

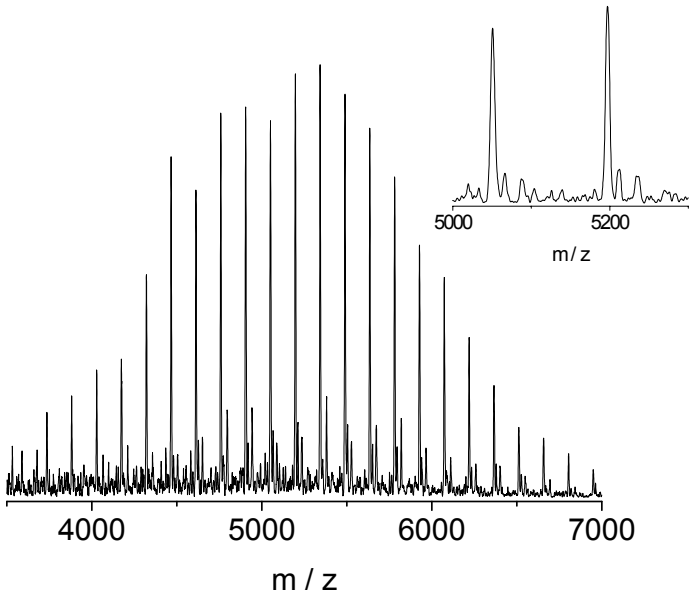

Figure 140 MALDI-ToF MS of using dithranol as matrix and silver trifluoroaceticacid as cationizing agent for the $PEEGE_{34}$-alkyne.

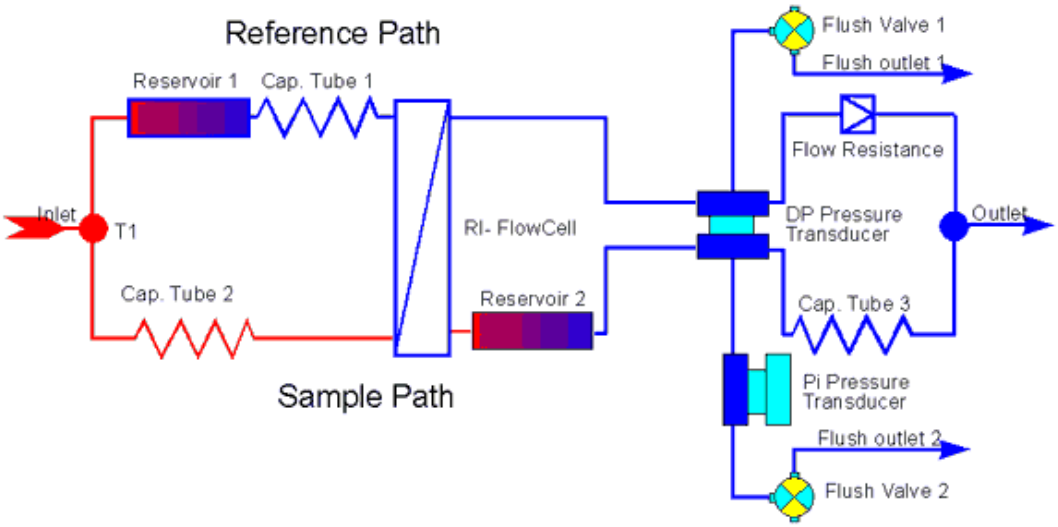

Figure 141 Schematic representation of the Dr. Bures ETA-2010 viscometer.

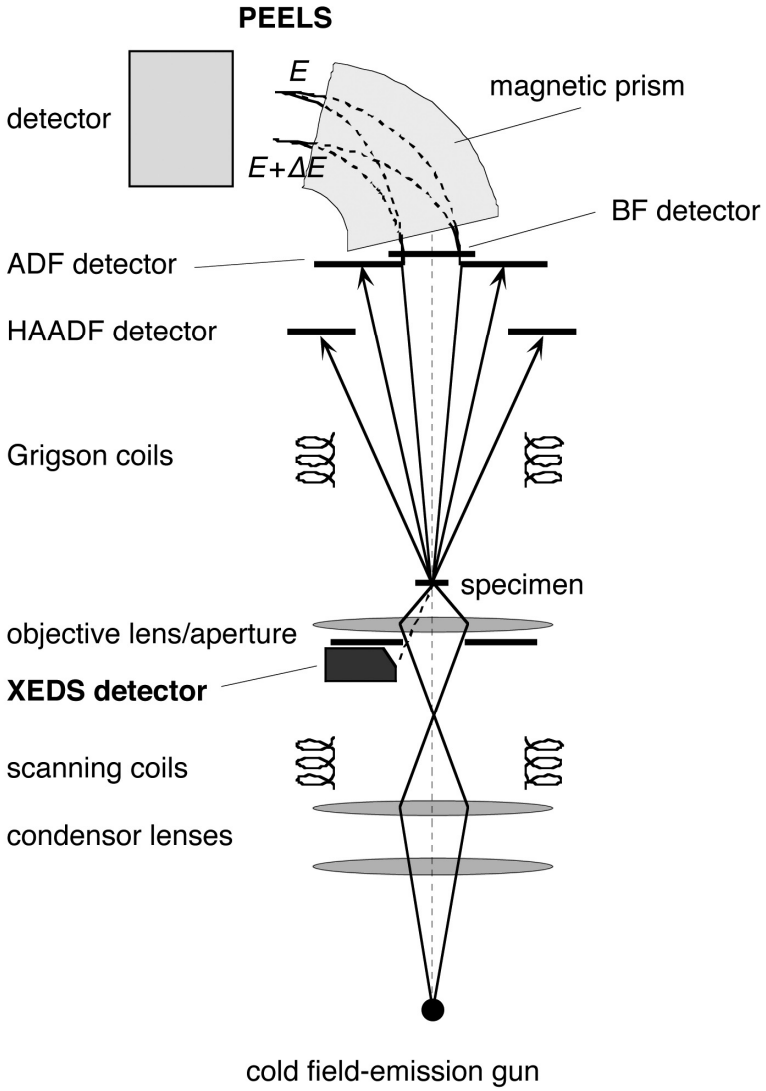

Figure 142 Schematic representation of a TEM.

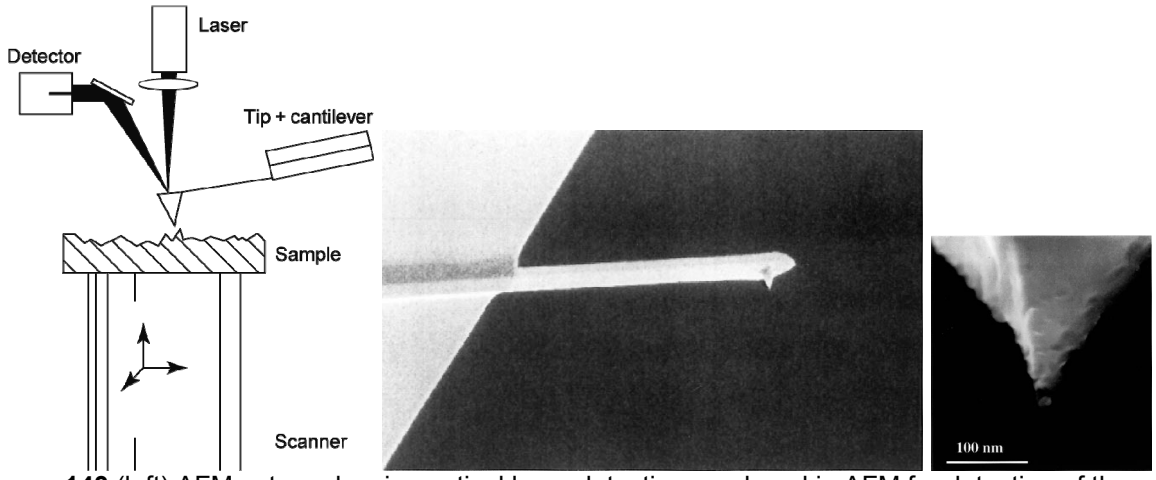

Figure 143 (left) AFM set-up showing optical lever detection employed in AFM for detection of the cantilever deflection caused by tip–sample force interactions. (middle) Scanning electron micrograph of etched Si probe, which consists of a 125-μm long cantilever and a sharp tip. (right) Apex of a Si tip.

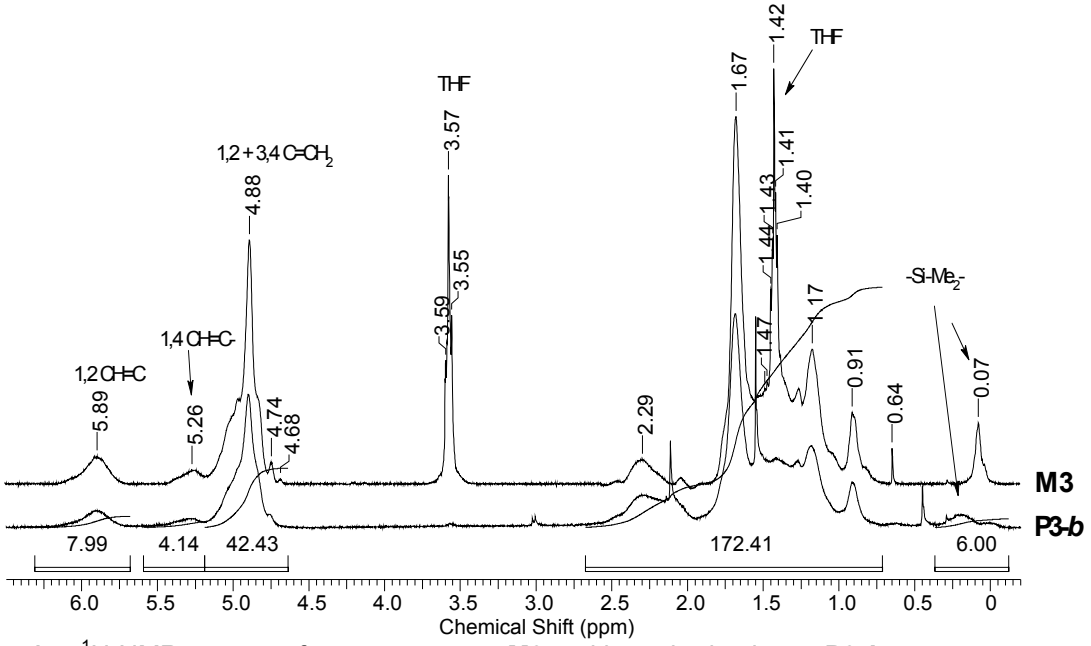

Figure 144 ^{1}H-NMR-spectra of macromonomer **M3** and branched polymer **P3-*b***.

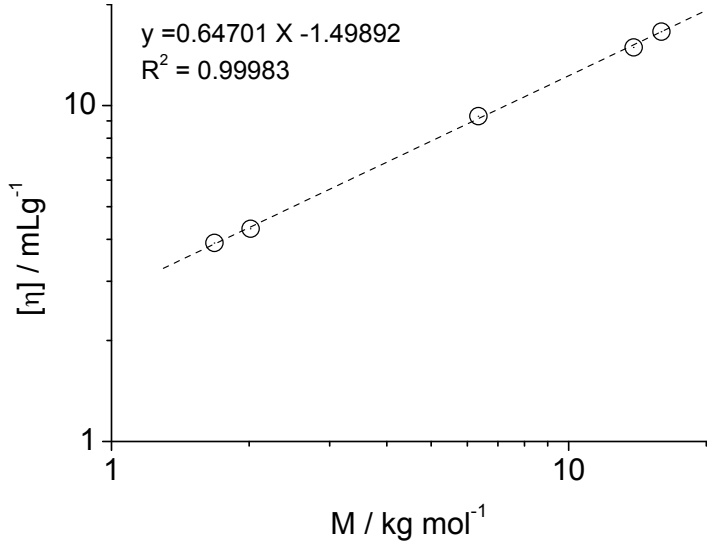

Figure 145 Mark-Houwink Plot for the macromonomers **M2-M7** (chapter 5)

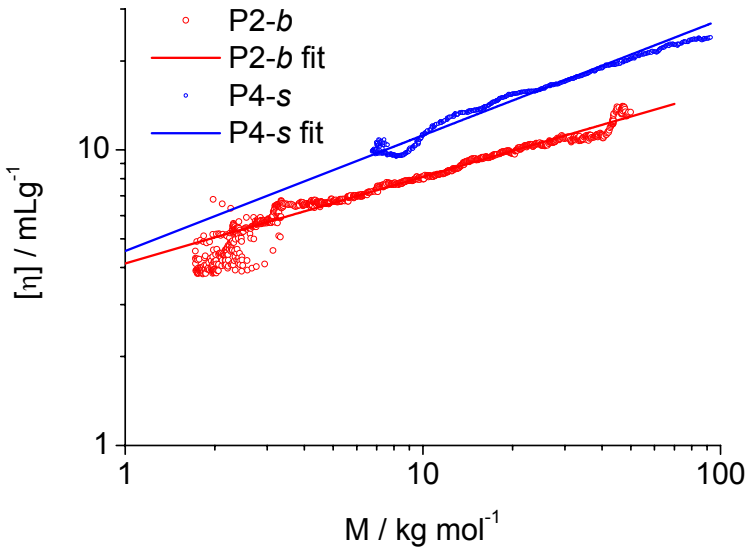

Figure 146 Mark-Houwink Plot for the branched polymers **P2-*b*** and **P4-*s***.

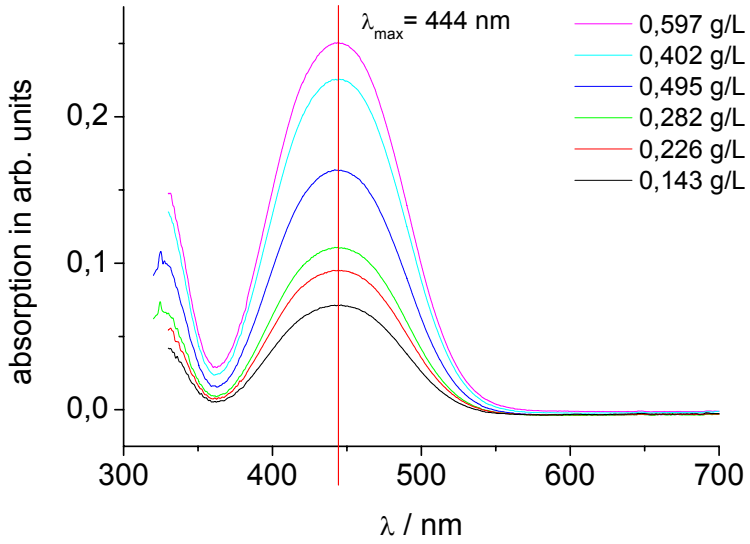

Figure 147 UV-vis spectra of $HSiMe_2Fc$ recorded in THF.

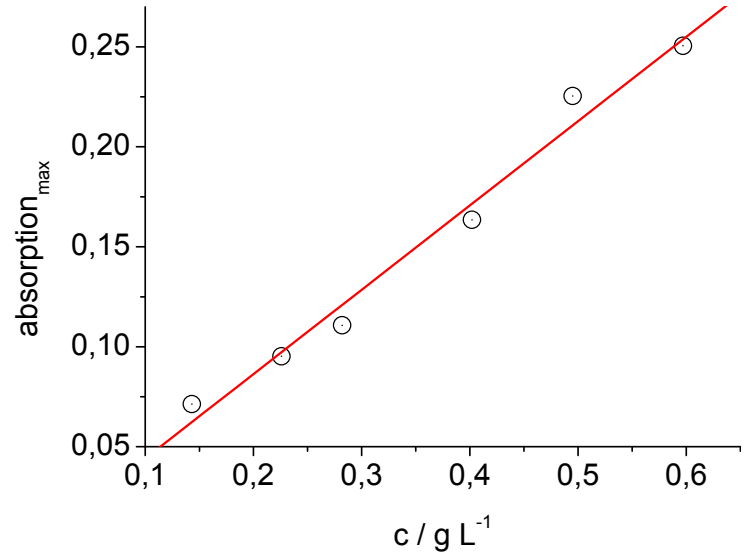

Figure 148 Calibration plot based on the data of Figure 147

11. Curriculum Vitae

AKADEMISCHE AUSBILDUNG

Johannes Gutenberg-Universität Mainz **seit 10/2004**
Promotion

Schwerpunkt: Anionische Polymerisationen
Thema: „Untersuchung des Einflusses von hyperverzweigten Strukturelementen bei amphiphilen Blockcopolymeren auf supramolekularer Ebene und Entwicklung von neuartigen ferrocenyl-funktionalisierten Polymeren für die Biosensorik“ unter Anleitung von Prof. Dr. H. Frey

Johannes Gutenberg-Universität Mainz **02/2004 – 09/2004**
Diplomarbeit

Schwerpunkt: Polykondensation
Thema: „Synthese von hyperverzweigten Triazen-Polyestern als Precursor für Nanofoams“ unter Anleitung von Prof. Dr. H. Frey

---

STUDIUM

Johannes Gutenberg-Universität Mainz **10/1999 – 09/2004**
Abschluss als Diplomchemiker

PRAKTIKA UND AUSLANDSERFAHRUNG

Graduate School of Science, Nagoya University **09/2002 – 03/2003**
Auslandssemester in Nagoya (Japan), gefördert durch ein DAAD Stipendium

Vianova Resins GmbH & Co. KG **07/2000 – 10/2000**
Tätigkeit als Werkstudent in der „Forschung Melaminharze“

BERUFLICHE AUSBILDUNG

Clariant GmbH **09/1996 – 06/1999**
Ausbildung zum Chemielaboranten

SCHULBILDUNG

Gymnasium **09/1993 – 06/1996**
Abitur am Gustav-Heinemann Gymnasium in Rüsselsheim

Gesamtschule **09/1987 – 06/1993**
Realschulabschluss an der Integrierten Gesamtschule in Kelsterbach

Grundschule **09/1983 – 06/1987**
Besuch der Karl-Treutel Schule in Kelsterbach

PUBLIKATIONSLISTE

Artikel

1. A Two-Step Route to Hyperbranched Polyisoprenes via AB_n-Macromonomers, Francisco-Javier López-Villanueva, Frederik Wurm, Andreas F.M. Kilbinger, Holger Frey, *Macromolecular Rapid Communications* **2006**, *accepted*

Vorträge

1. A Two-Step Route to Hyperbranched Polyisoprenes via ABn-Macromonomers, Francisco-J. López-Villanueva, Frederik Wurm, Andreas F. M. Kilbinger and Holger Frey, *232nd ACS National Meeting* **September 2006**, San Francisco (USA)

2. Influence of Block Length for Ferrocenyl-Functionalized Block Copolymers as Precursor for Biosensoric Applications, Francisco-J. López-Villanueva, Alejandra García Marcos, Karl Fischer, Manfred Schmidt, Beatriz Alonso, Carmen M. Casado, M. Pilar García Armada, José Losada and Holger Frey, *232nd ACS National Meeting* **September 2006**, San Francisco (USA)

Poster

1. Ferrocenyl-Functionalized Block Copolymers as Precursor for Biosensoric Applications, Francisco-J. López-Villanueva, Alejandra García Marcos, Karl Fischer, Manfred Schmidt, Beatriz Alonso, Carmen M. Casado, M. Pilar García Armada, José Losada and Holger Frey, *MWFZ Jahrestagung* **Mai 2006**, Mainz (Deutschland)

2. Hyperbranched Ferrocenyl Containing Polymers, H. Schüle, F. J. López-Villanueva, E. Barriau, E. Berger-Nicoletti, B. Alonso, C. M. Casado and H. Frey, *MWFZ Jahrestagung* **Mai 2006**, Mainz (Deutschland)

3. Synthesis and Superstructures of Novel Linear and Linear-Hyperbranched Amphiphilic Block Copolymers, Francisco-J. López-Villanueva, Emilie Barriau, Tobias W. Schleuss, Rüdiger Berger, Andreas F. M. Kilbinger and Holger Frey, *232nd ACS National Meeting* **September 2006**, San Francisco (USA)

4. Ferrocenyl Block Copolymers in Biosensoric Applications, Francisco-J. López-Villanueva, Alejandra García Marcos, Karl Fischer, Manfred Schmidt, Beatriz Alonso, Carmen M. Casado, M. Pilar García Armada, José Losada and Holger Frey, *GDCh Jahrestagung: Polymers & Coatings* **September 2006**, Mainz (Deutschland)

5. A Two-Step Route to *Ill*-Defined Functionalized Polydiene Stars via AB_n-Macromonomers, Francisco-J. López-Villanueva, Frederik Wurm and Holger Frey, *GDCh Jahrestagung: Polymers & Coatings* **September 2006**, Mainz (Deutschland)

6. Synthesis and Superstructures of Novel Linear and Linear-Hyperbranched Amphiphilic Block Copolymers, Francisco-J. López-Villanueva, Emilie Barriau, Tobias W. Schleuss, Hannah M. König, Rüdiger Berger, Ute Kolb, Andreas F. M. Kilbinger and Holger Frey, *Workshop - Biologically Inspired Nano-Architectures, SFB 625* **September 2006**, Mainz (Deutschland)

7. Synthesis and Biosensoric Applications for Ferrocenyl-Functionalized Block Copolymers, Francisco-J. López-Villanueva, Alejandra García Marcos, Karl Fischer, Manfred Schmidt, Beatriz Alonso, Carmen M. Casado, M. Pilar García Armada, José Losada and Holger Frey, *Workshop - Biologically Inspired Nano-Architectures, SFB 625* **September 2006**, Mainz (Deutschland)

PERSÖNLICHES

Staatsangehörigkeit Spanisch

Geburtstag/-ort 20. März 1977 in Rüsselsheim

12. References

[1] R. Geddes, "*The Polysaccharides: Glycogen: a structural viewpoint*", Academic Press, London, New York, **1985**, Vol. 3.
[2] A. Guilbot, C. Mercier, "*The Polysaccharides: Starch*", Academic Press, London, New York, **1985**, Vol. 3.
[3] L. Kenner, B. Lindberg, "*The Polysaccharides: Starch*", Academic Press, London, New York, **1983**, Vol. 2.
[4] P. A. Sandford, J. Baird, "*The Polysaccharides: Industrial Utilization of Polysaccharides*", Academic Press, London, New York, **1983**, Vol. 2.
[5] http://mse.iastate.edu/microscopy/plants.html
[6] H. Staudinger, E. Husemann, *Liebigs Ann Chem* **1937**, *527*, 195.
[7] K. H. Meyer, P. Bernfeld, *Helv Chim Acta* **1940**, *23*, 875.
[8] A. Sunder, J. Heinemann, H. Frey, *Chem-Eur J* **2000**, *6*, 2499.
[9] D. A. Tomalia, H. Baker, J. Dewald, M. Hall, G. Kallos, S. Martin, J. Roeck, J. Ryder, P. Smith, *Polym J* **1984**, *17*, 117.
[10] T. M. Miller, T. X. Neenan, *Chem Mater* **1990**, *2*, 346.
[11] J. M. J. Fréchet, *Science* **1994**, *263*, 1710.
[12] M. Fischer, F. Vögtle, *Angew Chem Int Edit* **1999**, *38*, 885.
[13] A. W. Bosman, H. M. Janssen, E. W. Meijer, *Chem Rev* **1999**, *99*, 1665.
[14] G. R. Newkome, C. N. Moorefield, F. Voegtle, "*Dendrimers and Dendrons: Concepts, Syntheses, Applications*", Wiley-VCH, Weinheim, **2001**.
[15] P. Froehling, *J Polym Sci Pol Chem* **2004**, *42*, 3110.
[16] B. Helms, E. W. Meijer, *Science* **2006**, *313*, 929.
[17] S. E. Stiriba, H. Frey, R. Haag, *Angew Chem Int Edit* **2002**, *41*, 1329.
[18] P. J. Flory, *J Am Chem Soc* **1952**, *74*, 2718.
[19] C. Drohmann, M. Möller, O. B. Gorbatsevich, A. M. Muzafarov, *J Polym Sci Pol Chem* **2000**, *38*, 741.
[20] C. Lach, P. Müller, H. Frey, R. Mülhaupt, *Macromol Rapid Comm* **1997**, 253.
[21] M. Johansson, E. Malmström, A. Hult, *J Polym Sci Pol Chem* **1993**, *31*, 619.
[22] G. Yang, M. Jikei, M.-A. Kakimoto, *Macromolecules* **1998**, *31*, 5964.
[23] K. E. Uhrich, C. J. Hawker, J. M. J. Fréchet, S. R. Turner, *Macromolecules* **1992**, *25*, 4583.
[24] C. J. Hawker, F. K. Chu, *Macromolecules* **1996**, *29*, 4370.
[25] Y. H. Kim, O. W. Webster, *J Am Chem Soc* **1990**, *112*, 4592.
[26] C. Gao, D. Yan, *Prog Polym Sci* **2004**, *29*, 183.
[27] M. Jikei, M. Kakimoto, *Prog Polym Sci* **2001**, *26*, 1233.
[28] A. Hult, M. Johansson, E. Malmström, *Adv Polym Sci* **1999**, *143*, 1.
[29] E. M. Harth, S. Hecht, B. Helms, E. E. Malmstrom, J. M. J. Fréchet, C. J. Hawker, *J Am Chem Soc* **2002**, *124*, 3926.
[30] K. Ito, S. Kawaguchi, *Adv Polym Sci* **2006**, *142*, 129.
[31] W. Burchard, *Adv Polym Sci* **1999**, *143*, 113.
[32] H. Xu, J. Gao, Y. Wang, Z. Wang, M. Smet, W. Dehaenb, X. Zhang, *Chem Commun* **2006**, 796.
[33] R. K. Kainthan, J. Janzen, E. Levin, D. V. Devine, D. E. Brooks, *Biomacromolecules* **2006**, *7*, 703.
[34] J. M. J. Fréchet, R. Lee, C. J. Hawker, *J Am Chem Soc* **1991**, *113*, 4583.
[35] D. Hölter, A. Burgath, H. Frey, *Acta Polym* **1997**, *48*, 30.
[36] H. Frey, D. Hölter, *Acta Polym* **1999**, *50*, 67.

[37] R. Schubbe, K. Angermund, G. Fink, R. Goddard, *Macromol Chem Physic* **1995**, *196*, 478.
[38] L. K. Johnson, C. M. Kilian, M. Brookhart, *J Am Chem Soc* **1995**, *117*, 6414.
[39] L. K. Johnson, S. Mecking, M. Brookhart, *J Am Chem Soc* **1996**, *118*, 267.
[40] S. Mecking, L. K. Johnson, L. Wang, M. Brookhart, *J Am Chem Soc* **1998**, *120*, 888.
[41] B. H. Zimm, W. H. Stockmayer, *Journal of Chemical Physics* **1949**, *17*, 1301.
[42] W. H. Stockmayer, M. Fixman, *Ann NY Acad Sci* **1953**, *57*, 334.
[43] H. Yamakawa, "*Modern theory of polymer solutions*", Harper and Row, New York, **1971**.
[44] J. G. Kirkwood, J. Riseman, *J Chem Phys* **1948**, *16*, 565.
[45] J. G. Kirkwood, *J Polym Sci* **1954**, *12*, 1.
[46] J. M. J. Fréchet, M. Henmi, I. Gitsov, S. Aoshima, M. R. Leduc, R. B. Grubbs, *Science* **1995**, *269*, 1080.
[47] D. Y. Yan, Z. P. Zhou, A. H. E. Müller, *Macromolecules* **1999**, *32*, 245.
[48] Z. Jia, D. Yan, *J Polym Sci Pol Chem* **2005**, *43*, 3502.
[49] S. Muthukrishnan, H. Mori, A. H. E. Müller, *Macromolecules* **2005**, *38*, 3108.
[50] R. Hanselmann, D. Holter, H. Frey, *Macromolecules* **1998**, *31*, 3790.
[51] W. Radke, G. Litvinenko, A. H. E. Muller, *Macromolecules* **1998**, *31*, 239.
[52] P. Bharathi, J. S. Moore, *J Am Chem Soc* **1997**, *119*, 3391.
[53] P. Bharathi, J. S. Moore, *Macromolecules* **2000**, *33*, 3312.
[54] R. Tokar, P. Kubisa, S. Penczek, A. Dworak, *Macromolecules* **1994**, *27*, 320.
[55] A. Dworak, W. Walach, B. Trzebicka, *Macromol Chem Physic* **1995**, *196*, 1963.
[56] A. Sunder, R. Hanselmann, H. Frey, R. Mulhaupt, *Macromolecules* **1999**, *32*, 4240.
[57] A. Sunder, H. Frey, R. Mülhaupt, *Macromol Symp* **2000**, *153*, 187.
[58] H. Kautz, A. Sunder, H. Frey, *Macromol Symp* **2001**, *163*, 67.
[59] R. K. Kainthan, E. B. Muliawan, S. G. Hatzikiriakos, D. E. Brooks, *Macromolecules* **2006**, *39*, 7708.
[60] N. Hadjichristidis, S. Pispas, G. Floudas, "*Block Copolymers: Synthetic Strategies, Physical Properties, and Applications*", Wiley-Interscience, New Jersey, **2003**.
[61] *http://www2.basf.de/basf2/html/plastics/deutsch/pages/styrol/index.htm*
[62] L. R. Hutchings, R. W. Richards, *Macromolecules* **1999**, *32*, 880.
[63] R. Matmour, R. Francis, R. S. Duran, Y. Gnanou, *Macromolecules* **2005**, *38*, 7754.
[64] M. Trollsas, J. L. Hedrick, *J Am Chem Soc* **1998**, *120*, 4644.
[65] U. Bayer, R. Stadler, *Macromol Chem Physic* **1994**, *195*, 2709.
[66] S. J. Teertstra, M. Gauthier, *Prog Polym Sci* **2004**, *29*, 277.
[67] A. Hakiki, R. N. Young, T. C. B. Mcleish, *Macromolecules* **1996**, *29*, 3639.
[68] Z. S. Yuan, M. Gauthier, *Macromolecules* **2005**, *38*, 4124.
[69] N. Hadjichristidis, M. Pitsikalis, S. Pispas, H. Iatrou, *Chem Rev* **2001**, *101*, 3747.
[70] N. Hadjichristidis, H. Iatrou, M. Pitsikalis, S. Pispas, A. Avgeropoulos, *Prog Polym Sci* **2005**, *30*, 725.
[71] C. Park, J. Yoon, E. L. Thomas, *Polymer* **2003**, *44*, 6725.
[72] Z. Li, M. A. Hillmyer, T. P. Lodge, *Macromolecules* **2006**, *39*, 765.
[73] Z. Li, M. A. Hillmyer, T. P. Lodge, *Langmuir* **2006**, *22*, 9409.
[74] I. Gitsov, K. L. Wooley, J. M. J. Fréchet, *Angew Chem Int Edit* **1992**, *31*, 1200.
[75] J. C. M. van Hest, D. A. P. Delnoye, M. W. P. L. Baars, M. H. P. van Genderen, E. W. Meijer, *Science* **1995**, *268*, 1592.
[76] J. C. M. van Hest, M. W. P. L. Baars, C. Elissenroman, M. H. P. van Genderen, E. W. Meijer, *Macromolecules* **1995**, *28*, 6689.
[77] A. F. Zhang, L. J. Shu, Z. S. Bo, A. D. Schlüter, *Macromol Chem Physic* **2003**, *204*, 328.
[78] H. Frauenrath, *Prog Polym Sci* **2005**, *30*, 325.

[79] A. G. Marcos, T. M. Pusel, R. Thomann, T. Pakula, L. Okrasa, S. Geppert, W. Gronski, H. Frey, *Macromolecules* **2006**, *39*, 971.
[80] E. Barriau, A. García Marcos, H. Kautz, H. Frey, *Macromol Rapid Comm* **2005**, *26*, 862.
[81] J. Rodríguez-Hernández, F. Chécot, Y. Gnanou, S. Lecommandoux, *Prog Polym Sci* **2005**, *30*, 691.
[82] J. M. J. Frechet, *Prog Polym Sci* **2005**, *30*, 844.
[83] K. Inoue, *Prog Polym Sci* **2000**, *25*, 453.
[84] S. Förster, T. Plantenberg, *Angew Chem Int Edit* **2002**, *41*, 689.
[85] T. P. Lodge, *Macromol Chem Physic* **2003**, *204*, 265.
[86] D. G. Bucknall, H. L. Anderson, *Science* **2003**, *302*, 1904.
[87] M. Lazzari, M. A. López-Quintela, *Adv Mater* **2003**, *15*, 1583.
[88] K. Yu, L. Zhang, A. Eisenberg, *Langmuir* **1996**, *12*, 5980.
[89] J. K. Cox, K. Yu, B. Constantine, A. Eisenberg, R. Bruce Lennox, *Langmuir* **1999**, *15*, 7714.
[90] L. Luo, A. Eisenberg, *Langmuir* **2001**, *17*, 6804.
[91] P. Bhargava, J. X. Zheng, P. Li, R. P. Quirk, F. W. Harris, S. Z. D. Cheng, *Macromolecules* **2006**, *39*, 4880.
[92] D. M. Vriezema, M. C. Aragones, J. A. A. W. Elemans, J. J. L. M. Cornelissen, A. E. Rowan, R. J. M. Nolte, *Chem Rev* **2005**, *105*, 1445.
[93] S. Förster, M. Antonietti, *Adv Mater* **1998**, *10*, 195.
[94] W. Huck, *Chem Soc Rev* **2005**, *34*, 191.
[95] A. Göthlich, S. Koltzenburg, G. Schornick, *Chem Unserer Zeit* **2005**, *39*, 262.
[96] M. P. Mcgrath, E. D. Sall, S. J. Tremont, *Chem Rev* **1995**, *95*, 381.
[97] I. Gitsov, "*Advances in Dendritic Macromolecules"*, Elsevier Science, Amsterdam, **2002**, Vol. 5.
[98] J. Allgaier, A. Poppe, L. Willner, D. Richter, *Macromolecules* **1997**, *30*, 1582.
[99] J. A. Opsteen, J. C. M. van Hest, *Chem Commun* **2005**, 57.
[100] W. Burchard, W. Richtering, *Progr Colloid & Polymer Sci* **1989**, *80*, 151.
[101] D. E. Koppel, *J Chem Phys* **1972**, *57*, 4814.
[102] B. J. Frisken, *Appl Opt* **2001**, *40*, 4087.
[103] D. Baskaran, *Macromol Chem Physic* **2001**, *202*, 1569.
[104] L. R. Hutchings, J. M. Dodds, S. J. Roberts-Bleming, *Macromolecules* **2005**, *38*, 5970.
[105] L. R. Hutchings, J. M. Dodds, S. J. Roberts-Bleming, *Macromol Symp* **2006**, *240*, 56.
[106] A. Togni, T. Hayashi, Eds., "*Ferrocenes. Homogeneous Catalysis, Organic Synthesis, Materials Science"*, VCH, Weinheim, **1995**.
[107] E. W. Neuse, *J Inorg Organomet P* **2005**, *15*, 3.
[108] F. Vögtle, "*Dendrimers I-IV, Topp. Curr. Chem., Vol. 197, 210, 212, 217"*.
[109] A. Salmon, P. Jutzi, *J Organomet Chem* **2001**, *637*, 595.
[110] S. Nlate, J. Ruiz, V. Sartor, R. Navarro, J. C. Blais, D. Astruc, *Chem-Eur J* **2000**, *6*, 2544.
[111] H. C. Yoon, M. Y. Hong, H. S. Kim, *Anal Chem* **2000**, *72*, 4420.
[112] C. A. Nijhuis, F. Yu, W. Knoll, J. Huskens, D. N. Reinhoudt, *Langmuir* **2005**, *21*, 7866.
[113] I. Cuadrado, M. Moran, C. M. Casado, B. Alonso, F. Lobete, B. Garcia, M. Ibisate, J. Losada, *Organometallics* **1996**, *15*, 5278.
[114] B. Alonso, I. Cuadrado, M. Moran, J. Losada, *J Chem Soc Chem Comm* **1994**, 2575.
[115] C. M. Casado, I. Cuadrado, M. Morán, B. Alonso, M. Barranco, J. Losada, *Appl Organometal Chem* **1999**, *13*, 245.
[116] I. Manners, *J Polym Sci Pol Chem* **2002**, *40*, 179.
[117] N. Kuramoto, Y. Shishido, K. Nagai, *J Polym Sci Pol Chem* **1997**, *35*, 1967.

[118] B. Alonso, B. González, B. García, E. Ramírez-Oliva, M. Zamora, C. M. Casado, I. Cuadrado, *J Organomet Chem* **2001**, *637*, 642.
[119] N. Hida, F. Takei, K. Onitsuka, K. Shiga, S. Asaoka, T. Iyoda, S. Takahashi, *Angew Chem Int Edit* **2003**, *42*, 4349.
[120] R. W. Heo, F. B. Somoza, T. Randall, *J Am Chem Soc* **1998**, *120*, 1621.
[121] M. Cazacu, A. Vlad, M. Marcu, C. Racles, A. Airinei, G. Munteanu, *Macromolecules* **2006**, *39*, 3786.
[122] E. W. Neuse, L. Bednarik, *Macromolecules* **1979**, *12*, 187.
[123] L. Cao, I. Manners, M. A. Winnik, *Macromolecules* **2001**, *34*, 3353.
[124] M. Baumert, J. Frohlich, M. Stieger, H. Frey, R. Mulhaupt, H. Plenio, *Macromol Rapid Comm* **1999**, *20*, 203.
[125] D. A. Durkee, H. B. Eitouni, E. D. Gomez, M. W. Ellsworth, A. T. Bell, N. P. Balsara, *Adv Mater* **2005**, *17*, 2003.
[126] H. C. Kolb, M. G. Finn, K. B. Sharpless, *Angew Chem Int Edit* **2001**, *40*, 2004.
[127] V. V. Rostovtsev, L. G. Green, V. V. Fokin, K. B. Sharpless, *Angew Chem Int Edit* **2002**, *41*, 2596.
[128] R. Huisgen, G. Szeimies, L. Moebius, *Chem Ber* **1967**, *100*, 2494.
[129] J.-F. Lutz, H. G. Börner, K. Weichenhan, *Macromol Rapid Comm* **2005**, *26*, 514.
[130] B. Helms, J. L. Mynar, C. J. Hawker, J. M. J. Fréchet, *J Am Chem Soc* **2004**, *126*, 15020.
[131] H. Li, F. Cheng, A. M. Duft, A. Adronov, *J Am Chem Soc* **2005**, *127*, 14518.
[132] D. A. Ossipov, J. Hilborn, *Macromolecules* **2006**, *39*, 1709.
[133] M. Morton, "*Anionic Polymerization: Principles and Practice"*, Academic Press, **1983**.
[134] N. Hadjichristidis, H. Iatrou, S. Pispas, M. Pitsikalis, *J Polym Sci Pol Chem* **2000**, *38*, 3211.
[135] D. Uhrig, J. W. Mays, *J Polym Sci Pol Chem* **2005**, *43*, 6179–6222.
[136] A. Mavroudis, N. Hadjichristidis, *Macromolecules* **2006**, *39*, 535.
[137] Y. Zhao, T. Higashihara, K. Sugiyama, A. Hirao, *J Am Chem Soc* **2005**, *127*, 14158.
[138] A. Hirao, M. Hayashi, *Acta Polym* **1999**, *50*, 219.
[139] I. Fallais, J. Devaux, R. Jérôme, *J Polym Sci Pol Chem* **2000**, *38*, 1618.
[140] J. Jagur-Grodzinski, *J Polym Sci Pol Chem* **2002**, *40*, 2116.
[141] G. Montaudo, F. Samperi, M. S. Montaudo, *Prog Polym Sci* **2006**, *31*, 277.
[142] D. Taton, A. Leborgne, M. Sepulchre, N. Spassky, *Macromol Chem Physic* **1994**, *195*, 139.
[143] S. E. Stiriba, H. Kautz, H. Frey, *J Am Chem Soc* **2002**, *124*, 9698.
[144] J. Ding, C. Price, C. Booth, *Eur Polym J* **1991**, *27*, 891.
[145] J. Ding, F. Heatley, C. Price, C. Booth, *Eur Polym J* **1991**, *27*, 895.
[146] C. Billouard, S. Carlotti, P. Desbois, A. Deffieux, *Macromolecules* **2004**, *37*, 4038.
[147] E. Barriau, "*Hyperbranched polyether polyols as building blocks for complex macromolecular architectures"*, Institute of Organic Chemistry, Johannes Gutenberg-University, Mainz **2006**
[148] S. Mori, H. G. Barth, "*Size Exclusion Chromatography"*, Springer, Heidelberg, **1999**.
[149] P. Dimitrov, A. Porjazoska, C. P. Novakov, M. Cvetkovska, C. B. Tsvetanov, *Polymer* **2005**, *46*, 6820.
[150] M. Przybylski, M. O. Glocker, *Angewandte Chemie-International Edition in English* **1996**, *35*, 807.
[151] V. Bütün, R. B. Top, S. Ufuklar, *Macromolecules* **2006**, *39*, 1216.
[152] J. H. Kim, M. K. Lee, C. Y. Ryu, J. W. Lee, S. S. Hwang, T. S. Park, K. U. Kim, H. S. Yoon, B. I. Ahn, K. H. Char, J. H. Ryu, R. P. Quirk, *Polym J* **1994**, *26*, 1111.
[153] J. H. Ahn, Y. D. Shin, S. Y. Kim, J. S. Lee, *Polymer* **2003**, *44*, 3847.

[154] H. Gilman, A. H. Haubein, *J Am Chem Soc* **1944**, *66*, 1515.
[155] P. A. Tipler, "*Physik"*, 3rd edition, München, **1994**.
[156] R. Xu, "*Particle Characterization: Light Scattering Methods"*, Kluver Academic Publishers, New York, **2002**.
[157] M. I. Mishenko, L. D. Travis, A. A. Lacis, "*Scattering, Absorption, and Emission of Light by Small Particles"*, Cambridge University Press, Cambridge, **2002**.
[158] W. Burchard, M. Schmidt, W. H. Stockmayer, *Macromolecules* **1980**, *13*, 1265.
[159] J. C. M. Lee, H. Bermudez, B. M. Discher, M. A. Sheehan, Y. Y. Won, F. S. Bates, D. E. Discher, *Biotechnol Bioeng* **2001**, *73*, 135.
[160] Y. Guo, H. Yui, H. Minamikawa, B. Yang, M. Masuda, K. Ito, T. Shimizu, *Chem Mater* **2006**, *18*, 1577.
[161] A. Rosenauer, "*Transmission Electron Microscopy of Semiconductor Nanostructures - An Analysis of Composition and Strain State"*, Springer, Berlin, **2003**, Vol. 182.
[162] R. A. Meyers, "*Encyclopedia of Analytical Chemistry"*, John Wiley & Sons Ltd., Chichester, **2000**.
[163] J. P. Spatz, A. Roescher, S. Sheiko, G. Krausch, M. Möller, *Adv Mater* **1995**, *8*, 731.
[164] J. P. Spatz, M. Möller, M. Noeske, R. J. Behm, M. Pietralla, *Macromolecules* **1997**, *30*, 3874.
[165] H. A. Al-Muallem, D. M. Knauss, *J Polym Sci Pol Chem* **2001**, *39*, 3547.
[166] D. M. Knauss, H. A. Al-Muallem, *J Polym Sci Pol Chem* **2000**, *38*, 4289.
[167] L. H. Sommer, E. W. Pietrusza, F. C. Whitmore, *J Am Chem Soc* **1947**, *69*, 188.
[168] J. L. Speier, J. A. Webster, G. H. Barnes, *J Am Chem Soc* **1957**, *79*, 974.
[169] United States. 3,775,452 (1973), inv. B. D. Karstedt;
[170] J. L. Speier, *Adv Organomet Chem* **1979**, *17*, 407.
[171] I. Ojima, S. Patai, Z. Rappoport, "*The Chemistry of Organic Silicon Compounds"*, Wiley, New York, **1989**.
[172] A. J. Chalk, J. F. Harrod, *J Am Chem Soc* **1965**, *87*, 16.
[173] M. A. Brook, "*Silicon in Organic, Organometallic, and Polymer Chemistry"*, JOHN WILEY AND SONS, INC., **2000**.
[174] I. Wender, P. Pino, J. F. Harrod, A. J. Chalk, "*Organic Synthesis via Metal Carbonyls"*, John-Wiley, New York, **1977**.
[175] Y. Tanaka, Y. Takeuchi, M. Kobayashi, H. Tadokoro, *J Polym Sci Part A-2* **1971**, *9*, 43.
[176] X. Guo, R. Farwaha, G. L. Rempel, *Macromolecules* **1990**, *23*, 5047.
[177] X. Guo, G. L. Rempel, *Macromolecules* **1992**, *25*, 883.
[178] J. T. Gotrol, W. W. Graessley, *Macromolecules* **1984**, *17*, 2767.
[179] J. M. J. Fréchet, D. A. Tomalia, "*Dendrimers and other Dendritic Polymers"*, John Wiley & Sons Ltd, **2001**.
[180] P. F. W. Simon, A. H. E. Müller, T. Pakula, *Macromolecules* **2001**, *34*, 1677.
[181] F.-J. Lopez-Villanueva, F. Wurm, A. F. M. Kilbinger, H. Frey, *American Chemical Society, Polymer Preprints, Division of Polymeric Materials: Science & Engineering* **2006**, *232*, PMSE 11.
[182] M. R. Ambler, *J Appl Polym Sci* **1980**, *25*, 901.
[183] M. Zuideveld, C. Gottschalk, H. Kropfinger, R. Thomann, M. Rusu, H. Frey, *Polymer* **2006**, *47*, 3740.
[184] M. Murali, A. B. Samui, *J Polym Sci Pol Chem* **2006**, *44*, 53.
[185] B. Alonso, C. M. Casado, I. Cuadrado, M. Moran, A. E. Kaifer, *Chem Commun* **2002**, 1778.
[186] M. P. Armada García, J. Losada, I. Cuadrado, B. Alonso, B. González, E. Ramírez-Oliva, C. M. Casado, *Sensor Actuat B-Chem* **2003**, *88*, 190.

[187] M. P. Armada García, J. Losada, I. Cuadrado, B. Alonso, B. González, C. M. Casado, J. B. Zhang, *Sensor Actuat B-Chem* **2004**, *101*, 143.
[188] F. Le Floch, H. A. Ho, P. Harding-Lepage, M. Bedard, R. Neagu-Plesu, M. Leclerc, *Adv Mater* **2005**, *17*, 1251.
[189] J. M. Gibbs, S. J. Park, D. R. Anderson, K. J. Watson, C. A. Mirkin, S. T. Nguyen, *J Am Chem Soc* **2005**, *127*, 1170.
[190] H. Frey, C. Schlenk, *Top Curr Chem* **2000**, *210*, 69.
[191] J. Bernard, M. Schappacher, E. Ammannati, A. Kuhn, A. Deffieux, *Macromolecules* **2002**, *35*, 8994.
[192] Z. Jia, Y. Zhou, D. Yan, *J Polym Sci Pol Chem* **2005**, *43*, 6534.
[193] Q. H. Sun, K. T. Xu, H. Peng, R. H. Zheng, M. Haussler, B. Z. Tang, *Macromolecules* **2003**, *36*, 2309.
[194] Z. Li, J. W. Y. Lam, Y. Dong, Y. Dong, H. H. Y. Sung, I. D. Williams, B. Z. Tang, *Macromolecules* **2006**, *39*, 6458.
[195] D. A. Rider, K. A. Cavicchi, K. N. Power-Billard, T. P. Russell, I. Manners, *Macromolecules* **2005**, *38*, 6931.
[196] J. Massey, K. N. Power, I. Manners, M. A. Winnik, *J Am Chem Soc* **1998**, *120*, 9533.
[197] K. T. Kim, C. Park, G. W. M. Vandermeulen, D. A. Rider, C. Kim, M. A. Winnik, I. Manners, *Angew Chem* **2005**, *117*, 8178.
[198] J. Heinze, *Angew Chem* **1984**, *96*, 823.
[199] P. T. Kissinger, W. R. Heineman, *J Chem Ed* **1983**, *60*, 702.
[200] H. D. Abruña, *Coordin Chem Rev* **1988**, *86*, 135.
[201] R. S. Nicholson, I. Shain, *Anal Chem* **1964**, *36*, 706.
[202] J. S. Moore, S. I. Stupp, *Macromolecules* **1990**, *23*, 65.
[203] P. Juhasz, C. E. Costello, *Rapid Commun Mass Sp* **1993**, *7*, 343.
[204] W. F. Little, R. Eisenthal, *J Am Chem Soc* **1960**, *82*, 1577.
[205] D. R. Thevenot, K. Toth, R. A. Durst, G. S. Wilson, *Biosens Bioelectron* **2001**, *16*, 121.
[206] S. Rodriguez-Mozaz, M. P. Marco, M. J. L. de Alda, D. Barcelo, *Anal Bioanal Chem* **2004**, *378*, 588.
[207] S. Rodriguez-Mozaz, M. J. L. de Alda, D. Barcelo, *Anal Bioanal Chem* **2006**, *386*, 1025.
[208] J. Wang, *Anal Chim Acta* **2002**, *469*, 63.
[209] L. Gorton, *Electroanal* **1995**, *7*, 23.
[210] S. J. Updike, G. P. Hicks, *Nature* **1967**, *214*, 986.
[211] T. A. Skotheim, H. D. Abruña, "*Electroresponsive Molecular and Polymeric Systems*", Marcel Dekker, New York, **1988**, Vol. 1.
[212] J. Wang, "*Analytical Electrochemistry, Second Edition*", Wiley-VCH, New York, **2000**.
[213] A. Malinauskas, J. Kulys, *Anal Chim Acta* **1978**, *98*, 31.
[214] G. Angeletti, A. Bjørseth, "*Organic Micropollutants in the Aquatic Environment*", Kluwer Academic, Dordrecht, **1991**.
[215] C. Sonnenschein, A. M. Soto, *J Steroid Biochem* **1998**, *65*, 143.
[216] H. W. Duckworth, J. E. Coleman, *J Biol Chem* **1970**, *245*, 1613.
[217] C. Kranz, H. Wohlschlager, H. L. Schmidt, W. Schuhmann, *Electroanal* **1998**, *10*, 546.
[218] M. Hedenmo, A. Narvaez, E. Dominguez, I. Katakis, *J Electroanal Chem* **1997**, *425*, 1.
[219] J. Sänger, C. Tefehne, R. Lay, W. Gronski, *Polym Bull* **1996**, *36*, 19.
[220] D. Guillaneux, H. B. Kagan, *J Org Chem* **1995**, *60*, 2502.

[221] I. Cuadrado, C. M. Casado, B. Alonso, M. Moran, J. Losada, V. Belsky, *J Am Chem Soc* **1997**, *119*, 7613.
[222] A. D. Schlüter, J. P. Rabe, *Angew Chem Int Edit* **2000**, *39*, 864.
[223] D. A. Foucher, B.-Z. Tang, I. Manners, *J Am Chem Soc* **1992**, *114*, 6246.
[224] R. F. Lane, A. T. Hubbard, *J Phys Chem* **1973**, *77*, 1401.
[225] F.-J. López-Villanueva, A. Garcia Marcos, K. Fischer, M. Schmidt, B. Alonso, C. M. Casado, M. P. Garcia Armada, J. Losada, H. Frey, *Polymer Preprints (American Chemical Society, Division of Polymer Chemistry)* **2006**, *47*, 1087.
[226] M. F. Cardosi, A. P. F. Turner, "*Advances in Biosensors, Mediated Electrochemistry: A Practical Approach to Biosensing"*, JAI Press, London, **1991**, Vol. 1.
[227] S. F. White, A. P. F. Turner, U. Bilitewski, R. D. Schmid, J. Bradley, *Anal Chim Acta* **1994**, *295*, 243.
[228] R. Garjonyte, A. Malinauskas, *Sensor Actuat B-Chem* **1999**, *56*, 85.
[229] R. Garjonyte, A. Malinauskas, *Sensor Actuat B-Chem* **1999**, *56*, 93.
[230] "*International Tables for X-ray Crystallography"*, Kynoch Press, Birmingham, England, **1974**, Vol. 4.